



HAL
open science

Design and synthesis of fluorescent glyco-dots for detection and cell imaging

Lei Dong

► **To cite this version:**

Lei Dong. Design and synthesis of fluorescent glyco-dots for detection and cell imaging. Organic chemistry. Université de Lyon, 2019. English. NNT : 2019LYSE1153 . tel-02299416

HAL Id: tel-02299416

<https://theses.hal.science/tel-02299416>

Submitted on 27 Sep 2019

HAL is a multi-disciplinary open access archive for the deposit and dissemination of scientific research documents, whether they are published or not. The documents may come from teaching and research institutions in France or abroad, or from public or private research centers.

L'archive ouverte pluridisciplinaire **HAL**, est destinée au dépôt et à la diffusion de documents scientifiques de niveau recherche, publiés ou non, émanant des établissements d'enseignement et de recherche français ou étrangers, des laboratoires publics ou privés.



N°d'ordre NNT : 2019LYSE1153

THESE de DOCTORAT DE L'UNIVERSITE DE LYON

opérée au sein de
l'Université Claude Bernard Lyon 1

Ecole Doctorale N° 206
Chimie, Procédés, Environnement

Spécialité de doctorat : Chimie
Discipline : Chimie Organique

Soutenue publiquement le 17/09/2019, par :
Lei DONG

Conception et synthèse de glyco-sondes fluorescentes pour des applications en détection

Devant le jury composé de :

| | | |
|-------------------|---|--------------------|
| Bruno ANDRIOLETTI | Professeur des Universités Université Lyon 1 | Examineur |
| Guo-Rong CHEN | Professeure East China University of Science and Technology (ECUST) | Examinatrice |
| Xiao-Peng HE | Professeure East China University of Science and Technology (ECUST) | Examineur |
| Boris VAUZEILLES | Directeur de Recherches CNRS Université Paris-sud | Rapporteur |
| Sébastien VIDAL | Directeur de Recherches CNRS Université Claude Bernard Lyon 1 | Directeur de thèse |
| Joanne XIE | Professeure des Universités ENS Paris-Saclay | Rapporteuse |

Acknowledgements

First of all, I feel very grateful for my supervisor, Dr. Sébastien Vidal, to give an opportunity to become a member of Laboratoire de Chimie Organique 2 at Institut de Chimie et Biochimie Moléculaires et Supramoléculaires, Université Claude Bernard Lyon 1, and to provide guidance and direction for three years. He always encouraged me and gave me many useful suggestions which could help me finish my PhD projects and thesis successfully. Except experimental knowledges, I have learned many aspects from him: the optimistic and strict attitude for science, the responsible and friendly attitude for students and co-operators, the relaxed and tolerant attitude for family and life.

Then, I would like to thank Prof. Chen Guorong, Prof. He Xiaopeng, the professors of Organic chemistry in East China University of Science and Technology (ECUST) in China. They collaborated with us to measure many fluorescent data of probes *in vitro* and explore the biological applications *in vivo*. They recommended me to the lab of Dr. Sébastien Vidal and helped me to apply for the scholarship from CSC. I would like to thank the post-doctor, doctor and master students in ECUST, including Fu Mengqi, Liu Lifang, Zhang Minyu, Han Haihao and Hu Xile, for supporting these essential fluorescent data in my projects.

Then, I appreciate the support from Dr. Ladaviere Catherine to provide the SEC analysis data, and Dr. Thierry Granjon for access to the fluorescence spectrometer. I am also grateful for Prof. Peter Goekjian, Prof. Pierre Strazewski, Dr. David Gueyrard and Dr. Michele Fiore in LCO2 to give effective help.

During my project, my group members (current and former) were willing to explain the lab regulation, solve my questions about science and life, bear with my poor French and nonstandard English. Therefore, I really prefer to show my thanks to Yoann Pascal, Nicolas Duguet, Baptiste Thomas, Maxime Pommier, Yann Bertholo, Fanny Demontrond, Dimitri Fayolle, Idriss Habibu, Bastien Raison, and other friendly members in LCO2.

Meanwhile, I would like to express my gratitude to many staff members in the analytical labs, the NMR spectroscopy lab and the mass spectroscopy lab. They did a lot of work to support my PhD program. I sincerely feel fortunate to have many Chinese friends in Lyon, Because of their assistance and support, I didn't feel alone, and enjoyed the colourful life in three years.

Great thanks to China scholarship council for financial support.

I honestly thank my girlfriend, Miss Liu Hang, for the support and company when I wrote my PhD manuscript. I could overcome lots of difficulties with her encouragement.

Finally, I sincerely would like to dedicate my work to my parents, Dong Ming-sheng and Zhu Xiu-ying. They gave the most selfless love and everything what they have to me in past 28 years. I am greatly grateful for their support.

List of Abbreviations

| | |
|------------------|---|
| ACQ | aggregation caused quench |
| Ac | acetyl |
| AFU | α -L-fucosidase |
| AIE | aggregation induced emission |
| aq. | aqueous |
| ASGPr | Asialoglycoprotein receptor |
| Boc | <i>tert</i> -butyloxycarbonyl |
| BSA | bovine serum albumin |
| BSP | 1-benzenesulfinyl piperidine |
| BTz | 2-mercaptobenzothiazole |
| calcd | calculated |
| ConA | Concanavalin A |
| COSY | correlation spectroscopy |
| CuAAC | Cu (I)-catalyzed azide-alkyne cycloaddition |
| Cys | cysteine |
| DCM | dicyanomethylene-4 <i>H</i> -pyran |
| DIPEA | <i>N,N</i> -diisopropylethylamine |
| DLS | dynamic light scattering |
| DMAP | 4-dimethylaminopyridine |
| DME | 1,2-dimethoxyethane |
| DMF | <i>N,N'</i> -dimethylformamide |
| DMSO | dimethylsulfoxide |
| DNA | deoxyribonucleic acid |
| DOSY | diffusion ordered spectroscopy |
| DTT | dithiothreitol |
| EDCI | <i>N</i> -ethyl- <i>N'</i> -(3-dimethylaminopropyl)carbodiimide hydrochloride |
| equiv. | equivalent |
| FL | fluorescence spectra |
| FRET | Förster resonance energy transfer |
| Fuc | fucose |
| Gal | galactose |
| β -Gal | β -D-galactosidase |
| Glc | glucose |
| β -Glc | β -D-glucosidase |
| GSH | glutathione |
| h | hour |
| Hcy | Homocysteine |
| HPLC | high performance liquid chromatography |
| HOBT | <i>N</i> -hydrobenzotriazole |
| IC ₅₀ | half inhibitory concentration |
| ICT | intermolecular charge transfer |

| | |
|-----------------------|---|
| <i>J</i> | coupling constant |
| LOD | limit of detection |
| LPS | Lipopolysaccharide |
| Man | mannose |
| <i>m</i> -CPBA | <i>meta</i> -chloroperoxybenzoic acid |
| min | minute(s) |
| MS | mass spectrometry |
| <i>m/z</i> | mass to charge ratio (mass spectrometry) |
| NBS | <i>N</i> -bromosuccinimide |
| NIR | near infrared |
| NMR | nuclear magnetic resonance |
| PDI | perylene diimide |
| PET | photo-induced electronic transfer |
| PNA | Peanut agglutinin |
| ppm | parts per million (NMR data) |
| PSTA | <i>p</i> -toluenesulfonic acid |
| Py | pyridine |
| RT | room temperature |
| SEC | size-exclusion chromatography |
| SIN-1 | 5-amino-3-(4-morpholinyl)-1,2,3-oxadiazolium chloride |
| TFA | trifluoroacetic acid |
| THF | tetrahydrofuran |
| TLC | thin layer chromatography |
| TMS | trimethylsilyl |
| TPE | tetraphenylethylene |
| UV | ultraviolet–visible spectroscopy |
| VcNa | sodium ascorbate |
| λ_{ex} | maximum excitation wavelength |
| λ_{em} | maximum emission wavelength |
| Φ | quantum yield |

General introduction

With scientific and social progress, various methods for the specific and sensitive detection of metals, proteins and other biomolecules are widely utilized in environmental protection, disease surveillance, drug therapy, agricultural production, industry and other significant areas. Fluorescent probes are widely developed based on ICT, PET, FRET and other fluorescence mechanisms, and applied to the detection of contaminants or in cell imaging. But the ACQ effect usually quenched the fluorescence intensity and thus limited the applications of organic probes in cell imaging and living systems. Therefore, the concept of aggregated-induced emission (AIE) appears as a possible solution to these problems and several fluorescent glycoclusters, glyco-probes and glyco-complexes were designed and reported for biological analysis.

Our first project aimed to design and synthesize fluorescent glyco-polymers with multiple glycosides for cell targeting and drug delivery while fluorescence will allow the detection of the targeted cells. To overcome the ACQ effect and interference from natural biological background fluorescence, we conjugated dicyanomethylene-4*H*-pyran (DCM) and tetraphenylethene (TPE) to obtain near-infrared AIE fluorescent probes. The glycosides provided good water solubility and self-assembly in water led to detection systems and imaging cancer cells.

TPE-based glycopolymers were synthesized from TPE monomers incorporating two monosaccharides by CuAAC conjugation and these monomers were polymerized by either CuAAC or thiol-ene “click” reactions. The TPE-based glycopolymers did not display a large chain length (typically less than 7 units) and the expected fluorescent properties could not be reached.

We then designed and synthesized glyco-dots self-assembled by DCM probes and TPE-based glycoclusters. The glyco-dots displayed high water-solubility and selective response to peroxynitrite (ONOO⁻) both *in vitro* and in cell assays. The glyco-dots could detect endogenous and exogenous ONOO⁻ but no specific cell recognition.

We designed and synthesized AIE fluorescent probes which could self-assemble with TPE-based glycoclusters. The resulting glyco-dots were readily water soluble and displayed excellent sensitivity and selectivity for thiophenol detection *in vitro* and in environmental water samples.

We finally combined both TPE and DCM moieties to synthesize a novel AIE fluorophore (TPE-DCM) with long-wavelength emission. Then conjugation with glycosides through CuAAC led to AIE fluorescent probes with long-wavelength emission, excellent water-solubility. Application to the detection of glycosidases *in vitro* and in cell assays or animal models was possible with these probes.

Résumé

Avec le progrès scientifique et les besoins sociétaux, diverses méthodes de détection spécifiques et sensibles des métaux, des protéines et d'autres biomolécules sont largement utilisées dans la protection de l'environnement, la surveillance des maladies, la pharmacothérapie, la production agricole, l'industrie et d'autres domaines importants. Les sondes fluorescentes sont largement développées sur la base des phénomènes de transfert d'énergie (ICT, PET, FRET) et appliquées par exemple à la détection de contaminants ou à l'imagerie cellulaire. Mais l'effet d'agrégation (ACQ) atténue généralement l'intensité de la fluorescence et limite ainsi les applications de sondes organiques (souvent peu solubles dans l'eau) dans l'imagerie cellulaire et les systèmes vivants. Par conséquent, le concept d'« aggregated induced emission » (AIE) représente une solution à ces problèmes d'agrégation et plusieurs glyco-clusters, glyco-sondes et glyco-complexes fluorescents ont été conçus et reportés pour des applications en analyse biologique.

Notre premier projet visait à concevoir et à synthétiser des glyco-polymères fluorescents pour le ciblage cellulaire et l'adressage de médicaments, tandis que la fluorescence permettrait la détection des cellules ciblées. Pour surmonter l'effet ACQ et les interférences provenant de la fluorescence biologique naturelle, nous avons conjugué le dicyanométhylène-4H-pyrane (DCM) et le tétraphényléthène (TPE) afin d'obtenir des sondes fluorescentes (AIE) émettant dans le proche infrarouge. Les glycosides ont fourni une bonne solubilité dans l'eau et l'auto-assemblage a conduit à des systèmes de détection et à une imagerie des cellules cancéreuses.

Les glyco-polymères à base de TPE ont été synthétisés à partir de monomères de TPE incorporant deux monosaccharides par conjugaison azide-alcyne (CuAAC) et ces monomères ont été polymérisés par des réactions de CuAAC ou thiol-ène. Les glyco-polymères à base de TPE ne présentaient malheureusement pas une assez grande longueur de chaîne (généralement moins de 7 unités) et les propriétés fluorescentes attendues ne pouvaient donc pas être atteintes.

Nous avons ensuite conçu et synthétisé des glyco-dots auto-assemblés par des sondes DCM et des glyco-clusters à base de TPE. Les glyco-dots ont présenté une hydrosolubilité élevée et une réponse sélective au peroxy-nitrite (ONOO^-) à la fois *in vitro* et dans des analyses cellulaires. Les glyco-dots pourraient détecter ONOO^- endogène et exogène, mais sans reconnaissance cellulaire spécifique.

Nous avons conçu et synthétisé des sondes fluorescentes AIE pouvant s'auto-assembler avec des glyco-clusters à base de TPE. Les glyco-dots résultants étaient facilement solubles dans l'eau et présentaient une sensibilité et une sélectivité excellentes pour la détection du thiophénol *in vitro* et dans des échantillons d'eau environnementaux.

Nous avons finalement combiné les deux fragments TPE et DCM pour synthétiser un nouveau fluorophore AIE (TPE-DCM) avec émission à longue longueur d'onde. Ensuite, la conjugaison avec des glycosides par CuAAC a conduit à des sondes AIE fluorescentes à émission de longue longueur d'onde, avec une excellente solubilité dans l'eau. Une application à la détection de glycosidases *in vitro* et dans des dosages cellulaires ou sur des modèles animaux a été possible avec ces sondes.

Table of contents

| | |
|--|----|
| Chapter I: Introduction | 1 |
| I.1 Small molecular fluorescent probe | 3 |
| I.1.1 Fluorescent probes..... | 3 |
| I.1.2 Organic fluorescent probes..... | 4 |
| I.1.3 Novel design principle -- Aggregated-induced emission (AIE) | 13 |
| I.2 Glycoconjugate as fluorescent probes | 20 |
| I.2.1 Carbohydrates in biology | 20 |
| I.2.2 Glycosylated fluorescent probes | 21 |
| I.3 Glycoclusters and self-assembled glyco-probes | 23 |
| I.3.1 Glycoclusters..... | 23 |
| I.3.2 Self-assembled nanoparticles and glyco-probes..... | 26 |
| I.5 Conclusion | 29 |
| I.6 Project purpose | 30 |
| Chapter II: Design and Synthesis of TPE-Based Glycopolymers | 35 |
| II.1 Introduction | 37 |
| II.1.1 Conjugation methodologies | 37 |
| II.1.2 Project design..... | 41 |
| II.2 Design and synthesis of bisymmetric TPE-scaffold..... | 42 |
| II.2.1 Synthesis of TPE by Julia olefination | 42 |
| II.2.2 Synthesis of TPE by Knoevenagel condensation..... | 43 |
| II.2.3 Nitration of TPE..... | 44 |
| II.3 Synthesis of TPE-based glycopolymers by thiol-ene “click” reaction | 46 |
| II.3.1 Synthesis of mannose-decorated TPE monomer..... | 46 |
| II.3.2 Synthesis of TPE-based glycopolymer by thiol-ene reaction | 46 |
| II.4 Synthesis TPE glycol-polymers through twice “click” reaction | 47 |
| II.4.1 Synthesis of galactose-decorated TPE-monomer for “click” reaction..... | 47 |
| II.4.2 Synthesis of galactose-decorated TPE polymer | 48 |
| II.5 Conclusion..... | 51 |
| Chapter III: Self-assembled Glyco-dots for Peroxynitrite Detection and Cell Imaging | 53 |
| III.1 Introduction..... | 55 |
| III.1.1 Fluorescent probes for intracellular peroxynitrite detection..... | 55 |
| III.1.2 Project design | 59 |
| III.2 Synthesis of TPE-glycoclusters and DCM probes | 61 |
| III.2.1 Synthesis of TPE-based glycoclusters | 61 |
| III.2.2 Synthesis of DCM probes..... | 61 |
| III.3 Self-assembly of glyco-dots and detection of ONOO ⁻ | 62 |
| III.3.1 Detection of ONOO ⁻ using DCM probes..... | 62 |
| III.3.2 Analysis of the mechanism of DCM probes for ONOO ⁻ detection..... | 64 |
| III.3.3 Glycoclusters selection for perfecting water-solubility of DCM probes | 65 |
| III.3.4 Explore combination mode between TPE-glycoclusters and DCM probes.... | 67 |
| III.3.5 Size and shape variation of DCM probes after self-assembly with TPE-based | |

| | |
|--|------------|
| glycoclusters..... | 70 |
| III.3.6 Influence of time on fluorescence intensity..... | 73 |
| III.3.7 ROS and RNS selectivity of series glyco-dots | 74 |
| III.3.8 ONOO ⁻ titration | 75 |
| III.4 Detection of ONOO ⁻ in biological systems..... | 77 |
| III.4.1 Series glyco-probes responding ONOO ⁻ in cells | 77 |
| III.4.2 Cytotoxicity of self-assembled glyco-dots | 78 |
| III.4.3 Glyco-dots responding to endogenous ONOO ⁻ | 78 |
| III.4.4 Cell selectivity of glyco-dots..... | 79 |
| III.4.5 Conjectures of combination mode between DCM probes and glycoclusters in biological assays..... | 82 |
| III.5 Conclusion | 82 |
| Chapter IV: Self-assembled AIE Glyco-dots for Thiophenol Detection..... | 85 |
| IV.1 Introduction..... | 87 |
| IV.1.1 Fluorescent probes for thiophenol detection..... | 87 |
| IV.1.2 Project design..... | 90 |
| IV.2 Synthesis of probe for PhSH detection..... | 91 |
| IV.2.1 Synthesis of 1-carbonyl-1'-methoxy-terraphenylethylene..... | 91 |
| IV.2.2 Synthesis of the DCM fluorophore (TPE-DCM)..... | 92 |
| IV.2.3 Synthesis of probes by sulfonylation | 93 |
| IV.3 Novel AIE probe for thiophenol detection | 94 |
| IV.3.1 The fluorescence response of TPE-DCM probes to thiophenol detection | 94 |
| IV.3.2 Fluorescence properties of IV-7 for thiophenol response | 95 |
| IV.3.3 The response mechanism of IV-7 to thiophenol detection..... | 96 |
| IV.3.4 Solvent influence | 97 |
| IV.3.5 pH influenced fluorescence of probe for thiophenol detection | 97 |
| IV.3.6 Selectivity for thiophenol detection | 98 |
| IV.3.7 AIE fluorescent performance for thiophenol detection..... | 98 |
| IV.3.8 Time influence | 99 |
| IV.4 Self-assembly of TPE-glycocluster and TPE-DCM-based probe for PhSH detection .. | 100 |
| IV.4.1 TPE-glycoclusters self-assembly with IV-7 for thiophenol detection | 100 |
| IV.4.2 AIE affecting fluorescence of glyco-dots for thiophenol response | 102 |
| IV.4.3 Response time of glyco-dots for thiophenol detection..... | 103 |
| IV.4.4 Influence of thiophenol concentration | 103 |
| IV.4.5 Detection of thiophenol in environmental water samples..... | 105 |
| IV.4.6 Size variation of glyco-dots after intermolecular self-assembly | 106 |
| IV.5 Conclusion..... | 107 |
| Chapter V: Long-wavelength AIE Fluorescent Glycoclusters for Glycosidase Detection | 109 |
| V.1 Introduction | 111 |
| V.1.1 Fluorescent probes for glycosides detection..... | 111 |
| V.1.2 Project design..... | 116 |
| V.2 Synthesis of the TPE-DCM probes..... | 118 |
| V.2.1 Synthesis of a carbonyl TPE moiety | 118 |
| V.2.2 Synthesis of the NIR fluorophore (TPE-DCM)..... | 118 |

| | |
|---|-----|
| V.2.3 Carbohydrates decorated on fluorophore through glycosylation | 119 |
| V.2.4 Conjugation through C ₃ or TEG linkers..... | 121 |
| V.2.5 Design and synthesis of TPE-DCM-based glycoclusters | 122 |
| V.3 Water-soluble TPE-DCM-based glycoclusters for galactosidase detection..... | 124 |
| V.3.1 Fluorescence detection of β -galactosidase | 124 |
| V.3.2 Influence of probe concentration..... | 125 |
| V.3.3 Reverse AIE effect of TPE-DCM-glycoclusters | 125 |
| V.3.4 Influence of time for β -Gal detection with probe V-17a | 126 |
| V.3.5 pH influence | 127 |
| V.3.6 TPE-DCM-glycoclusters quantifying β -Gal concentration..... | 127 |
| V.3.7 Selectivity of V-17a for β -Gal detection | 128 |
| V.3.8 Carbohydrate selectivity with V-17a for β -Gal detection | 129 |
| V.3.9 Dynamic light scattering analysis..... | 129 |
| V.3.10 V-17a detection of endogenous β -Gal and imaging cells..... | 130 |
| V.4 Conclusion..... | 131 |
| VI. Experimental Section | 133 |
| VI.1 General information..... | 135 |
| VI.1.1 Reagents and solvents | 135 |
| VI.1.2 Nuclear magnetic Resonance | 135 |
| VI.1.3 Mass spectrometry..... | 135 |
| VI.1.4 High Performance Liquid Chromatography. | 135 |
| VI.1.5 C18 Chromatography | 135 |
| VI.1.6 Absorption, fluorescence and DLS spectrometry | 135 |
| VI.1.7 High-resolution transmission electron microscope | 136 |
| VI.1.8 Dynamic light scattering | 136 |
| VI.1.9 Cell culture | 136 |
| VI.1.10 Generation of shASGPR1..... | 136 |
| VI.2 Synthesis..... | 137 |
| VI.2.1 General procedures..... | 137 |
| VI.2.2 Synthesis..... | 138 |
| VI.3 Fluorescence measurement..... | 172 |
| VI.3.1 Supramolecular glyco-probe with DCM probe and TPE-glycocluster for ONOO ⁻ detection..... | 172 |
| VI.3.2 Supramolecular glyco-probe with TPE-DCM probe and TPE2S for thiophenol detection | 173 |
| VI.3.3 TPE-DCM-based glycocluster for glycosidase response..... | 174 |
| Reference | 175 |

Chapter I

Introduction

With scientific and social progress, various methods for the specific and sensitive detection of ions, proteins and other biomolecules are widely utilized in environmental protection, disease surveillance, drug therapy, agricultural production, industry and other significant areas^[1-3]. The detection methods are developed through several analytical techniques such as electrochemical analysis, high performance liquid chromatography, atomic absorption spectroscopy^[4-7]. However, expensive price, complex operations or long testing time limit their use in non-specialized environments. Fluorescence analysis shortens the testing time, increases the analytical sensitivity, and simplifies the process among other advantages^[8]. For these reasons, it plays an important role in many fields such as chemistry, biology, medicine, pharmacy and diagnostics^[9-12]. Herein, we will introduce some general fluorescent dyes including their characteristics, development, synthesis, and recent applications in biological systems.

I.1 Small molecular fluorescent probe

Modern chemical analysis and chemical biology depend on the design of efficient “fluorescent probes” for the accurate deciphering of biological processes. Such fluorescent probes are typically composed of a fluorophore unit decorated with special targeting or detecting groups. Since Roger Yonchienien and co-workers^[13] designed and synthesized the first fluorescence sensor that could produce luminescence by complexation of aromatic dyes with calcium ion in 1980s, fluorescent probes as advanced methods entered a fast-developing period from detecting simple ions *in vitro* to imaging biological processes *in vivo*.

I.1.1 Fluorescent probes

Fluorescent probes are composed of a reporting group (fluorophore) and a detecting group (e.g. chelating ions). To be applied in several biological imaging, additional moieties have been introduced such as DNA, peptides and carbohydrates on fluorophores to selectively recognize particular proteins, organelles, cells, or tissues^[14]. The fluorescent probes were classified as substitutional probes, chelating-coordinating probes, and reactive probes according to their diverse detection mechanisms.

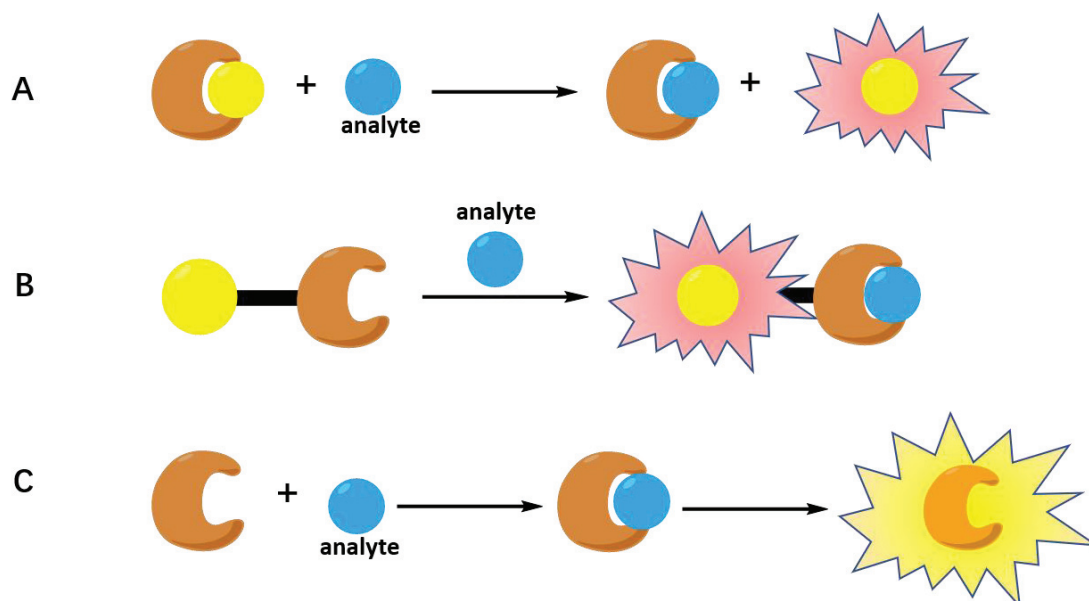


Figure 1: Three main principles for fluorescent probes. (A) Substitutional probe, (B) chelating-coordinating probe, (C) reactive probe.

Substitutional probes (Fig. 1A) were obtained by turn-off the fluorescence upon binding to receptors. Then the analyte to be detected will bind to the receptor and release the fluorescent probe to generate a fluorescence signal^[15, 16].

Chelating-coordinating probes (Fig. 1B) should follow the 3R rule (Receptor-Relay-Reporter) meaning that the receptor and reporter are linked through a covalent bond or interacted with non-covalent bond. When the analyte is interacting with the receptor, the reporter generates a different signal due to the intramolecular variation of electron density based on additional interactions on the scaffold (hydrogen bond, electrostatic force, coordinating bond)^[17-19].

As fluorescent reporter and analyte detector, reactive probes can be divided into two categories (Fig. 1C). The analyte can interact with the probe and trigger a fluorescence signal by changing its electronic properties. Also, the analyte can catalyse an intramolecular reaction in the probe leading to a change in fluorescence signal. These reactive probes are usually sensitive, selective, and reliable for the recognition of specific analytes due to the irreversibility of the chemical reaction^[20-22].

I.1.2 Organic fluorescent probes

Aromatic molecules after absorbing light with specific wavelength can activate intramolecular electron in higher energy level. Fluorescence is one method to release redundant energy from a singlet excited state to ground state through photo-emission^[23]. However, many factors impact the energy release including structure difference, solvent influence, solubility, π - π stacking, responding modes and others which effect molecular energy transfer. Here, three typical fluorescence mechanisms and a novel fluorescence emergence process will be introduced.

I.1.2.1 Mechanisms influencing fluorescence

Three main types of fluorescence mechanisms can be distinguished according to their interaction between probes and analytes: Intermolecular Charge Transfer (ICT), Photo-induced Electronic

Transfer (PET), Förster Resonance Energy Transfer (FRET).

Intermolecular Charge Transfer (ICT) is an essential mechanism, characterized by an intramolecular charge transfer between positive and negative charges generated upon excitation of a ground state, which is commonly used to design fluorophore, change emissive wavelength, and decorate fluorescent properties^[24]. The ICT probe (Fig. 2) had usually a “push-pull” electronic system with electronic donor (D such as alcohol, amine) and electronic acceptor (A such as carbonyl, nitrile) connected with covalent bonds, and capable of transferring charges through π - π conjugated systems. The charge of the analyte or positive ions will influence the variation of wavelength and fluorescence intensity.

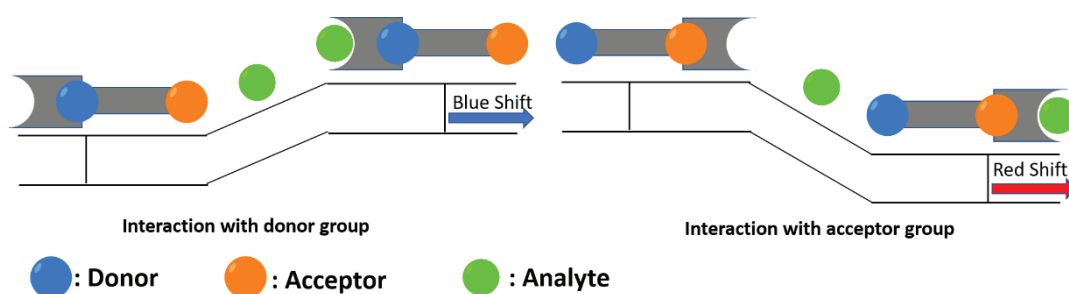


Figure 2: The mechanism of intermolecular charge transfer (ICT).

Ionic probes are usually modified in their density distribution of intramolecular electronic cloud to quench or increase fluorescence after chelating ions with electronic charges. Many probes followed by sensitive fluorescence enhancement were applied to detect metal ion in sewage and intracellular biomarker for disease diagnosis. Two quinoline-based probes for Zn^{2+} detection and imaging the ions in lysosomal have been designed^[25]. The probes provided ratiometric and blue-shift fluorescence changes upon coordination with zinc ion in aqueous solution, and detected intracellular and subcellular ions sensitively. A sensitive Zn^{2+} probe incorporating 1,8-naphthalimide as fluorophore and DPA as detector emitted green fluorescence for Zn^{2+} and blue luminescence for Cd^{2+} (Fig. 3)^[26]. Two different chelating models influenced the density distribution of electronic cloud in whole fluorophore. However, the chelating bond connecting probe and analyte is unstable, reversible and non-specific when others similar analytes existed. But ICT mechanism is still widely studied in various designs thought and applied to regulate and decorate properties of fluorophores with other essential mechanisms^[27, 28].

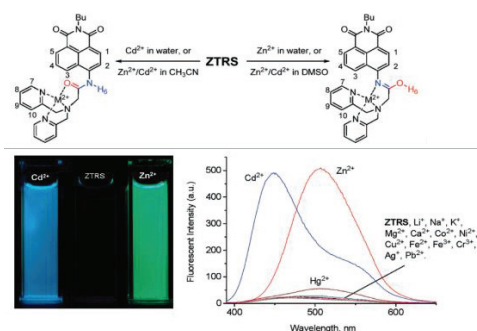


Figure 3: The probe based on ICT effect for Zn^{2+} detection^[26].

Photo-induced Electronic Transfer (PET) involves the intramolecular electronic transfer between donor (D) and acceptor (A) after excitation of the probe with light to stimulate the fluorescent core and reach an excited state. Due to the intramolecular electronic density changes, the fluorescent probe can respond accurately and provide a specific signal difference (Fig. 4)^[29, 30]. Compared with the quenched ground state, the fluorescence intensity usually has a remarkable enhancement, or the emissive wavelength shifts drastically upon interaction of the probe with the analyte. As classic PET application of probe design, many rich-electronic chemical groups (such as amino linkers or phenols) were decorated on fluorophores but not connected through π - π conjugation (double bond). The electronic cloud is activated after absorbing excited light, then transferred to fluorophore leading to break or weaken the electronic D-A system to quench the whole fluorescence. After coordinating or reacting with analyte, the fluorescence is recovered followed by PET process blocked and D-A system rebuilt^[31-33]. However, the fluorescence response is not stable and sensitive enough since electron-rich groups were usually interfered at different pH or in the presence of cations, which restricted its application in acidic environments^[34, 35].

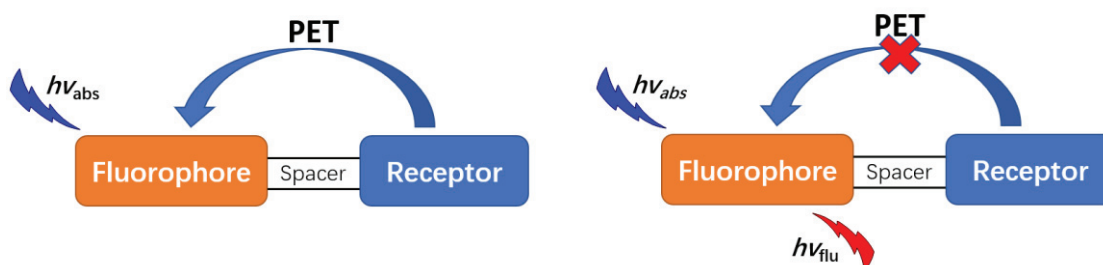


Figure 4: The mechanism of photo-induced electronic transfer (PET).

A novel PET probe for HClO detection in cancer cells consisted of BODIPY fluorophore and 2,4-dimethylpyrrole as detector. The green fluorescence ($\lambda_{em} = 505$ nm) was recovered when the probes were oxidized by HClO along with annihilation of the PET state (Fig. 5)^[36]. Similarly, near-infrared fluorescent probe showed red increased luminescence after detection of electron-rich group with Pim protein kinases (an important biomarker in brain and cancer, prostate cancer, breast cancer)^[37]. Some probes were also designed to detect specific intracellular small molecules for cancer imaging through neutralizing the ion pair electron of amine or decreasing electron density. A turn-on fluorescein-based probe through NO-induced deamination of an aromatic primary amino group showed fluorescence increase and high selectivity for NO detection in solution and in cancer cells, but only responded in neutral and weakly basic solution^[38].

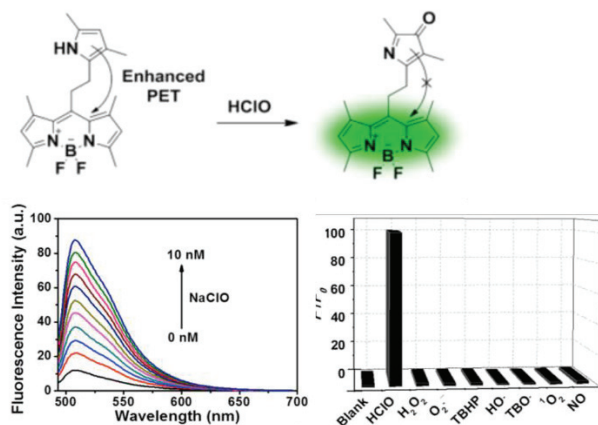


Figure 5: The probe based on PET effect for HClO detection^[36].

Förster Resonance Energy Transfer (FRET) is not a radiative process. A ground state acceptor (A) releases luminescence after absorbing the fluorescence from an excited donor (D) through dipole-dipole interactions (Fig. 6). The absorption of the acceptor must overlap with the emission of the donor and the efficiency of the energy transfer depends on several parameters such as the extent of spectral overlap between D and A, the relative orientations of the transition dipoles, the distance between D and A^[39, 40]. The distance appears as the most essential parameter because FRET occurs with about 10 to 100 Å distances between D and A, largely compatible with the dimensions of most biomacromolecules. FRET was therefore prevalently applied for bioanalysis and biological imaging due to the simple ratiometric fluorescent system. Unlike one-signal probes, FRET sensors contain two different fluorophores which can release a ratiometric fluorescence signal, used for the quantitative detection of analytes and eliminating ambiguities arising. Conventional FRET probes have been designed in the form of two covalently linked fluorescent moieties. However, the two organic fluorophore systems can still be hard to synthesize owing to the proper controlling of the D/A distance, and limited modifiable position for fluorophore connection and detector decoration. Recently, fluorophores were self-assembled with nanoparticles, carbon nanodots or quantum dots to build up new supramolecular FRET systems overcoming some disadvantages^[41].

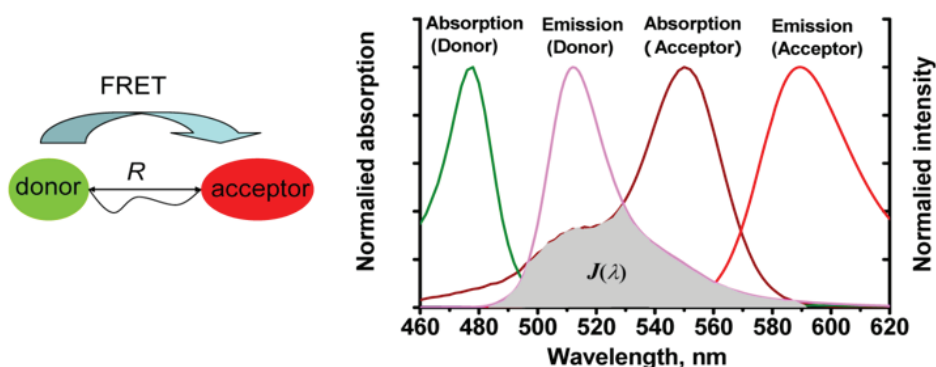


Figure 6: The mechanism of Förster resonance energy transfer (FRET) and relative spectra overlapping between donor and acceptor^[41].

A FRET-based ratiometric fluorescent probe consisting of amino-coumarin and fluorescein for

HNO detection and imaging in cancer cells (Fig. 7)^[42]. The blue emission (470 nm) of coumarin (excited at 415 nm) was observed when the FRET was blocked due to a change in absorption of acceptor (A) moiety and quenching its fluorescence. The fluorescence signal of fluorescein (517 nm) was observed with a decreased fluorescence of coumarin when the probe reacted with HNO and released the two hydroxyls on fluorescein. Meanwhile, FRET system was recovered with new absorption at 495 nm receiving energy from coumarin. The probe exhibited good selectivity for HNO, good sensitivity (1.4 μM) and obvious colour change in cell imaging.

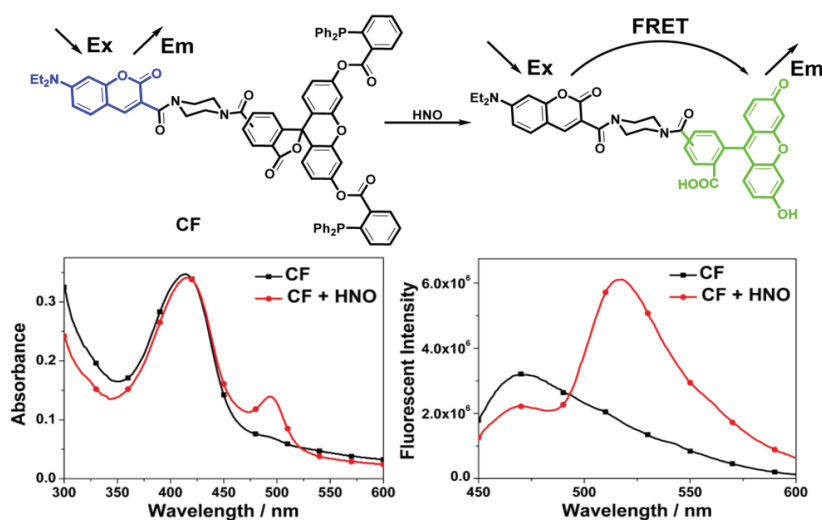


Figure 7: The FRET probes composed of coumarin and fluorescein for HNO detection^[42].

However, complicated fluorophore design, high synthetic difficulty, low water-solubility and uncertain activity for analytes detection restricted applications and development of several FRET probes. Therefore, intermolecular self-assembly through hydrogen bond, π - π stacking, aggregation or others Van der Waal's forces, is a simple, fast, and efficient choice to construct FRET-based ratiometric fluorescent systems. A special probe consisting of green quantum dots and red fluorescent proteins for visualizing intracellular pH variation (Fig. 8). The pH-sensitive protein could respond red fluorescence after absorbing energy from quantum-dot and quenching the green signal in basic environment. This probe with high sensitivity, wide working range, ratiometric responding signal, allowed to monitor different pH environmental changes *in vitro* and *in vivo*^[43].

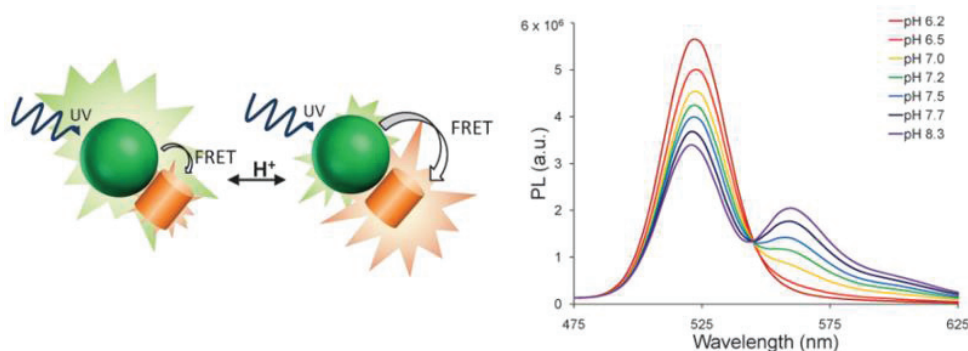


Figure 8: Self-assembled FRET probe as pH variation monitor^[43].

I.1.2.2 Organic fluorophore and its application

Various organic fluorescent scaffolds including pyrene, coumarin, fluorescein, rhodamine, 1,8-naphthalimide, BODIPY, DCM derivatives, cyanine, tetraphenylethylene and their structural analogues, were frequently applied in advanced areas. Here, we introduced some classic fluorophores and their derivatives that have excellent fluorescent characteristics and the exemplary use of sophisticated, custom-made probes.

The coumarin scaffold is a particular structure in organic chemistry, occurring in numerous natural products and performing excellent functions in pharmacology. Normally decorating the 7-position (Fig. 9A) with electronic-donating groups highly increases the fluorescence intensity. The structure of 7-hydroxycoumarin (Fig. 9B) which absorbs UV light ($\lambda_{\text{ex}} = 360$ nm) and emits blue light ($\lambda_{\text{em}} = 450$ nm) was sensitive for pH with wavelength changes^[44]. The 7-aminocoumarin scaffold is another common fluorescent core with tunable emission through the 7-amino was modification with electronic-poor groups^[45]. Coumarins are usually synthesized by the Pechmann condensation involving the acid-catalyzed reaction of a phenol and a β -carbonyl ester^[46].

The boron dipyrromethene (BODIPY) is employed as a reactive probe in various bioanalysis, because of its characteristic properties of neutral charge, small Stokes shift, insensitivity of fluorescence to environmental changes (Fig. 9C and 9D)^[47]. Scientists designed and synthesized series of infrared emitting BODIPY through extending π - π conjugated systems or changing the boron ligands to affect fluorescence properties and use it to detect some important ions in living system in combination with proteins^[48], to generate singlet oxygen for photodynamic therapy, as well as to build up various FRET systems through bioluminescence resonance energy transfer (BRET) effect^[49, 50].

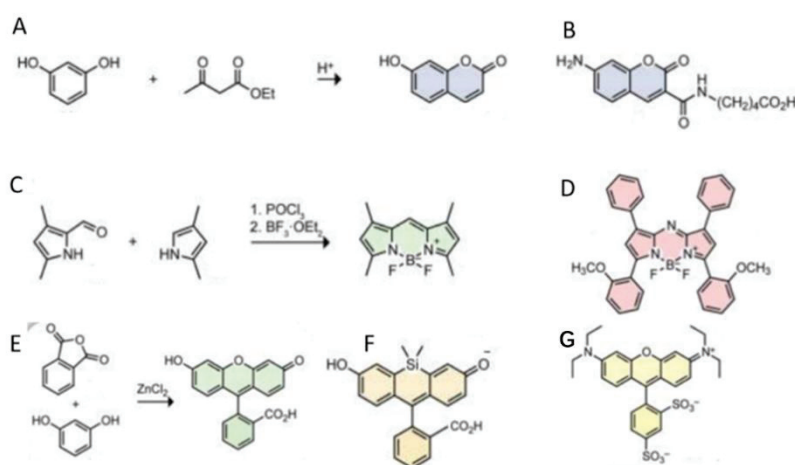


Figure 9: (A) Synthesis of 7-hydroxycoumarin, (B) 7-aminocoumarin derivatives. (C) Synthesis of BODIPY scaffold, (D) aza-BODIPY derivatives. (E) Synthesis of fluorescein, (F) Si-fluorescein. (G) is disulfonic rhodamine^[23].

Fluorescein including its derivatives (Fig. 9E and 9F) and rhodamines (Fig. 9G) are two similar fluorescent scaffolds, which have become ubiquitous small-molecular fluorophores since their synthesis in 1871^[51] and 1887^[52]. Fluorescein having two hydroxyl is very sensitive to environmental pH changes and acting as a special “on-off” pH probe^[53, 54]. Therefore, protecting hydroxyl with some electronic-rich groups could weaken the pH sensitivity in solvent and increase

the quantum yield^[55]. Compared with fluorescein, rhodamine has more advantages including lower pH-sensitivity, higher photostability, outstanding quantum yield, and sustainable spectral properties. The traditional rhodamines absorb the green light and emit a yellow light ($\lambda_{ex}/\lambda_{em} = 565 \text{ nm}/586 \text{ nm}$). Usually, modification on the phenyl ring or changing the substituent patterns on the aniline nitrogen of rhodamine can modulate the fluorescence properties^[56]. Decorating the carboxyl with amino-compounds, could quench the fluorescence due to prevented cyclization disturbing the π - π conjugated and electronic “push-pull” systems. Utilizing this characteristic, scientists designed and synthesized some rhodamine-based probes to coordinate ion or react with amine^[57-59].

Most of traditional fluorophore with short wavelength emission were usually interfering with biological background light which restricted their application in cell imaging, monitoring drug delivery or disease diagnosis. Therefore, near-infrared (NIR) fluorescent scaffolds have been designed with decreased energy loss when penetrating skin, imaging tissue and avoiding the interference of blue background light^[60-62]. Dicyanomethylene-4*H*-pyran (DCM) is a NIR fluorophore displaying a typical ICT-based chromophore with standard structure of donor- π -acceptor (D- π -A)^[63]. DCM attracted considerable views from chemists owing to its excellent photophysical advantages such as wide absorption range, high sensitivity for electronic changes, long emission wavelength, high fluorescent quantum yield, and controllable fluorescence properties (Fig. 10). Normally, chemists decorated specific detector on the hydroxyl or amino groups to control the DCM fluorescence. Recently, numerous DCM derivatives have been reported in OLED materials, logic gates, optical chemosensors, biological imaging, and disease diagnosis^[64].

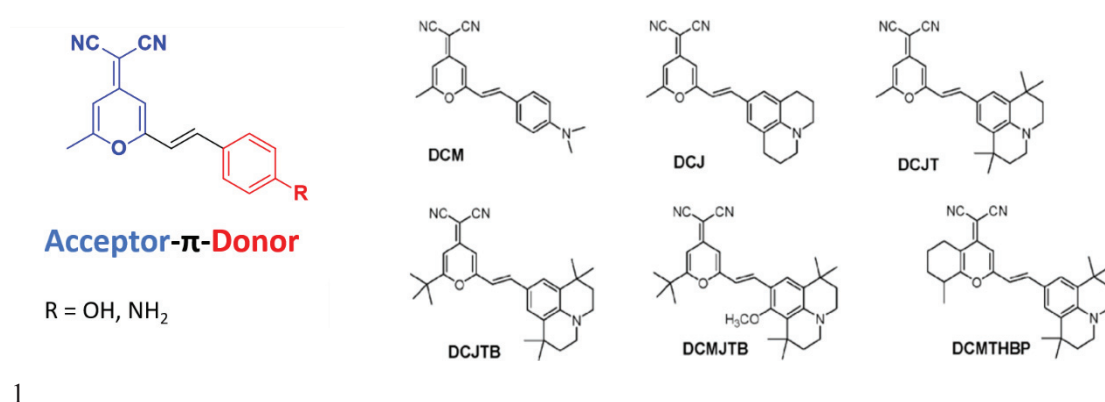


Figure 10: The ICT process of DCM and some chemical structures of typical reported DCM dyes^[64].

Pyrophosphate anion (PPi) is an essential biomolecule in metabolic system, bioenergetic, intercellular information transfer, and protein synthesis, but it is easy to detect with metal ions. An “on-off-on” probe (Fig. 11A) which could change fluorescence intensity through coordinating with Cu²⁺ and PPi was reported^[65]. The probe-Cu complex displayed near-infrared wavelength emission ($\lambda_{emis} = 650\text{nm}$) and efficient quantum yield ($\Phi = 0.4$) after detecting PPi and enhanced fluorescence. According to the excellent response for PPi, a macromolecular probe (Fig. 11B) was studied for the detection of Cu²⁺ and PPi. The hydrophilic probe exhibits fluorescence-*off* upon detection with Cu²⁺ selectively and recover the fluorescence-*on* after polymer-Cu system responding to molecules such as ATP, ADP, AMP, phosphate and other analogues of PPi^[66]. However, poor water-solubility of both probes restricted the further applications in intracellular detection.

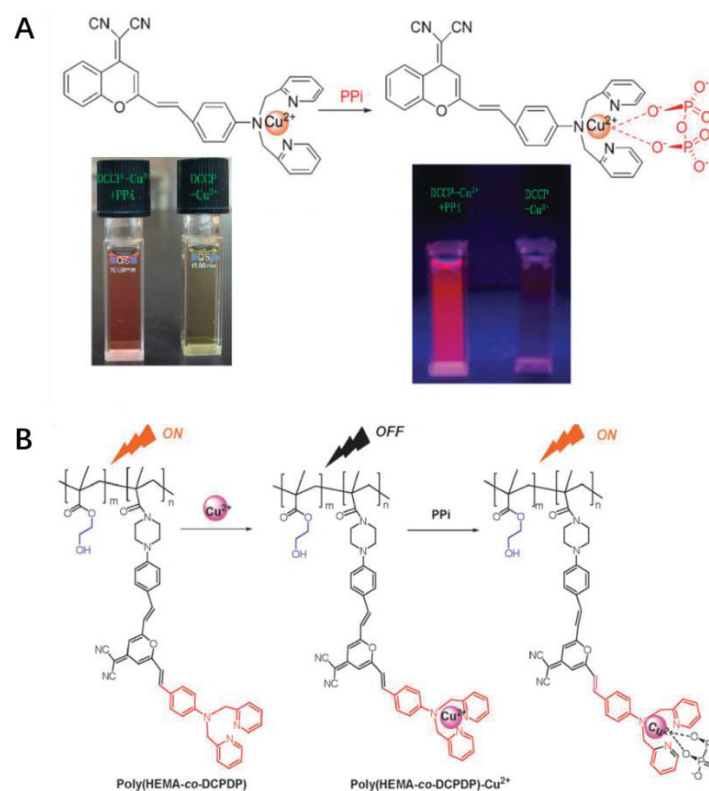


Figure 11: (A) DCM probe^[65] and (B) relative polymer for detecting Cu^{2+} and PPI^[66].

DCM and its derivatives are extensively developed red brighter emission by extending π - π conjugated systems or decorating aromatic rings. Hydrogen peroxide (H_2O_2) is an important reactive oxygen species (ROS) in physiological and pathological processes such as cancer, neurodegenerative diseases, Alzheimer's diseases, and cardiovascular disorders^[67-69]. A two-photon excitation (860 nm) NIR probe for monitoring H_2O_2 based on DCM fluorophore exhibited obvious fluorescence variation (13-fold enhancement), excellent sensitivity and selectivity for responding H_2O_2 in short time. The perfect photostability of the NIR probe could allow to monitor the endogenous and exogenous H_2O_2 in cancer cells^[70]. Through decorating the phenol on a similar fluorophore, a colorimetric molecular probe for intracellular glutathione detection was designed (Fig. 12C and 12D). 2,4-Dinitrobenzenesulfonyl group, as electron-poor substituent could quench the fluorescence. The resulting DCM-sulfonate have high activity to react with GSH, DTT, Cys, Hcys accompanied by fluorescence recovery. The probe has good photostability for H_2O_2 detection in HeLa cells^[71].

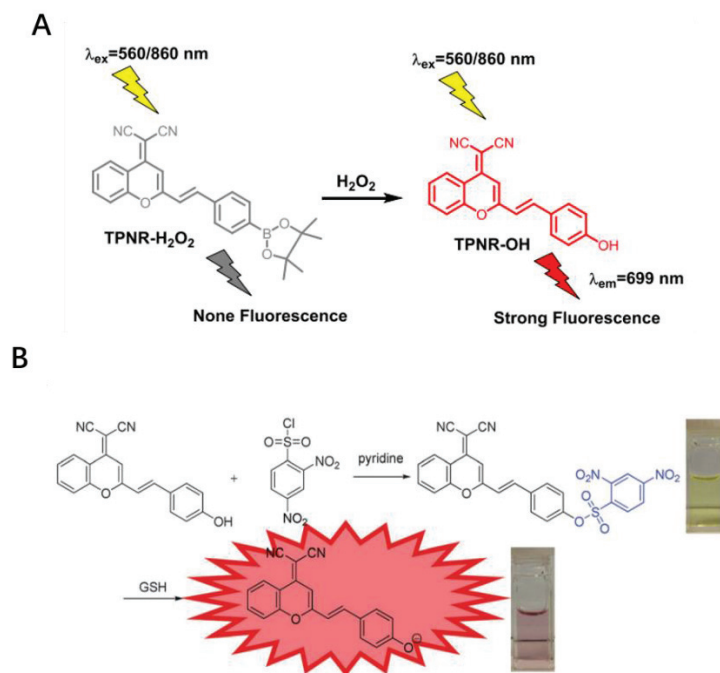


Figure 12: (C)^[70] and (D)^[71] is two DCM-derivatives for monitoring intracellular biomarkers.

The photostability, near-infrared wavelength emission and high quantum yield attracted chemists to develop DCM to other imaging areas. Tracking and delivering activated drugs *in vivo* or *in situ* is critical but remains mainly challenging. The quenched fluorescence of near infrared amino-DCM dye and decorated camptothecin (CPT) was achieved by disulfide bond (Fig. 13)^[72]. The two released thiol groups after cleavage of disulfide bond by excess intracellular GSH, could clean the amide bond on DCM to recover the red emission and release the CPT in cancer cell^[71, 73]. The novel complex exhibited preferable sensitivity and selectivity for biological thiols, wider responding pH range, excellent water-solubility, short reactive time. Meanwhile, the particular recognition between carbohydrates and lectins was applied to design probes for HepG2 cell imaging and liver cancer diagnosis via ASGPr receptors on cell surface. Several functional 2D materials (2D graphene oxide, MoS₂) conjugated with monosaccharide decorated DCM interacted with lectin (peanut agglutinin) and then pull the water-soluble probe out of 2D materials to generate a fluorescence signal enhancement^[74-76]. These functional fluorescent materials self-assembled with galactose-based DCM dyes, displayed selective recognition of HepG2 cells.

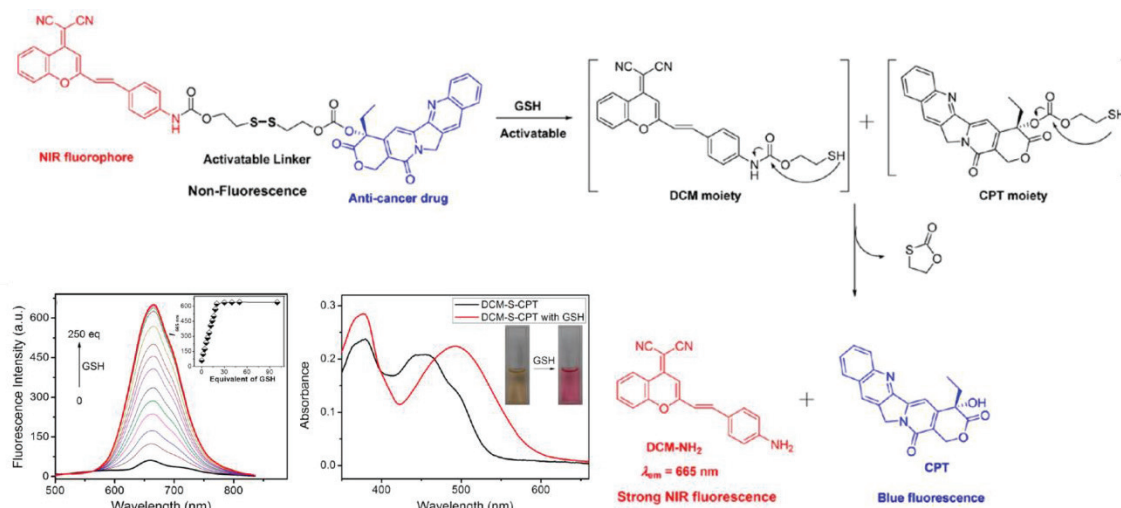


Figure 13: NIR amino-DCM probes traced drug releasing through intracellular biological thiols^[72].

However, typical DCM core with pyran or benzopyran ring are too hydrophobic restricted its further application. Improved DCM dyes (Fig. 14B-D) through replacing pyran or benzopyran by pyridine or quinoline^[77]. The nitrogen atom increased the electronic pull-push system resulting to the red-shift of its absorption and emission. Some hydrophilic groups (Fig. 14E) such as sulfonate group (SO_3^{2-}) or oligoethyleneglycol (TEG) linker was substituted on the nitrogen of fluorophore to improve its water solubility and biological compatibility^[78]. Another classic method was N-ethyl substitution to endow an excellent AIE property, which overcame ACQ effect resulting to quench or decrease fluorescence intensity in aqueous solution (more details will be introduced in the next section).

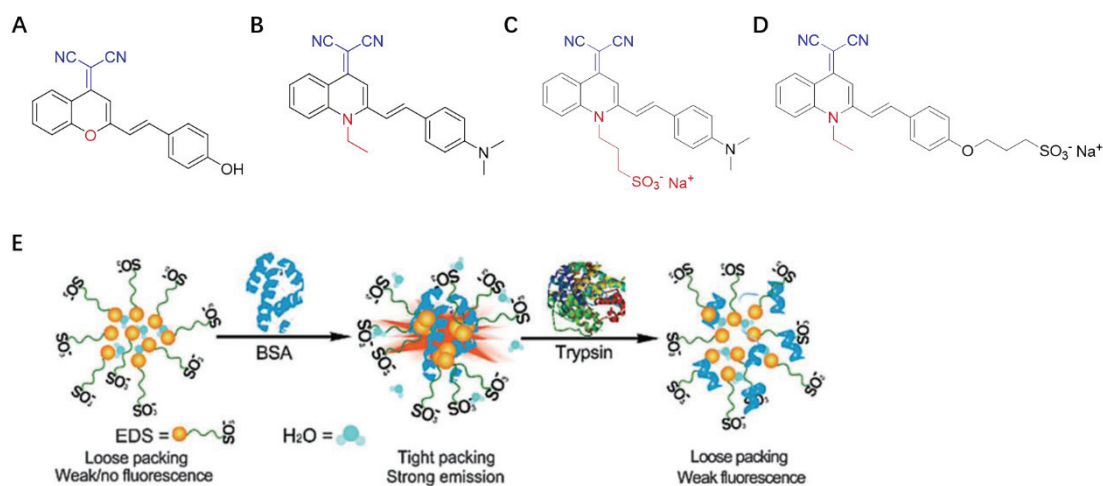


Figure 14: (A) Typical DCM dye, (B-D) series of novel N-substituted DCM dyes^[77], and (E) the application process of BSA detection in aqueous solution^[77].

I.1.3 Novel design principle -- Aggregated-induced emission (AIE)

Organic fluorescent probes have mainly hydrophobic structures with poor water-solubility. But biological applications or intracellular assays are in aqueous environment therefore excellent water-solubility becomes a decisive parameter for evaluating applicability of organic probes. However,

aggregated-caused fluorescence quenching (ACQ) is another limiting process restricting application of many NIR fluorophores in cell imaging and disease diagnosis.

I.1.3.1 Aggregation-induced emission (AIE effect)

ACQ effect is concentrated quenched or aggregation-caused quenched (Fig. 15). Light emissions from familiar fluorophores usually quenched in aggregate state (such as in poor solvent) or at high concentration. This ACQ effect highly limits the fluorescent sensors application in biological imaging and acquired diluted solution of probes for bioanalysis, which reduced the sensitivity and decreased the accuracy of tracing intracellular biomolecule. Aromatic molecules can accumulate on the surface of some biomolecules or in hydrophobic micro-environments thus increasing the concentration of probes and quench the fluorescence, partially or completely^[79, 80]. The aromatic rings on fluorophores usually display intensive intermolecular π - π stacking interactions in high concentration or in aggregated states.

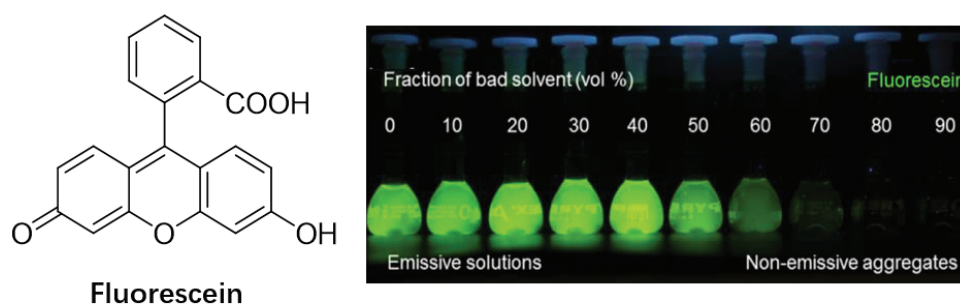


Figure 15: ACQ effect quenched fluorescence with water ratio increase^[81].

Aggregation-induced emission is also called as AIE effect. The studies of AIE fluorophores developed rapidly since Prof. Benzhong Tang and co-workers put forward the concept in 2001, designed and synthesized the first typical AIE probes^[82]. AIE probes are fluorogenic molecules without light emission when dissolved in compatible organic solvents but reaching intensive emission after intermolecular aggregation (Fig. 16) in solvent such as water or aqueous buffers. For example, the luminescence of perylene was quenched but the fluorescence of hexaphenylsilole (HPS) was enhanced by increasing ratio of water fraction in THF solution.

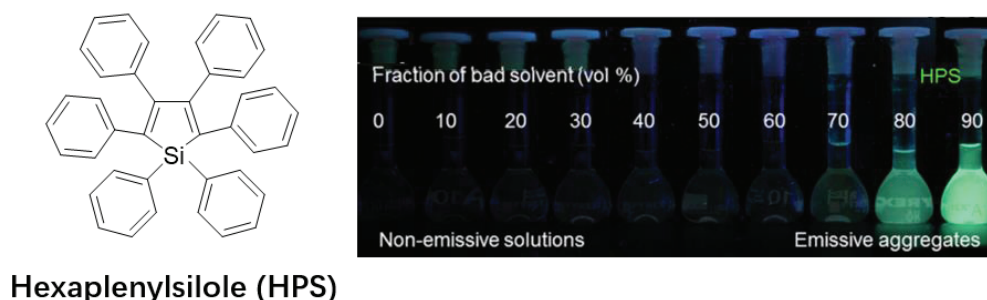


Figure 16: AIE effect enhanced fluorescence with water ratio increase^[81].

AIE phenomenon is normally derived from intramolecular rotating units such as benzene rings. Comprehension of the potential mechanism for AIE phenomenon is crucial and necessary to search for fundamental photophysical knowledge on account of its guidance for the design of novel

fluorophores, exploring the biological application and promote technological innovations. Many researchers speculated that decisive factors influencing properties of AIEgens were conformational planarization, E/Z isomerization, twist intermolecular charge transfer or structural restriction, and J-aggregation formation^[83]. Benzhong Tang and co-workers recently elucidated the influence factors of AIE is RIR, RIV and RIM, proved by experimental and theoretical results^[84].

RIR is restriction of intramolecular rotation, the most important parameter of influencing the fluorescence intensity (Fig. 17A). The rotor-containing fluorophores keep low-frequency motions in dilute solvent, leading to fast nonradiative decline of the excited states that quenched the fluorescence. However, the restricted rotation of benzene rings in aggregated states blocked the energy release through radiationless pathway, meanwhile the radiative channel is recovered followed by fluorescence signal increase^[85]. Besides, compared to traditional organic fluorophores with large π - π stacking plans, the highly twisted structure of AIEgens impedes intermolecular π - π stacking by keeping certain distance to protect the “turn-on” fluorescent states^[85]. The environmental temperature and pressure sometimes can affect the fluorescence intensity of AIEgen due to interfering intramolecular rotation and changing solvent density^[86]. Lifetime is an essential parameter for evaluating the properties of AIE fluorophores when the molecule was aggregated in poor solvent to extend lifetime from picosecond to nanosecond^[87]. Moreover, other effects such as electronic conjugation as well impose some influence for RIR process. The aromatic part with polycyclic substituents, compared with phenyl, enhanced the quantum yield in good solvent, but decay the AIE ability due to the large molecular volume when increased the water ratio in THF solution^[88, 89]. Reported AIE mechanisms are typically through AIE properties of hexaphenylsilole (HPS), but applications have been done by others AIE cores such as tetraphenylethylene (TPE) derivatives verifying the RIR principles^[90, 91].

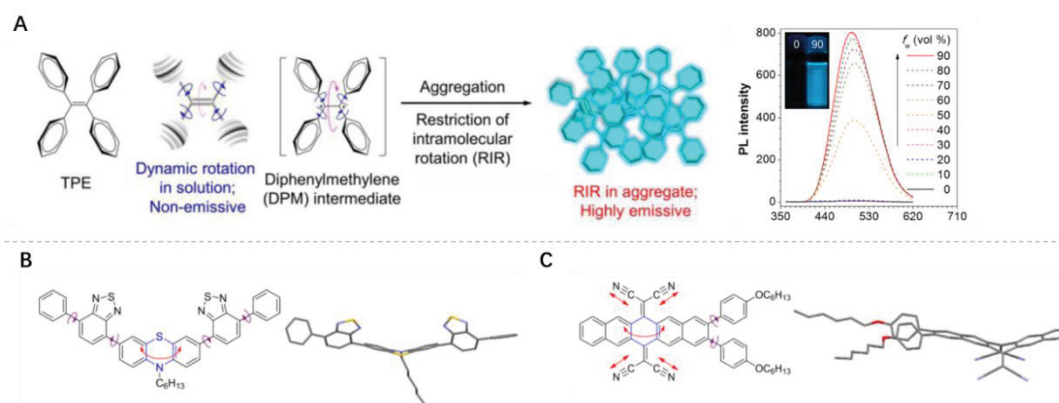


Figure 17: (A) RIR effect of TPE generates AIE properties. (B) and (C) are two AIEgens affected by RIM effect (RIR and RIV)^[84].

Restriction of intramolecular vibrations (RIV) is another pathway to generate AIE phenomenon. Different from RIR, RIV cores usually control the molecular vibrations to affect fluorescent signal^[92, 93]. Restriction of Intramolecular Motions (RIM) mixes intramolecular rotation and vibration together so that it exhibits characteristics of both mechanisms (Fig. 17B and 17C)^[94].

I.1.3.2 Popular AIE fluorophores and their imaging application

Even though the traditional fluorophores have excellent optical properties and applications,

molecules can undergo compact packing and thus strong π - π stacking interactions in aggregated states, further leading to the undesirable ACQ effect. Therefore, researchers developed various strategies to optimize present organic dyes to maintain their properties of the conventional luminescence and granted the benefits of AIE characteristics. The improvements of ACQgens promoted development of novel fluorophores and diversified the known AIEgens. The following discussion was categorized into three main groups: 1. conjugating AIE fluorescent structures on ACQgens; 2. replacing moieties of AIEgens with specific ACQ units; 3. designing new AIE structures from ACQ archetype based on the RIM principle. We will focus on the first strategy.

Combining AIE archetype into traditional ACQgens, is the most direct and popular method to improve intrinsic properties and reserve the excellent advantages of ACQ dyes. With AIEgens electronically conjugated to ACQ units, the resulting fluorescence probes can decay ACQ interference and provide AIE effect while keeping peculiarities of the building blocks.

Tetraphenylethylene (TPE), 2,3,3-triphenylacrylonitrile (TPAN), and triphenyl ethylene (TPEH) are three classic AIE archetypes decorated on ACQcores such as anthracene, pyrene, perylene diimide, and BODIPY, because of their simple synthetic method and outstanding AIE properties (Fig. 18). Experiments showed that TPE derivatives decorated on the perylene diimide dramatically increased the AIE effect on fluorophore, improve emissive wavelength and quantum yield owing to the electron-rich TPE structures.

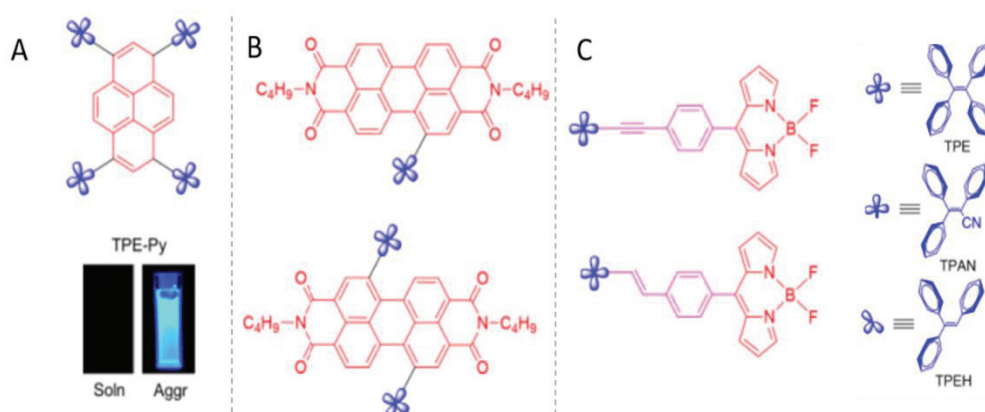


Figure 18: (A) is TPE-decorated pyrene and AIE effect in THF and water. (B) is different number of TPE decorated perylene diimide, and (C) is two TPE-BODIPY^[84].

Tetraphenylethylene (TPE) is a typical AIE fluorescent scaffold applied in bioanalysis and cell imaging. TPE derivatives normally release energy through nonradiative states through intramolecular phenyl rotation in good solvent after absorbing light but emit strong luminance (470 nm) when dissolved in aqueous environment due to phenyl rotation blocked. The crystal structure indicated a twist angle ($\sim 50^\circ$) between phenyl rings and the central vinyl bond. The immediate π - π stacking conformation promotes nonradiative recombination and red-shift emission. Intermolecular multiple C-H... π interactions between aromatic hydrogens and the vinyl bond reinforce the stability of the whole molecule in solid or aggregated state (Fig. 19A)^[95, 96]. The four phenyl rings rotation around the olefin centre can be triggered in the diradical diphenylmethane groups in excited state.

As the H-NMR spectrum showed (Fig. 19B), broken vinyl bond in excited state transform the ratio of the *Z* / *E* isomer from 93:7 to 50:50^[97]. The friction caused by intramolecular twisting and rotational motion in solvent media induce an energy relaxing pathway changing from photonic to thermal. In aggregated state, congenerous RIR effects and highly twisted structures impeding the intermolecular π - π stacking energy transfer, leading to recovering the fluorescence emission^[97-99].

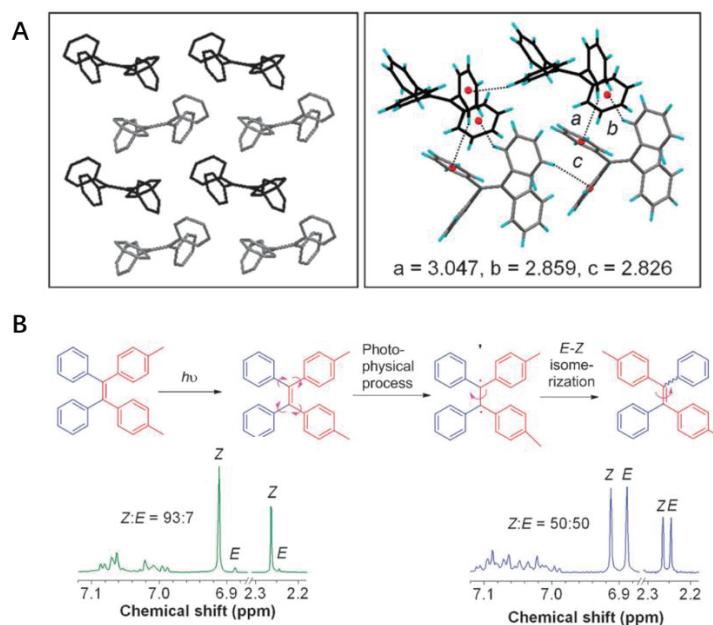


Figure 19: (A) Molecular packing pattern of TPE and intermolecular C-H... π interaction in the crystalline state^[95]. (B) *Z* / *E* isomerization of TPE in excited states^[97].

For the AIE properties, simple structure and intense fluorescence emission, researchers explored a number of synthetic and modified routes to functionalized TPE derivatives. McMurry coupling (Fig. 20A) is a typical method to afford symmetric TPEs. The ketones are condensed to the corresponding alkene catalysed by low valent titanium reduced from TiCl_4 / Zn system^[100] or TiCl_3 / Li system^[100, 101]. McMurry reaction is particularly prominent in homocoupling. Nevertheless, non-symmetric TPE were generally obtained in low yield and complex mixtures through McMurry reaction due to its nonselective coupling. Knoevenagel condensation is another efficient choice to construct double bonds that was frequently applied for non-symmetric TPEs (Fig. 20B)^[102]. The yield of Knoevenagel condensation depends on the pK_a of the base, usually requires electron-rich ketones, and electron-poor diphenylmethanes.

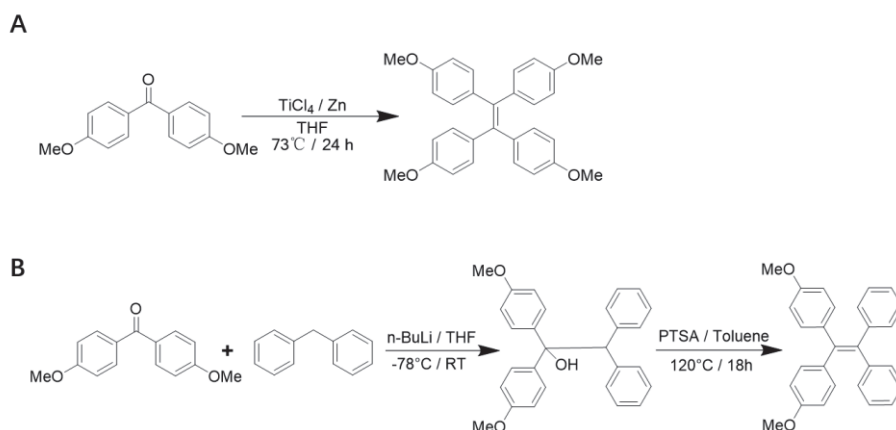


Figure 20: The schemes of (A) McMurry reaction and (B) Knoevenagel condensation for TPE synthesis.

Besides improving ACQgens structural to change their inherent optical properties, TPE has participated in probes design chelating heavy-metal ions, thiols, explosive gases, carbohydrates, and combined with proteins or DNAs. Song Song, The AIE effect of TPE in water (Fig. 21A) was studied with three types of TPE analogues with different glycol units to increase the solubility in water and evaluation of their AIE properties in CH_2Cl_2 and hexane. The fluorescence intensity of TPE derivatives was quenched after adding γ -cyclodextrin, because the aggregated TPE was separated as cyclodextrin-TPE mono-metric species. Addition of cholate in the mixture could recover the TPE aggregated fluorescence intensity due to competition with γ -cyclodextrin^[103]. BSA-TPE derivatives with AIE properties were designed as fluorescent probes for label-free detection of protease and α 1-antitrypsin, which could provide the “off-on-off” fluorescence signals in water (Fig. 21B)^[84].

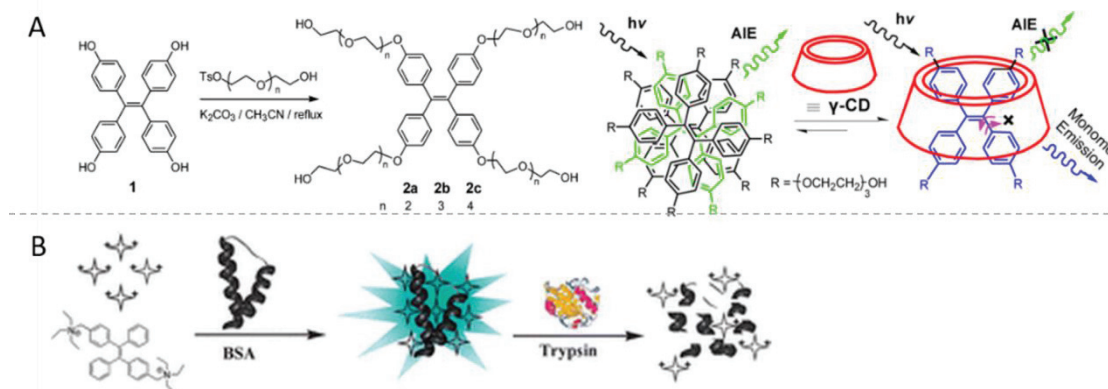


Figure 21: (A) AIE altered fluorescence of TPE derivatives^[103] and (B) relative application of TPE in bioanalysis^[84].

TPE derivatives are usually designed as energy providers or indicators due to their high photostability. A TPE-based probe for imaging mitochondria membrane through triphenylphosphonium (TPP) tracking was reported (Fig. 22A). Introduction of a phosphonium reactive electron-poor group on the TPE core enhanced the electronic “pull-push” effect and red-shifted the emission wavelength (525-535 nm). Outstanding AIE properties in aqueous media were observed for biomolecules, showing clear imaging and sensitive mitochondria membrane targeting but no fluorescence after incubating with the phosphonium reactive carbonyl cyanide *m*-chlorophenylhydrazine (CCCP) in HeLa cells^[91]. Ratiometric NIR fluorescent probes for detecting

intracellular pH variation were obtained with TPE as the energy donor because of its AIE properties, conjugated with hemicyanine-rhodamine derivatives that have sensitive “turn-on” response acidic media (Fig. 22B). The probe emitted blue fluorescence (TPE light) in neutral solution excited at 420 nm without through-bond energy transfer (TBET). When π - π stacking recovered in rhodamine moiety in acidic pH, the intense red emission (740 nm) appeared followed by a blue fluorescence decay. The probe exhibited good ratiometric fluorescent response under pH range from 7.4 to 2.5 without any disturbance by common ions and biomolecules. Excellent photostability and nontoxicity facilitated monitoring pH changes with different colours in HeLa cells ^[104].

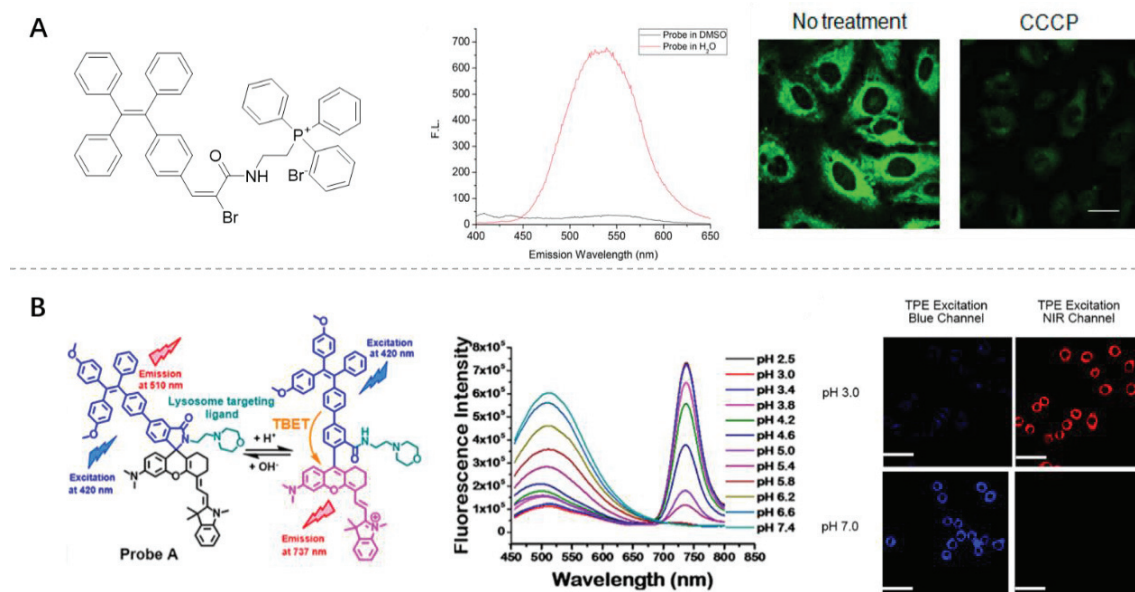


Figure 22: (A) TPE as indicator targeted mitochondria membrane^[91]. (B) Ratiometric near-infrared TPE hemicyanine-rhodamine probes for intracellular acidic pH detection ^[104].

The advantages of DCM dyes have been introduced above. Even though TPE dyes exhibit outstanding optical properties and wide application, the shorter emissive wavelength still restricted its biological imaging and further experiments in tissue or *in vivo* due to interference of the blue biological fluorescence background. From simple structures of DCM and TPE, combining the two units together to extend the emissive wavelength has been reported^[105]. The probes incorporated TPE, DCM and triphenylamine (TPA) exhibited fluorescence quenched inceptively by twisted intramolecular energy transfer (TICT) but enhanced in aqueous solution due to AIE effect. The probe can self-assemble with bovine serum albumin (BSA), nanoparticles, to imaging *in vitro* and *in vivo*. Nevertheless, the complex structure, intricate synthetic route and large organic aromatic system restricted excellent water-solubility, biocompatibility, and further functionalization. Hence, quinoline-malononitrile based fluorophores displayed obvious AIE effect and simple synthesis ^[78]. Compared with long-chain group on the nitrogen atom, short alkyl chain as ethyl have less resistance of rotation to perform good AIE effect. The reverse effect influences fluorescent properties even if the two structure are similar (Fig. 23A). The specific *N*-substituted DCM structures still possessing NIR emission and high affinity for BSA, was designed as indicator to cell imaging and trypsin tracking in cells. Besides, dyes were functionalized with various electron-poor groups to construct “turn-on” probe for detecting small biomolecules. The AIE DCM-based fluorescent “turn-on”

probes for detecting galactosidase that is an essential biomarker for primary ovarian cancers and cell senescence have been developed^[106, 107]. The electron-poor galactose conjugated on the phenolic hydroxyl group quenched the fluorescence but slightly improved its water-solubility. Galactosidase hydrolysed the glycosidic bond recovering the phenol and fluorescence. Meanwhile, the change in solubility did not alter the fluorescence intensity due to AIE effect. The probe displayed good enzyme selectivity, preferable linear relationship with enzyme increasing, distinct fluorescence signal in intracellular imaging (Fig. 23B)^[108].

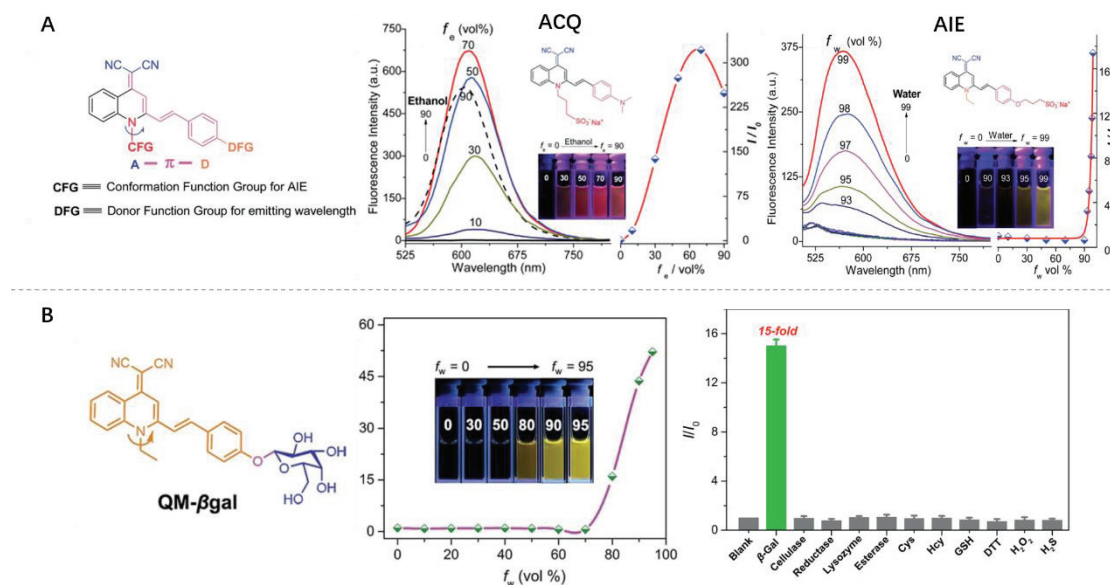


Figure 23: (A) Nanoparticles composed of AIE-DCM and BSA for cell imaging^[78]. (B) AIE fluorescent “turn-on” probe for intracellular galactosidase detection^[108].

I.2 Glycoconjugate as fluorescent probes

Even though fluorescent probes have been applied in biological imaging, detection of biomolecules, tracking drug release and diagnosis with proven results, the low affinity or specificity for cells or tissues, high toxicity, non-recognition and poor solubility were still challenging for further biological or medical applications. Carbohydrate play an indispensable role in living cells not only for energy source, but also transfer information between cells. Here, we will introduce carbohydrates and some typical designs of glycoclusters and carbohydrate-decorated systems.

I.2.1 Carbohydrates in biology

Carbohydrates are one of the most necessary elements in living organisms, and play important roles in energy supply and signal transmission widely present in cell and its surface. Numerous carbohydrates present in living organisms, are normally conjugated with other fundamental biomolecules to form different glycolipids or glycoproteins. These glycoconjugates existing in most tissue, and participate in basic biological processes such as cell adhesion, cell recognition, cell differentiation, development of the neuronal works, immune response, signal transmission, intracellular trafficking of proteins, metastasis and bacterial infections^[109]. As the relationship of

carbohydrates and biological processes are elucidated, scientists are interested in biology, chemistry, biochemistry and pharmacy to define the biological roles and functions to examine its potential therapeutic application^[110-112].

As the crucial molecules for signal transmission, glycoproteins are widely presented in mammalian cells and tissues, especially on the surface of the cytomembrane. The function of oligosaccharide chains in glycoprotein include: (a) Participating in fold and association of glycoproteins to form and maintain the correct structure. (b) Influencing and regulating the secretion and stability of glycoproteins. (c) Participating in the recognition between biomolecules (such as antigen-antibody, enzyme-substrate and hormone-acceptor) and different cells^[111, 112].

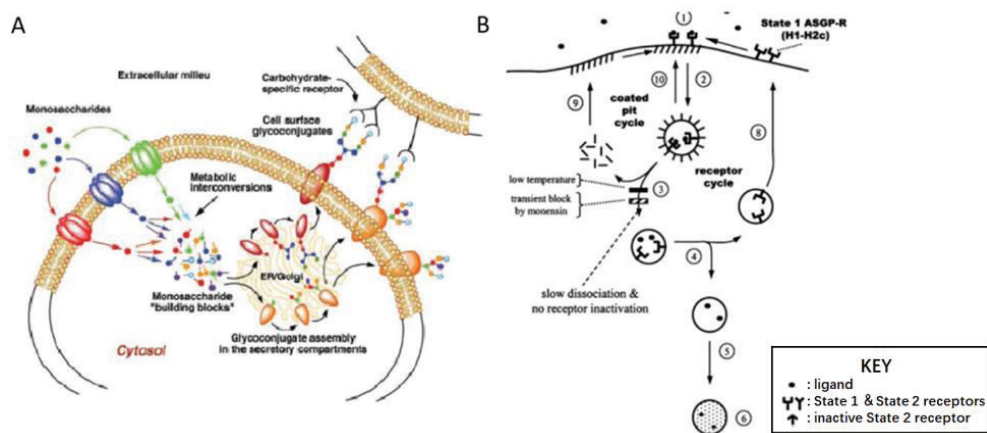


Figure 24: (A) Importance of glycoconjugates in biological processes^[109] and (B) the main pathway model for endocytosis mediated by ASGPr^[113].

Asialoglycoprotein Receptor (ASGPr) is secreted from parenchymal liver cells, and have two characteristics: hepatocyte-specific, and high affinity of galactose and *N*-acetylgalactosamine^[114]. Oligosaccharide or glycoproteins with galactose residues are recognized by ASGPr in the cytomembrane. The conjugate binding to ASGPr is present on the surface of the cell then aggregated and internalized through clathrin-mediated endocytosis^[113, 115]. Hence, fluorescent probes decorated with monosaccharides were designed for bioanalysis and biological imaging.

1.2.2 Glycosylated fluorescent probes

Based on the specific ASGPr recognition, fluorescent probes decorated with monosaccharide or oligosaccharide were reported. These glycosylated fluorescent probes have excellent water-solubility to improve their application in biochemistry. The reported probes displayed similar properties to the original fluorophore as reporting-group, and their monosaccharide could be used electively with particular proteins or lectins for targeting special cancer cells.

Yanhui Tang, Guorong Chen and co-workers decorated fluorophores at C3, C4-position on a glucose by azide-alkyne “click” reaction^[116]. The fluorescent probe could coordinate Cu^{2+} to quench the luminescence and then released a fluorescence signal after addition of CN^- in aqueous solution. Min Hee Lee, Ji Hye Han, Jong Seung Kim and co-workers reported a reactive fluorescent probe responding with intracellular thiols, that was modified 4-aminonaphthalimide scaffold with triethyleneglycol galactose as targeting-group and disulfide bond as detecting group (Fig. 25A)^[117]. The glyco-probe performed different fluorescence colour from blue to green because the thiols broke the disulfide bond and then release the amino group. This probe can work in a wide pH range

(4-10) Tris-HCl buffer, accurately provide a ratio fluorescence signal, specifically target HepG2 cells to detect the endogenous thiols. In our previous work, we decorated galactose or glucose on fluorescent quenched 4-aminonaphthalimide by “click” conjugation^[118]. These two glyco-probes exhibited sensitive “turn-on” signal after chelating Zn^{2+} ion in aqueous buffer. Glycol-probes have lower limit of detection (LOD), fluorescence enhancement, wider pH working range, and lower cell toxicity when compared to similar structures. The probes could detect Zn^{2+} in environmental water accurately, respond to different concentration of intramolecular Zn^{2+} , recognize, target and image HepG2 cells (Fig. 25B).

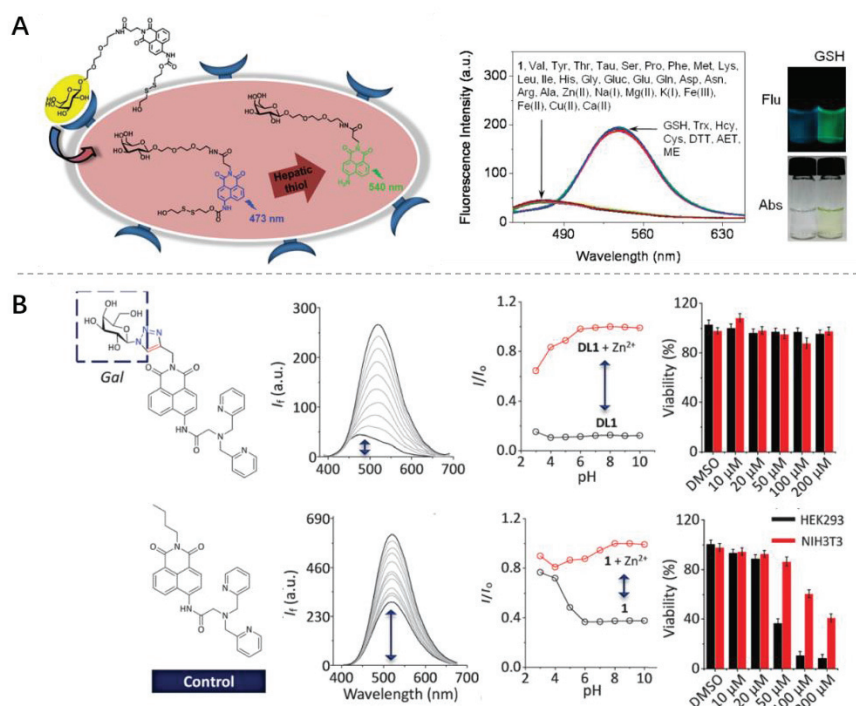


Figure 25: (A) Disulfide galactosyl naphthalimide detected intracellular thiols^[117] and (B) glycosylation enhanced traditional probes for Zn^{2+} detection^[118].

The galactosyl naphthalimide probe detecting the thiophenol have higher water-solubility than other probes. The LC-MS titration verified the mechanism of the probe reacting with thiophenol^[119]. Kaibin Li, Xiaopeng He and co-workers reported series galactosyl fluorescent probes and glucosylated derivatives as negative control^[120]. Therein the rhodamine glycoconjugated probes could measure the Hg^{2+} in buffer solution and water samples from Huangpu River (Shanghai), target HepG2 cell, detect the exogenous Hg^{2+} and decrease the cytotoxicity in biological assays. It's notable that they certified that the probe recognized HepG2 cell through ASGPr pathway based on receptor knocked-down experiments (Fig. 26A). The self-quenched pyrene-naphthalimide scaffold decorated with galactose and mannose respectively was synthesized, to interact to different lectins such as PNA and ConA^[121]. Because of the π - π conjugation between pyrene and naphthalimide, the specific lectins bonded to the glycosyl moiety disrupted the π - π conjugation to recover the FRET fluorescence. The molecular and biological experiments conformed the hypothesis and mechanism (Fig. 26B).

Glyco groups are not only water-soluble or targeting groups, but sometimes, they can act as an electron-poor group, controlling the fluorescence properties. The common pathway is to decorate

galactose on phenolic hydroxy which typically plays the role of electron provider in probe systems. The resulting probes usually monitor galactosidase^[23, 122-124]. However, typical fluorophores generally possess only one modifiable position for controlling their fluorescent switch. Access to two decorating positions will increase difficulty of compound synthesis but change intrinsic optical properties. Hence, researchers have to develop others novel pathways to realize their purpose.

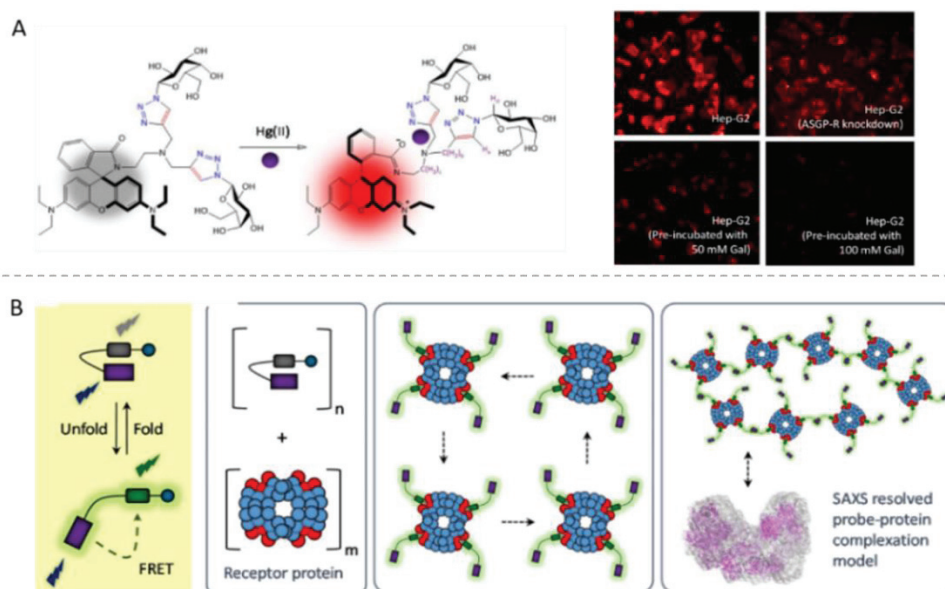


Figure 26: (A) Galactosyl rhodamine detected exogenous Hg^{2+} ^[120] and (B) the self-quenched pyrene-naphthalimide recognizing specific lectins^[121].

I.3 Glycoclusters and self-assembled glyco-probes

Biomolecular recognition between carbohydrates and proteins are essential for the initiation of critical processes in living organic systems such as fertilization, intercellular signal transmission, host-pathogen interactions, immune response and cancer metastasis^[125]. However, monosaccharide or individual carbohydrate residues tend to combine weakly with their complementary proteins. Since multivalent recognition leads to stronger affinity enhancements than predicted from constitutive interaction which is called “glycoside cluster effect”, glycoclusters have found a wide range of biological applications^[126-128].

I.3.1 Glycoclusters

The “glycoside cluster effect” is the combination of the multiple ligand copies on a central core leading to improved binding with biological targets^[129-134]. Hence, to design multivalent glycoclusters, a wide series of “artificial glycoforms” have been synthesized and studies in complex multivalent binding interactions. Aromatic cores are excellent and polyvalent platforms for the design of glycoclusters^[135]. Since J. Yariv, M. M. Rapport and Liselotte Graf firstly reported the “aromatic core” containing clustered glycosides in 1962^[136], the development of multivalent glycoclusters have been driven on the expressways. Despites the hydrophobic aromatic core, the multihydroxyl carbohydrates or glycans efficiently improved water-solubility to promote

applications in suitable biophysical measurements and biological investigations. Well-defined glycoclusters and glycodendrimers composed of single aromatic or heteroaromatic cores have been reported, and gradually applied in various areas such as anti-adhesins, drug delivery systems, imaging agents, biosensors, and vaccines, combined with advanced nanomedicine^[128]. Here, some typical models of glycoclusters were summarized containing aromatic scaffolds as multi-substituted benzenes, polyaromatic cores, and fused-polycyclic cores.

The multiple-substituted benzenes were classified as disubstituted, trisubstituted, tetra- and hexa-substituted benzene cores. The construction of divalent glycoclusters depends on with multivalent lectins that would form homogeneous and cross-linked lattices with multivalent glycoclusters (Fig. 27)^[137, 138]. The glycoside moieties are connected on the aromatic cores with *N*-, *O*-, *S*-, or *C*-linkers through direct glycosylation or “click” reaction catalysed with Cu⁺ ion or organometallic strategies^[139]. Even though these glycoclusters have excellent water-solubility and biological activates, the small π -system, non-fluorescence and limited assembly strategies restricted further applications and development.

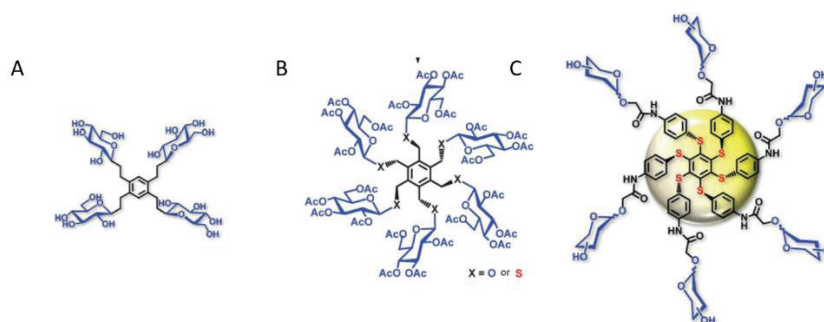


Figure 27: Example of (A) tetravalent and (B) hexavalent glycoclusters with benzene core and (C) hexaphenylbenzene core^[140].

Based on the glycoclusters with individual benzene core, some glycoconjugates using polyaromatic cores were presented with more substituents, simple synthesis, wider π - π stacking systems and excellent optical properties. Series of prevalent polyaromatic scaffold have been designed including hexaphenylbenzene, cyclotriphosphazene, tetraphenylmethane, azobenzene, tetraphenylethylene, cyclotrimeratrylene and perylene diimide. Here, we will discuss two aromatic cores, tetraphenylethylene (TPE) and perylene diimide (PDI) based glycoclusters^[140].

TPE have good AIE properties and are widely exploited in the development of AIE- based bio/chemosensors for detection of ions, DNA, ATP, nuclease and acetylcholinesterase assay. Qi Chen, Ning Bian, Baohang Han and co-workers reported the first TPE glycoclusters application for alkaline phosphatase detection^[141]. The electropositive glycoclusters self-assembled with the anionic monododecylphosphate to provide an aggregating fluorescence. The increasing enzyme hydrolysing the phosphate disrupted the aggregation to disperse the glycoclusters with fluorescence “switch-off” (Fig. 28A). The ionic glucosamine conjugated on TPE decreased the detecting sensitivity and selectivity due to nonspecific electrostatic interactions. Hence, decorating neutral targeting groups on TPE scaffolds was investigated for the fluorescence “turn-on” detection of lectins. Since first TPE-based glycoclusters recognized *Ricinus Communis* and

Sambucus sieboldiana agglutinins, TPE was widely applied in lectin or protein detection through AIE effect^[142]. A specific TPE sensor was exploited to detect influenza virus such as cholera toxin through specific aggregation (Fig 28B). The reported compound showed high lectin selectivity for cholera toxin without signal interference from BSA^[143].

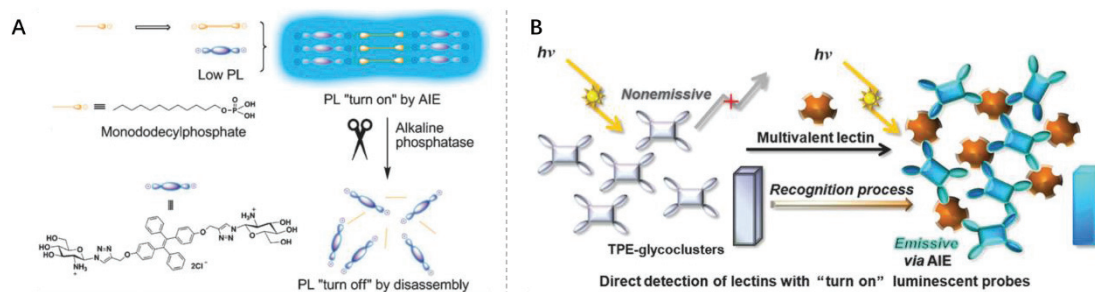


Figure 28: (A) First TPE-based glycoclusters for alkaline phosphatase detection^[141]. (B) Intermolecular aggregation for influenza viruses recognition^[143].

Complementary studies have shown glucosyl TPE sensors to monitor glucosidase^[144]. The glucoside was hydrolyzed by specific enzyme enhancing fluorescence intensity in aqueous buffer based on the solubility change and molecular aggregated (Fig. 29A). In parallel, classic aggregation phenomena was applied to recognize some lectins (ConA) by α -thiomannosylated TPE. Carbohydrates interacted with ConA, and then a fluorescent signal was emitted due to restricted rotation of benzenes (Fig. 29B). However, addition of thyroglobulin (Tg), whose structure is similar to ConA, could interrupt the recognition between the epitope and lectins^[145]. Overall, similar tendencies were observed the efficiency of recognition depended on the protein and the surface characteristics such as size, valency, shape, and hydrophobicity.

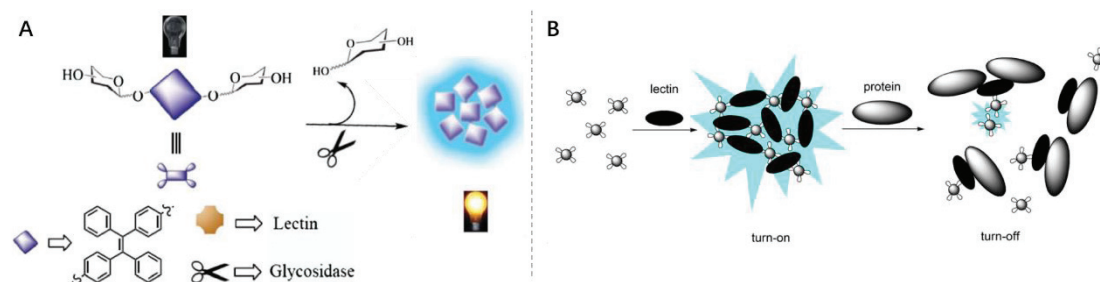


Figure 29: (A) Solubility changed after enzyme cutting glucoside^[144] and (B) fluorescence switched TPE aggregation through recognition^[145].

Perylenediimide (PDI) scaffold is another excellent aromatic centre with four or six modifiable positions to decorate two different functional groups^[146]. The large conjugated π -system and electronic “pull-push” systems from bay region to imide region, generates red fluorescence emission (about 600 nm). Kerang Wang, Hongwei An, Xiaoliu Li and co-workers designed and synthesized water-soluble PDI-glycocluster decorated with 12 mannoses for ConA detection^[147]. Due to multiple mannoses, compound exhibited high affinity for ConA with two order of magnitude higher than the corresponding monosaccharide. The intermolecular π - π stacking interactions quenched fluorescence in basic states. With increasing concentration of ConA, the carbohydrate-lectin recognition disrupted the stacking and recovered red emission. The reported glycoclusters displayed

good selectivity for ConA but no response for BSA and peanut agglutinin (PNA). In cell imaging, the compound can recognize and dye macrophage-like cells. Although numerous glycoclusters presented preferable affinity for lectin and protein recognition and detection, the weak fluorescence restricted its application in cell imaging so that it was utilized as carrier to target and transport other molecules.

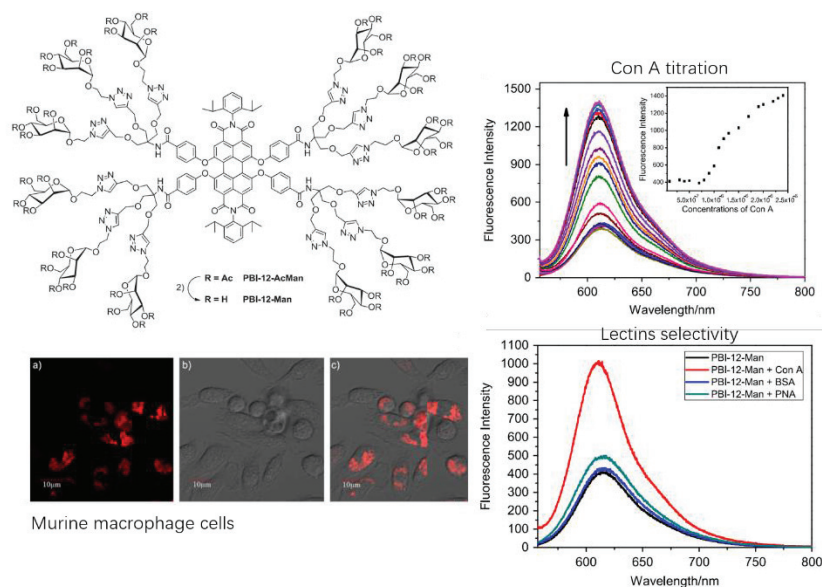


Figure 30: PDI-glycoclusters conjugating with mannoses for Con A response^[147].

1.3.2 Self-assembled nanoparticles and glyco-probes

Nanoparticles (NPs) are in the advanced areas of rapidly developing nanotechnology and drew numerous attentions on the design and applications of these novel nanomaterials. Traditional NPs commonly contains two- or three-dimension carbon materials such as graphene, carbon dots, carbon nanotubes, quantum dots, rare earth doped NPs, gold NPs, and silica NPs. Because of the particular shape- or size-dependent structure and optical properties, these nanomaterials play an important role in several scientific fields^[148]. Due to obvious targeting and water-soluble characteristics of glycoclusters and glycoconjugates, nowadays NPs are employed as specific carrier combined with glycoclusters to self-assemble into biological nanomaterials, which widely exhibited excellent functions in biology and medicine including proteomic and genomic studies, disease diagnostics, targeting drug delivery, pharmaceutical screening, biological therapeutics and medical imaging (including *in vivo* imaging, cancerous sensors, and selective recognizing tumours) [8, 149, 150]. Here, we introduced glycoconjugate NPs and their prevalent designs and applications.

Gold nanoparticles (GNPs) normally have a relative narrow size from 2-100 nm range but typically in 2-20nm range. The reported GNPs with carbohydrates displayed spherical geometry, and other morphologies of nanostructures such as nanorods and nanostars may also be observed^[151]. Quantum confinement, scattering and surface plasmon resonance are three main essential factors affecting the optical, electronic, fluorescent properties due to the difference of size, shape size, distribution in solution and the surface functionalization with GNPs [152-154]. Prevalent methods for the combination of carbohydrates with nanoparticles use neoglycoconjugates with thiol-terminated linkers (or disulfide), or ligand exchange of thiol-terminated carbohydrates on the performed GNPs (Fig. 31A)^[155]. Glycoconjugated GNPs exhibited excellent response based on colorimetric assays

through multivalent interactions with lectins combined with a change in optical properties by self-conjugation [156]. Detecting proteins by electrochemical sensing and mass spectrometry analysis also has been reported [157, 158]. The other field using glycosyl-GNPs is diagnosing some disease in aqueous environment. Vargas-Berenguel and co-workers designed specific systems to transport drugs through the recognition between lactose and peanut agglutinin (PNA) / galectin-3 (Gal-3) (Fig. 31B)[159].

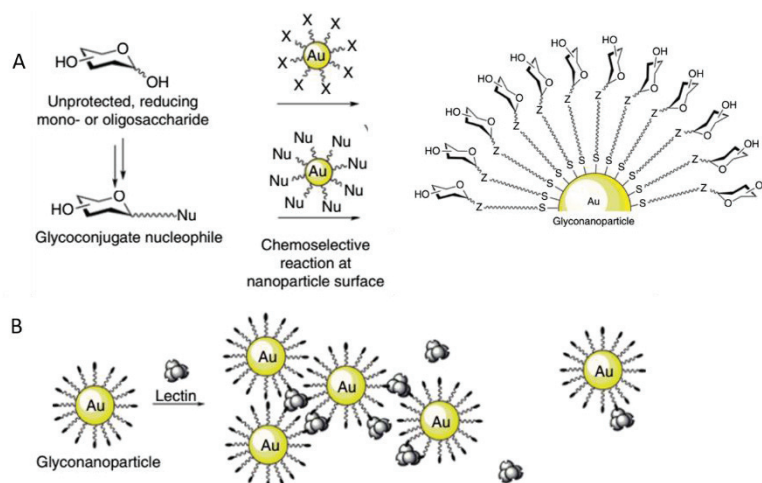


Figure 31: (A) The main pathways to construct glyconanoparticles^[155], and (B) the multivalent interactions of GNPs and lectins^[159]

Carbon nanomaterial is another classic candidate for conjugation with carbohydrates. Buckminsterfullerenes (0D), carbon nanotubes (CNTs, 1D) and graphene oxide (GO, 2D) are three common kind of materials with unique and extraordinary physical and electrical properties. Many researchers modified the surface of carbon materials constructing specific systems to apply in photovoltaics, drug delivery, materials chemistry, biological recognition and imaging diagnosis. Through the plethora of chemistry, decorating on the surface of carbon materials is a popular method to build up a covalent bond with carbohydrates typically through cycloaddition reactions [110]. Noncovalent functionalization usually requires some hydrophobic compound or molecules for adsorption on the surface of materials through π - π interactions. These conjugations quenched fluorescence and increased concentration on relatively in small area. Yang and co-workers first reported sensors constructed by stacking of specific human thrombin aptamer labelled with fluorophore and GO, which have efficient low limit of detection (2 nM) [160]. Xiaopeng He and his co-workers decorated monosaccharides on fluorescent scaffolds (such as pyrene, rhodamine, Dicyanomethylene-4*H*-pyran) and conjugated them with graphene to construct functional carbon nanomaterials to recognize different lectins and release electrical or fluorescent signals (Fig. 32A)^[161-163]. Carbon materials have excellent performance, however their toxicity restricted s applications *in vivo* experiments or clinical medicine. Due to their pure carbon structure, the materials cannot be removed through metabolism, and then aggregate in organs such as liver. Even though some glycoconjugated carbon materials could be hydrolyzed by lysosome, the exposed materials still existed after glycolysis and remained toxic^[164, 165].

Considering the cytotoxicity of nanomaterials in living systems, cyclodextrins (CDs) are specific macrocyclic oligosaccharides, built from 1,4-limited linked α -D-glucopyranose units. Common CDs

possess six, seven or eight glucopyranose units to form α -, β -, and γ - type of CDs with hydrophilic surface and hydrophobic core. Therefore CDs, have been widely applied in various multivalent systems to be employed in molecular recognition, catalysis, polymerization, drug delivery, and hydrolysis^[126]. Multivalent carbohydrate systems with terminal sugar ligands bind lectins through glycoside clustering. The hydrophobic CD cavity enable to hold hydrophobic organic molecules and assemble into “lectin- carbohydrate- ligand” guest complexes, which are employed in lectins recognition, drug delivery, metal complexes, rotaxanes and other systems^[166]. For example, the pyrene decorated β -CDs could quench the fluorescence of glycosyl rhodamine by π - π interactions to form a water-soluble, self-assembly system (Fig. 32B). The fluorescence signal was emitted with a colour change, after the lectins recognized the glycoside and disrupted the primary system^[167].

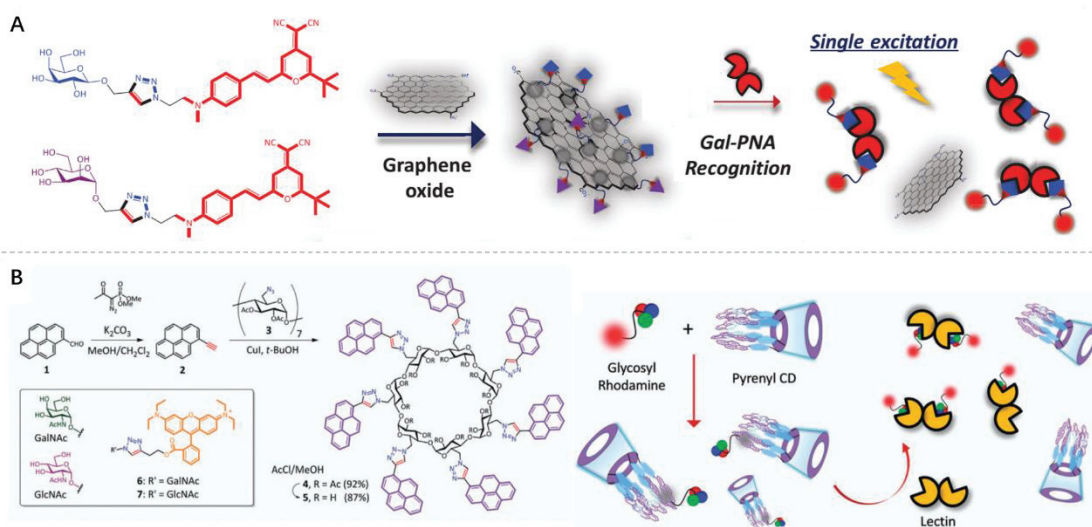


Figure 32: (A) Functional materials conjugated by glyco-DCM and GO for PNA detection^[162]. (B) Self-assembled rhodamine-CDs systems for lectin detection^[167]

We have designed and synthesized a self-assembly composed of near infrared DCM dye and PDI-based glycoclusters. Glycoclusters constructed amphiphilic glyco-dots with hydrophilic surface and hydrophobic core containing DCM probes with organic structure (Fig. 33A)^[168]. Extensive π - π stacking with the large PDI planar aromatic moiety, influenced electronic distribution of DCM dyes and quenched fluorescence. The experimental data of HRTEM, and DLS showed individual shape and size for glycoclusters that became larger after addition of DCM (Fig. 33B). The quenched fluorescence cannot be interfered by pH variation in aqueous buffer after conjugation. The fluorescence was recovered by DCM leaving the whole system when high affinity proteins for DCM were added in solution such as BSA, HSA and FBS, whereas no obvious signal change was observed for some lectins such as PNA, ConA and SBA (Fig. 33C). According to cell imaging data, the PDI-DCM glycol-dot have excellent cell selectivity through selective carbohydrate-protein recognition (Fig. 33D). Knocking down specific receptors from the cell surface decreased the fluorescence intensity demonstrated the specific recognition process.

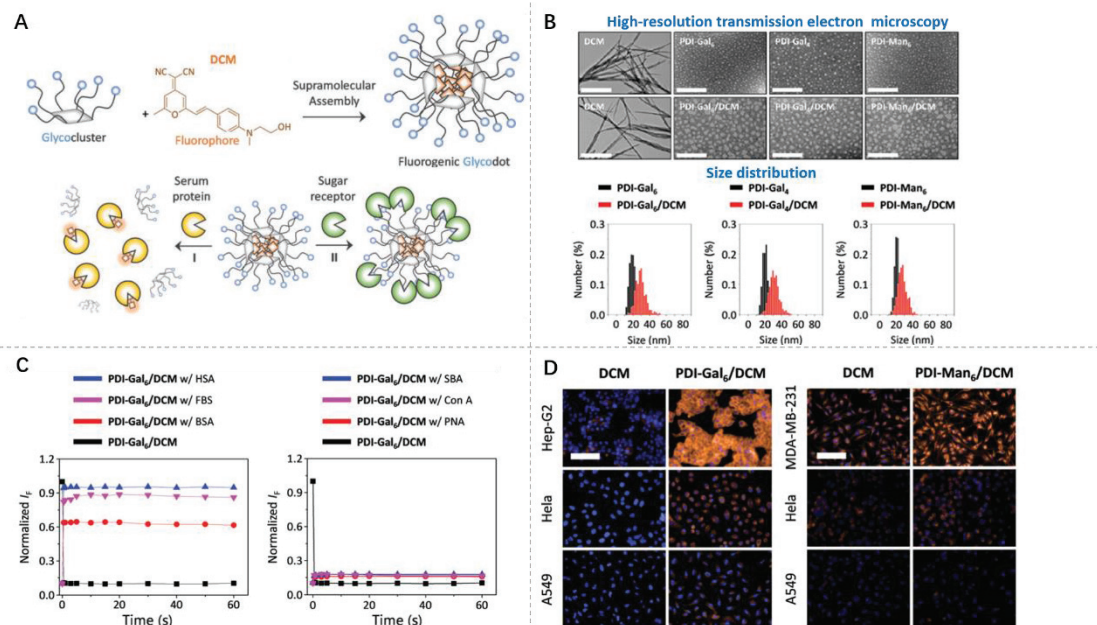


Figure 33: (A) The working diagram of glyco-dots. (B) HRTEM and DLS measuring size before and self-assembly with DCM. (C) and (D) respectively are lectin selectivity and cell recognition^[168].

1.5 Conclusion

In this chapter, we have introduced general basic information about organic fluorescent probes. Three principles and fluorescence mechanisms are essential for the design of fluorophores, the control of optical properties, the understanding of working mechanisms of probes for detections and improve biological applications. Förster resonance energy transfer (FRET effect) is a prevalent mechanism, because it can provide ratiometric fluorescence variation with increasing concentration of analysts. Based on the poor water-solubility and aggregated caused quenched (ACQ effect) decaying fluorescence intensity of typical fluorophores, the concept of aggregated induced emission (AIE effect) was put forward in 2011, which improved the weak emission of organic fluorophores through decorating AIE part. The three mechanisms including RIR, RIV and RIM plays decisive roles guiding novel AIEgens design and synthesis. Then several typical fluorophores were presented, DCM derivatives, as a standard ICT dye, with advantages such as preferable Stokes shift, near infrared emissive wavelength, simple structure, convenient synthetic route. s one of classic AIEgens, tetraphenylethylene (TPE) was applied to DNA imaging and protein detection because of its good photostability.

Carbohydrates play essential roles in biology such as energy source, information transfer, or immunity. ASGPr acceptor is a receptor at the surface of hepatic (HepG2) cells, which can recognize and internalize galactose into cells. Hence, conjugation of galactosides on traditional fluorophore is an efficient pathway to enhance water-solubility, promote cell compatibility and endow specific cell targeting and selectivity. Some small glyco-probes were reported for ions or biomolecular detection and imaging specific cells through fluorescence variation targeting particular tumor. Nevertheless, low affinity between protein and single glycoside leading to limited selectivity, and complicated

fluorophores design impeded further application in biological assay.

According to the “glycoside cluster effect”, numerous carbohydrates on a core have multivalent recognition with a protein, improving affinity. “Click” reactions including copper catalysed azide-alkyne cycloaddition (CuAAC) or thiol-ene reaction are applied due to high yield and convenient modification. Aromatic cores with modifiable positions for conjugation with carbohydrates were welcomed because they can aggregate and form a hydrophobic moiety for adsorption of organic molecules. TPE, as a classic AIE fluorophore, was frequently applied in lectin or protein detection through modified solubility or RIR effect triggering fluorescence. However, the large volume of glycoclusters makes difficult to cross the cytomembrane even if it has remarkable receptor affinity. Nanoparticles are a good choice for lectin detection with distinct UV change or another signal variation. Gold nanoparticle, carbon nanomaterials and cyclodextrin are prevalent materials for carbohydrate conjugation which can increase partial concentration of sugars, control optical properties and enhance lectin affinity. Intermolecular self-assembly is another suitable manner to improve properties of probes and transport into cells.

I.6 Project purpose

In our previous studies, glycoclusters with different cores have been reported for their interactions with cell or bacteria lectins. Fluorescent reporters, based on rhodamine ^[120], naphthalimide ^[169] and DCM ^[162] were designed, synthesized, and applied to detect particular ions, biomolecules, lectins, or cancer cells. However, single monosaccharide conjugation only allowed limited affinity and sensitivity for proteins. Glycoclusters have an increased valency for a better affinity to receptors but also a large volume leading to restricted penetration into cells. We will design glyco-probes with high recognition and affinity ligands for receptors, possessing sensitive and selective detection for biomolecules and cell imaging and that can be used as delivery systems.

We have designed TPE-based glycopolymers from TPE monomers incorporating two monosaccharides by CuAAC reaction and thiol-ene “click” reactions. After intermolecular polymerization, we expected the TPE-based glycopolymer having more than 20 units and emitting intense fluorescence. The multiple glycosides will give high affinity to cell receptor and target specific cells through “glycoside cluster effect”. Meanwhile, the TPE hydrophobic core of the polymer will enable to contain and transport organic fluorescent probes or drugs for delivery to cancer cells, for imaging, and therapeutics diagnosis (Fig. 34).

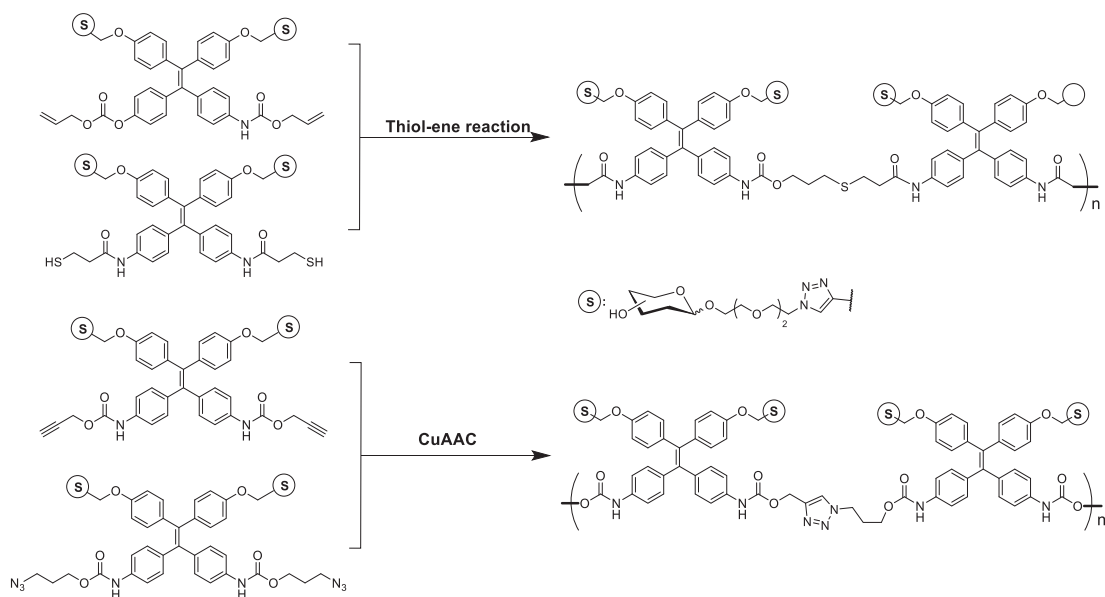


Figure 34: Two synthesis routes of TPE-based glyco-polymer through CuAAC reaction or Thiol-ene “click” reaction.

ACQ effect always restricts the fluorescence intensity of traditional probes working in aqueous solution. We have combined TPE moieties and DCM cores together through C=C bond, to design novel AIE fluorophore (TPE-DCM) with long-wavelength emission, excellent photostability and tunable optical properties. After obtaining TPE-DCM, we have decorated 2,4-nitrobenzenesulfonate on the fluorophore to quench the emission before thiophenol detection. However, the ACQ effect may influence the fluorescence when AIE probes have been aggregated in aqueous solution. So, we have used TPE-glycoclusters to contain the TPE-DCM probes for thiophenol response, but displaying the AIE properties of probs after intermolecular self-assembly (Fig. 36).

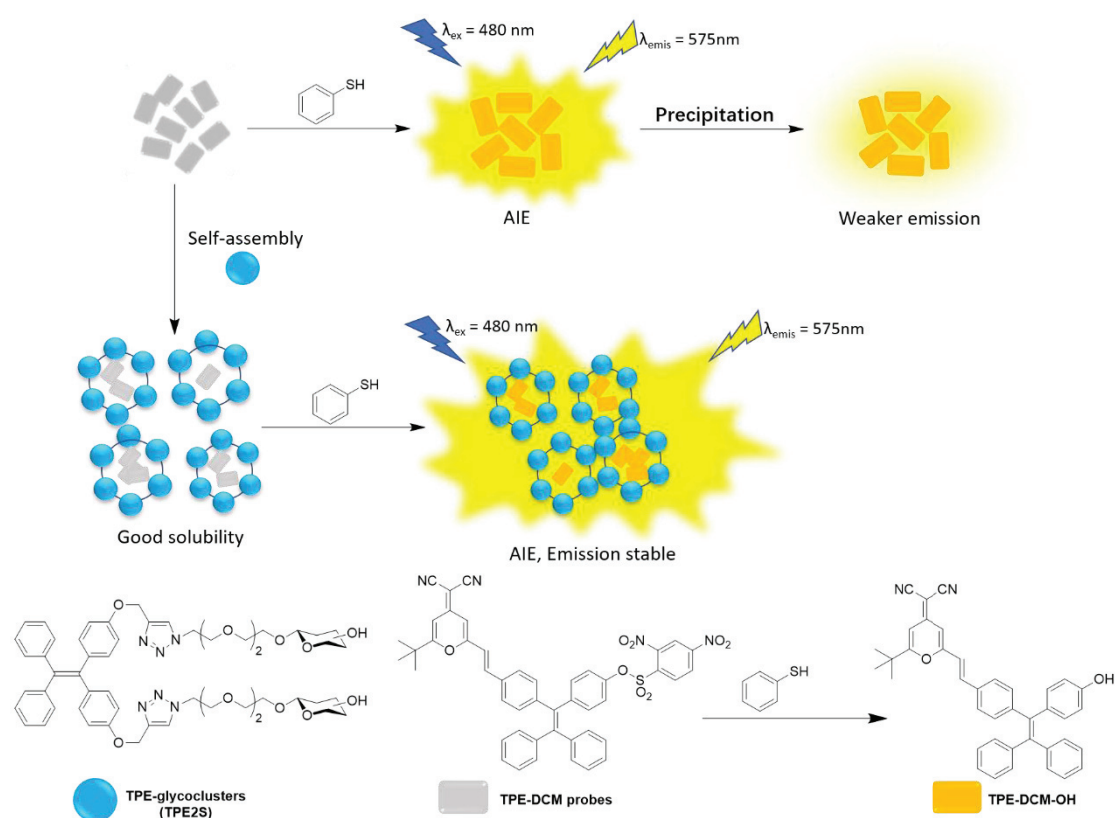


Figure 36: The response mechanism of glyco-dot for thiophenol and relevant compound structures.

Although TPE-glycoclusters improve the water-solubility and transport of probes into cells, the stability of the supramolecular assemblies can be limited when incubated with cells and in the presence of proteins such as BSA or HSA. Hence, based on the TPE-DCM fluorophore, we have decorated several monosaccharides by CuAAC. The covalent bond between glycoside and fluorophore provide probe excellent water-solubility, and control fluorescence in aqueous solution through AIE effect. The TPE-DCM-based glycoclusters will be employed to detect β -galactosidase *in vitro* and *in vivo*, and further applied for imaging cancer cells or senescent cells. After hydrolysis of the galactose by the enzyme, the water-solubility decreased leading to intermolecular aggregating and release fluorescence emission signal by AIE effect (Fig. 37).

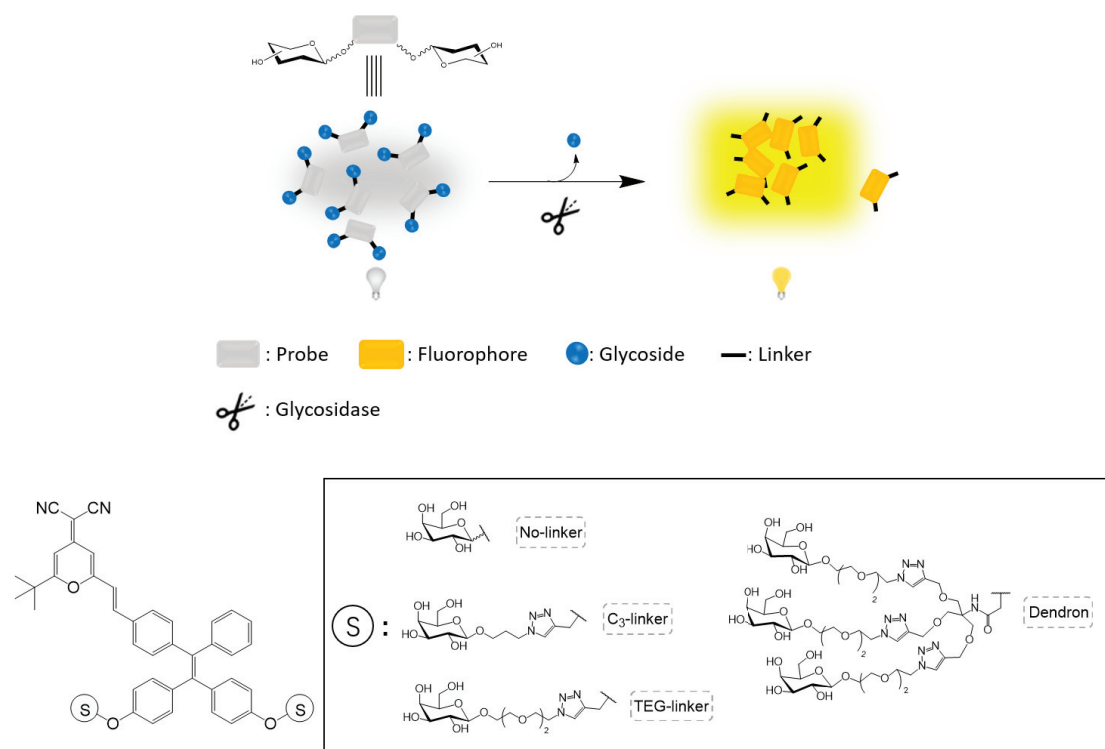


Figure 37: The response mechanism of TPE-DCM-based glycoclusters for glycosidase detection through AIE effect, and relevant glycoclusters with different linkers.

Chapter II

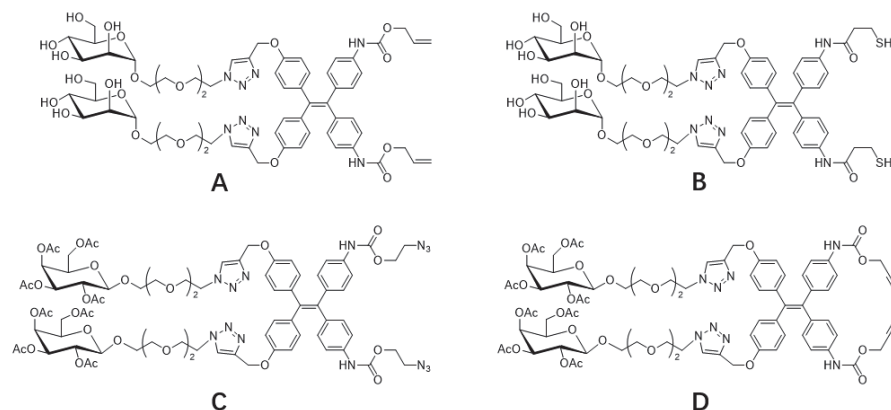
Design and Synthesis of TPE-Based Glycopolymers

II.1 Introduction

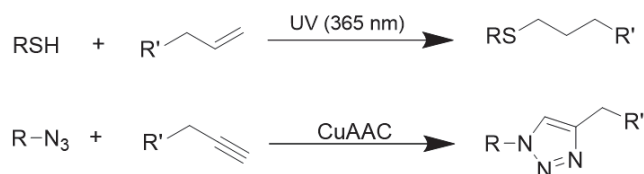
Tetraphenylethylene (TPE) is a representative AIE fluorophore with excellent photostability and multiple modifiable positions for functionalization. Many studies have reported applications for lectin recognition, enzyme detection and cell imaging. However, the blue emissive wavelength of the TPE core is overlapping with biological background fluorescence, so that it is not adapted for imaging cells. TPE remains a good aromatic core for the design of glycoclusters with relative hydrophobic core leading to aggregation in aqueous buffer. Hence, we have designed TPE-based glycopolymers with different monosaccharides based on the following monomers and thiol-ene reaction or azide-alkyne “click” reaction. The glycopolymers will have high water-soluble surface and hydrophobic cavities deliver of specific probes.

Thiol-ene reaction and azide-alkyne “click” conjugations were related since both are compatible with aqueous conditions for the final stage polymerization process (scheme 1).

Monomers:



Click reaction:



Scheme 1: The structures of monomers and the processes of thiol-ene reaction or azide-alkyne conjugation.

II.1.1 Conjugation methodologies

II.1.1.1 Cu(I) catalysed azide-alkyne “click” reaction (CuAAC)

Traditional azide-alkyne cycloaddition required high temperatures and long reaction times without any catalysts and produced mixtures of 1,4- and 1,5-disubstituted triazole regioisomers. However, the copper-catalyzed azide-alkyne cycloaddition (CuAAC), has been applied to the synthesis of glycoclusters, glycopolymers and nanoparticles^[170]. Compared with the others metal catalysts, such as the Ru-catalyzed “click” reaction that produced 1,5-disubstituted triazoles, CuAAC has lower sensitivity towards solvent and reaction conditions, less stringent steric demand of the azide substituent than found for RuAAC, and higher yield (Fig. 1A). CuAAC click reaction

is a stepwise process different from general “[3+2]” cycloadditions, which is supported by DFT calculations and kinetic evidence [171, 172]. The mechanism of CuAAC has two plausible pathways distinguished by two Cu species in the transition states. At the beginning, Cu(I) is coordinated with the alkyne after removing the proton from terminal alkyne. The intermediate I_a reacts with the nucleophilic azide and forms an unstable six-membered ring intermediate III_a . Rearrangement to the five-membered ring IV followed by reductive elimination affords the desired triazole [173]. Later on, Fokin and co-workers could demonstrate the CuAAC mechanism using isotopically labeled ^{63}Cu / ^{65}Cu and discovered the gem-di-copper defining intermediated III_b through Path 2 (Fig. 1B) [171].

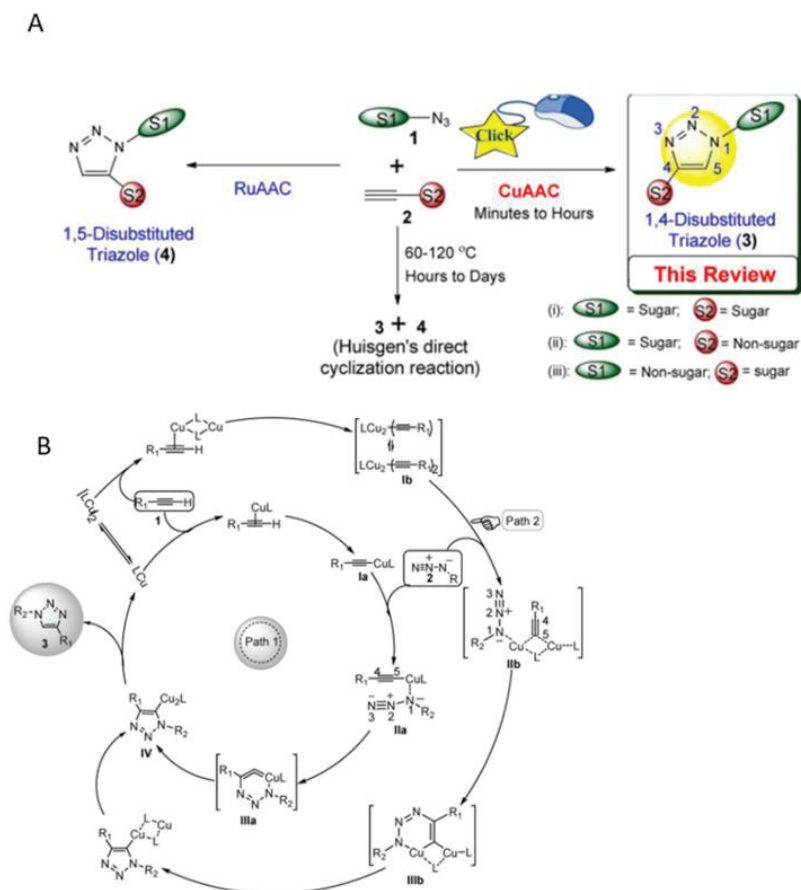


Figure 1: (A) Regioselective comparison of azide-alkyne cycloadditions with different catalyst and (B) two mechanisms of click reaction catalyzed with Cu(I) [170].

According to the mechanism, the Cu(I) play an important role in the whole processes. Hence, how to choose the three sources of Cu(I) is critical in CuAAC reaction, including (a) direct utilization of Cu(I); (b) reduction from Cu(II), and (c) oxidation from elemental Cu(0). Normally the second source (b) that reducing from Cu(II) such as copper sulfonate or copper acetate have been more practical because the catalytic system is compatible with aqueous conditions and provide high concentration of Cu(I). The aqueous condition can dissolve the CuSO_4 -sodium ascorbate system which catalyzed the “click” reaction and resulted in the formation of triazole products with high yield and excellent regioselectivity. Cu(I) salt is another prevalent method to catalyse this cycloaddition without reductant. This situation normally required deoxygenated aprotic solvents such as THF, CH_3CN , CH_2Cl_2 . The copper iodide, copper bromide, copper chloride and coordinated

complexes have been reported addition of some common bases to improve the reaction efficiency. In addition, “click” reaction could be performed in polar solvents including water and others aqueous alcohol depending on the solubility of starting materials^[174]. Combination of “click” reaction with microwaves (μW) or ultrasound irradiation under continuous flow conditions, aqueous media, solid supports, and room-temperature ionic liquid, are reported as useful tools to improve the reaction. For example, the microwave assistance can reduce the reaction time (from 12 h to 10-15 min) and generate to desired cycloaddition with higher yield.

II.1.1.2 Thiol-ene reaction

Encouraged by the useful applications of CuAAC, thiol-ene reaction, as an ancient reaction known for over 100 years, begins to recover specific interest in different synthetic systems (Fig. 2A). Thiol-ene have four features which attract much attention in versatile process: (a) Thiol-ene conjugation easily occurs in various conditions such as radical pathway, or accelerated with nucleophiles, acids and bases in some high polar solvent such as water and DMF. (b) Many types of double bonds can participate in the hydrothiolation including activated and non-activated species and multiple-substituted olefinic bonds. (c) Thiols are employed for the reaction although the reactive activities depend on the length of S-H bond and the cleavage mechanism. (d) Air and water insensitive procedures can be completed in a matter of seconds at room temperature and normal pressure ^[175].

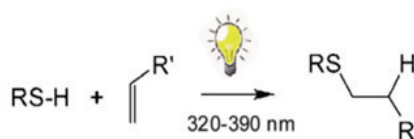


Figure 2: Hydrothiolation of C=C bond with anti-Markovnikov orientation^[175].

Generally, thiol-ene reaction involves radical process induced by UV light, which goes through the initiation, propagation, and termination steps (Fig. 2B). The thiol is stimulated with photo initiator under irradiation to generate a thiyl radical after the hydrogen radical cleavage. The thiyl radical then adds to the C=C bond on olefin to yield an intermediate carbon-centered radical which subsequently combines with another thiol to transfer a hydrogen radical. The newly produced thiyl radical continues to repeat the propagation process. And the termination steps involve typical radical-radical coupling processes. The thiol-ene reaction is a radical step-growth polymerization with anti-Markovnikov orientation. The reactive speed and yield depend on the structure and activities of both thiol and ene partners. Three classic thiols, alkyl 3-mercaptopropionates, alkyl thioglycolates, and alkylthiols have high reactivity to yield radical and combine with C=C bond. And the activities of alkene lie on their structure obviously: norbornene > vinyl ether > propenyl > alkene \approx vinyl ester > N-vinylamide > allyl ether \approx allyl triazine \approx allyl isocyanurate > acrylate > N-substituted maleimide > acrylonitrile > methacrylate > styrene > conjugated diene. TEC has been widely employed in polymerization, for the synthesis of multivalent glycoclusters, glyconanoparticles and self-assembled systems ^{[176] [177]}.

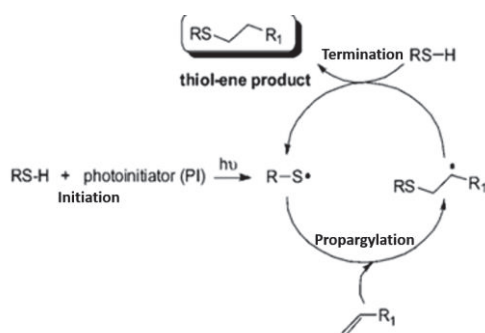
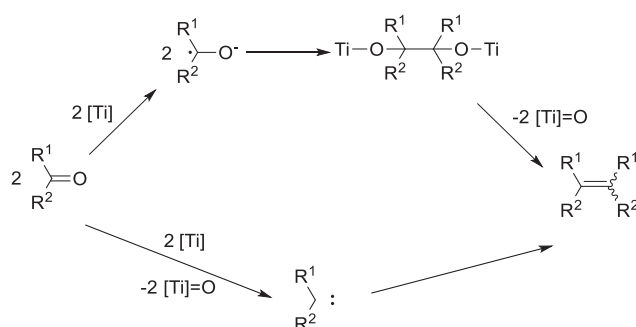


Figure 3: Radical mechanism of thiol-ene reaction ^[176].

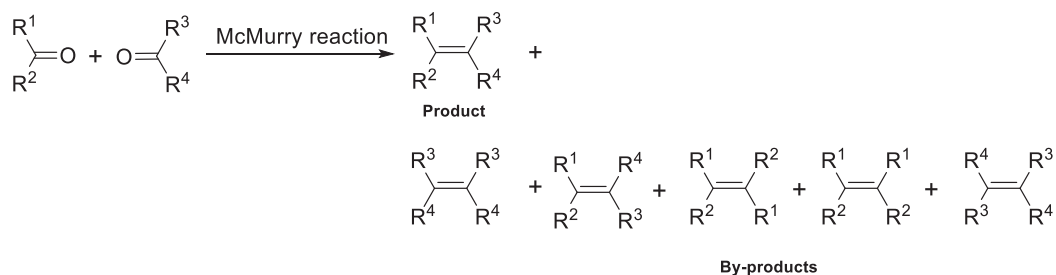
II.1.1.3 McMurry reaction

The McMurry reaction is a general method starting from aromatic ketone to obtain symmetric TPE. TiCl_4 -Zn catalyst system have been largely used for diversified TPE construction^[178]. Ketones were easily given electrons by Ti to provide a radical anion which will self-condense to the dianion (Scheme 2).



Scheme 2: Two proposed mechanisms of McMurry reaction ^[179]

Elimination of two molecules of TiO_2 affords the tetra-substituted olefin^[179]. Even though the McMurry reaction appears as a powerful tool to obtain highly substituted alkene, it is not suitable to provide non-symmetrical alkene, since a statistical distribution will be obtained and will have to be purified hardly when two different ketones will be used (Scheme 3). When synthesized TPE with two functional groups, it's not a most suitable method due to complicated products from two starting materials cross reaction.



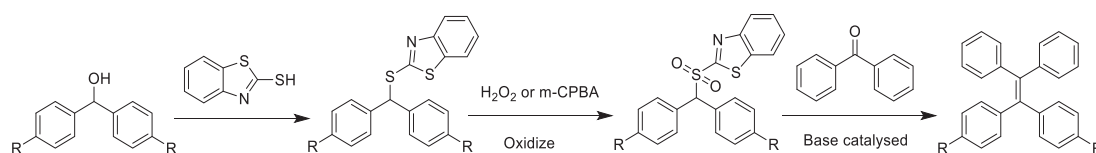
Scheme 3: Statistical products were obtained when synthesis of non-symmetric TPE through McMurry reaction.

We therefore investigated a Julia olefination approach that would allow the chemoselective

coupling of non-symmetric TPE.

II.1.1.4 Julia olefination

Julia olefination is a method to synthesize alkene from ketones or aldehydes. The synthesis of non-symmetric TPE will then proceed through the reaction of a sulfone and a ketone under basic conditions (Scheme 4). A diphenylmethanol derivative can be readily converted to the sulfone. Condensation with a diarylketone will afford a TPE derivative^[180, 181].

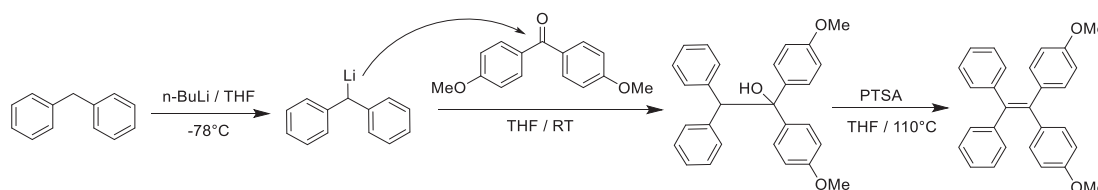


R: H or OMe

Scheme 4: Synthesis of non-symmetric TPE through Julia olefination.

II.1.1.5 Knoevenagel condensation

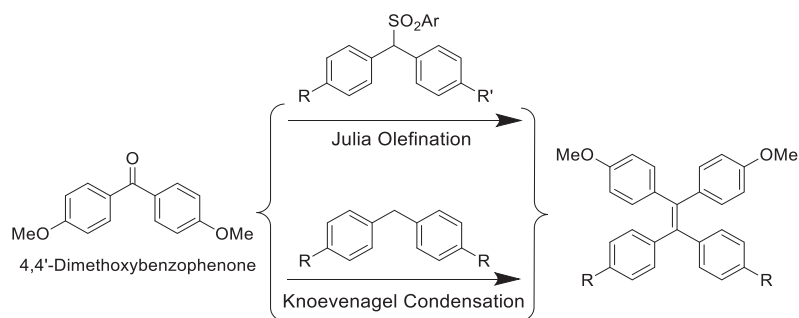
Knoevenagel condensation is another approach to synthesize TPE or non-symmetric TPE^[102, 182]. Butyllithium was used as a strong base to remove a proton on diphenylmethane in dry THF at -78°C. The Li-intermediate would then condense with the carbonyl to generate the alcohol intermediate which would lead to the desired olefin after *p*-toluene sulfonic acid catalysed dehydration (Scheme 5).



Scheme 5: Synthesis of non-symmetric TPE through Knoevenagel condensation.

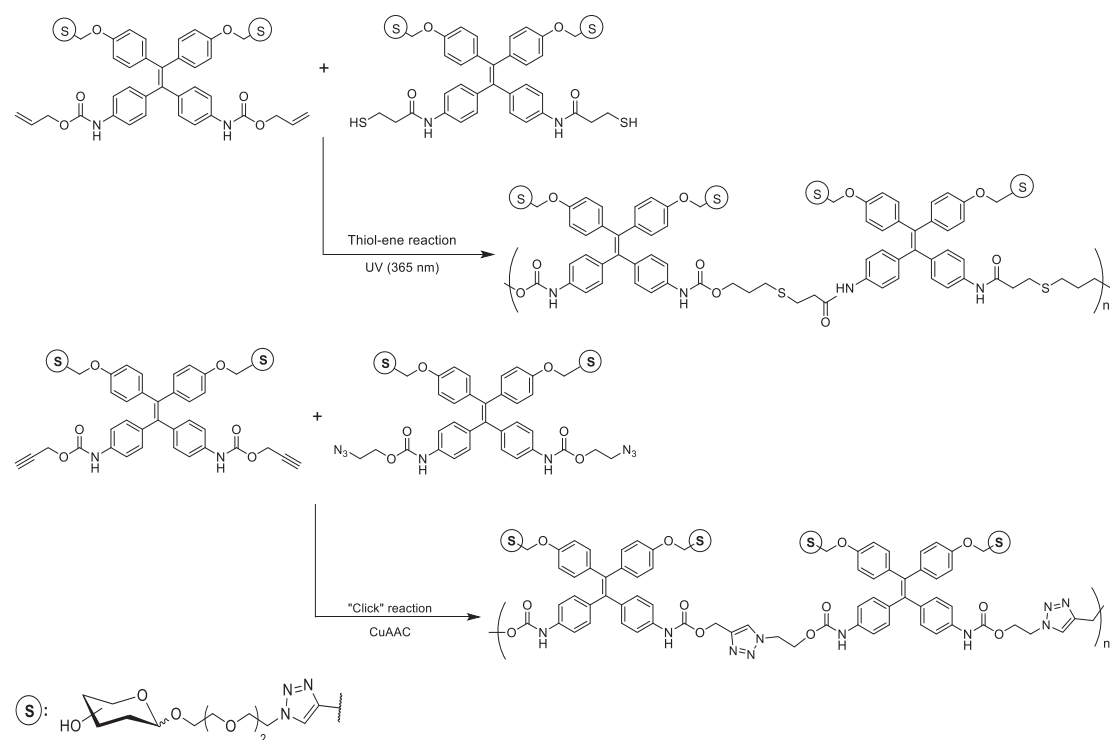
II.1.2 Project design

We have previously reported TPE-based glycoclusters decorated with four monosaccharides have been reported for bacteria lectin detection^[183]. For glycopolymers construction, the synthesis of a TPE-based glyco-monomer containing two different functional groups for incorporation of carbohydrates on one side and polymerization on the other side. However, traditional McMurry reaction is only appropriate to synthesize symmetric TPE cores. Julia olefination is a general method to build double bonds and was never applied for TPE synthesis. Knoevenagel condensation is an excellent method for the synthesis of non-symmetric TPE cores. Therefore, choosing a coupling pathway is the first question to be investigated (Scheme 6).



Scheme 6: Julia olefination and Knoevenagel condensation for TPE-core synthesis

We propose to polymerize monomers through two different “click” reactions: Thiol-ene reaction catalysed by UV-light is a convenient choice for glycopolymerization with water-soluble glyco-TPE monomers under 365 nm light catalysis. CuAAC is also investigated for the preparation of glycopolymers. The TPE-monomer will be desymmetrized through a dimethoxybenzophenone hosting the carbohydrate moieties and a precursor system for the polymerizable functionalities (thiol, ene, azide, alkyne).



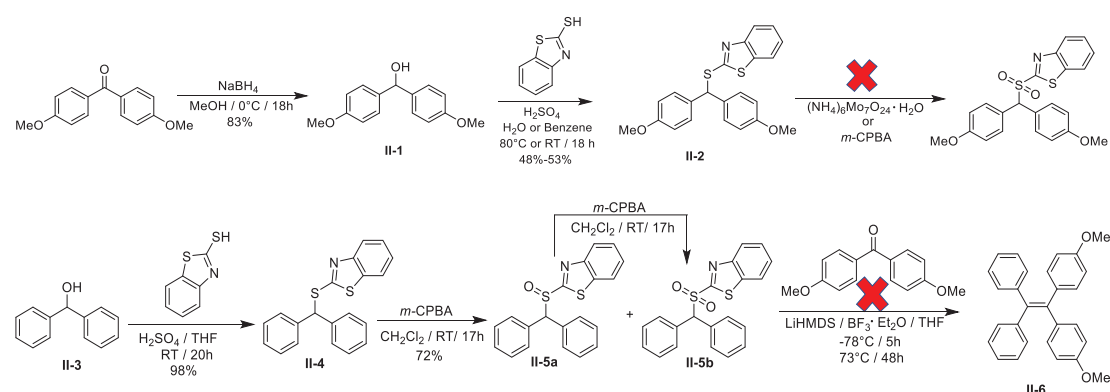
Scheme 7: Synthesis routes of thiol-ene reaction and CuAAC for polymerization of TPE monomers.

II.2 Design and synthesis of bisymmetric TPE-scaffold

II.2.1 Synthesis of TPE by Julia olefination

4,4'-Dimethoxybenzophenone was reduced with NaBH_4 at 0°C to obtain alcohol **II-1** then substitution by 2-mercaptobenzothiazole (BtzSH) in H_2O or benzene to afford thioether [184, 185]. **II-**

2 oxidation with H_2O_2 and $(\text{NH}_4)_6\text{Mo}_7\text{O}_{24}\cdot 4\text{H}_2\text{O}$ in ethanol failed^[186]. Hence, 3-chloroperbenzoic acid (*m*-CPBA) was used as more moderated oxidant but still obtained the fail results. We supposed that the electron-rich aromatic groups may decrease the reactivity of the sulphur atom (Scheme 8).

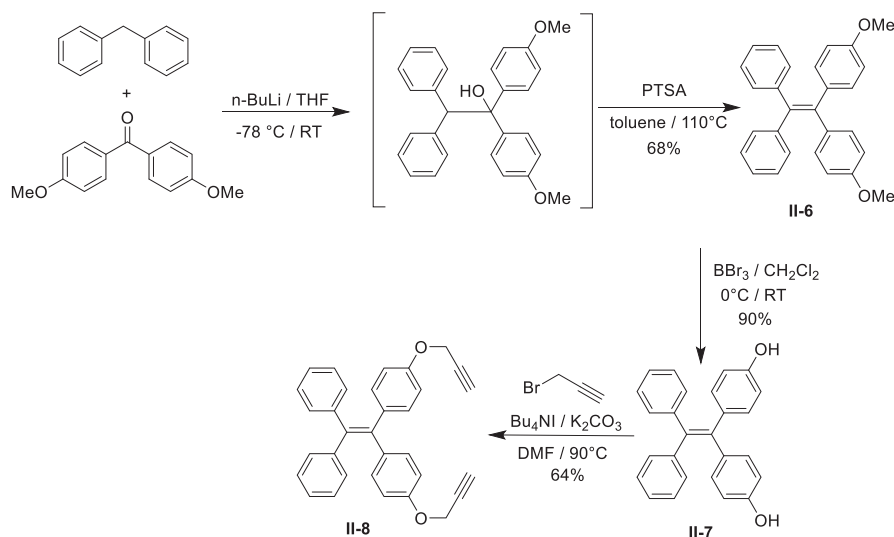


Scheme 8: Two TPE synthesis routes through Julia olefination.

We therefore decided to synthesize the sulfone **II-5b** from diphenylmethanol. Compound **II-4** was obtained after substitution with BtzSH and followed by oxidation with *m*-CPBA in CH_2Cl_2 afforded a mixture of sulfoxide **II-5a** and sulfone **II-5b**. Re-oxidation of **II-5a** can provide more sulfone **II-5b**. In Julia olefination steps, compound **II-5b** was deprotonated then condensation with 4,4'-dimethoxybenzophenone failed even with $\text{BF}_3\cdot\text{OEt}_2$ to activate the carbonyl group or with heating. We speculated that the main reason leading to unsuccessful Julia olefination was the large molecular volumes of both starting materials. The tertiary α -sulfonyl anion was too hindered with two aromatic rings and so its nucleophilicity towards dimethoxybenzophenone was too poor to allow condensation (Scheme 8). Julia olefination was not efficient to synthesize the TPE core (**II-6**).

II.2.2 Synthesis of TPE by Knoevenagel condensation

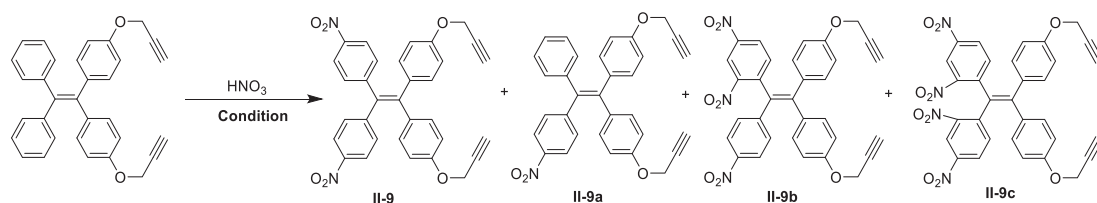
Diphenylmethane used as starting material was deprotonated by *n*-butyllithium^[182]. The resulting Li-substituted intermediate was stable in THF solution and condensation with 4,4'-dimethoxybenzophenone afforded the tertiary alcohol, which was dehydrated leading to the non-symmetric TPE **II-6**. The compound **II-6** exhibited standard AIE properties^[102] that non-fluorescence in organic solvent but emit blue fluorescence on TLC plates. BBr_3 was used to obtain the bis-phenol **II-7**. Propargylation could only achieve in the presence of Bu_4NI acting as a cation for the insoluble phenolate. Dipropargyl TPE (**II-8**) has two positions to conjugate monosaccharides and two blank phenyl ring will then be used for further functionalization (Scheme 9).



Scheme 9: Knoevenagel condensation to provide non-symmetric TPE.

II.2.3 Nitration of TPE

We next turned our attention to the introduction of two para-amino-substituents on the unsubstituted phenyl rings. These resulting aniline moieties will then be used to introduce the polymerizable functionalities. Nitration is rather difficult and the outcome of the reaction is highly dependent on the NO_2^+ source and reaction conditions. Referring to similar nitrification on aromatic ring^[187], concentrated HNO_3 and H_2SO_4 were mixed in a CH_2Cl_2 solution of compound **II-8** at 0°C . The by-product (**II-9c**) with four nitro groups were obtained (Table 1, Entry 1) according to $^1\text{H-NMR}$ analysis. We supposed that compound **II-8** with two methoxy groups has high reactivity to nitration since it is electron-rich. AcOH was used as catalyst without H_2SO_4 at 0°C to smoothen the nitration conditions (Table 1, Entry 2). But a similar result was obtained and we then considered weaker acidic environment and decreased the temperature drastically (Table 1, Entry 3).



Scheme 10: Nitration of TPE **II-8** and relevant products

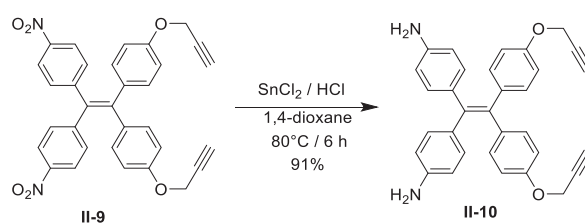
Table 1 : Nitration of TPE **II-8** under different conditions

| Entry | Reaction Conditions | II-9 | II-9a | II-9b | II-9c |
|-------|---|-------|-------|-------|-------|
| 1 | $\text{HNO}_3 / \text{H}_2\text{SO}_4, \text{CH}_2\text{Cl}_2, 0^\circ\text{C}$ | 0 | 0 | 0 | Major |
| 2 | $\text{HNO}_3 / \text{AcOH}, 0^\circ\text{C}$ | 0 | 0 | 0 | Major |
| 3 | $\text{HNO}_3 / \text{H}_2\text{SO}_4, \text{CH}_2\text{Cl}_2, -78^\circ\text{C}$ | Major | Minor | Major | Major |
| 4 | $\text{HNO}_3, \text{CH}_2\text{Cl}_2, -78^\circ\text{C}$ | Major | Minor | Minor | Minor |

Condition: TLC analysis traced the reaction process

But the best condition were found with concentrated HNO₃ as initiation agent without H₂SO₄ stirring in CH₂Cl₂ at -78°C to obtain the **II-9** with 75% yield (Table 1, Entry 4). But some pivotal factors influenced the reaction yield and the distribution of by-products. Nitric acid dropwise and slow addition was required to provide optimal yield of the desired di-nitro-TPE **II-9**. TLC analysis was the easiest method to monitor the reaction with typical R_f value of 0.31, 0.42, 0.17, and 0.07 for **II-9**, **II-9a**, **II-9b**, **II-9c** respectively. Vigorous stirring was also required for homogenous system from the biphasic water / CH₂Cl₂ layers. Quenching the reaction totally to basic pH was mandatory before purification to avoid that would decompose or further react to *o*-nitrated species.

Compound **II-10** was obtained from **II-9** by SnCl₂ in 1,4-dioxane with concentrated HCl solution. After reduction, the fluorescence colour of compound **II-10** changed to blue compared with the yellow fluorescence of **II-9** due to intramolecular electronic “pull-push” system disappearance (Scheme 11).



Scheme 11: **II-9** was reduced to obtain bis-propargyl-bis-anilino-TPE **II-10**.

A ¹H-NMR analysis of compounds **II-9** and **II-10** provided a typical para-substituted phenyl ring pattern with two sets of AB systems for each TPE (Fig. 4). The bis-propargyl-bis-anilino-TPE **II-10** was therefore a key intermediate in our project with two propargyl groups available for conjugation with azido-carbohydrate via CuAAC and the two aniline moieties for conjugation with polymerizable functionalities.

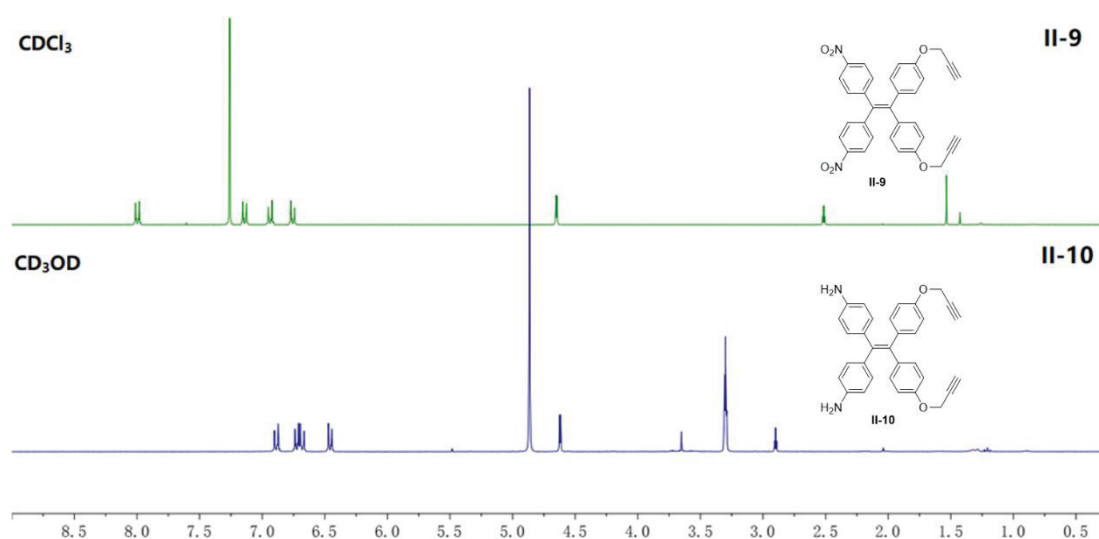
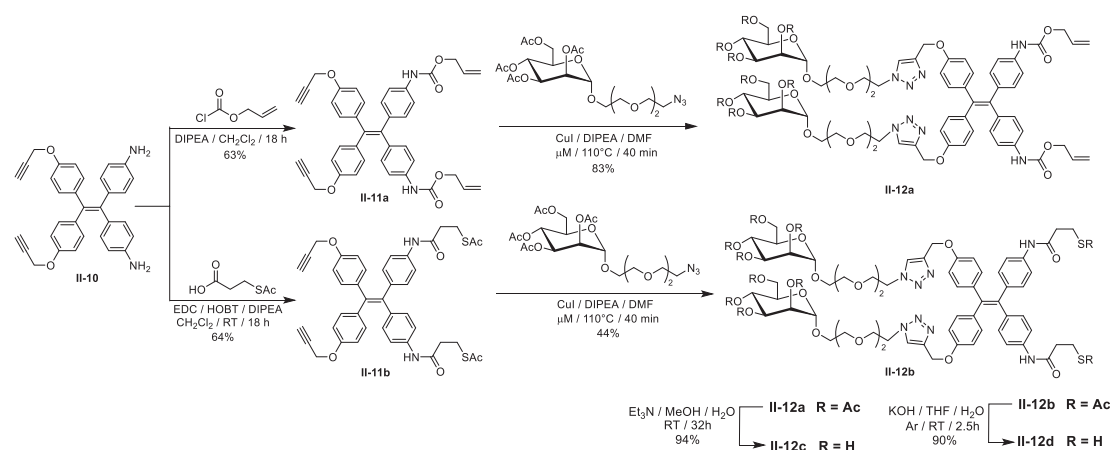


Figure 4: ¹H-NMR spectra of compound **II-9**, and **II-10**.

II.3 Synthesis of TPE-based glycolymers by thiol-ene “click” reaction

II.3.1 Synthesis of mannose-decorated TPE monomer

Allyl chloroformate and 3-(acetylthiol)propionic acid were reacted with the diamino TPE core affording carbamates **II-11a** and **II-11b**. Then acetyl protected mannosides with an azide group was on the TPE core. Microwaves irradiation accelerated “click” reaction and improved reaction yield were obtained with elevated temperature^[183]. It’s worth noting that copper should be removed completely with EDTA solution during workup because the compounds containing two triazole and several oxygen atoms could chelate copper ions easily. Residual copper was difficult to clear away in subsequent steps which would influence cytotoxicity in biological assay. For acetyl deprotection, compound **II-12a** was stirred in basic aqueous solution during 18h then purified to obtain the glyco-monomer **II-12c**. When **II-12b** was subjected to deacetylation under the same conditions, the corresponding monomer **II-12d** wasn’t obtained but got a dimer analogue emitting intense blue fluorescence which molecular weight measured from mass spectrometry. The exposed thiols would generate disulfide bonds and conjugated together in basic aqueous solution after acetyl deprotection. Hence, compound **II-12b** was deprotected by KOH in THF / MeOH solution under inert atmosphere (Ar) to obtain the other glycol-monomer **II-12d** without dimerization (Scheme 12).



Scheme 12: Synthesis scheme of two glycol-TPE monomers for thiol-ene reaction.

II.3.2 Synthesis of TPE-based glycolpolymer by thiol-ene reaction

The TPE monomer **II-12c** and **II-12d** were stirred in a solution of MeOH and H₂O under 365 nm UV irradiation. ¹H-NMR indicated that the two starting materials remained unchanged in solution. Excess 2,2-dimethoxy-2-phenylacetophenone (DPAP), as a useful photoinitiator, was added in solution to promote free radical generation under 365 nm UV light. After stirring 5 h, the resulting solution became cloudy and a suspension appeared with some undissolved materials. Hence, the obtained solid and solution were separated, concentrated and dried before ¹H-NMR and MS analysis. For liquid portion, ¹H-NMR showed the characteristic peaks of the allyl moiety on monomer **II-12c** had almost disappeared, but the peaks of mannose could not be observed. Besides, MS analysis didn’t find any relevant molecular weight of the polymer but only a series peaks at m/z 1300-1500 which indicated that no polymer was present in the filtrate. The solid could not dissolve in water,

MeOH, THF even DMSO and DMF thus no $^1\text{H-NMR}$ spectrum could be obtained while analysis did not provide any useful data. From this disappointing result, we hypothesized that TPE dyes could absorb UV light, release energy by intramolecular rotation or fluorescence emission, therefore free radical generation was restricted preventing polymerization in solution. As a conclusion, thiol-ene conjugation was not suitable for the polymerization of TPE glyco-monomers (Fig. 5).

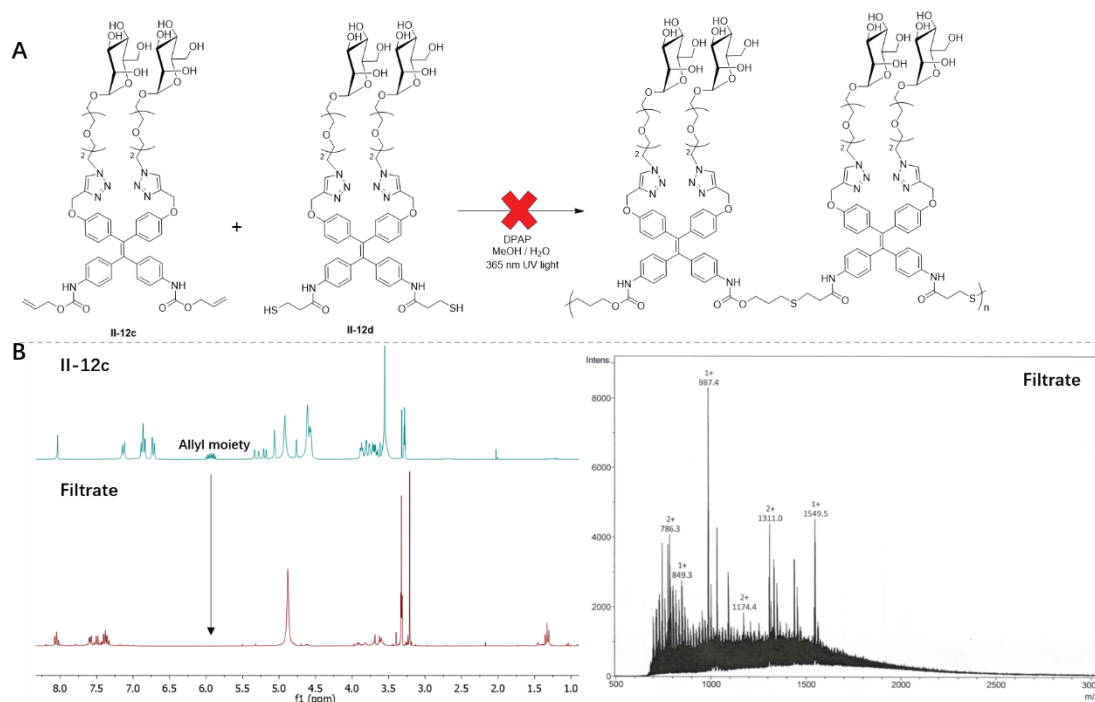


Figure 5: (A) Synthesis scheme of TPE-based glycopolymer by thiol-ene reaction. (B) $^1\text{H-NMR}$ and MS analysis of filtrate after polymerization.

II.4 Synthesis TPE glycol-polymers through double “click” reaction

II.4.1 Synthesis of galactose-decorated TPE-monomer for “click” reaction

Starting from diamino TPE **II-10**, acetyl protected galactose derivative with an azide group was conjugated by CuAAC. Under microwave irradiation, compound **II-13** was obtained in low yield (25%) catalysed by CuI and DIPEA at 110 °C. Therefore, CuSO₄ and sodium ascorbate catalysis at room temperature improved reaction yield to 72%. Vigorous stirring was necessary to mix the biphasic solvent system of CH₂Cl₂ for **II-10** and water for salts. When purifying the crude compound **II-13**, copper should be removed by EDTA solution.

to guarantee the oxydo-reduction cycle of $\text{CuSO}_4 / \text{VcNa}$. Then we increased the reaction time from 18 h to 5 days (conditions C, Scheme 14) leading to polymer **II-16c**, expecting a larger reaction time to lead to higher degree of polymerization. Finally, CuI catalysis was also investigated (conditions D, Scheme 14) to evaluate another CuAAC conjugation method leading to polymer **II-16d**. Direct polymerization by carbamoylation of diamine-TPE **II-13** was polymerized to provide polymer **II-17**.

All polymers **II-16a-d** and **II-17** displayed fluorescence emission from TLC plates analysis ($\lambda_{\text{ex}} = 490 \text{ nm}$). $^1\text{H-NMR}$ analysis of the polymer **II-16a** indicated disappearance of the alkyne monomer peak ($\delta = 2.5 \text{ ppm}$, Fig. 6A) while a new signal ($\delta = 4.3 \text{ ppm}$, Fig. 6B) could be observed for polymer **II-17** corresponding to the symmetric ethylene linker between two monomer units.

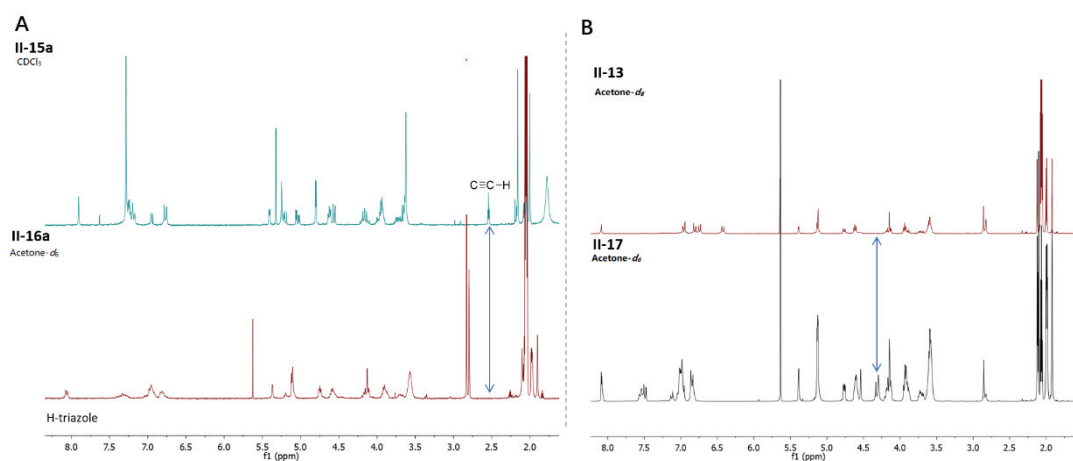


Figure 6: $^1\text{H-NMR}$ comparisons of polymers and relevant starting materials.

However, $^1\text{H-NMR}$ could not measure molecular weight or polymerization degree. Hence, size exclusion chromatography (SEC) analysis, as efficient chromatography normally used to separate each portion and analyse molecular weight for polymers, was employed to measure the average molecular weight of our polymers. Through this specific chromatography, molecules with larger volume would be eluted earlier than smaller compounds. First, compound **II-16a**, **II-16d**, and **II-17** were submitted to SEC analysis (Fig. 7A). Compared with **II-17**, **II-16a** and **II-16d** showed wider molecular ranges and higher molecular weight with higher polymerization degree which certified that CuAAC was more efficient than direct carbamoylation for TPE synthesis of TPE-based polymers. Then, SEC data of CuAAC polymers revealed that $\text{CuSO}_4 / \text{VcNa}$ catalysis provided the largest molecular weight whether in water or MeOH . Lengthening reactive time didn't increase the degree of polymerization but rather the opposite. Microwaves irradiation promoted intramolecular cyclization to obtain low degree of polymerization. DOSY NMR analysis certified that homogenous molecular weight distributions of polymers **II-16a** and **II-17** were obtained with a narrow distribution below $5 \text{ m}^2 / \text{s}$ was observed (Fig. 7B).

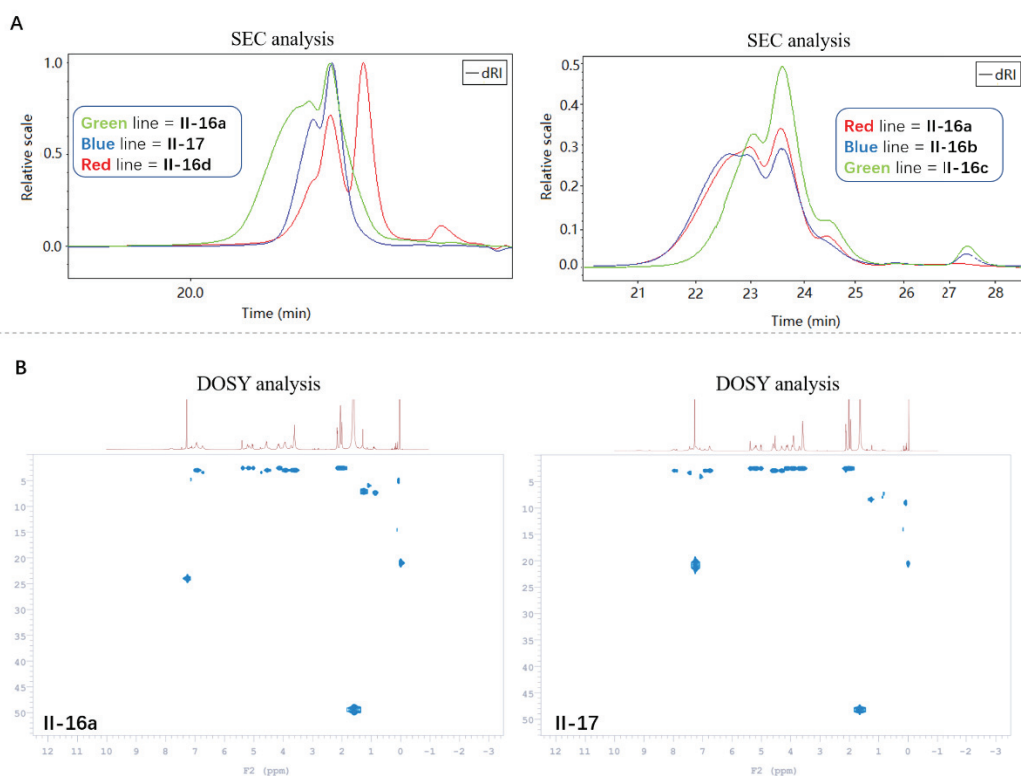


Figure 16: (A) Molecular size of series polymers were measured by SEC analysis. (B) Homogenous size of components in compound **II-16a** and **II-17**.

After calculating the molecular weight of monomer and compared with molecular weight of each polymers measured from SEC data, the compounds of **II-16a** or **II-16b** contained six monomers units and should be called oligomers but not polymers, which was far less than our anticipation of 15 units or more (Table 2). The polymerization failed probably because: (i) the large volume and molecular weight of TPE monomer increased the difficulty of polymer generation; (ii) after a few (2-4) monomers polymerized, the oligomers may aggregate into micelles with TPE inside that would prevent propargyl or azide to further react with other monomers.

Table 2: Molecular weight distribution analysed by SEC and DOSY

| Sample | SEC analysis | | | DOSY analysis | | Degree of polymerization | |
|---------------|--------------|------------|-----------------------|---------------------|-----------------------|--------------------------|----------|
| | Mn (g/mol) | Mw (g/mol) | \bar{M}_w/\bar{M}_n | Mw (g/mol, monomer) | D calc ^[a] | | D obs |
| II-16a | 7340 | 9427 | 1.28 | 3365 | 2.57 | 2.70 | 6 |
| II-16b | 7383 | 9687 | 1.31 | 3365 | 2.54 | 2.70 | 6 |
| II-16c | 5639 | 7082 | 1.26 | 3365 | 2.88 | 3.16 | 4 |
| II-16d | 4349 | 6517 | 1.50 | 3365 | Not measured | Not measured | 4 |
| II-17 | 6459 | 7290 | 1.37 | 1595 | 2.84 | 2.62 | 6 |

[a]: The calculation of **D cal⁺** referred to reported study ^[188].

Even though the polymerization was difficult and led too low molecular weight species, we deacetylated the polymers **II-16a-d** and **II-17**. The resulting polymers were supposed to be water soluble with the carbohydrate moieties. But the material obtained was poorly soluble in water and

also in organic solvents. So unfortunately, we could not investigate further these polymers for biological assays or interactions with proteins.

A possible improvement would be to graft larger saccharide units (as oligosaccharides or glycodendrons) or to use a solubilizing moiety such as a carboxylic acid or a specific protein of the TPE-monomer. Nevertheless, we have decided to stop this project this stage and to focus on other approaches.

II.5 Conclusion

Tetraphenylethylene is a typical AIE fluorophore with multiple modifiable position. TPE-based glycoclusters have designed, synthesized, and applied to recognize specific cells, target lectins and detect glycosidases. Aggregation in aqueous solution made TPE emit strong fluorescence without ACQ influence. Hence, we have designed and synthesized TPE-based glycopolymers with high fluorescence intensity in aqueous solution for probe or drug delivery and cell targeting.

We attempted to construct our basic TPE core through Julia olefination and Knoevenagel condensation. Julia olefination was not suitable to synthesize disymmetric TPE with two functional groups. We synthesized TPE core with two “blank” positions on phenyl rings by Knoevenagel condensation. Then, a moderated reactive condition was explored for bisymmetric dinitro TPE core synthesis. Reduction of the nitro to amino groups provided the desired TPE core with two functional groups.

We tried “thiol-ene” reaction to conjugate TPE monomers together. Through amidation was decorated vinyl or acetyl-protected thiol groups on TPE then conjugation with mannose derivatives with TEG linkers was accomplished. After deprotection, two water-soluble TPE-based monomers were mixed with photoinitiator (DPAP) in water irradiated by 365 nm UV light. But probably TPE absorbing 365 nm light, restricted the radical reaction process. A substance with low solubility in water, as we speculated, could be the targeted polymers but no direct evidence could prove its structure.

Hence, we changed structure of TPE monomers and adopted two “click” reactions to construct the polymer. Relevant propargyl and azide groups were modified on TPE through amidation before conjugation with galactose on fluorophore. Then, we explored the best reactive conditions for the second “click” reaction including $\text{CuSO}_4 / \text{VcNa}$, $\text{CuI} / \text{microwave}$, and additional amidation. Through SEC and DOSY analysis, $\text{CuSO}_4 / \text{VcNa}$ system was the best condition providing the highest polymerization degree and molecular weight.

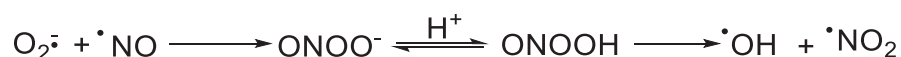
However, polymerization of the TPE core resulted in ball-shape structures restricting intermolecular polymerization, leading to only oligomers containing six monomers. And after deprotection, the limited number of glycosides were not sufficient to offset hydrophobicity from conjugated TPE core. Resulting TPE glyco-oligomers neither dissolve in aqueous nor organic solution, which probably explains why compounds generated by thiol-ene have similar solubility properties.

Chapter III

Self-assembled Glyco-dots for Peroxynitrite Detection and Cell Imaging

III.1 Introduction

Peroxynitrite (ONOO⁻) is an important reactive oxidant and nitration agent found physiological and pathological processes. It has been demonstrated to cause neuronal death in vivo such as brain ischemia, amyotrophic lateral sclerosis, Alzheimer's disease and Parkinson's disease^[189, 190]. ONOO⁻ can damage tissue by releasing hydroxyl radical ([•]OH) and nitrogen dioxide (NO₂[•]). Also, due to its efficient nitration and oxidant properties, biomolecules such as DNA, proteins, thiols and lipids were easily damaged triggering cancer, septic shock, atherosclerosis and multiple sclerosis^[191]. Peroxynitrite was normally generated from ubiquitous superoxide radical anion (O₂^{•-}) and enzymatically produced nitric oxide radical ([•]NO), but quickly formed to ONOOH and then decomposed in acidic environment (Scheme 1)^[192] Fluorescent analysis is sensitive, rapid, accurate to capture the ephemeral ONOO⁻ in cells. Hence, detecting the level of intracellular ONOO⁻ is a key indicator for monitoring or predicting diseases effectively. Over the past decade, fluorescent probes for ONOO⁻ detection and imaging in cell with different mechanisms were reported frequently.



Scheme 1: The production and decomposition of peroxynitrite (ONOO⁻).

III.1.1 Fluorescent probes for intracellular peroxynitrite detection

Peroxynitrite has high oxidative activity towards weak or unstable chemical bonds and groups, such as heteroatom (Se, Te) oxidation, activated C=C bond oxidative cleavage, phenol oxidation, ether oxidation and arylboronic acids oxidation.

Keli Han and co-workers reported two near-infrared reversible cyanine (Cy) based fluorescent probes for ONOO⁻ detection (Fig. 1A). Selenium (Se) or tellurium (Te), as detectors, were incorporated in a cyanine dye to quench fluorescence by redundant lone pair electrons on heteroatoms. Active peroxynitrite could oxidize these heteroatoms to generate Se=O or Te=O bond quenching the original PET effect and recovering fluorescence emission. However, reductant such as cysteine or GSH could restore the Se or Te and recovered the intramolecular PET effect. The two probes exhibited sensitive fluorescent response and linear increase with increasing concentrations of ONOO⁻ until saturations with 23.3-fold enhancement. Excellent selectivity for ONOO⁻ was observed in comparison with other oxidants in solution. Near-infrared probes emitted red fluorescence when reacted with endogenous ONOO⁻, thus sufficiently avoiding the biological background interference. Nevertheless, the 600s required to reach maximum fluorescence and weak quantum yield were not satisfactory for further biological applications^[193, 194].

Phenol oxidation is another prevalent design for fluorescence modification and the design of probes. A phenol group can be readily oxidized to semiquinone which will redistribute the phenyl electrons system. The phenone was further oxidized leading to C-N bond cleavage. According to this mechanism, JinHee Park, Jong-In Hong and co-workers reported two-photon fluorescent probe for peroxynitrite detection^[195]. However, long reaction time, nonlinear concentration relationship and fluorophore instability for ONOO⁻ prevented application in cell assay. Xiulan Li, Jingli Hou, Yangping Liu and co-workers decorated 4-(methylamino)phenol and triphenylphosphonium

bromide on 1,8-naphthalimide to design a fluorescence “turn-on” probe. The probe exhibited selectivity to oxidants, lower limit of detection and distinctly imaging in RAW264.7 cell (Fig. 1B) [196]. Tao Peng, Xingmiao Chen, Dan Yang and co-workers designed a rhodamine-based fluorescence “turn-on” probe through improving rhodamine’s stability to ONOO⁻ and water-solubility. The terminal probes showed fluorescence enhancement in chemical and biological media, imaging ONOO⁻ in live cells and tissues[197]. However, long response time was still restricting this type of detection model.

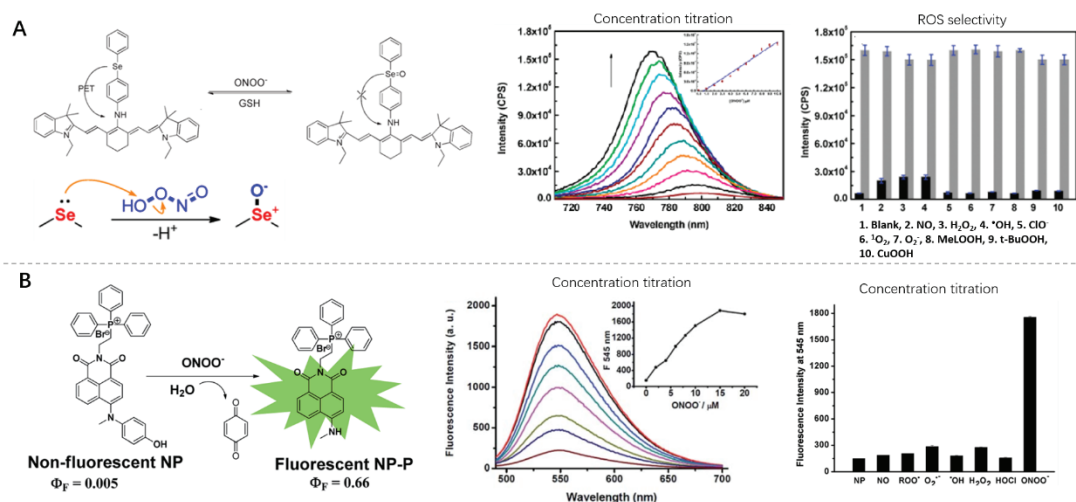


Figure 1: (A) Cyanine probe for ONOO⁻ detection by Se oxidation^[194]. (B) 1,8-naphthalimide based probes for ONOO⁻ detection through phenol oxidation^[196].

To control fluorescence, trifluoromethyl ketone is another moiety for ONOO⁻ detection. Based on this mechanism, Dan Yang, Huali Wang, Jiangang Shen and co-workers modified trifluoromethyl ketone derivatives on the hydroxy of fluorescein to “turn-off” fluorescence (Fig. 2A)^[198]. After reaction with ONOO⁻, the trifluoromethyl caging moiety was removed and restoring the intramolecular electronic “pull-push” system. The probe showed more obvious fluorescence intensity variation for ONOO⁻ than other oxidants and linear relation to ONOO⁻ concentrations after stirring 15 min. Detection of ONOO⁻ in neuronal cells was also possible. Zhenning Sun, Huali Wang, Dan Yang and co-workers designed BODIPY-based fluorescent probe working by PET effect^[199]. Green signal was emitted after oxidation by ONOO⁻ in aqueous buffer or *in vivo*. Shorten emissive wavelength and little Stokes shift are the main defects restricting fluorescence intensity measurements and further applications. Hence, Jianjian Zhang, Xu Zhen, Jianfeng Zeng and Kanyi Pu developed a near-infrared (NIR) fluorescence and photoacoustic (PA) dual-model probe for ONOO⁻ detection^[200]. The cyanine-based probe was quenched through disrupting the intramolecular ICT effect by carbonate modification. The probes showed higher NIR (59-fold) and PA (5-fold) enhancement, excellent water-solubility, and are the first detecting systems for endogenous ONOO⁻ in living systems by NIR and PA dual-mode imaging.

Fluorophores playing dual-roles as reporter and detector are a smart model for probe design. Xiaotong Jia, Qiangqiang Chen, Xuhong Qian and co-workers developed molecular probes composed of two cyanine fluorophores (Cy3 and Cy5) with different reactivity towards ONOO⁻ (Fig.

2B). The fluorescence signal was changed from red (660 nm) to green (530 nm) when the structure of probe **PNCy3Cy5** was decomposed by peroxynitrite. The ratiometric probe exhibited high selectivity and sensitivity for ONOO^- detection which can be applied in semiquantitative determination of ONOO^- in living cells. Notably, the probes particularly localized on mitochondria, where endogenous ONOO^- was principally generated [201]. Dan Cheng, Yue Pan, Young-Tae Chang and co-workers conjugated coumarin and rhodamine to construct a two-photon and FRET fluorescent system. Rhodamine emitting red fluorescence (~ 650 nm) was the fluorescent reporter and detector. When ONOO^- added to the activated $\text{C}=\text{O}^+$ bond of the pyrylium moiety, the conjugated system in rhodamine derivatives was disrupted. The coumarin, as energy provider, released blue fluorescence signal. This probe exhibited excellent ONOO^- selectivity versus other reactive oxygen species (ROS) and reactive nitrogen species (RNS) and monitored endogenous ONOO^- with minimal cytotoxicity. Moreover, a ratiometric probe could monitor ONOO^- variation produced by LPS stimulation in inflamed mouse model which was useful for biological imaging and disclosed ONOO^- state in physiological and pathological conditions (Fig. 2C)[202].

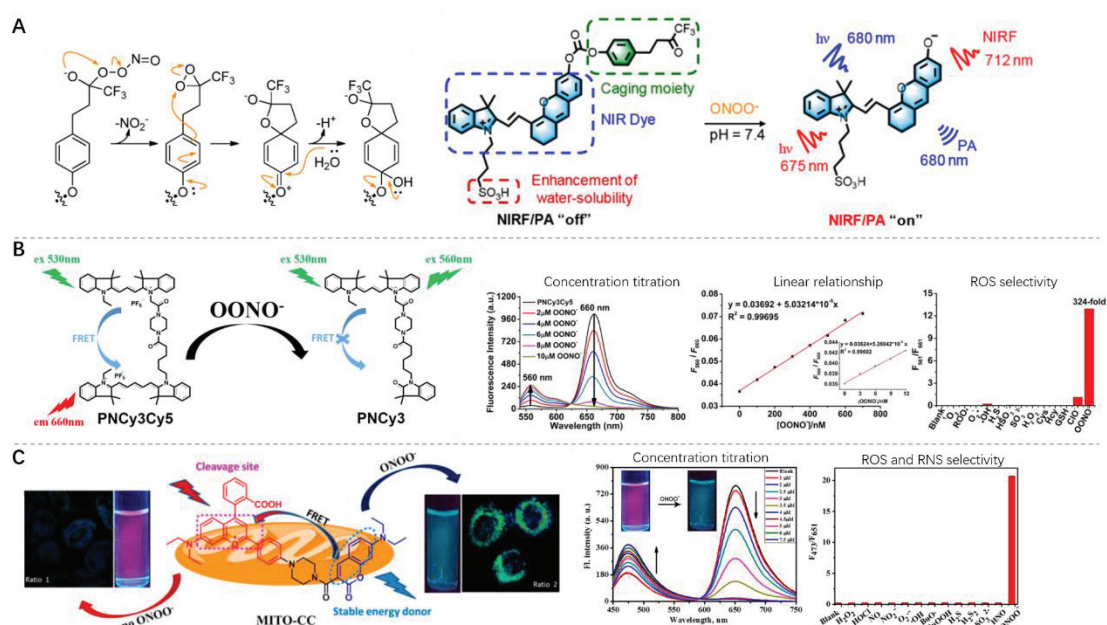


Figure 2: (A) Cyanine-based probes for ONOO^- detection by trifluoromethyl ketone oxidation[200]. (B) Cyanine-based[201] and (C) coumarin-rhodamine-based[202] FRET probes for ONOO^- detection through fluorophore decomposing.

Arylboronic acid oxidation is a rapid, sensitive and accurate pathway which was employed for ONOO^- detection. Adam Sikora, Jacek Zielonka, B. Kalynaraman and co-workers reported boronic acid pinacol ester have high reactivity towards ONOO^- which is 200 times faster than HClO and a million times faster than H_2O_2 [203]. The nucleophilic addition of ONOO^- to the boron atom led to the elimination of a molecule of NO_2 “insertion” in the B-C bond leading to an aryl-pinacol-borate intermediate. Further decomposition to generate phenol and a pinacol borate after reaction with water (Fig. 3A). Currently, arylboronic acids and pinacol esters are frequently designed for ONOO^- monitoring in biological imaging.

signal. The self-assembly pathways promote water-solubility of organic probes. Xiaolong Sun, Karel Lacina, Tony D. James and co-workers reported a system based on 1,8-naphthalimide (Fig. 4C) [207]. The exposed boronic acid was condensed with a diol from fructose. The addition of ONOO⁻ removed the boronic acid to recover PET. The PET effect was impeded when the electron-rich nitrogen was H-bond to the boronic acid, and then recovered after cleavage of the boronic acid by ONOO⁻. After conjugation with fructose, high water-soluble fluorescent “on-off-on” model showed selectivity for ONOO⁻, but interfered by ClO⁻ [20]. Whereafter, Kaibin Li and co-workers designed long-wavelength DCM based probes using a similar pathway (Fig. 4D). They demonstrated that fructose could easily construct B-O bond to block PET effect in contrast to weak fluorescence improvement by galactose, glucose, mannose, fucose and other disaccharides without fructose units [190].

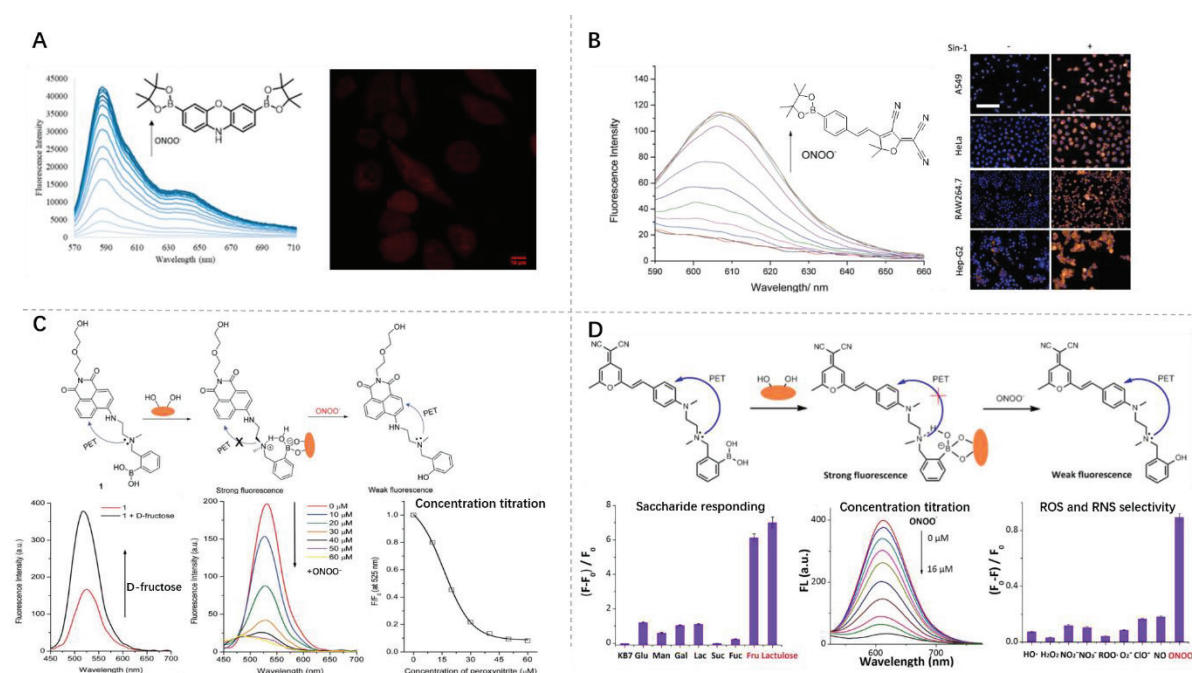


Figure 4: (A) Phenoxazine^[205] and (B) DCM-like^[206] probes decorated with boronic acid pinacol ester for ONOO⁻ detection. (C) Complexation of 1,8-naphthalimide probe and fructose to monitor ONOO⁻[20]. (D) Complexation self-of DCM probe and lactulose to monitor ONOO⁻[190].

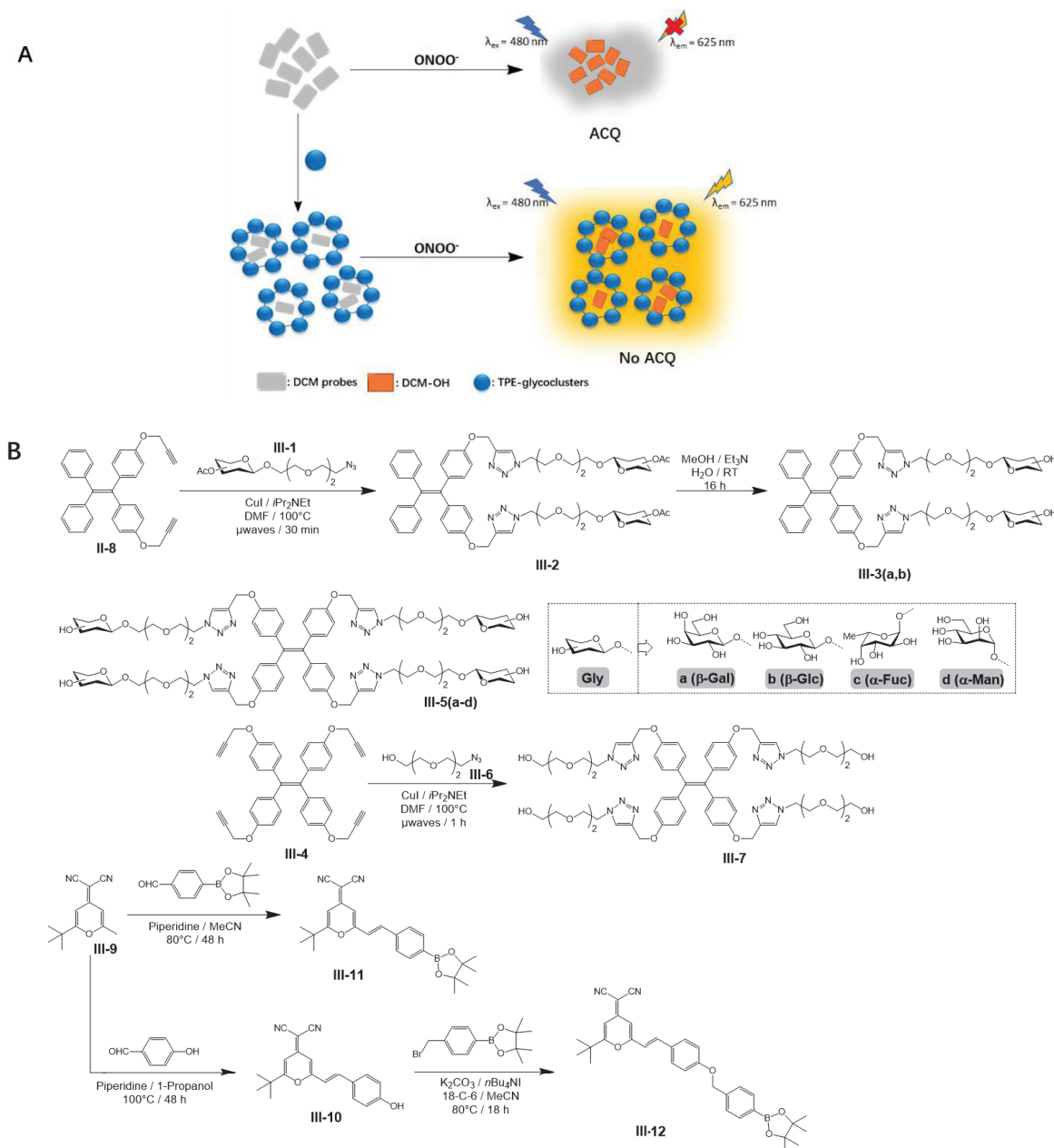
III.1.2 Project design

Even though TPE-based polymers displayed poor solubility which prevented application for detection or drug delivery, we considered the excellent ability of TPE-glycoclusters to self-assemble with hydrophobic partners. In our previous studies, DCM-based probes have been designed, synthesized and self-assembled into “glyco-dot” materials to imaging cells. Excellent optical properties, long-wavelength emission and simple synthetic procedures certified their fluorescent properties for biomolecule detection and cell imaging.

We designed two DCM-probes with different boronic acid moieties: (i) boronic acid pinacol ester was connected on phenyl ring (**III-11**) through blocking intramolecular electronic “push-pull” system to quench fluorescence; (ii) the same phenyl boronic acid pinacol ester was connected with a methylene bridge (**III-12**) on hydroxyl DCM to quench fluorescence by PET effect. However, such organic structure may possess low water-solubility leading to weak emission influenced by

ACQ effect in aqueous buffer.

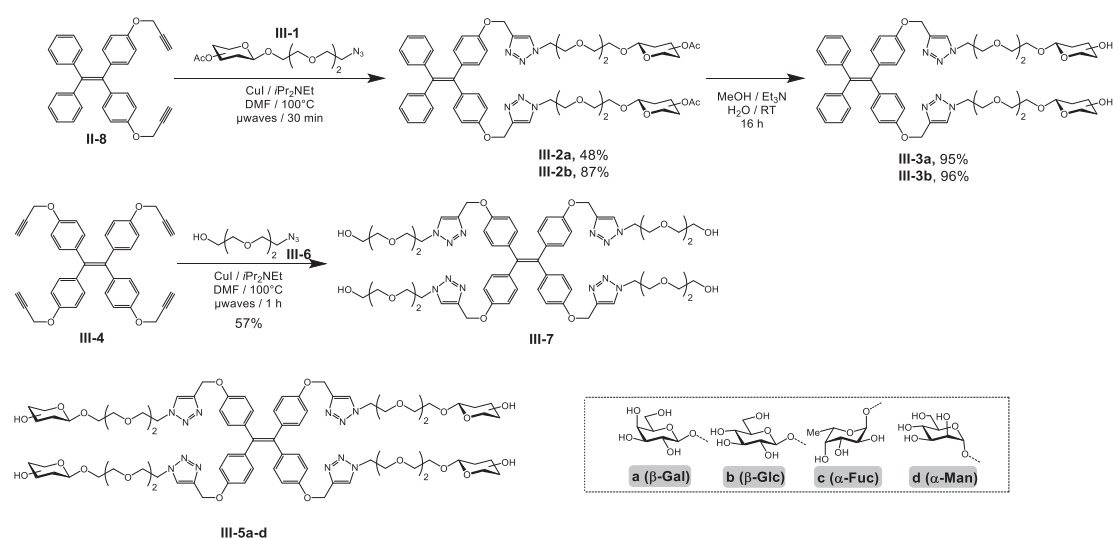
We have therefore used TPE-based glycoclusters as water-solubility agents (Scheme 2A). “Click” conjugation of different monosaccharide azide derivatives on dipropargyl- or tetrapropargyl-TPE obtained two kinds of TPE-based glycoclusters to recognize and target specific cells (Scheme 2B). In our previous studies, an interesting FRET relationship was found between TPE-glycocluster and DCM dyes when mixed in aqueous solution. This phenomenon showed that TPE-based glycoclusters could capture DCM molecules and construct “glyco-dot”. According to this discovery, we decided to adopt TPE-glycoclusters to transport DCM probes and improve their water-solubility. Self-assembled glyco-complex would construct glyco-balls with hydrophilic surface for dissolving in water and hydrophobic centre containing DCM probes. Amphiphilic glyco-dots would be responding to ONOO⁻ cancer cell and monitor intracellular ONOO⁻ for biological imaging.



III.2 Synthesis of TPE-glycoclusters and DCM probes

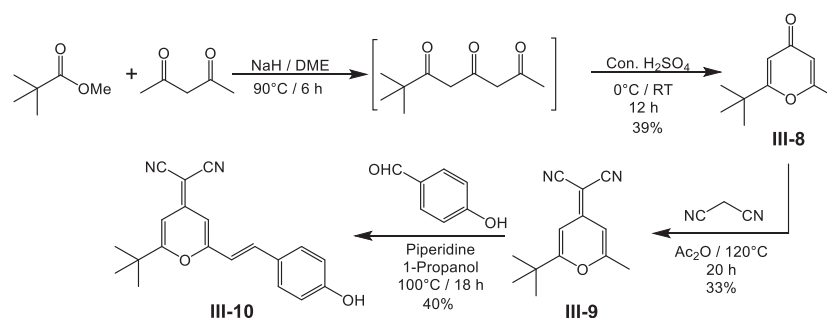
III.2.1 Synthesis of TPE-based glycoclusters

TPE-based glycoclusters containing two monosaccharides was started from dipropargyl TPE compound **II-8**. Through “click” reaction, acetyl protected galactose or glucose was decorated on TPE cores under microwave (Scheme 3). To avoid Cu metal ion interfering in biological assay, the purification should remove residual copper ions by using EDTA solution during aqueous extraction workup. Then TPE-based glycoclusters **III-2a,b** was deprotected in MeOH solution with Et₃N to obtain final products **III-3a,b**. TPE-based glycoclusters containing four monosaccharides **III-5a-d** are similarly^[183]. As a negative control, mono-azido-triethyleneglycol **III-6** was conjugated with tetrapropargyl-TPE core **III-4** to afford compound **III-7** with TEG linkers.



Scheme 3: Synthesis of TPE-based glycoclusters and a negative control compound.

III.2.2 Synthesis of DCM probes

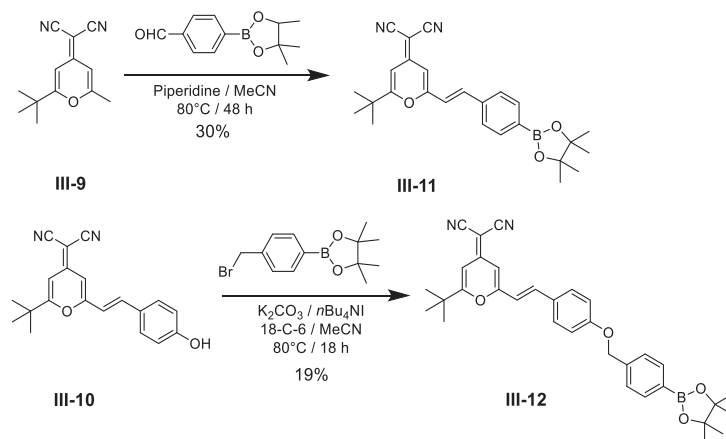


Scheme 4: Synthesis scheme of hydroxyl DCM dye

DCM dyes synthesis was started from 2,6-dimethyl-4*H*-pyran-4-one to obtain two active methyl positions for further symmetrical modifications. In our project, blocking one side of the 2,6-dimethylpyranone to synthesize the desired monofunctionalized DCM core was required. Hence, methyl pivalate and 2,4-pentanedione were used as starting materials to synthesize compound **III-**

8 with tert-butyl blocking one side of the pyranone. Then malononitrile was condensed in a Knoevenagel reaction generated compound **III-9**. Aldolization with 4-hydroxybenzaldehyde afforded the DCM dye **III-10** (Scheme 4).

DCM probe **III-11** was synthesized from compound **III-9** and 4-formylphenylboronic acid pinacol ester in CH₃CN piperidine. 4-Bromomethylphenylboronic acid pinacol ester was substituted on hydroxyl DCM dye (**III-10**) catalysed by K₂CO₃ and tetrabutylammonium(*n*-Bu₄NI) in refluxing CH₃CN. Adding 18-crown-6 in the mixture could increase reactivity through detection of the K⁺ cation (Scheme 5).



Scheme 5: Synthesis scheme of two DCM-based probes.

III.3 Self-assembly of glyco-probes and detection of ONOO⁻

In this section, the fluorescence data of two DCM probes (**III-11** and **III-12**) were discussed including optical variation after conjugating with TPE-based glycoclusters and response to ONOO⁻. The water-solubility of TPE glycoclusters with different monosaccharides and further ASGPr recognition in biological assay prompted us to select TPE-glycoclusters decorated with two or four galactoses. In this section, the TPE2S was **III-3a** decorated with two galactosides, and TPE4S was **III-5a** decorated with four galactosides.

III.3.1 Detection of ONOO⁻ using DCM probes

Even though the DCM probes **III-11** and **III-12** have several heteroatoms, the major part of their structures is still highly hydrophobic. Hence, 20% MeCN was required in PBS buffer to dissolve the probes in aqueous solution (Fig. 5).

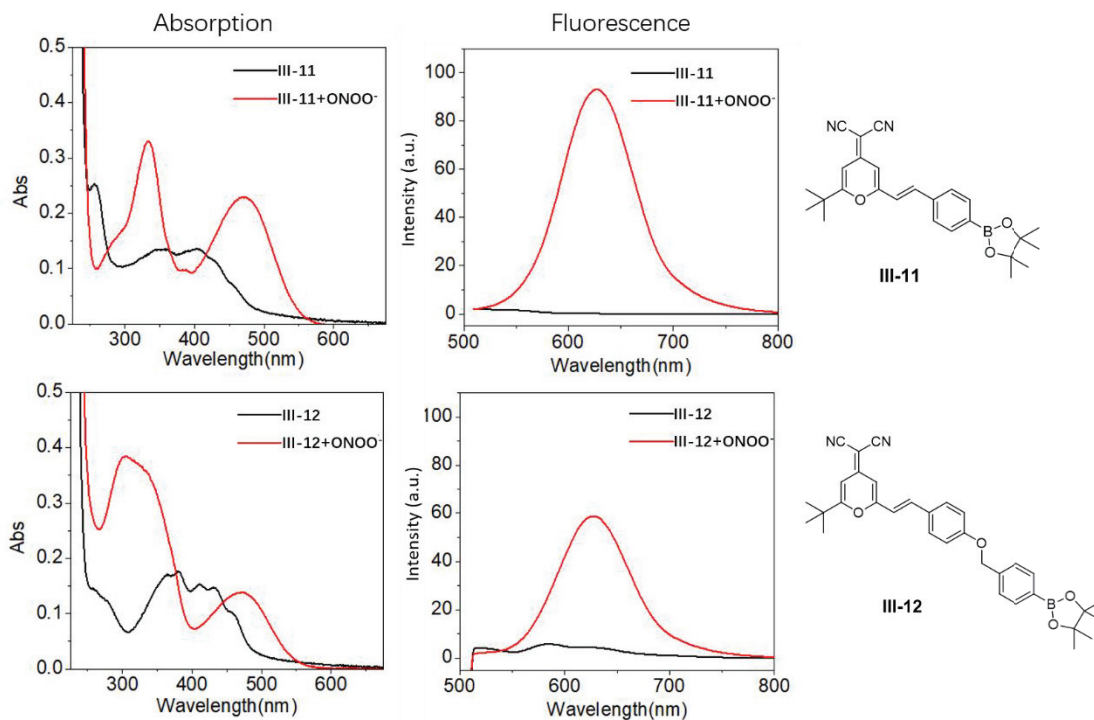


Figure 5: UV absorption and fluorescence emission changes of **III-11** (40 μM) and **III-12** (40 μM) upon addition of ONOO^- (excess) in PBS buffer with 20% MeCN.

After addition of ONOO^- , the maximum absorption wavelength of both probes were red-shifted. Two newly formed absorption peaks (red line) replacing initial absorption peaks (black line) illustrated that the distribution of electrons was changed after reaction with ONOO^- . Fluorescence emission intensity was increased as expected after exposition to ONOO^- . The maximum absorption wavelength of **III-11** was red-shifted from 405 nm to 480 nm and a fluorescence emission peak was generated at 625 nm (Table 1). Similarly, the maximum absorption wavelength of **III-12** was red-shifted from 435 nm to 480 nm and fluorescence emission peak was generated at 625 nm. For probe **III-12**, PET effect didn't quench fluorescence sufficiently resulting in higher basic fluorescence intensity and weaker fluorescence enhancement compared with **III-11**.

Table 1: Comparison of λ_{ex} , λ_{em} , stokes shift and quantum yields for probes **III-11** (10 μM) and **III-12** (10 μM) before and after adding ONOO^- in PBS + 20% MeCN

| | λ_{ex} (nm) | λ_{em} (nm) | Stokes shift (nm) | Quantum yield (Φ) |
|--------------------------------|----------------------------|----------------------------|-------------------|--------------------------|
| III-11 | 405 | 550 | 145 | 0.001 (470 nm) |
| III-11+ONOO⁻ | 470 | 625 | 155 | 0.111 (470 nm) |
| III-12 | 435 | 580 | 145 | 0.008 (480 nm) |
| III-12+ONOO⁻ | 480 | 625 | 145 | 0.106 (480 nm) |

Nevertheless, 20% MeCN in PBS buffer is not suitable for applications in biological system. Hence, we measured fluorescence variations of both probes in PBS buffer without any organic solvent (Fig. 6). Minor and unstable signal variations were obtained in pure water after adding ONOO^- . Poor water-solubility leading to quenching of fluorescence by ACQ effect, or low reactivity of probes with ONOO^- in aqueous buffer were speculated as two main reasons. Therefore, mass

spectrometry analysis of mixtures of probes with ONOO^- indicated the presence of compound **III-10** as a proof of proper reactivity of probes with ONOO^- . The resulting restricted fluorescence signal was therefore due to the ACQ effect observed for compound **III-10**. Next, we measured the fluorescence intensity variations of probe **III-12** (10 μM) before and after adding ONOO^- in PBS buffer with different ratio of MeCN. Fluorescence intensity was persistently decaying with H_2O portion increasing in the presence of ONOO^- . ACQ effect almost quenched fluorescence in 100% PBS buffer even though probe **III-12** had been switched-on fluorescence through DCM dye generation.

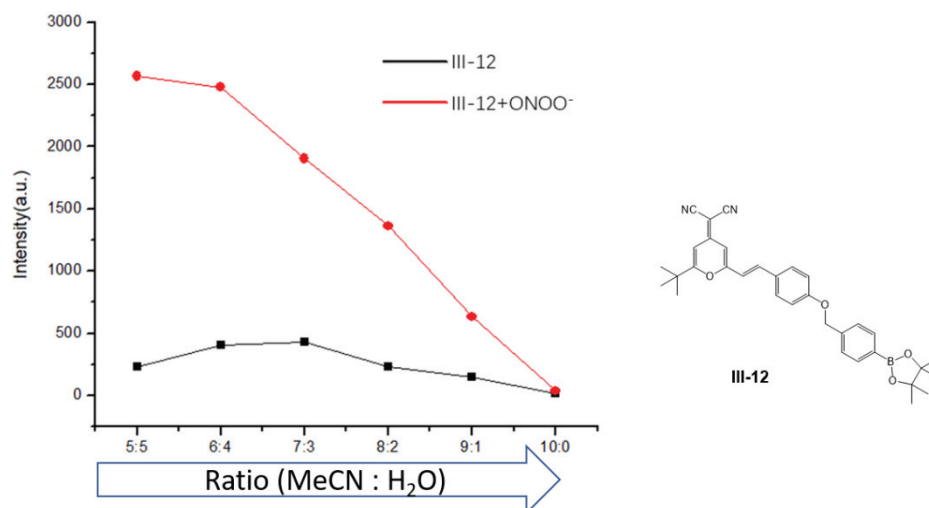
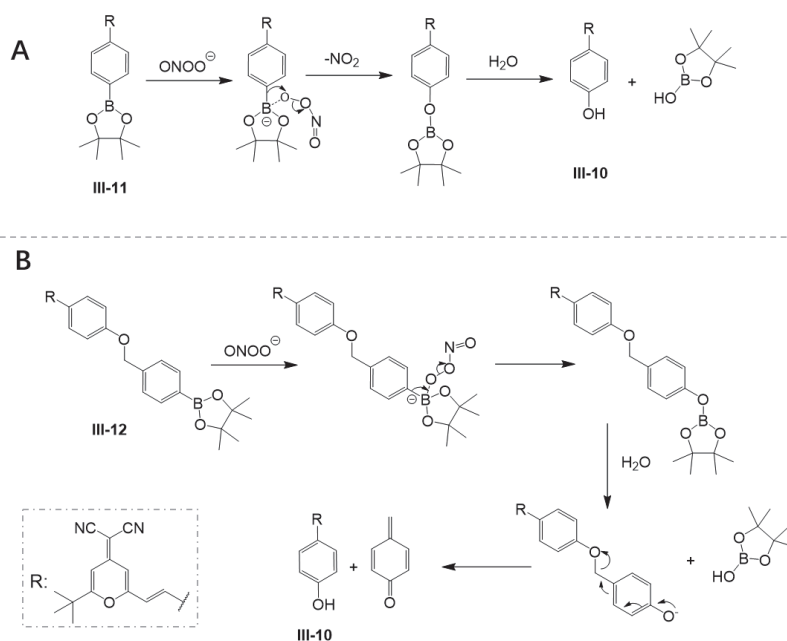


Figure 6: ACQ effect decayed fluorescence intensity after **III-12** responding to ONOO^- in solution with increasing H_2O portion.

III.3.2 Analysis of the mechanism of DCM probes (**III-11** and **12**) for ONOO^- detection



Scheme 6: Mechanism of DCM probes (A) **III-11** and (B) **III-12** for ONOO^- detection.

The mechanisms of DCM probes (**III-11**, **12**) for detecting ONOO⁻ were speculated and shown in Scheme 6^[206]. For probes **III-11**, the electron-poor boron atom was electrophilic enough to allow condensation with the negative oxygen atom on peroxyxynitrite. Rearrangement to the borate with loss of nitrite and further hydrolysis afforded the desired phenol **III-10**. In this process, fluorescence emission was recovered through ICT effect.

The mechanism of probe **III-12** was different from **III-11**, which fluorescence was quenched by PET effect from phenyl boronic acid pinacol ester. After generating the similar borate and hydrolysis to the intermediate phenol, spontaneous elimination of quinone methide afforded the desired phenol **III-10**. The corresponding mass peak at $m/z = 339$ certified **III-10** after DCM probes had been exposed to ONOO⁻ in PBS buffer with 20% MeCN. HPLC analysis also indicated that probes **III-11** and **III-12** are readily converted into DCM phenolic dye **III-10** after addition of ONOO⁻ (Fig. 7).

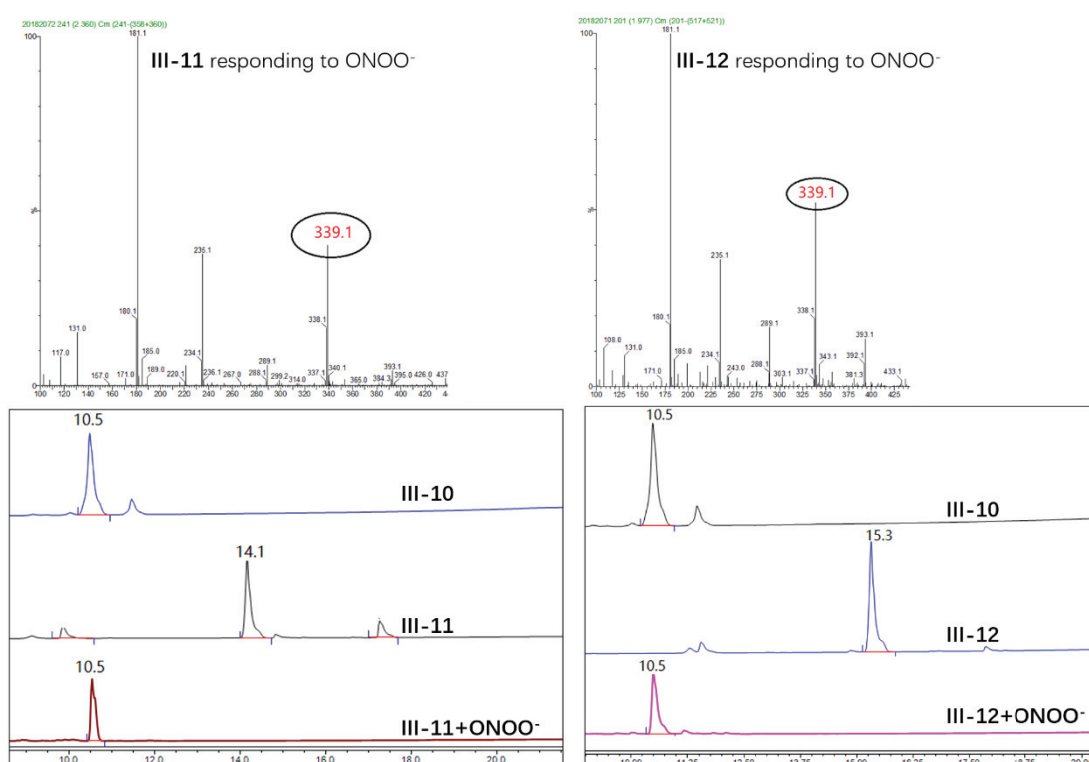


Figure 7: (Top) mass spectrometry and (bottom) HPLC analyses of DCM probes (**III-11** and **III-12**) upon addition of ONOO⁻.

III.3.3 Glycoclusters selection for perfecting water-solubility of DCM probes

In our previous studies^[168], PDI-based glycoclusters (PDI) have been synthesized and displayed sufficient water-solubility and high affinity for DCM dyes. In a similar approach, TPE-based glycoclusters (TPE2S, **III-3a**) having a central hydrophobic core would self-assemble in water into aggregate with DCM probe inside to promote its solubility. Hence, DCM probe (**III-12**, 10 μM) was mixed with two glycoclusters (100 μM) based on PDI or TPE core in PBS buffer before adding ONOO⁻ (Fig. 8).

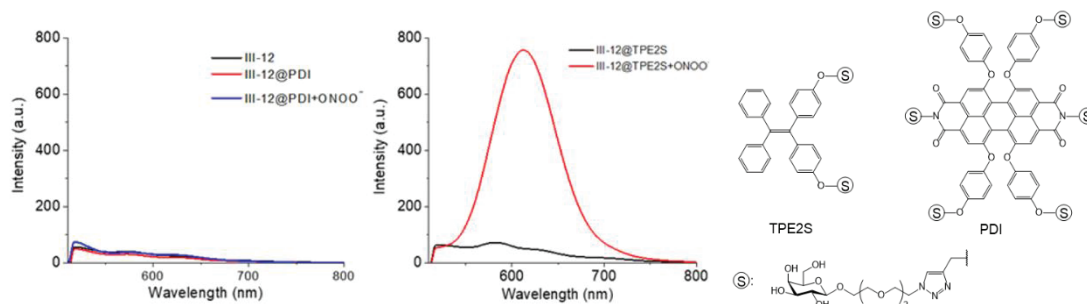


Figure 8: PDI-based and TPE-based glycoclusters self-assembled with **III-12** for ONOO⁻ response in PBS buffer.

In our PDI study^[168], we have demonstrated that the PDI glycocluster could self-assemble with the DCM dye to generate a glyco-dot and also allow cell penetration and more importantly disruption of these glyco-dots to release the DCM dye and trigger the turn-on fluorescence. The same PDI glycocluster with DCM probe **III-12** did self-assemble into glyco-dots, then addition of ONOO⁻ did trigger the formation of **III-10**, but the DCM dye did not escape from the PDI-based glycoclusters since no emission could be observed (Fig. 8 left). On the contrary, TPE2S glycocluster allowed the formation of glyco-dots with DCM dye **III-12** and addition of ONOO⁻ triggered the disruption of these aggregated since a strong emission was observed due to DCM phenolic dye **III-10** (Fig. 13 center). TPE2S glycocluster would prevent the ACQ effect of probe **III-10** and therefore promote the detection of ONOO⁻ analyte. Based on these positive results, we changed the addition sequence of the three molecules (**III-12**, TPE2S, ONOO⁻) and monitored fluorescence variations of TPE ($\lambda_{\text{ex}} = 320 \text{ nm}$) and DCM ($\lambda_{\text{ex}} = 480 \text{ nm}$) (Fig. 9).

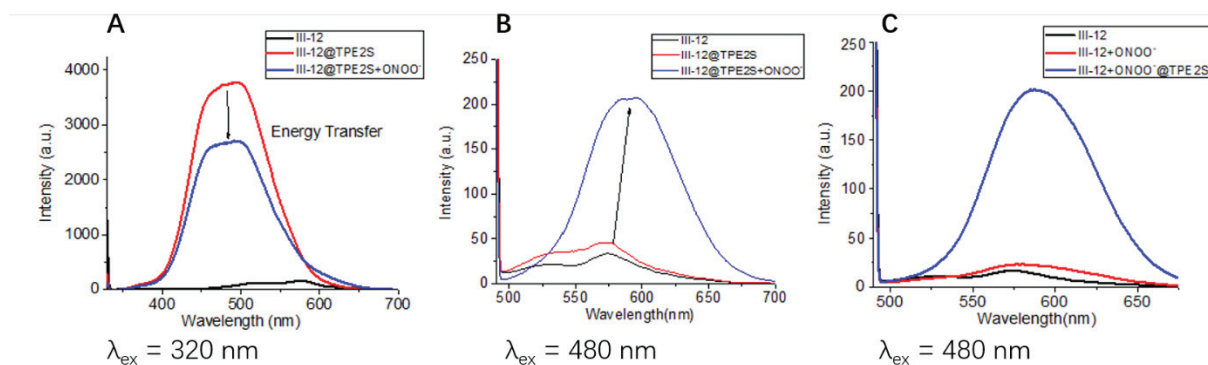


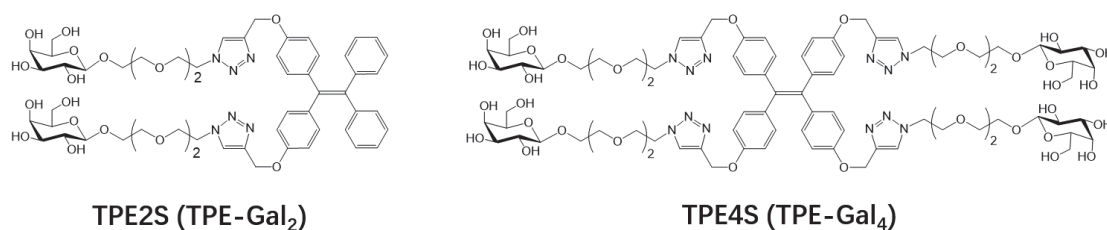
Figure 9: Fluorescence variations in different addition sequence: (A) **III-12**, TPE2S and ONOO⁻, $\lambda_{\text{ex}} = 320 \text{ nm}$; (B) **III-12**, TPE2S and ONOO⁻, $\lambda_{\text{ex}} = 480 \text{ nm}$; (c) **III-12**, ONOO⁻ and TPE2S, $\lambda_{\text{ex}} = 480 \text{ nm}$.

Intense fluorescence emission appeared at 490 nm after addition of TPE2S (100 μM) in a PBS solution of **III-12** (10 μM) with excitation wavelength at 320 nm. The signal intensity decayed after adding ONOO⁻ (Fig. 9A) and we speculated that ONOO⁻ partially oxidized the TPE structure, or emission from TPE was absorbed by the DCM dye in a FRET process. In order to prove our speculation, the excitation wavelength was changed to 480 nm to monitor the DCM fluorescence variations (Fig. 9B). Compared with the low intensity of DCM dye **III-12** (black line) in PBS buffer, TPE2S addition enhanced fluorescence intensity since intermolecular self-assembly improved solubility and impeded ACQ effect. Fluorescence enhancement of the DCM signal was observed

with a short red-shift after adding ONOO^- (Fig. 9B). These results demonstrated that the TPE2S glycoclusters could self-assemble with the DCM probe **III-12** and generate a slight increase of the fluorescence signal through partial inhibition of the ACQ effect in pure PBS buffer. Then we adjusted the addition sequence of each molecule by mixing **III-12** with ONOO^- , and then adding TPE2S in the solution. The small intensity enhancement before adding TPE2S could certify that probe **III-12** reacted with ONOO^- but emission was influenced by ACQ. Adding TPE2S increased the intensity of the fluorescence signal meaning that the glycoclusters TPE2S could self-assemble with DCM dye **III-10** (Fig. 9C).

III.3.4 Explore combination mode between TPE-glycoclusters and DCM probes

In this section, the combination of DCM probes **III-11** and **III-12** with TPE-based glycoclusters (TPE2S and TPE4S) in aqueous buffer were explored. For all the measurements *in vitro*, the TPE2S and TPE4S were the TPE core decorated with several galactosides (Scheme 7).



Scheme 7: The structure of TPE2S and TPE4S for fluorescence measurements *in vitro*.

III.3.4.1 Intermolecular interactions of DCM probes **III-11** and **III-12** with glycoclusters TPE2S and TPE4S

The fluorescence intensity variations were measured with increasing concentration of probes **III-11** (0 to 30 μM) and **III-12** (0 to 80 μM) in glycoclusters TPE2S and TPE4S (20 μM) in PBS solution with excitation wavelength at 320 nm (Fig. 10).

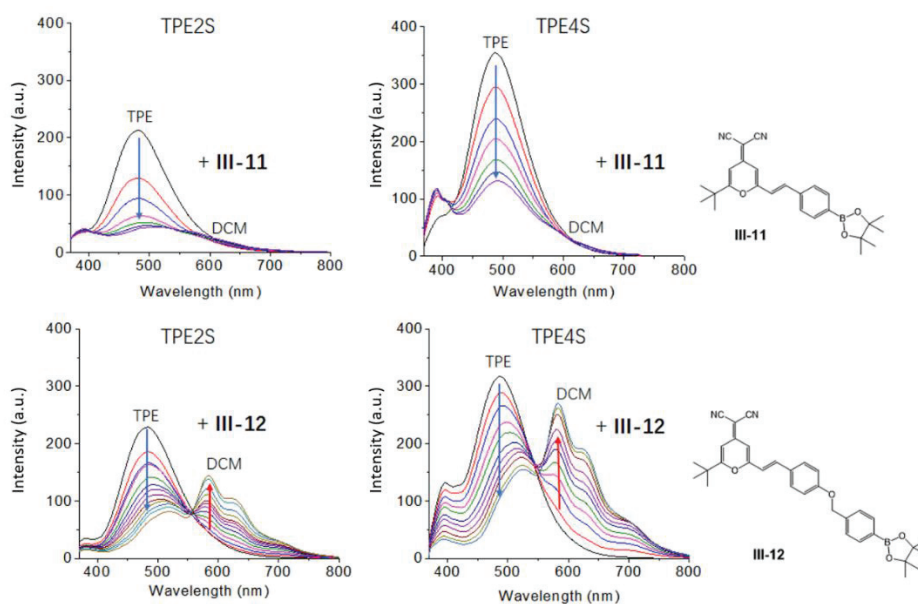


Figure 10: Fluorescence variation of addition of DCM probes **III-11** (0-30 μM) and **III-12** (0-80 μM) with TPE2S or TPE4S (20 μM) in PBS solution ($\lambda_{\text{ex}} = 320 \text{ nm}$).

The fluorescence emission of the two DCM probes were different after incubation with TPE-glycoclusters. TPE2S or TPE4S are emitting intense blue signal in their aggregated states even though they have been modified with monosaccharides. Probe **III-11** quenched the fluorescence of TPE when it was added in glycoclusters solution. But the emission of DCM at 600 nm did not appear as it could have been expected from receiving energy from TPE. Two possible pathways may explain this phenomenon: (i) The fluorescence switch of **III-11** was still quenched by the boronate moiety even though it could accept energy transfer from TPE glycoclusters. (ii) The distance between the two molecules should be close enough so that energy transfer could happen. However, the energy from TPE was released through nonradiative pathways but not through fluorescence emission. The fluorescence spectrum of **III-12** (Fig. 10, bottom) demonstrated that the fluorescence emission intensity of DCM probe at 600 nm was increasing when adding **III-12** in the mixture. Intramolecular PET effect didn't quench fluorescence of **III-12** completely so that the probe could absorb energy from TPE and then release its specific emission.

III.3.4.2 Intermolecular interaction of compound **III-10** with glycoclusters

We performed a titration of the two DCM probes **III-11** (0 to 30 μM) and **III-12** (0 to 50 μM) into a solution of a TPE-based glycoclusters (TPE2S or TPE4S, 20 μM) and excess ONOO⁻ (100 μM) to further explore their self-assembly mode. After reaction with ONOO⁻, both probes were oxidized to the phenolic DCM **III-10**. Hence, this experiment would investigate the association modes between glycoclusters and DCM derivatives.

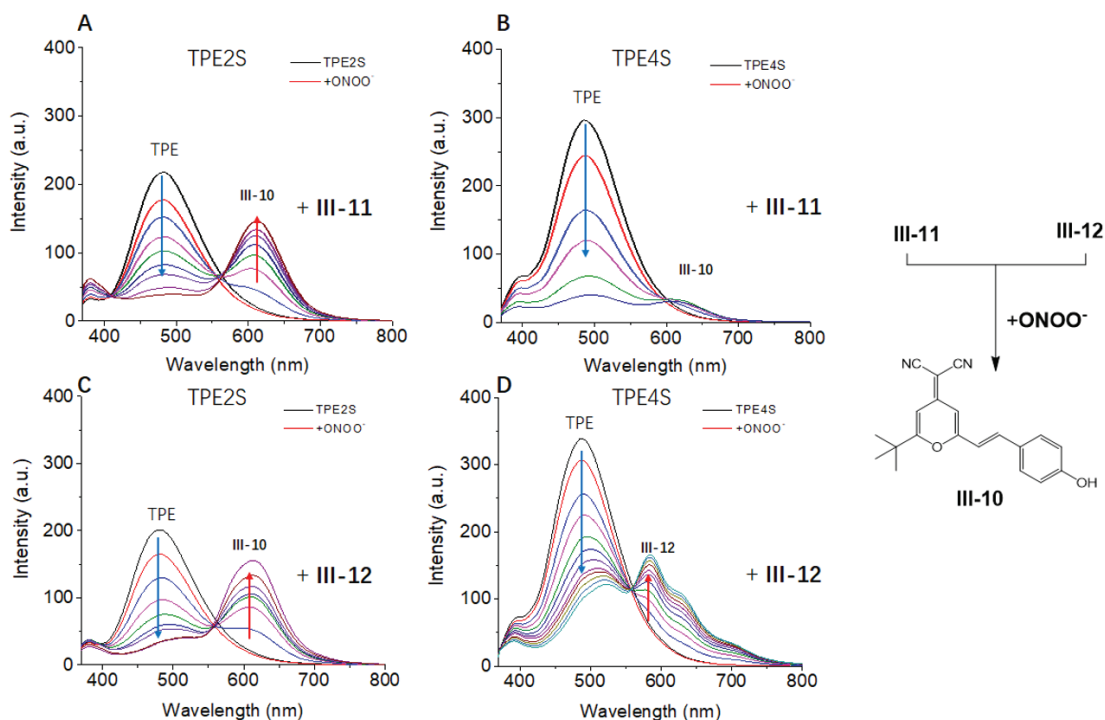


Figure 11: Fluorescence variation of adding DCM probes **III-11** (0-30 μ M) and **III-12** (0-50 μ M) in TPE2S or TPE4S (20 μ M) PBS solution mixed with excess ONOO⁻ (100 μ M) (λ_{ex} = 320 nm).

DCM **III-10** was the common product after probes **III-11** and **III-12** reacted with ONOO⁻. So, the compound interacting with TPE-glycoclusters should be **III-10** which generated single fluorescence peak at 620 nm (λ_{ex} = 320 nm). With increasing the concentration of probes **III-11** (Fig. 11A) or **III-12** (Fig. 11C) in TPE2S solution with excess ONOO⁻, a ratiometric fluorescence signal was observed with emission intensity at 620 nm increasing along with blue emission decreasing at 490 nm. FRET phenomenon relationship observed between **III-10** and TPE2S indicated that the distance between the two molecules was close enough and that the two molecules were still in contact after reaction with ONOO⁻. But the complexes formed with TPE4S and each DCM probe displayed different fluorescence signal changes. After **III-11** was reacted with ONOO⁻, the newly generated **III-10** didn't emit fluorescence even though it received energy from TPE4S (Fig. 11B). This observation supposed that TPE4S could contain **III-10** in a smaller molecular volume in its hydrophobic core for a good energy transfer, but intermolecular FRET effect was observed in opposition to **III-11** conjugated with TPE4S for detection of ONOO⁻ (Fig. 10). **III-12** and TPE4S complex exhibiting FRET effect seemed to provide inconsistent results since the same product **III-10** generated from the **III-12** after reaction with ONOO⁻ should provide the same fluorescence signal as the TPE4S associated with **III-11** (Fig. 11B). But we thought this result was still correct because the red fluorescence with two peaks (Fig. 11D) was from unreacted **III-12** aggregating with TPE4S but not phenolic DCM probe **III-10**. This incomplete reactivity of DCM probe **III-12** towards ONOO⁻ was not observed with TPE2S (Fig. 11C) with the stronger fluorescence signal of **III-10** after conjugation with TPE2S overlapping the signal of unreacted **III-12**.

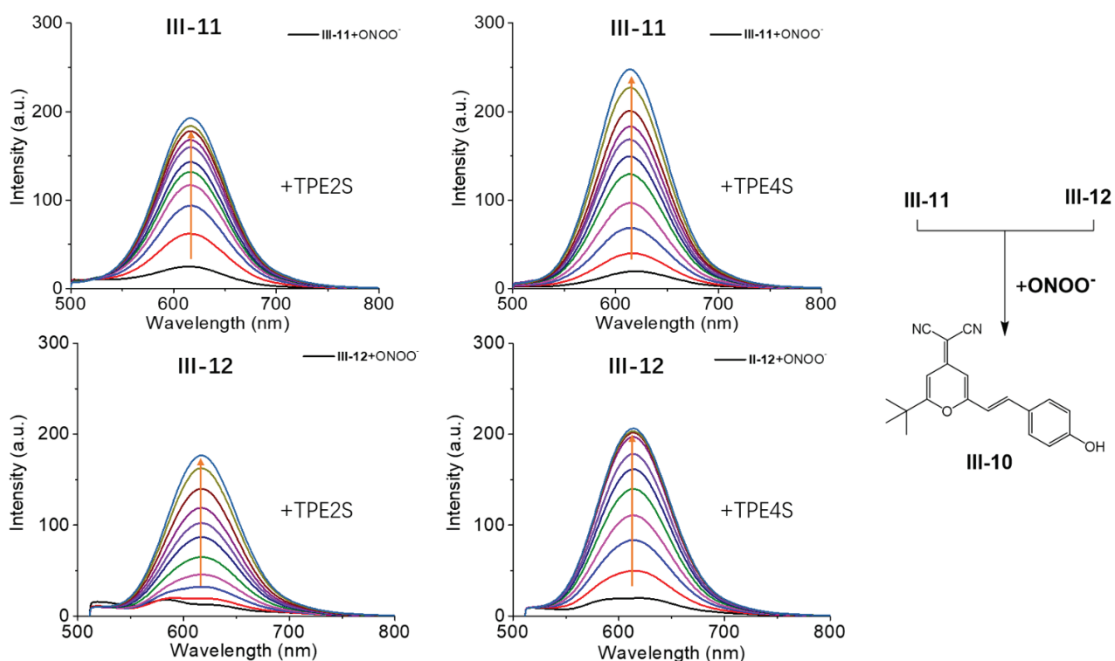


Figure 12: Fluorescence variation by adding TPE-glycolusters (0-200 μM) in DCM probes **III-11** and **III-12** (10 μM) solutions pre-mixed with ONOO^- (100 μM) ($\lambda_{\text{exc}} = 480 \text{ nm}$).

In order to verify that TPE-glycolusters could still interact with **III-10** and improve its fluorescence, we titrated TPE2S and TPE4S into the solutions of **III-11** or **III-12** pre-reacted with ONOO^- (Fig.12). DCM probes **III-11** and **III-12** were incubated with ONOO^- and the fluorescence of the generated compound **III-10** was quenched by ACQ effect in PBS solution. Following addition of TPE-glycolusters, DCM compound **III-10** emitted a strong fluorescence signal at 620 nm due to water-solubility improvement and inhibition of the ACQ effect. Higher concentration of glycolusters in buffer would construct more amphiphilic glyco-dots to contain DCM and promote intense fluorescence emission. We selected 150 μM as a suitable concentration of glycolusters for DCM conjugation in subsequent experiments. This fluorescence enhancement proved that TPE-glycolusters could aggregate and contain all the three DCM derivatives (**III-10**, **III-11** and **III-12**). The FRET effect depended on intermolecular distance and molecular size of probes and glycolusters (Table 2). At least, TPE-glycolusters (TPE2S and TPE4S) have excellent ability to interact with DCM probes for the detection of ONOO^- in PBS buffers.

Table 2: Combination between DCM probes and TPE-glycolusters

| | III-11 | III-12 | III-10 |
|-------|---------------|---------------|---------------|
| TPE2S | Aggregation | FRET | FRET |
| TPE4S | Aggregation | FRET | Aggregation |

Aggregation: TPE energy transfer but no emission from DCM excited at 320 nm. FRET: TPE energy transfer and DCM emitted fluorescence at $\sim 600 \text{ nm}$ when excited at 320 nm.

III.3.5 Size and shape variation of DCM probes after self-assembly with TPE-based glycolusters

In order to further verify that DCM probes could self-assemble with TPE-glycolusters occurred,

we measured molecule size changes and shape variations before and after self-assembly. To compare size changes of DCM probes, glycoclusters and self-assembled glyco-dots, dynamic light scattering (DLS) was a useful tool to observe the main diameter of each system.

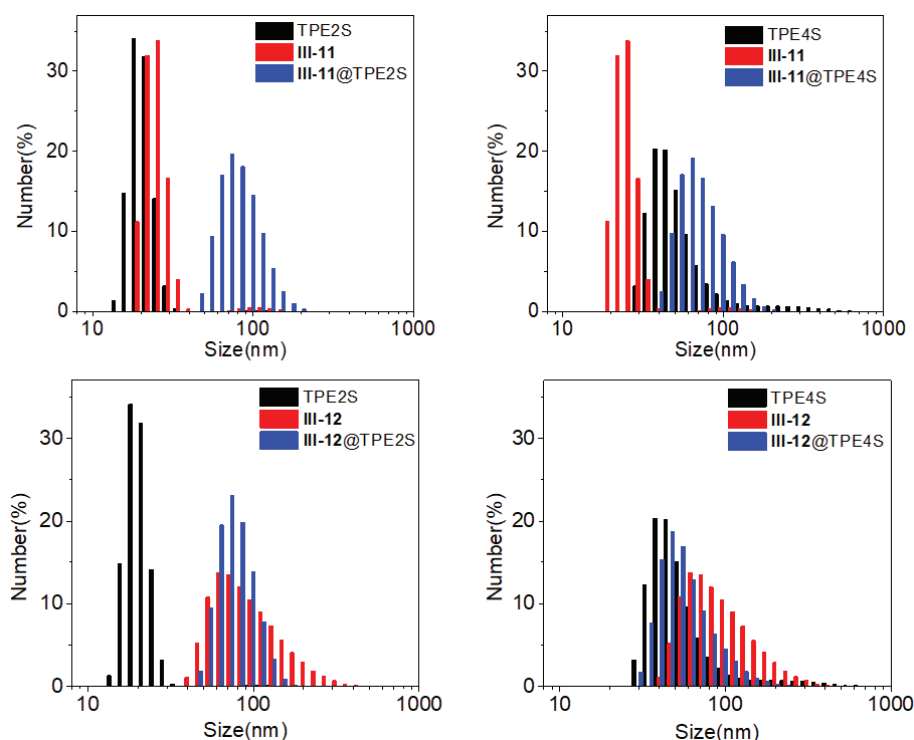


Figure 13: Aggregate size variation of DCM probes, TPE-glycoclusters and their complexes after self-assembly.

The size of TPE4S was larger than TPE2S due to two more monosaccharides decorated on the TPE core (Fig. 13). For the diameter of the DCM probes, **III-11** displayed around 10 nm molecular size, larger than the size of single molecules, which demonstrated that the hydrophobic probe was aggregated in aqueous solution. Probe **III-12** was displayed a larger size around 100 nm probably due to the extra phenyl ring on DCM dye increasing its hydrophobicity. After incubation of **III-11** with TPE2S or TPE4S, the novel size of the resulting glyco-dot was increased distinctly, and the small aggregates disappeared which indicated that the two molecules had been totally self-assembled together. The size of glyco-dots obtained from TPE2S and **III-12** was similar to the probes in solution. We supposed that TPE2S could dissolve the aggregate state of the DCM dye and then capture them in its hydrophobic core. The size of glyco-dot obtained from TPE4S and **III-12** certified our hypothesis indirectly with the observation of size shrinking after aggregation. Meanwhile, we speculated that DCM probes are indeed contained in hydrophobic TPE aggregate because the size of glyco-dot was slightly increased in comparison with the size of TPE4S.

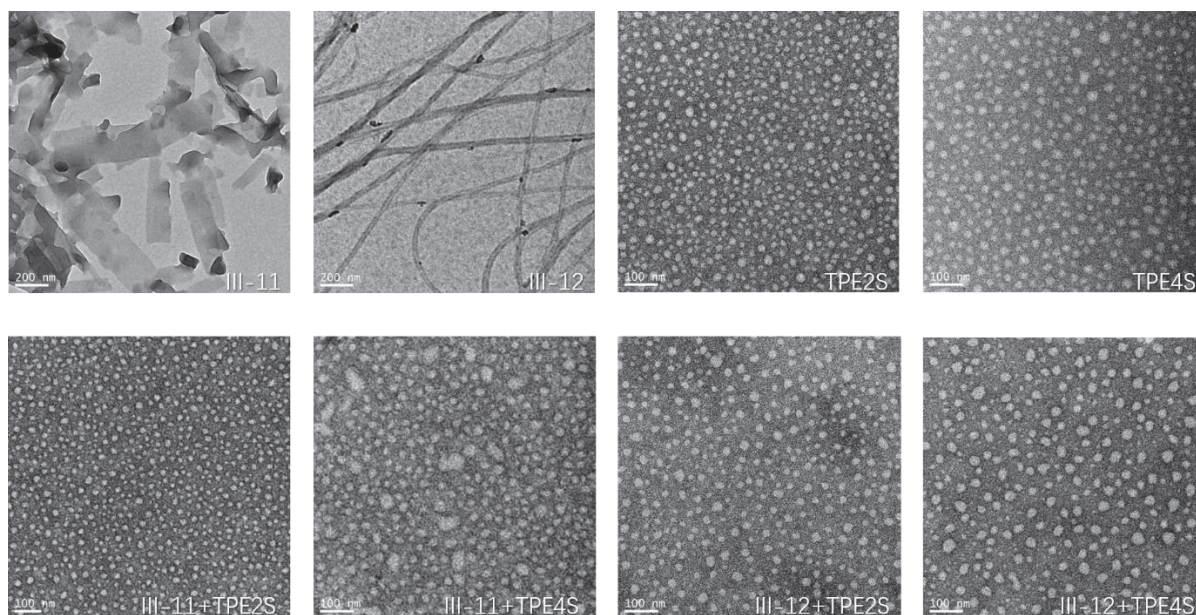


Figure 14: Aggregation of DCM probes, TPE-glycoclusters and their complexes after self-assembly obtained by TEM.

Even though structures were similar, the shapes of the two DCM probes were since **III-11** had a sheet shape while **III-12** displayed a filament structure. The shape of TPE4S aggregates was irregular and shape larger than for TPE2S. After self-assembly, all glyco-dots displayed similar appearance as glycoclusters. Nevertheless, the particular shape of the DCM probes was not demonstrating that DCM probes were associated to TPE aggregation (Fig. 14). Hence, DLS and TEM data illustrated that DCM probes could self-assemble with TPE-glycoclusters in aqueous solution, and TPE-glycoclusters could play the same role as organic solvents (20% MeCN was required for proper solubility) to improve water-solubility of DCM probes (Fig. 15). After addition of ONOO^- , the solution color of **III-11** was darker than **III-12**, which indicated that the reactivity of **III-11** was higher than **III-12** whether TPE-glycocluster or organic solvent improving the solubility and impeding the ACQ effect.

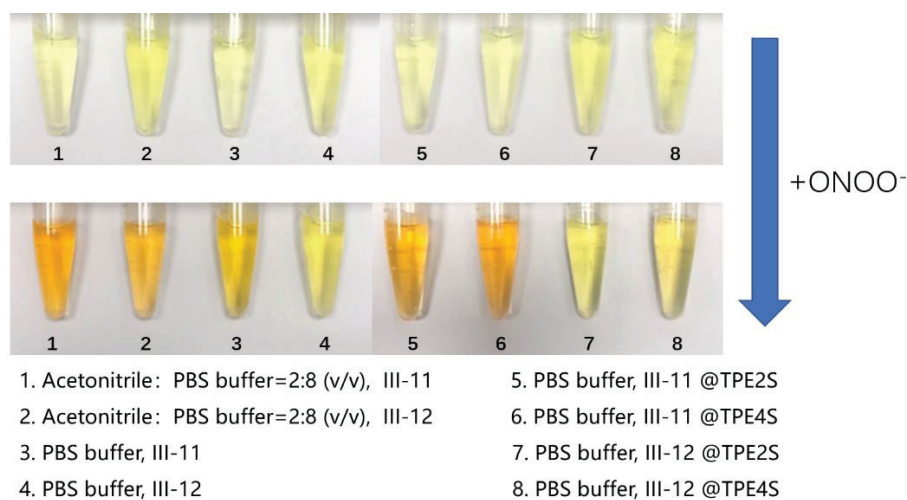


Figure 15: Solution colour comparisons in different condition before or after adding ONOO^- .

III.3.6 Influence of time on fluorescence intensity

Detection of ONOO^- require reaching reaction completion rapidly within a few minutes. Especially since ONOO^- is decomposed quickly and displays short lifetime in biological systems. Rapid fluorescence detection could provide accurate measurements. Hence, excess ONOO^- ($150 \mu\text{M}$)^[206] was generated from reaction of sodium nitrite with hydrogen peroxide then added in a solution of DCM probes ($10 \mu\text{M}$) and TPE-glycoclusters ($150 \mu\text{M}$) in PBS buffer. Fluorescence intensity was measured over time until fluorescence signal was reaching a maximum (Fig. 16).

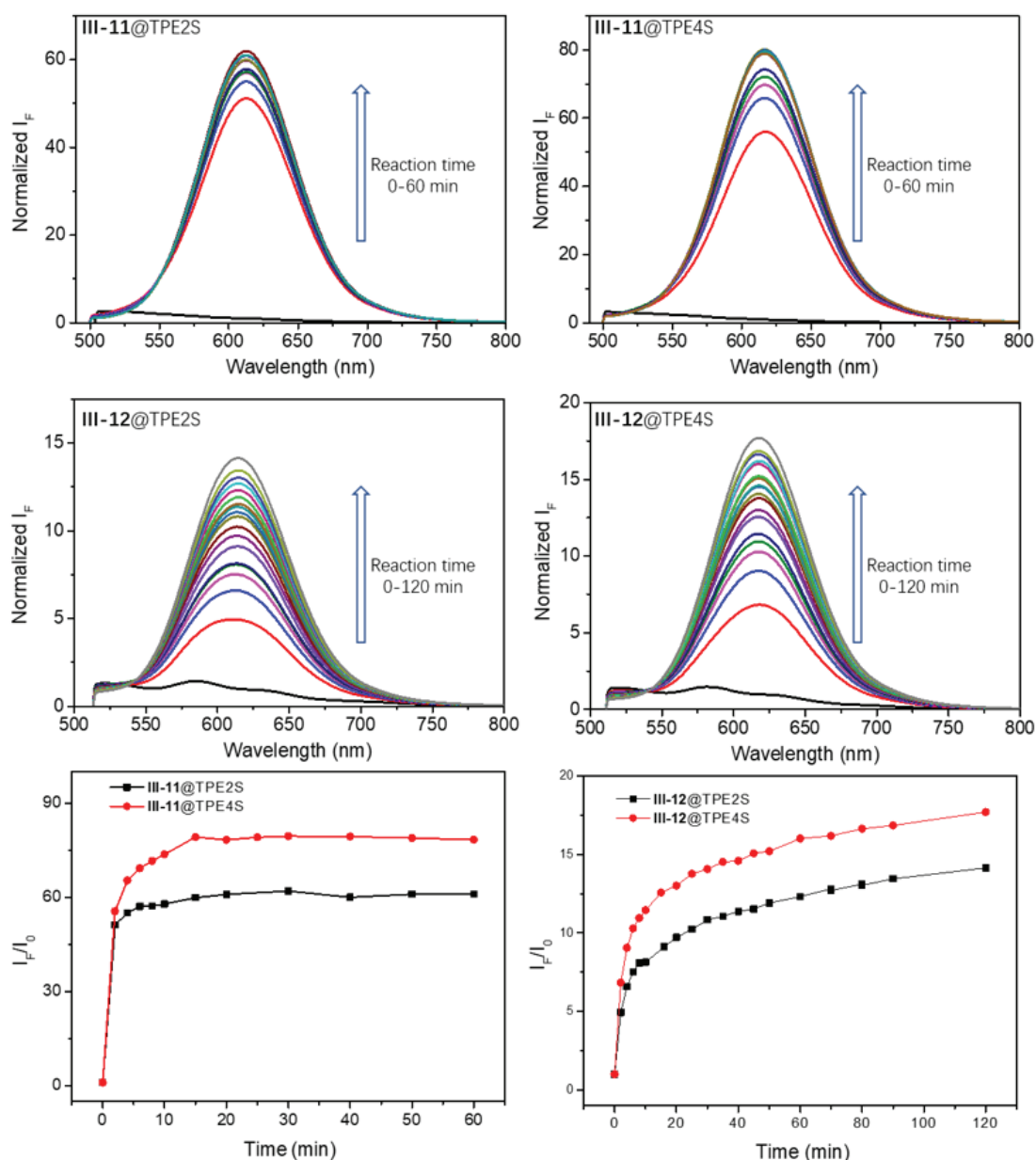


Figure 16: Fluorescence enhancement for ONOO^- detection as a function of time. DCM probes ($10 \mu\text{M}$), TPE-glycoclusters ($150 \mu\text{M}$), ONOO^- ($150 \mu\text{M}$) in PBS buffer ($\lambda_{\text{ex}} = 480 \text{ nm}$).

Glyco-dots obtained from DCM probes self-assembled with TPE-glycoclusters exhibited a fluorescence “turn-on” response to ONOO^- in PBS aqueous buffer. Excess ONOO^- ensured that all probes could react and release maximal signal intensity. Obvious fluorescence enhancements were

observed after addition of ONOO^- with increasing time. The DCM probe **III-11** displayed instantaneous fluorescence emission with a rapid signal enhancement and maximal signal intensity (60-80 a.u.) with 2 minutes. The DCM probe **III-12** showed similar results as **III-11** but with longer time to reach maximum and with lower fluorescence intensity (15-18 a.u.). The DCM probe **III-11** would generate the fluorescent dye **III-10** by a single “synthetic” step while probe **III-12** would require two mechanistic steps with the elimination of quinone methide. This second step might be slower in the case of **III-12** and this would be a plausible explanation for the lower intensity and longer reaction time observed for **III-12** vs **III-11**.

Also, TPE4S performed better than TPE2S in terms of fluorescence improvement leading to TPE4S / **III-11** as the best combination for such glyco-dots.

III.3.7 ROS and RNS selectivity of series glyco-dots

Reactive oxygen species (ROS) and reactive nitrogen species (RNS) participate in intracellular metabolism and influence physiological processes. Some reported probes were reacting with H_2O_2 , ClO^- , NO and other common ROS or RNS when responding to ONOO^- ^[203]. Hence, selectivity for different ROS and RNS is another requirement to evaluate probes for ONOO^- detection. Different ROS / RNS (150 μM) were added in solutions of DCM probes (10 μM) and TPE-glycoclusters (150 μM), and stirred during 10 min (determined as an optimal reaction time from Fig. 16).

All glyco-probes exhibited high emission intensity enhancement at 620 nm compared with no signal change for other ROS or RNS. These results demonstrated that glyco-dots self-assembled from DCM probes and TPE-glycoclusters could detect ONOO^- selectivity among another ROS and RNS.

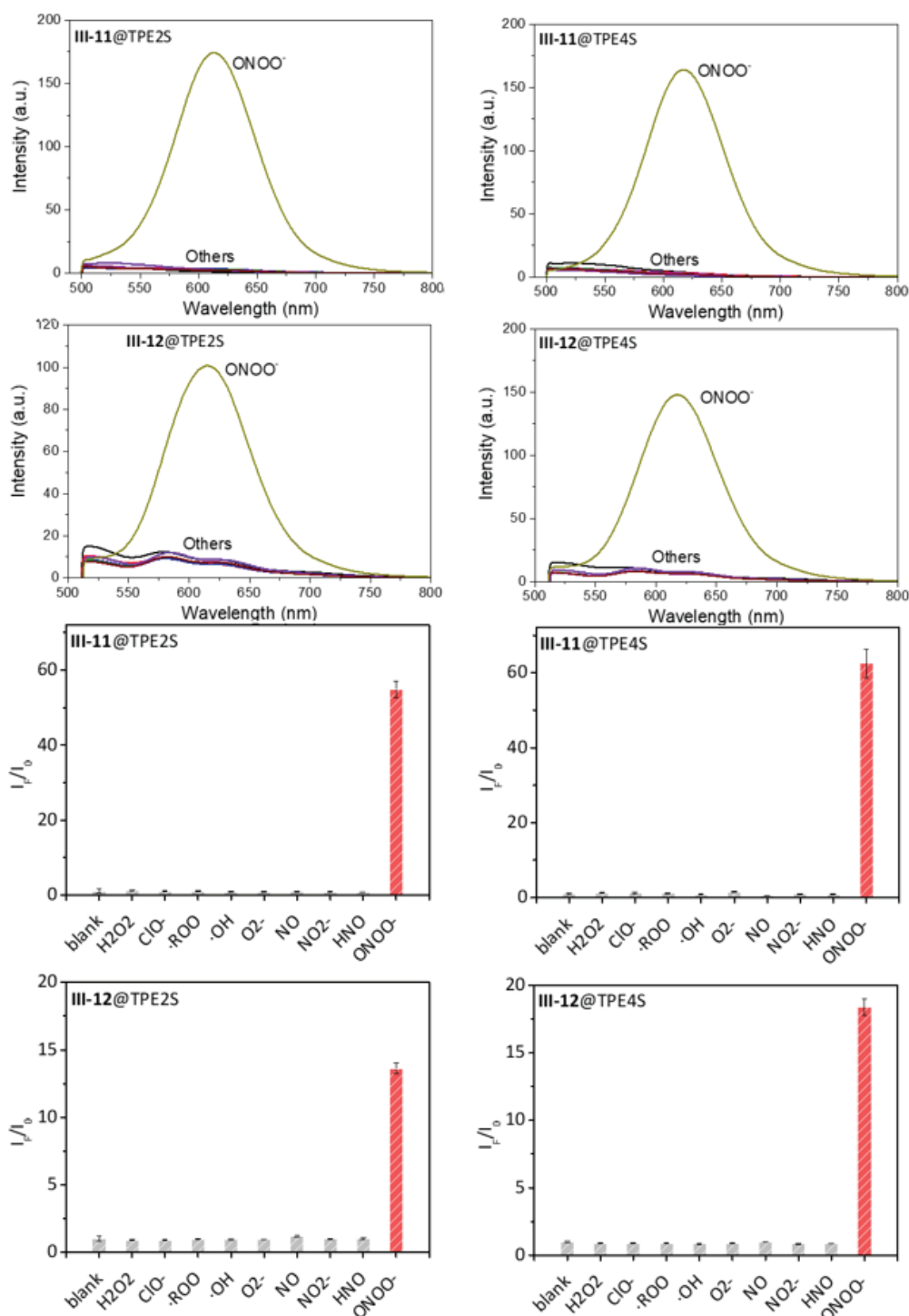


Figure 17: Selectivity of glyco-dots self-assembled from DCM probes (10 μM) and TPE-glycoclusters (150 μM) for ROS and RNS (150 μM) stirred 10 min in PBS buffer ($\lambda_{\text{ex}} = 480 \text{ nm}$). Please see the Experimental Section for more details.

III.3.8 ONOO $^-$ titration

Now that glyco-dots performed excellent properties for ONOO $^-$ detection, the concentration relationship between glyco-dots and ONOO $^-$ was studied. Hence, different concentrations of ONOO $^-$ were added in glyco-dots solution (Fig. 18).

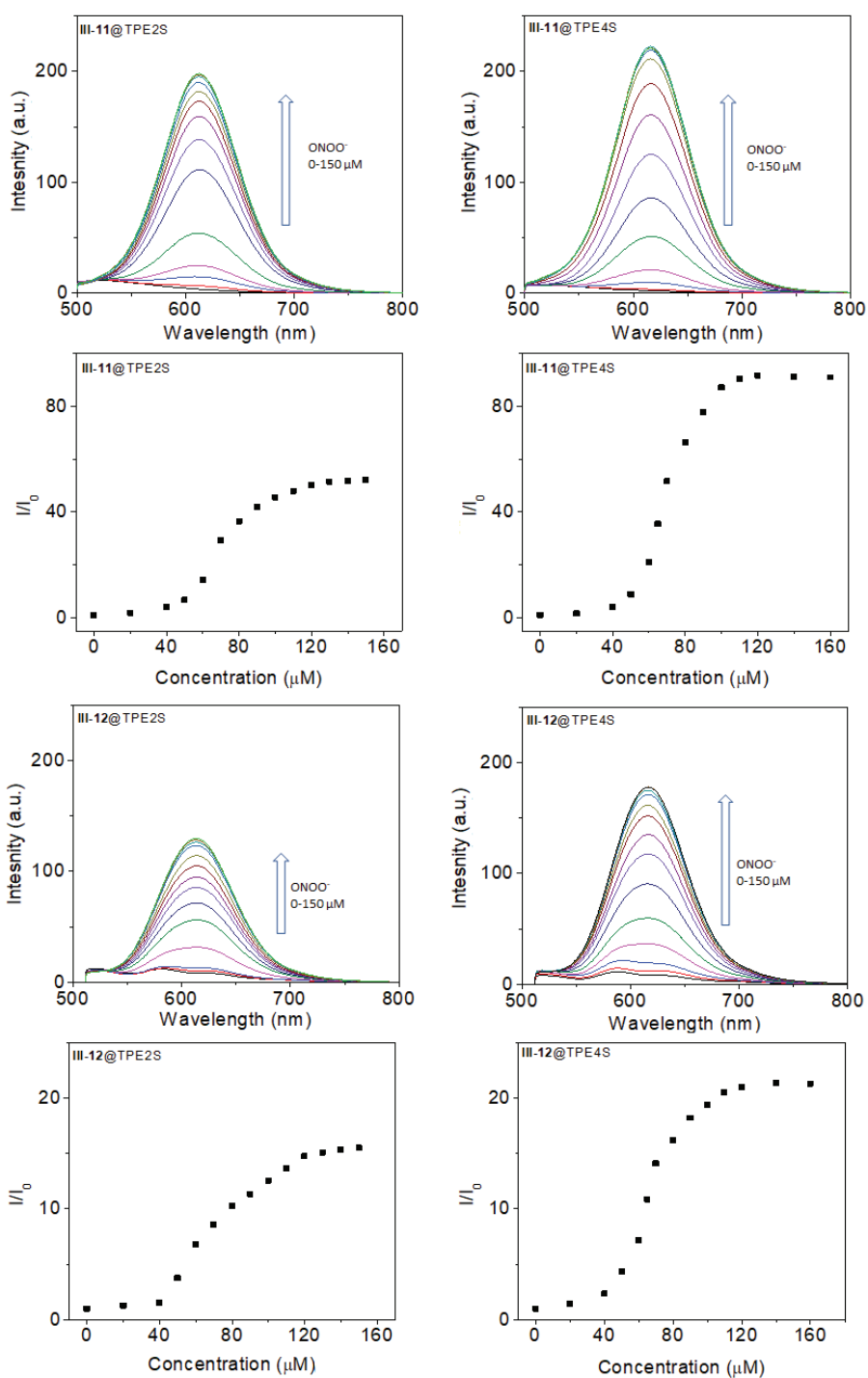


Figure 18: Fluorescence emission enhanced with increasing ONOO⁻ concentration. DCM probes (10 μM), TPE-glyco-clusters (150 μM) in PBS buffer ($\lambda_{\text{ex}} = 480 \text{ nm}$). Reaction time (10 min).

With ONOO⁻ concentration increasing, the fluorescence emission of glyco-dots were “turn-on” and the increase was monitored. Again, the TPE4S / III-11 association provide the best results in terms of maximal fluorescence signal. TPE4S or TPE2S did not influence the concentration of ONOO⁻ required to reach the maximum signal (nearly 120 μM in all cases). The only difference between the glyco-clusters would rely on the shaper increase in fluorescence signal for TPE4S versus

TPE2S. At low ONOO⁻ levels, almost no fluorescence signal could be detected because the ONOO⁻ pieces had a very low probability to encounter DCM probes in solution as these are embedded in a TPE-based aggregate. Then, at nearly 40 μM concentration of ONOO⁻, the reaction can now occur and trigger a sharp fluorescence signal increase for the next higher concentrations up to ~120 μM and then reaching saturation (>120 μM) of complete reaction of the DCM probes.

III.4 Detection of ONOO⁻ in biological systems

Glyco-dots exhibited excellent fluorescence properties for ONOO⁻ detection at the molecular level. Multiple monosaccharide copies conjugated on the TPE core were expected not only to increase water-solubility, but also to target receptors on the cell membrane and deliver DCM probes into cells. Hence, cell imaging experiments were performed to evaluate glyco-dots for biological application in cells.

III.4.1 Series glyco-dots responding ONOO⁻ in cells

In order to measure the fluorescence response of DCM probes and the delivery ability of TPE-based glycoclusters, the glyco-dots self-assembled from galactosylated TPE-based glycocluster TPE2S (**III-3a**) and TPE4S (**III-5a**) were incubated with SIN-1 (ONOO⁻ initiator) with HepG2 cells. Such galactosylated glyco-dots would interact with HepG2 cells through binding to the ASGPr.

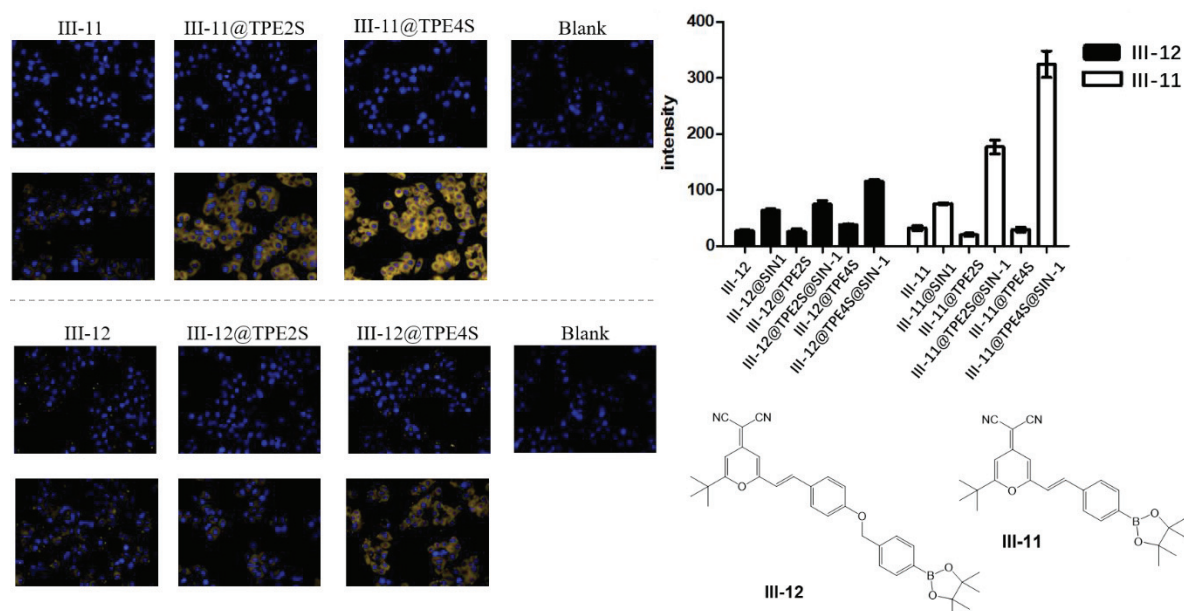


Figure 19: Glyco-dots self-assembled with DCM probes (**III-11**, **III-12**, 10 μM) and TPE-glycoclusters (**III-3a**, **III-5a**, 150 μM) for intracellular ONOO⁻ detection and HepG2 cells imaging.

The samples without SIN-1 incubation emitted weak basic fluorescence signal similar as blank samples, which illustrated that DCM probes did not emit fluorescence due to boronate moiety blocking the ICT effect and no interference from others intracellular biomolecules could be observed (Fig. 24). The samples incubated with SIN-1 with glyco-dots exhibited a fluorescence “turn-on” state

to release yellow emission in cells. From cell imaging pictures, the yellow fluorescence emission didn't overlap with the blue fluorescence emitted from the cell nucleus indicated that DCM probes was remained in the cytoplasm. Probe **III-11** had twice higher fluorescence signal response to ONOO⁻ than probe **III-12** as previously observed in HepG2 cell. The fluorescence detection required incubation with TPE-based glycoclusters. TPE4S performed better than TPE2S in terms of fluorescence improvement ability also similarly observed *in vitro*. **III-11** was performing better than **III-12** and was therefore used in the next experiments.

III.4.2 Cytotoxicity of self-assembled glyco-probes

Same fluorophores have high cytotoxicity and influence cell viability. Hence, cytotoxicity is an important factor to evaluate the further biological applications for experiments *in vivo*. High concentration of glyco-dots might influence bioactivity and viability of cells. Here, the four glyco-dots conjugated from two DCM probes (**III-11** and **III-12**) and two TPE-based glycoclusters (TPE2S and TPE4S) with different concentrations were incubated with HepG2 cells during 24 h and 48 h before measuring cell viability (Fig. 20).

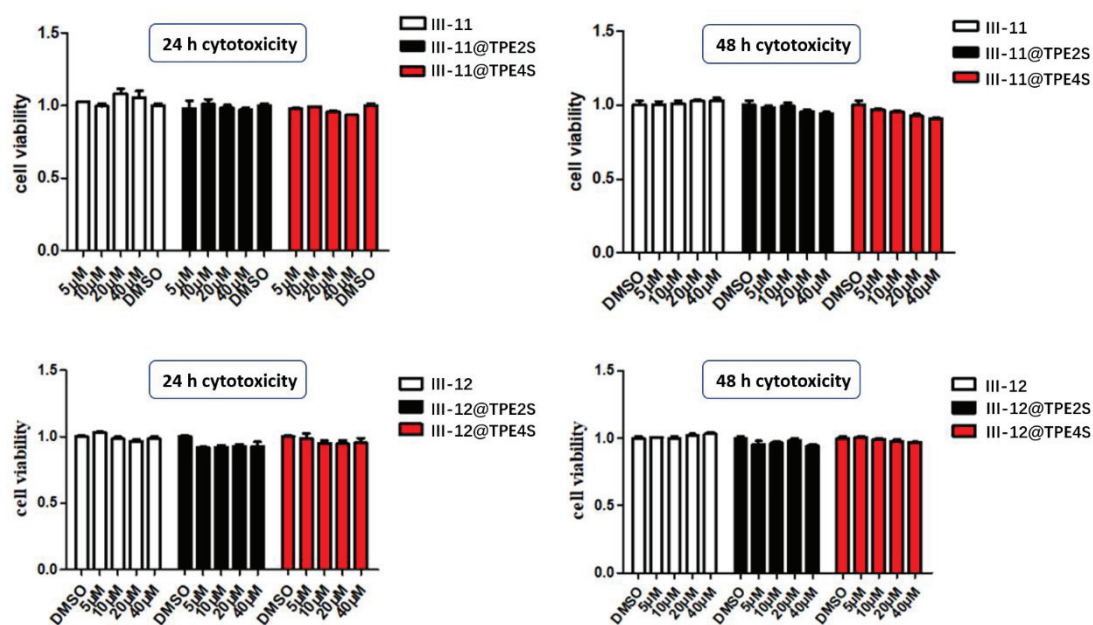


Figure 20: Cytotoxicity of glyco-dots with different concentrations during 24 h or 48 h for HepG2 cells.

The results showed that DMSO has no cytotoxicity for HepG2 cells. With increasing DCM probes concentration (0-40 μM), the concentration of TPE-based glycoclusters was kept 15-fold more than the DCM probes. All of glyco-dots exhibited almost 100% cell viability for HepG2 cells which was similar as DMSO. Hence, such glyco-dots had low cytotoxicity and are suitable for further cell assays.

III.4.3 Glyco-dots responding to endogenous ONOO⁻

Glyco-dots could detect exogenous ONOO⁻ in HepG2 cells. How about detecting endogenous ONOO⁻ which is needed because endogenous ONOO⁻ has low concentration in cells, not as high as

when incubating SIN-1 to produce exogenous ONOO⁻. RAW264.7 cells are mouse macrophages that was usually used to generate endogenous ONOO⁻ induced by LPS.

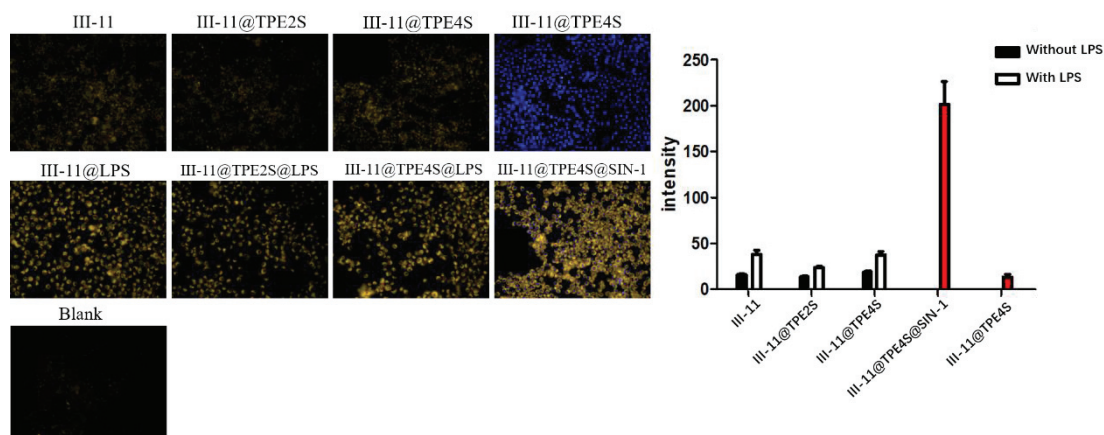


Figure 21: Glyco-dots self-assembled from **III-11** and TPE-based glycoclusters responding to endogenous ONOO⁻ in RAW.264.7 cells.

Endogenous ONOO⁻ generated by LPS (Fig. 21), could “switch-on” yellow fluorescence from DCM probes in RAW264.7 cells. According to emission intensity comparison, the signal with LPS were a little higher than without LPS. This result shows that the DCM probes had reacted with minute amount of endogenous ONOO⁻ sensitively. But the emission intensity had no distinct difference when incubating DCM probes with or without TPE-based glycoclusters. Hence, the functions of TPE2S and TPE4S could not be verified. Also, all DCM probes into cells could not completely react with endogenous ONOO⁻, since induction of SIN-1 provided a dramatic increase of the fluorescence signal due to exogenous ONOO⁻. In this case, all the DCM probes had reacted completely with ONOO⁻ and released the strongest fluorescence emission. In assumption, even though pure DCM probes, glyco-dots with TPE2S and glyco-dots with TPE4S were incubated at 5 μM, 10 μM and 20 μM, LPS generating endogenous ONOO⁻ only existed 1 μM which could not generate enough endogenous ONOO⁻ to react with probes hence leading to the minimal emission intensity. However, glyco-dots provide enough fluorescence signal to trace of endogenous ONOO⁻ induced by LPS.

III.4.4 Cell selectivity of glyco-dots

To explore the cell recognition and selectivity obtained through monosaccharides on glyco-dots, we incubated glyco-dots containing TPE2S or TPE4S conjugated with galactosides with HeLa cells [208], L02 cells [209] and 293T cells [210], which expressed almost no galactose-selective receptor (e.g. ASGPr) on the cell membrane (Fig. 22). SIN-1 as exogenous ONOO⁻ initiator was incubated together with glyco-dots to measure fluorescence response to ONOO⁻.

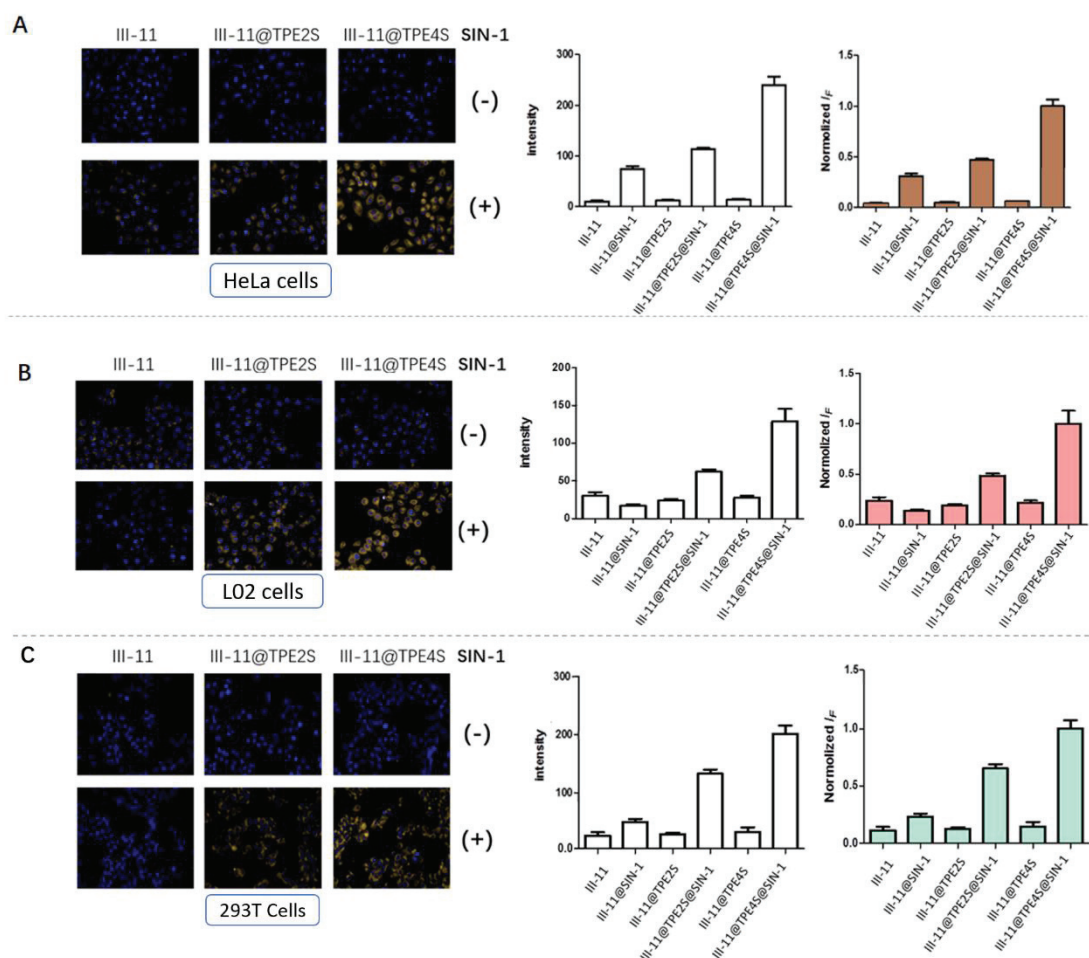


Figure 22: Glyco-dots self-assembled from **III-11** and TPE-based galactoclusters (**III-3a** and **III-5a**) detection of exogenous ONOO⁻ in (A) HeLa cells, (B) L02 cells and (C) 293T cells.

After incubating ONOO⁻ into cells, all samples incubated with the DCM probes displayed homologous fluorescence signal changes. Meanwhile, the samples incubating glyco-dots (with TPE-based glyoclusters) emitted higher fluorescence intensity than pure DCM samples with TPE4S samples exhibiting obvious intensity enhancement in comparison with TPE2S in all the cell line. The fluorescence signal observed here with these three cell lines lacking galactose receptors should have been zero or background level, if the internalization had happened through receptor-mediated endocytosis. The fluorescence signal observed here for the DCM probes reacting with ONOO⁻ is therefore indicating that DCM probes could be internalized into cells through a passive mechanism across the cell membrane. This result is very different from the selective targeting of HepG2 cells that we obtained with PDI-based glyco-dots^[168]. To further demonstrate our hypothesis, we prepared glyco-dots self-assembled from **III-11** and TPE-based glyoclusters with different number or kind of monosaccharides such as glucose, mannose and fucose (Fig. 23). Then the resulting glyco-dots were incubated with HepG2 cells together with SIN-1.

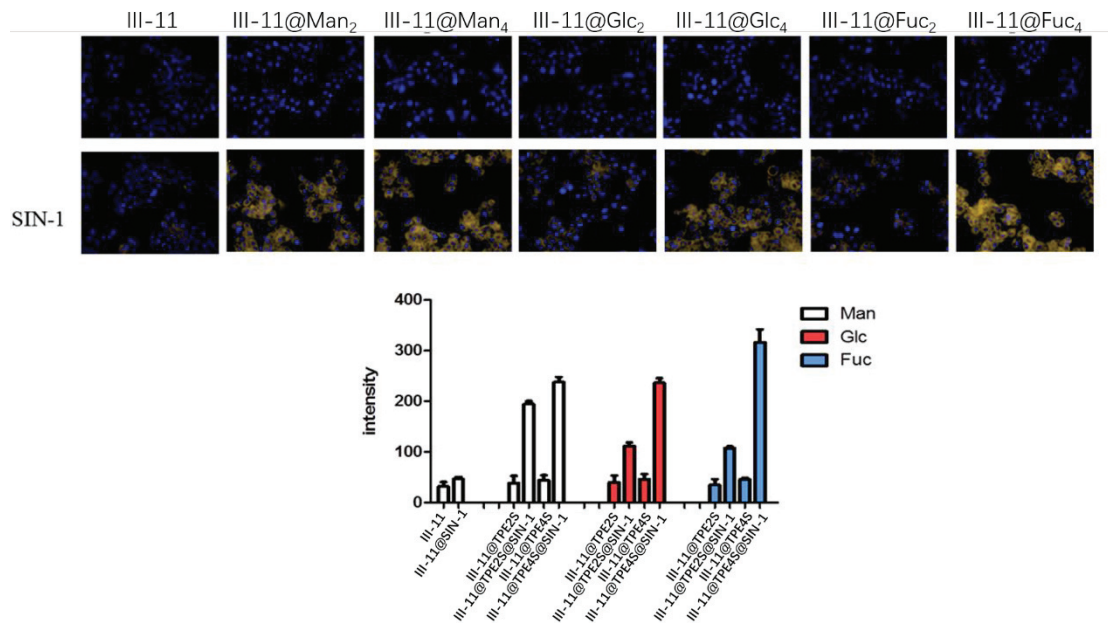


Figure 23: Glyco-dots conjugated with glucose, mannose or fucose TPE- based glycoclusters response to exogenous ONOO⁻ in HepG2 cells.

All samples incubated TPE-based glycoclusters released stronger fluorescence signal than the corresponding with pure DCM probes. TPE4S exhibited higher ability to promote DCM probe detection of ONOO⁻ in HepG2 cells. However, all the glyco-dots showed similar enhancement tendency as galactose-probe, which was unreasonable because mannose- and fucose-probes could not recognize ASGPr receptors on the cell membrane. To further illustrate the non-requirement of ASGPr for the endocytosis of the glyco-dots, we used a HepG2 cell line with the ASGPr knock-down, meaning no more galactose receptor at the cell membrane (Fig. 24). The results obtained highlighted the similar fluorescence signal too ONOO⁻ in both cases, therefore proving that endocytosis would not occur through a receptor-mediated process.

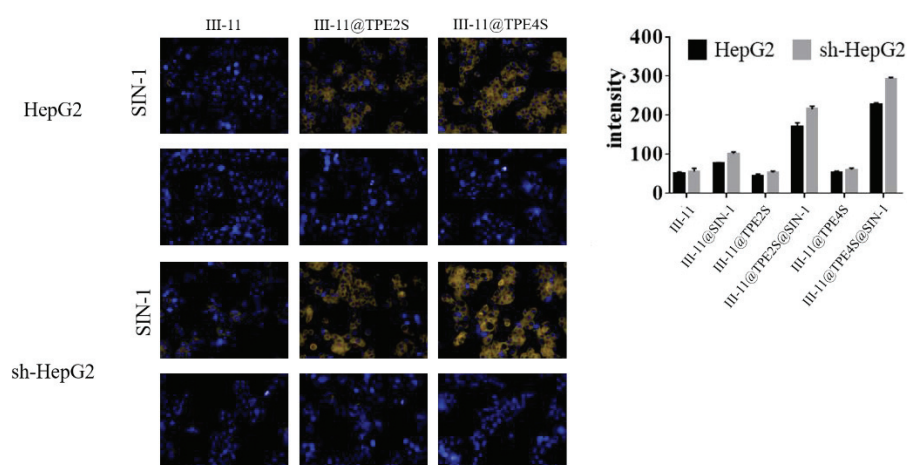


Figure 24: Galactose-probe responding ONOO⁻ in HepG2 cells with ASGPr knocking-down (sh-HepG2 cells).

In conclusion, glyco-dots incorporation DCM probe III-11 and the TPE4S species were the best

system for the detection of ONOO⁻ in cell. Nevertheless, while the carbohydrate moieties could provide proper water solubility, selectivity in targeting a specific cell line was not possible. This results is in sharp contrast with the high selectivity observed in a similar context with PDI-based glyco-dots^[168].

III.4.5 Combination e between DCM probes and glycoclusters in biological assays

According to above introduction, TPE-based glycoclusters could self-assemble with DCM probes to construct glyco-dots in aqueous solution at the molecular level. When incubating glyco-dots in biological assays, TPE-glycoclusters could improve water-solubility of DCM probes and promote cells imaging, but could not recognize ASGPr on the cytomembrane for targeting specifically HepG2 cells and transport probes into cells through endocytosis pathways. Hence, the possible combination mode between glycoclusters and DCM probes cannot be fully explained.

When mixing TPE-glycoclusters and DCM probes in aqueous solution, the resulting glyco-dot was obtained from TPE-glycoclusters adopting ball-structure with hydrophilic surface from its monosaccharides and hydrophobic core to contain DCM probes inside. This stable structure could dissolve aggregated DCM probes and improve fluorescence intensity by blocking the ACQ effect at the molecular level. The glyco-dots might not keep stable structure in biological assays when incubating with cells and responding to ONOO⁻. We speculated two possible processes when glyco-dots were incubated cells:

(i) The glyco-dots were decomposed by organic elements in cell culture. That is to say, the glyco-dots could not assemble when incubating with cells. For this possibility, glycoclusters improving fluorescence intensity of DCM probes into cells demonstrated its poor reliability, because the fluorescence intensity of glyco-dots should be same as samples with single DCM probes if glyco-dots were decomposed when incubated in cell culture.

(ii) The stability of glyco-dots was good in cell culture for proper contact with the cell membrane, which kept delivering and dispersing DCM probes to quench ACQ effect. Several monosaccharides on surface of glyco-dots could improve molecular water-solubility. The glyco-dots detecting ONOO⁻ and imaging several cells without influence from sugar-receptor recognition, verified our hypothesis that glycoclusters could work in biological assays. Whereas, DCM probes probably have higher affinity for protein or lipid bilayer to leave the TPE core, then crossed the cytomembrane and combined with serum proteins such as HSA in cytoplasm. After responding to ONOO⁻, oxidized DCM dye kept binding with intracellular protein and blocking the ACQ effect to release intense fluorescence in the cytoplasm.

III.5 Conclusion

Peroxynitrite (ONOO⁻) is an important reactive oxidant and nitrating agent existing in physiological and pathological processes. It has been demonstrated to cause neuronal death *in vivo* such as brain ischemia, amyotrophic lateral sclerosis, Alzheimer's disease and Parkinson's disease. Compared with others conventional detection methods, fluorescent analysis is sensitive, rapid, accurate tools to capture the ephemeral ONOO⁻ in cells. Hence, detecting the level of intracellular ONOO⁻ is a key indicator for monitoring or predicting diseases effectively. Over the past decade, fluorescent probes for ONOO⁻ detection and imaging in cells with different mechanisms were

reported frequently including phenyl group oxidation, aryl ether group oxidation, heteroatom (Se, Te) oxidation, aryl boronate oxidation. However, hydrophilic fluorescent probes for rapid ONOO⁻ detection, was still necessary to design and further develop efficient probes.

Through further modifying monosaccharide on TPE core with several propargyl groups, TPE-based glycoclusters containing different glycosides were designed and synthesized. Meanwhile, two DCM-based aryl boronate probes (**III-11**, **12**) for ONOO⁻ detection, were designed and synthesized. The probes could detect ONOO⁻ in PBS buffer mixed with 20% MeCN, but displayed quenched fluorescence emission in pure PBS buffer by ACQ effect even if probes reacted with ONOO⁻.

For improving water-solubility and blocked ACQ effect of DCM probes, we attempted to self-assemble TPE-glycoclusters and DCM probes to construct glyco-dots with hydrophilic surface and hydrophobic core. The two combinational relationships between glycoclusters and DCM dyes was explored and the intermolecular distance was closed enough to block ACQ effect, but FRET occurring depended on the volume of DCM and glycoclusters molecules. The 15:1 ratio of glycoclusters to DCM probes was the best concentration to construct glyco-dots and block ACQ effect. The glyco-dots conjugated with TPE4S had better performance than TPE2S due to two additional monosaccharides further improving water-solubility. DCM probes **III-11** showed higher activity than **III-12** for responding ONOO⁻ in short time. The resulting glyco-dots could respond to ONOO⁻ selectively and showed concentration dependent relationship with ONOO⁻ in PBS aqueous buffer. Through DLS and TEM analysis, we supposed that the DCM core was contained into the hydrophobic core of aggregated TPE glycoclusters, and not aggregate in solution to break ACQ effect. The glyco-dots self-assembled with **III-11** and TPE4S was the best combination for detecting ONOO⁻ at the molecular level.

In biological assays, even though all the glyco-dots had lower cytotoxicity, **III-11** conjugated TPE glycoclusters exhibited better fluorescence enhancement than **III-12**. The glyco-dots self-assembled with **III-11** and TPE-glycoclusters could respond to endogenous ONOO⁻ but no obvious improvement for glycoclusters was observed because lower concentration of endogenous ONOO⁻ didn't react completely with probes. The experiments of cell selectivity and glycoside selectivity, TPE-based glycoclusters could transport DCM probes into several cells and responding to ONOO⁻ without any restriction from ASGPr recognition. Hence, we hypothesized that glyco-dots had high cell compatibility for transporting DCM on cell surface, then DCM probes crossed the cytomembrane and combined with proteins in cytoplasm but TPE-glycoclusters still stay outside.

In conclusion, we have designed and synthesized a kind of glyco-dots self-assembled by DCM probes and TPE-glycoclusters. The glyco-dots having high water-solubility could respond to ONOO⁻ with fluorescence enhancement at the molecular and biological level. The glyco-dots could detect endogenous and exogenous ONOO⁻ but no specific cell recognition for targeting HepG2 cells could be observed.

Chapter IV

Self-assembled AIE glyco-dots for thiophenol detection

IV.1 Introduction

Thiophenol (PhSH) is an important organosulfur compound. This colorless liquid is the simplest aromatic thiol extensively applied in organic synthesis of agrochemicals, pharmaceuticals and dye industries^[211-213]. Aliphatic thiols such as cysteine (Cys), homocysteine (Hcy), glutathione (GSH) or other biological thiols participate in a range of biological functions^[214]. But thiophenol and aromatic derivatives are polluting compounds with high toxicity in fish and mouse that the median lethal dose (LC₅₀) of 0,01 to 0,04 mM or 46.2 mg / kg^[215, 216]. Exposure to the thiophenol liquid or vapor in water or soil for a long time is highly detrimental human health, and triggers series of severe systemic injures, such as damage of the central nervous system, muscle weakness and even death^[217].

IV.1.1 Fluorescent probes for thiophenol detection

Many efficient methods have been reported to detect aromatic thiols including HPLC^[218], UV detection and chromatography-mass spectrometry analysis^[219]. Fluorescent probes are widely developed and applied for thiophenol detection due to their high sensitivity, simple process and low detection limits. Normally, 2,4-dinitrophenyl group is common moiety in the design of fluorescent probes to modify fluorescence properties through intramolecular charges transfer (ICT), photo-induced electronic transfer (PET), Förster resonance energy transfer (FRET) or through-bond energy transfer (TBET). The 2,4-dinitrophenyl group can be conjugated on the fluorophore with a sulfonyl ester^[220], sulfonamide^[221] or ether^[222].

Fluorescent probes based on *N*-phenyl-1,8-naphthalimide were reported with various positions of dinitrobenzenesulfonyl group (DNs) as detector on phenyl ring^[223]. The probe with DN on *ortho*-position of the phenyl ring exhibited better fluorescence response than other position. The probe could release 20-fold fluorescence emission at 548 nm after responding to PhSH, rapidly, sensitively and selectively. An efficient two-photon fluorescent probe with red emission was developed for PhSH imaging^[224]. A moiety with two photon property was conjugated with a BODIPY ring transferring energy by TBET effect. The fluorescence was quenched by DN due to PET effect. After reaction with thiophenol, the intramolecular electron density was recovered followed by DN elimination to disrupt the initial PET structure. The probe displayed yellow fluorescence signal at 586 nm, linear variation of emission with PhSH concentration, high selectivity for thiophenol and distinct fluorescence imaging in HeLa cells. However, this large hydrophobic structure required 50% ethanol to improve solubility for PhSH detection (Fig. 1A). A squaraine-based near infrared fluorescent probe was developed for PhSH detection^[225]. As a colorimetric and “off-on” fluorometric dual-channel chemosensor, the probes exhibited high sensitivity (LOD: 9.9 nM), selectivity and rapid response in aqueous solution. Mannose was connected on fluorophore for water-solubility improvement. The fluorescence property of the probe was selective for PhSH over other thiol species in neutral environmental water samples (Fig. 1B).

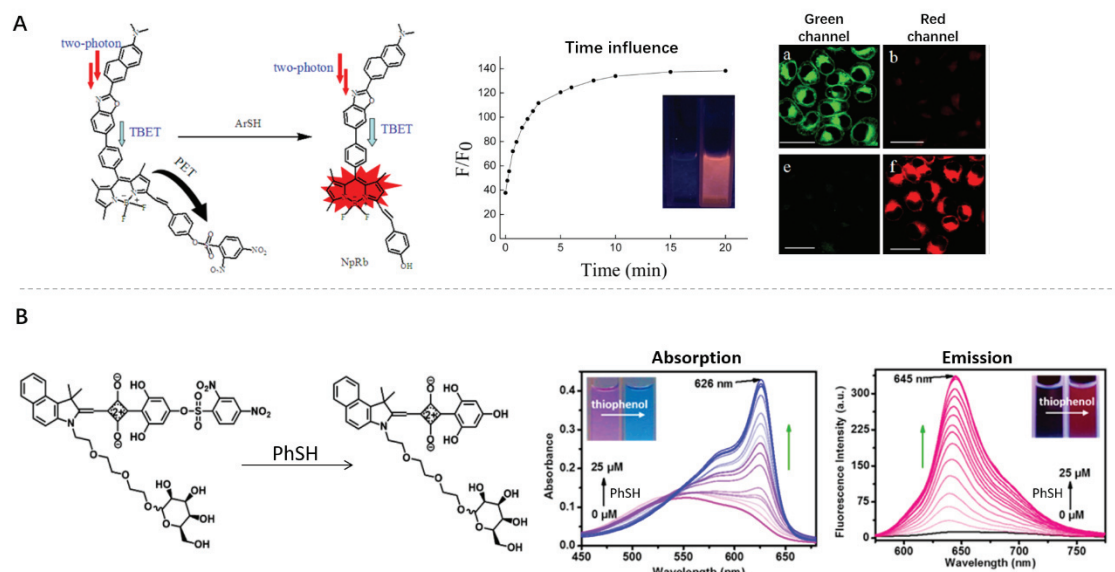


Figure 1: (A) Two-photon BODIPY-based fluorescent probe for thiophenol detection. (B) The colorimetric and near-infrared PhSH probe

The response mechanism of probes with sulfonamide connection are similar to the probes with sulfonate connection. Thiophenol has high nucleophilicity to react with the C-S bond between 2,4-dinitrobenzene and sulfonyl in basic environments. After SO₂-C bond cleavage, the residues with O-SO₂ or NH-SO₂ decomposed to release sulfur dioxide and generate hydroxy or amine groups, which could recover original electron distribution on the fluorophore to change emission intensity in aqueous solution. Hence, detection of thiophenol would require neutral or basic environment to (Fig. 2).

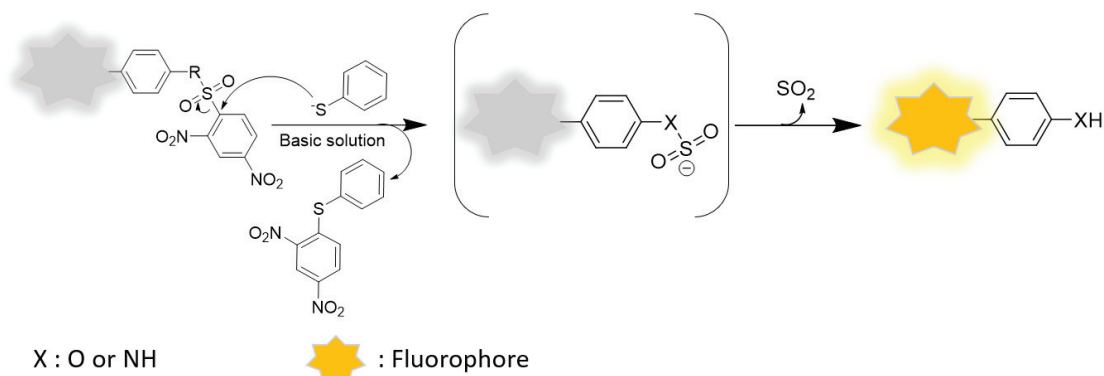


Figure 2: The response mechanism of probes for thiophenol detection.

A dicyanomethylene-benzopyran based NIR fluorescent probe was reported for thiophenol detection. 2,4-dinitrobenzene was combined on fluorophore and emission was quenched through a sulfonamide bond (Fig.3A)^[226]. After responding to thiophenol, the fluorescence emission at 670 nm had distinct enhancement in aqueous solution. This probe features remarkable large Stokes shift and displayed a rapid, highly selective and sensitive response to the analyte. The potential applications of this probe were demonstrated by the quantitative detection of thiophenol in environmental water and in living cells. But poor water-solubility required 30% MeCN which

altered emission intensity (Fig. 3A). A fluorescent probe based on triarylboron compound was developed for thiophenol detection. 2,4-dinitrobenzene could modulate the fluorescence emission through controlling PET and ICT effect. The probe showed very fast response toward thiophenol (within ~ 5 min) with limits of detection (LOD) in the micromolar range (Fig.3B)^[221]. With similar response mechanism, a novel fluorescent probe to detect thiophenol over aliphatic thiols was reported based on dicyanomethylene-4*H*-pyran as fluorophore^[227]. The piperazine moiety between the fluorophore and the detector quenched the fluorescence by PET effect. The fluorescent probe displayed excellent long-wavelength emission enhancement at 613 nm after responding to thiophenol and its derivatives sensitively and selectively. However, poor water-solubility was still to be improved for further applications (Fig. 3C).

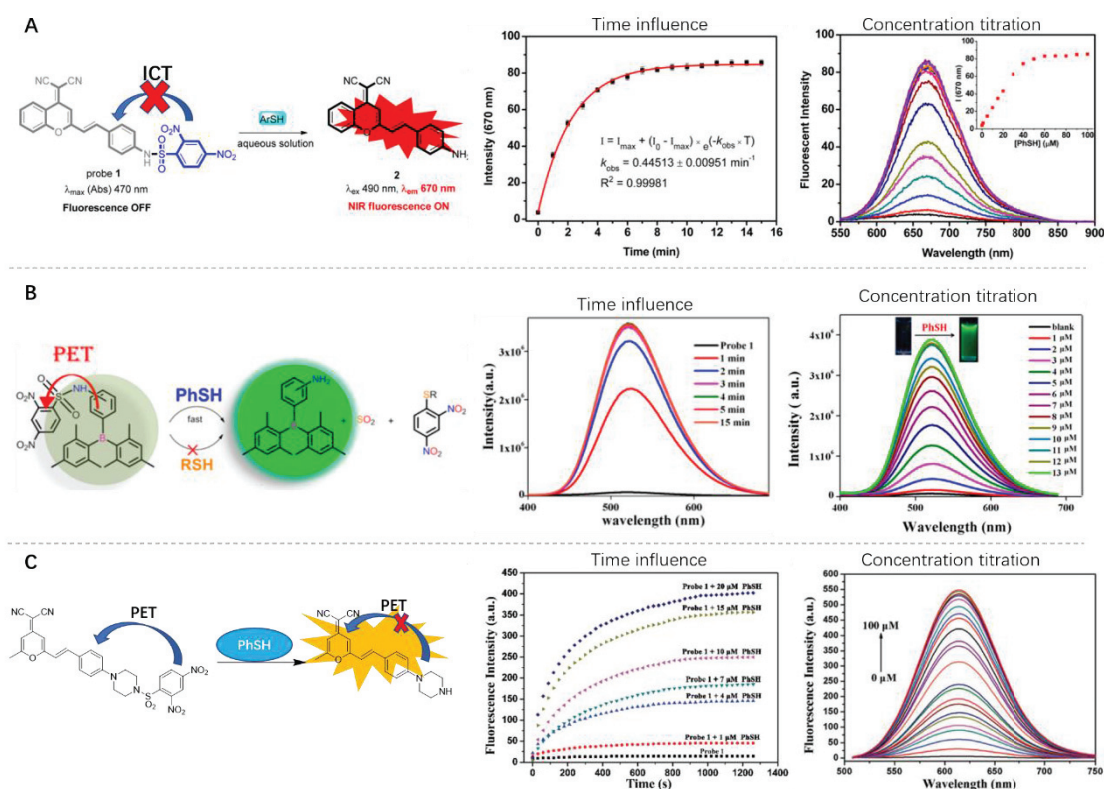


Figure 3: Three NIR fluorescent probes based on DCM dye for thiophenol detection through (A) ICT effect^[226] and (C) PET effect^[221, 227].

2,4-Dinitrophenyl ether is another detector for thiophenol response without sulfur dioxide generation. Nucleophilic thiophenol in basic solution could react with the C-O bond to promote the formation of the corresponding phenol. A benzothiazole based “turn-on” fluorescent probe for thiophenol detection was reported. The probe could release fluorescence emission at 480 nm with sensitive signal change (LOD = 3.3 ppm) in aqueous solution with 45% DMF^[228]. Through decoration of dicyanomethylene-benzopyran, a NIR colorimetric probe was developed with longer Stokes shift and distinct fluorescence enhancement. This probe showed sensitive and selective for detection of thiophenol in aqueous solution with 50% DMSO, and could respond to analyte in environmental sample, HeLa cells and living zebrafish^[229]. Lei Yang, Yuanan Su, Xiangzhi Song and co-workers reported an excellent fluorescent probe for discriminatory detection of cysteine / homocysteine, glutathione / hydrogen sulphide, and thiophenol^[214]. Through structural changes of

fluorophores, the probes contained three moieties each reacting with a specific analyte and generating a fluorescence signal with variant emission wavelength. This probe showed good selectivity for thiols and other common amino acids and anions. The sensing mechanism of this probe towards thiols was proved by the optical, HPLC and mass spectrometry analysis. Meanwhile, the probe could still detect each thiol with different signal in living cells (Fig. 4).

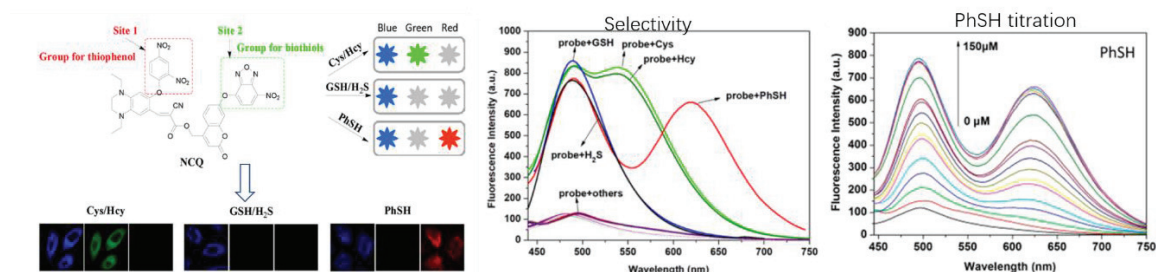
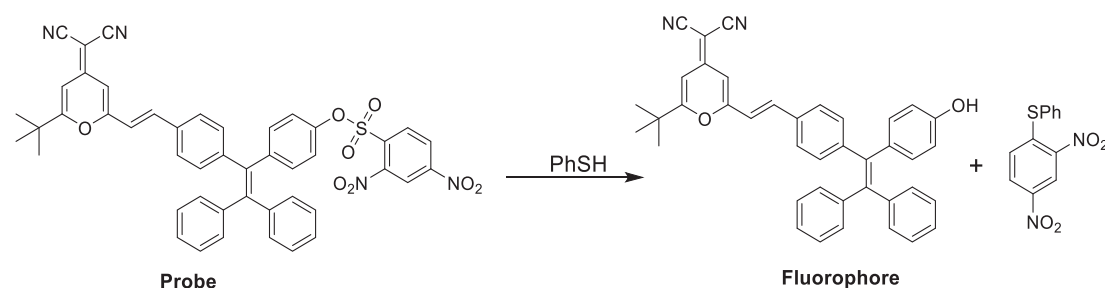


Figure 4: Triple-emission fluorescent probe for discriminatory detection of Cys / Hcy, GSH / H₂S and thiophenol^[214].

IV.1.2 Project design

Some fluorescent probes have been reported for thiophenol detection with sensitive and selective fluorescence response in environmental samples and living cells. However, poor water-solubility usually decreased their emission intensity, restricted LOD and application of some probe with NIR emission by ACQ effect. Tetraphenylethylene (TPE) have excellent AIE properties and stable photostability, but the short emission wavelength is limiting further applications in biological systems. DCM based fluorophore with long emission wavelength, good quantum yield and large Stokes shift, have been developed and applied for many analyte detections. However, the ACQ effect quenching fluorescence always restricted its performance in aqueous solution. To utilize the advantages of DCM and overcome the ACQ drawbacks, a novel fluorophore composed of conjugated TPE and DCM cores was designed. The new fluorophore (TPE-DCM) was predicted to display AIE properties from the TPE core, red fluorescence emission from the DCM moiety and outstanding photostability, when decorating 2,4-dinitrobenzenesulfonate on fluorophore (Scheme 1).



Scheme 1: TPE-DCM based probe for thiophenol detection.

The probe with large hydrophobic structure should hardly dissolve in water leading to aggregation or precipitation in aqueous solution, which may influence sensitivity and accuracy for thiophenol detection. According to the results of chapter III, TPE-glycolclusters could improve the solubility of probes and block ACQ effect for fluorescence intensity. Due to similar structures between TPE-

DCM and TPE-glycoclusters, we supposed that these two molecules could interact together to construct a glyco-dot with increased water-solubility (Fig. 5). We will not consider the stability of glyco-dots *in vivo* due to the absence of endogenous PhSH in living cells.

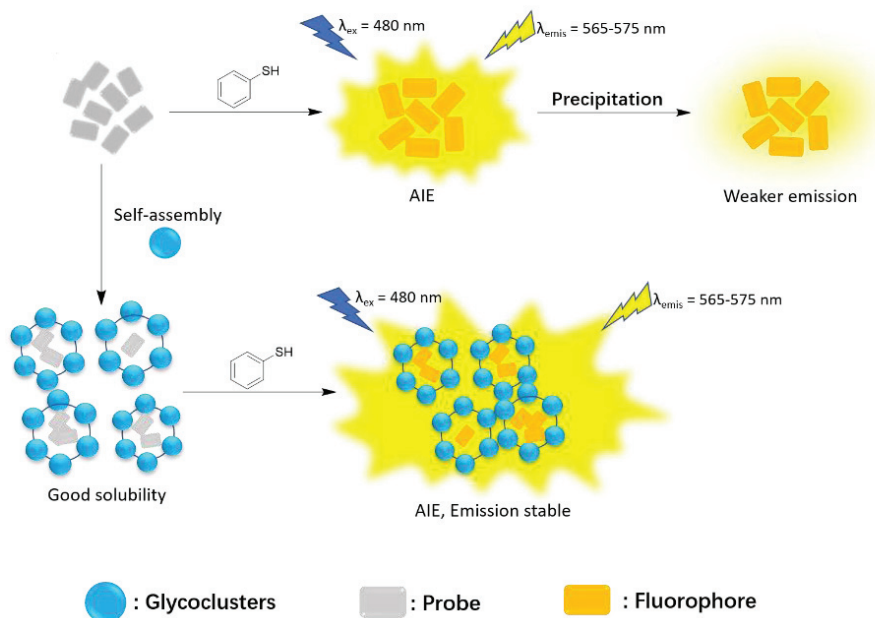
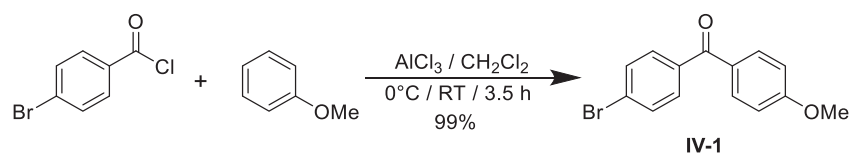


Figure 5: The response process of glyco-dots for thiophenol detection in aqueous solution.

IV.2 Synthesis of probe for PhSH detection

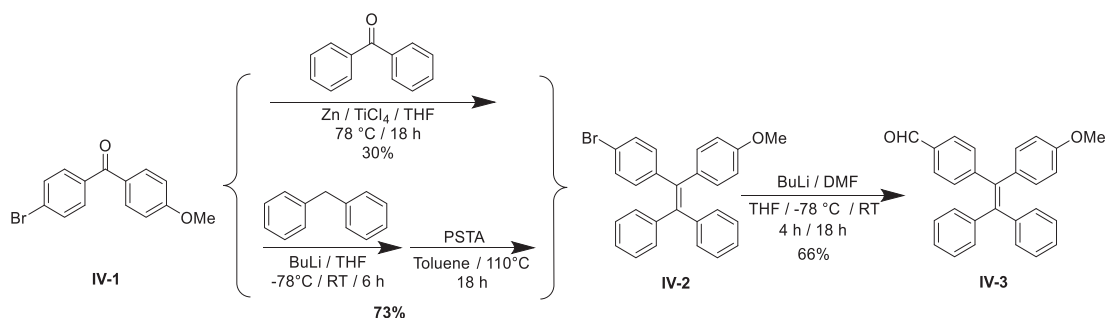
For probe detecting thiophenol in a 1:1 ratio, only one modifiable position on fluorophore is necessary to regulate fluorescence emission and combine with detector moiety. Hence, we should design and synthesize specific TPE core with one hydroxy protected by methyl and a carbonyl for DCM conjugation. After fluorophore construction and deprotection, combining 2,4-dinitrobenzene sulfonate and fluorophore will be explored.

IV.2.1 Synthesis of 1-carbonyl-1'-methoxy-terraphenylethylene



Scheme 2: Synthesis of 4-bromo-4'-methoxybenzophenone (**IV-1**).

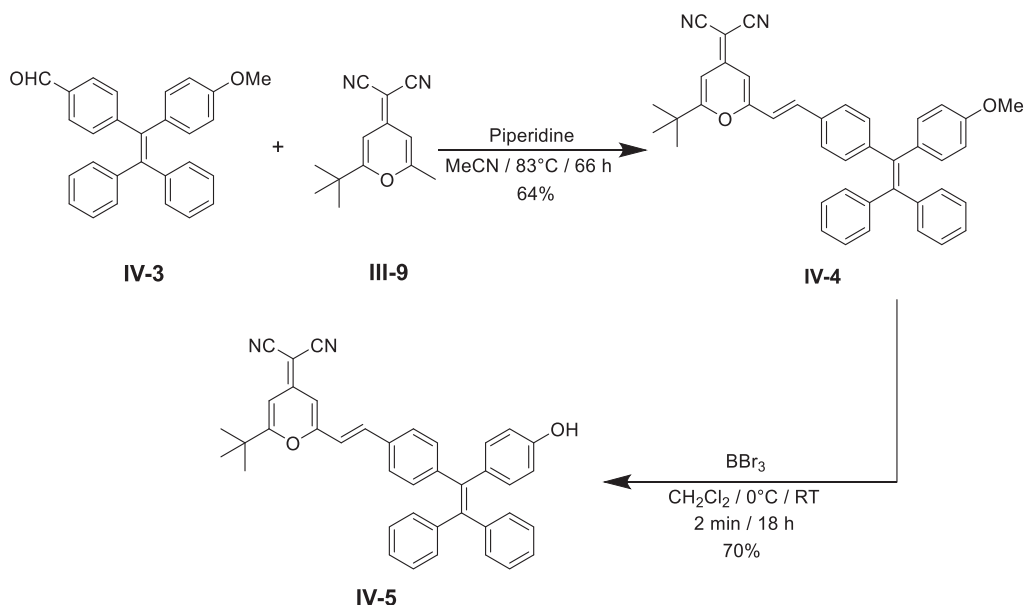
According to Friedel-Crafts acylation^[230], 4-bromobenzoyl chloride and methoxybenzene were dissolved in CH_2Cl_2 at 0°C under aluminium chloride (AlCl_3). This step displayed a high yield (99%) of ketone compound **IV-1** after purification by silica gel chromatography (Scheme 2).



Scheme 3: The synthesis of compound **IV-2** through McMurry reaction or Knoevenagel condensation, and synthesis of compound **IV-3**.

For synthesis of compound **IV-2**, we tried McMurry reaction to conjugate two kinds of ketone but only obtained 30% yield. So, we supposed Knoevenagel condensation could be employed to synthesize the target TPE compound, because the carbonyl of **IV-1** has higher reactivity for the lithiated intermediate than bromine when adding in solution after diphenylmethane activated by *n*-butyllithium. Compound **IV-2** was synthesized in 73% yield by Knoevenagel condensation (Scheme 3). In this step, the ratio of BuLi and diphenylmethane should be appropriate and the ketone **IV-1** should be used in excess and added rapidly in the solution to prevent excess Li-intermediates from substituting bromine. Then, lithium-halogen exchange followed by formylation with DMF provided **IV-3** in 66% yield.

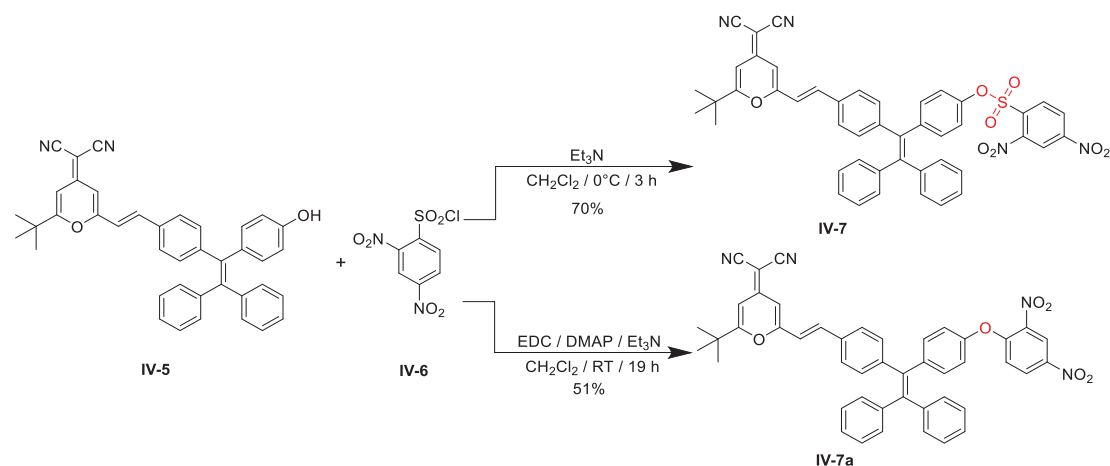
IV.2.2 Synthesis of the DCM fluorophore (TPE-DCM)



Scheme 4: The synthesis of the AIE fluorophore (TPE-DCM-OH, **IV-5**).

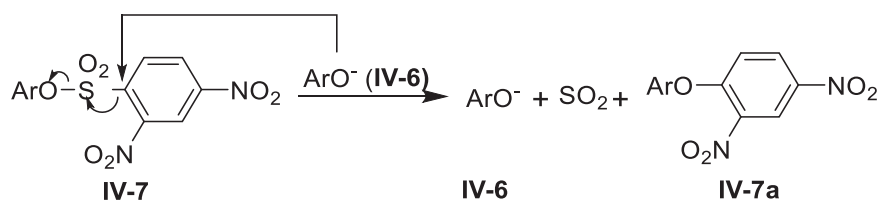
An aldol condensation between the carbonyl TPE **IV-3** with compound **III-9** catalysed by piperidine in MeCN during 66 h afforded the fluorophore **IV-4** with AIE moiety. Then, BBr_3 was used to deprotect the methyl group and obtain phenol **IV-5** for subsequent detector decoration (Scheme 4).

IV.2.3 Synthesis of probes by sulfonylation



Scheme 5: Synthesis scheme of two probes through the changes of reaction condition.

Sulfonylation of phenol **IV-6** provided two different outcomes depending on the reaction conditions. While standard conditions provided the sulfonate **IV-7**, extended reaction time and addition of a carbodiimide (EDC) led to the diarylether **IV-7a**. We hypothesized related mechanism that the S-C^{Ar} bond was cleaved by ArO⁻ (**IV-6**) easily, then generate ArO⁻ (**IV-6**), SO₂ and diarylether **IV-7a** (Scheme 6). The chemical shift of the three aromatic protons on 2,4-dinitrobenzene at the range of 8-9 ppm was different when compared the H¹-NMR of the two products (Fig. 6A). And HRMS results showed the mass of **IV-7** and **IV-7a** were 803.2177 (C₄₆H₃₅N₄O₈S) and 739.2555 (C₄₆H₃₅N₄O₆) respectively (Fig. 6B). Nevertheless, the fluorescence response to thiophenol is still possible while the ether **IV-7a** as previously reported^[231, 232]. Hence, the fluorescence changes will be measured and compared to select the better candidate for subsequent thiophenol detection.



Scheme 6: The transform mechanism from sulfonate **IV-7** to diarylether **IV-7a**.

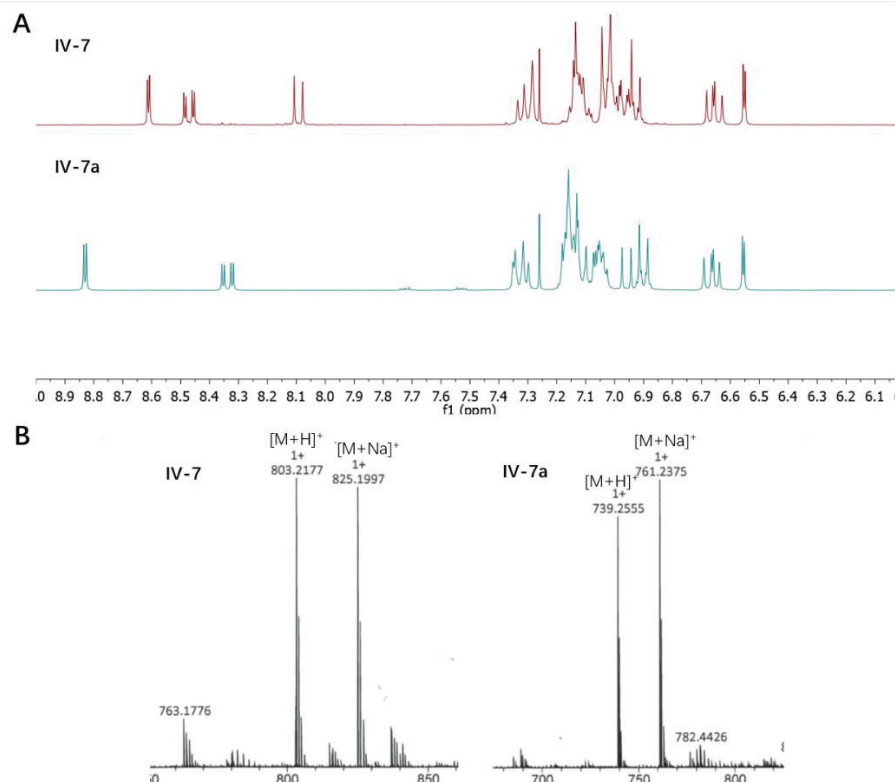


Figure 6: (A) $^1\text{H-NMR}$ and (B) HRMS analysis of probe **IV-7** and **IV-7a**.

IV.3 Novel AIE probe for thiophenol detection

The two TPE-DCM based fluorescent probes **IV-7** and **IV-7a** have been synthesized and characterized before measuring fluorescence properties for thiophenol detection *in vitro*. Although the probes have specific AIE properties, the influence of fluorescence intensity and reactivity with analyte should be verified. Meanwhile, the TPE-based glycoclusters will be investigated to improve the water-solubility for a better detection.

IV.3.1 The fluorescence response of TPE-DCM probes to thiophenol detection

The basic fluorescence variation of probes **IV-7** and **IV-7a** were measured to select the best candidate for subsequent experiments. Due to hydrophobic structures of probes and thiophenol, the PBS buffer required 10% THF to improve solubility in aqueous solution. The thiophenol (100 μM) was stirred with probes (10 μM) during 2-3 min and the fluorescence measured exciting at the longest absorption wavelength. The fluorescence intensity of **IV-7** have been quenched enough due to the electron-poor 2,4-dinitrosulfonate group. However, the missing sulfonate in diarylether **IV-7a** did not prevent ICT effect which was still active leading to fluorescence (Fig. 7A). After adding thiophenol and reacting with probes, the distinct fluorescence enhancement of probe **IV-7** at 570 nm was observed while a decrease of probe **IV-7a**. The mass spectrometry illustrate that the sulfonate detector has been removed from **IV-7** after responding to thiophenol and generate hydroxy TPE-DCM (**IV-5**). But Ar-O bond on **IV-7a** was not cleaved by thiophenol (Fig. 7B). Hence, the probe **IV-7** is the best candidate to detect thiophenol, and will be investigated in subsequent

experiments with 10 μ M concentration.

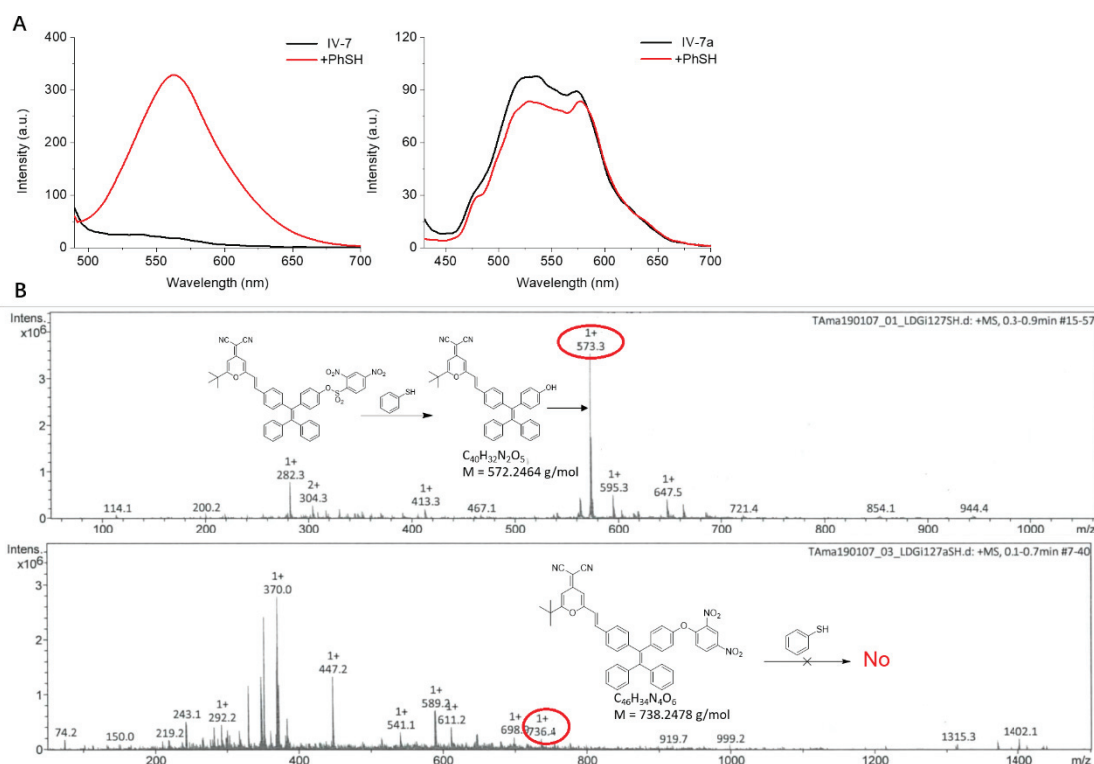


Figure 7: (A) The fluorescence variation of probe **IV-7** and **IV-7a** after reacting with thiophenol in aqueous solution. (B) Mass spectrometry analysis to verify the response to PhSH.

IV.3.2 Fluorescence properties of **IV-7** for thiophenol response

To determine the largest excitation and emission wavelength of probe **IV-7** for subsequent parameter measurement, the probe was dissolved in PBS buffer with 10% THF and the absorption and emission spectra measured, before adding thiophenol in solution and measuring the same parameter after 3 min stirring.

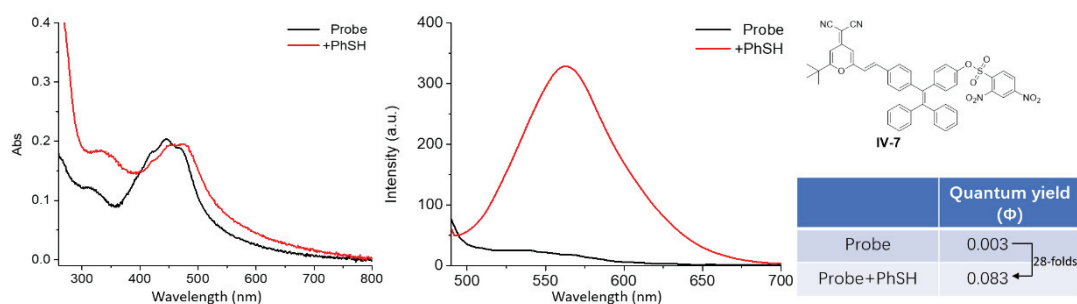


Figure 8: The absorption and emission of **IV-7** before and after adding thiophenol in solution.

The wavelength of absorption was shifted from 450 nm to 480 nm. Meanwhile, intense fluorescence emission was released followed by a slight emission wavelength red-shift from 550 nm to 570 nm. These phenomena demonstrated that the ICT effect was recovered when PhSH

reacted with the electron-poor detector and release hydroxy on fluorophore. The Stokes shift (90 nm) and 28-fold emission enhancement demonstrated that this probe could respond to thiophenol in aqueous solution.

IV.3.3 The response mechanism of **IV-7** to thiophenol detection

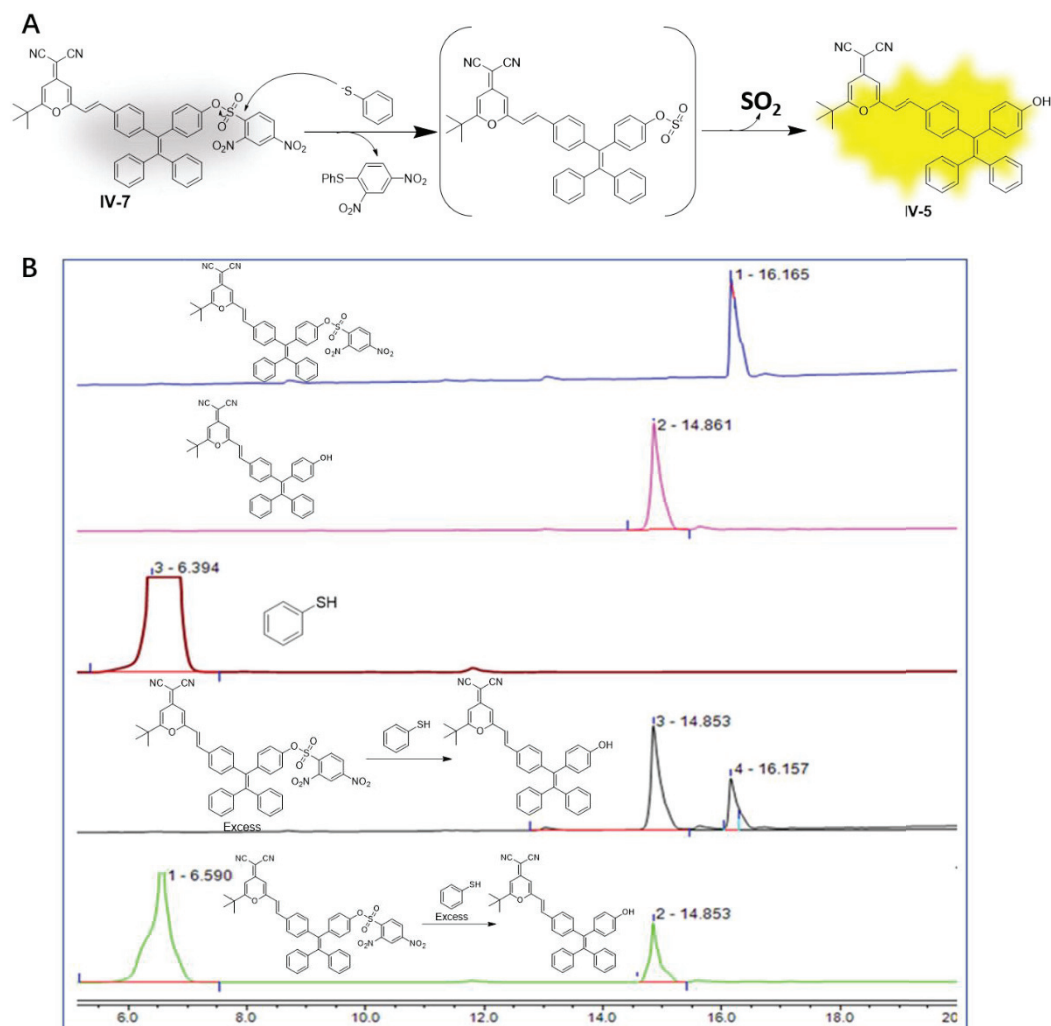


Figure 9 (A) The response mechanism of **IV-7** to thiophenol detection was proved by (B) HPLC analysis.

According to some reported probes with similar response mechanism^[220, 223-225], negative aromatic thiol ion have high nucleophilicity to react at the aromatic carbon on dinitrobenzene and cleave the S-O bond. The resulting intermediate was unstable with the loss of SO₂ to generate hydroxy TPE-DCM (**IV-5**) followed by SO₂ released. Hence, the probe responding in neutral or basic solution was a critical element to generate negative thiophenol (Fig. 9A). After **IV-5** generation, poor water-solubility led molecules to aggregate with intense fluorescence emission induced by AIE effect. To demonstrate the mechanism, HPLC analysis was employed to separate each compound. The probe **IV-7** displayed lower polarity than **IV-5** due to sulfonylation of the hydroxy group. The probe **IV-7** could react with PhSH and generate the hydroxy TPE-DCM **IV-5** completely followed by fluorescence enhancement. Hence, the probe **IV-7** has reactivity for thiophenol detection and generate AIE fluorescence from hydroxy TPE-DCM **IV-5**.

IV.3.4 Solvent influence

Due to the hydrophobicity of **IV-7** and thiophenol, adding appropriate organic solvent mixed with PBS was helpful to disperse molecules in solution, which could avoid aggregation. Hence, we compared the fluorescence enhancement in PBS solution with 10% of different organic solvents (Fig. 10).

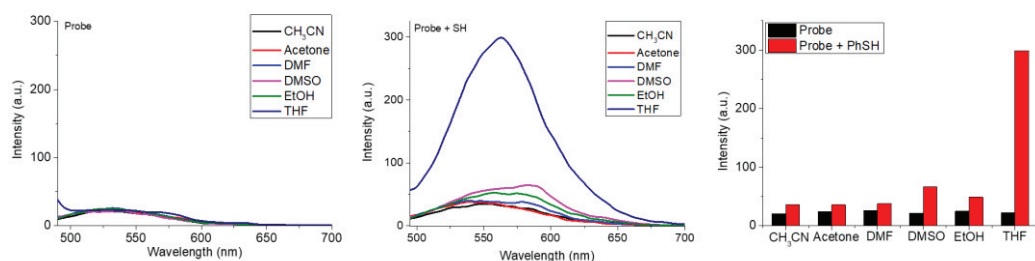


Figure 10: Solvent affected fluorescence intensity for thiophenol detection in PBS buffer mixed with 10% of different organic solvents.

Before adding thiophenol in solution, the probe emitted weak fluorescence. Then, THF displayed the best property to improve the fluorescence enhancement when reacted with PhSH. We speculated that THF with lower polarity could dissolve and disperse the probe and analyte in aqueous solution sufficiently, leading to an optimal access of PhSH to the probe in solution. Therefore, we would use 10% THF in PBS buffer as the solvent media for thiophenol experiments.

IV.3.5 pH influenced fluorescence of probe for thiophenol detection

The working pH range is an essential parameter to evaluate the optical properties and applications of the TPEDCM probe **IV-7**. Due to the response mechanism leading to a phenol **IV-5**, we speculated that the working pH of solution would influence fluorescence enhancement. Hence, the probe's response thiophenol was measured at different pH (from 3 to 10) in PBS buffer with 10% THF.

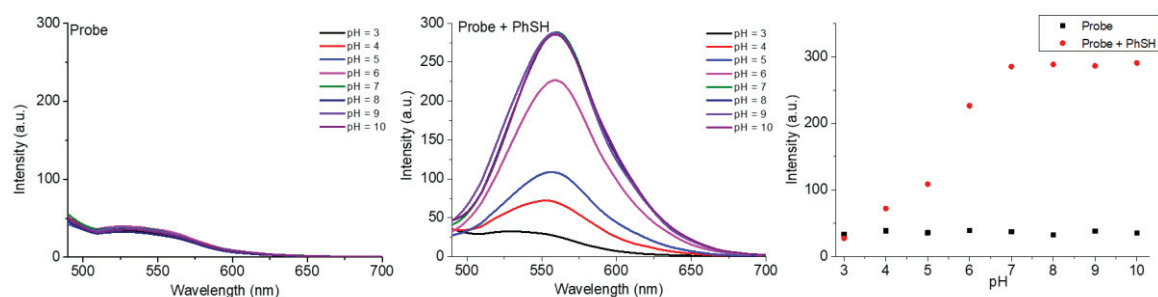


Figure 11: Probe **IV-7** detecting thiophenol in aqueous solution at different pH.

When the probe working in the acidic solution (pH = 3), the fluorescence intensity didn't increase after adding thiophenol, which illustrate the absence of PhS^- which could not trigger fluorescence when pH increased, the fluorescence intensity kept increasing to the maximum when pH reached neutral or basic range. The fluorescence variations with different pH certified that the negative

aromatic thiol ion was the crucial factor controlling “fluorescence-switch”.

IV.3.6 Selectivity for thiophenol detection

The selectivity for specific analyte is another critical parameter in functional evaluation. It is worthy to explore that if aliphatic thiols or common oxidants could influence the fluorescence. Therefore, we measured emission intensity with a series of common amino acids, oxidants and ions (50 μM) in 90% PBS buffer (pH 7.3, 10 mM) with THF, before adding excessive thiophenol and measuring fluorescence changes (Fig. 12A). The black is the fluorescence intensity of **IV-7** after responding to other analytes. And the red bar is the emission intensity of **IV-7** after adding thiophenol with corresponding analytes co-existence in the solutions. Then, **IV-7** was explored for its selective response some thiols including aliphatic thiols and thiophenol derivatives (Fig. 12B).

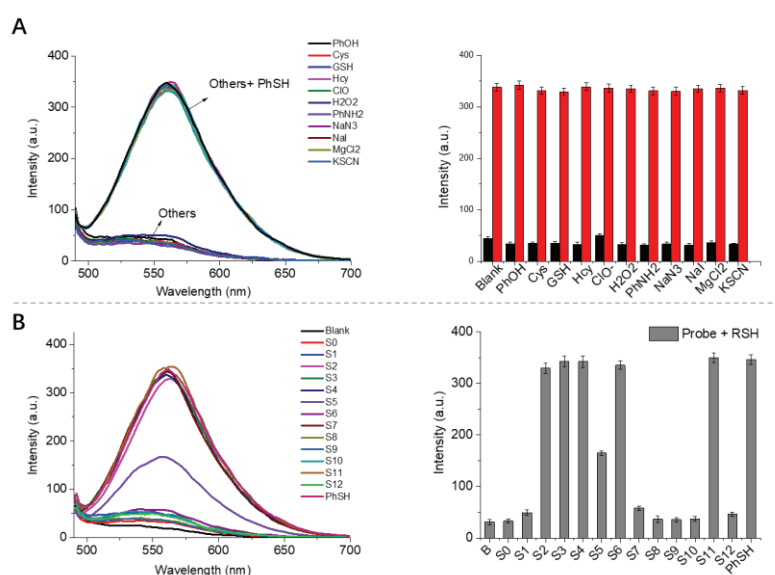


Figure 12: The selectivity of probe **IV-7** for (A) series of amino acids, oxidants, ions, and (B) thiols. *Reagent:* (B) blank, (S0) 1,2-ethanedithiol, (S1) Cyclohexanethiol, (S2) 4-aminothiophenol, (S3) 3-aminothiophenol, (S4) 4-methoxythiophenol, (S5) 4-nitrothiophenol, (S6) 4-methylthiophenol, (S7) 2-methyl-2-propanethiol, (S8) pyrimidinthione, (S9) α -thioglycerol, (S10) 2-mercaptobenzothiazole, (S11) 4,4'-thiobisbenzenethiol, (S12) 2-aminoethanethiol hydrochloride.

The absence of fluorescence variation proved that the probe had no response for some oxidants, amino acids with thiols and ions. After adding excess PhSH, the enhanced fluorescence emission verified that the existed ingredients could not disturb **IV-7** from responding to thiophenol in aqueous solution (Fig. 12A). The probe exhibited fluorescence enhancement for thiophenol and its derivatives, but no signal increase for aliphatic thiols detection (Fig. 12B). The probe emitting weaker emission for 4-nitrothiophenol (S5) was probably due to the electron-poor nitroaryl group thus decrease its nucleophilicity. So, the probe **IV-7** was allowed to detect several thiophenols and overcome interference from other analytes.

IV.3.7 AIE fluorescent performance for thiophenol detection

In order to overcoming the ACQ effect quenching DCM emission in aqueous solution, the TPE

moiety was conjugated with DCM to alter the optical properties. We investigated the fluorescence variation to thiophenol in neutral PBS buffer with different ratio of THF.

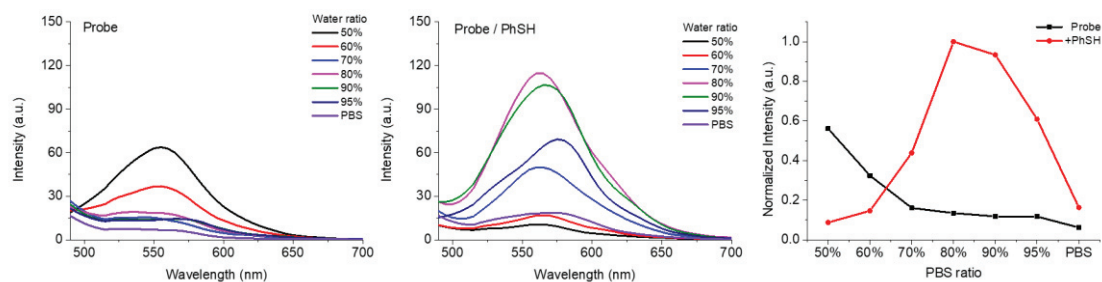


Figure 13: AIE fluorescence variation of **IV-7** for thiophenol detection with water ratio increase in THF.

The probe **IV-7** displayed fluorescence quenching influenced by ACQ effect with water ratio increasing. This phenomenon was probably due to the large volume of 2,4-dinitrobenzene on the fluorophore restricting the rotation of phenyls on TPE, thus changing the optical properties as traditional dyes with ACQ effect. After incubating thiophenol, the intramolecular rotation was recovered to exhibit AIE properties followed by water ratio increasing from 50% to 80%. Then the fluorescence intensity continued to decrease above 80% water ratio. We suppose that the aggregated molecules could be considered as a unit which fluorescence was quenched by ACQ effect when further aggregating together. The fluorescence intensity of probe was influenced by the balance between AIE and ACQ effect. Even though AIE effect has efficient ability to improve emission intensity of hydrophobic probe in aqueous solution, enough water-solubility is still a necessary parameter for further application.

IV.3.8 Time influence

Response time is an important parameter not only to evaluate the sensitivity of the probe for the analyte, but might influence subsequent experimental results such as concentration titration. Thus, we incubated with probe **IV-7** (10 μ M) and excess thiophenol (100 μ M) in aqueous solution with 10% THF, and monitored the fluorescence variation over time.

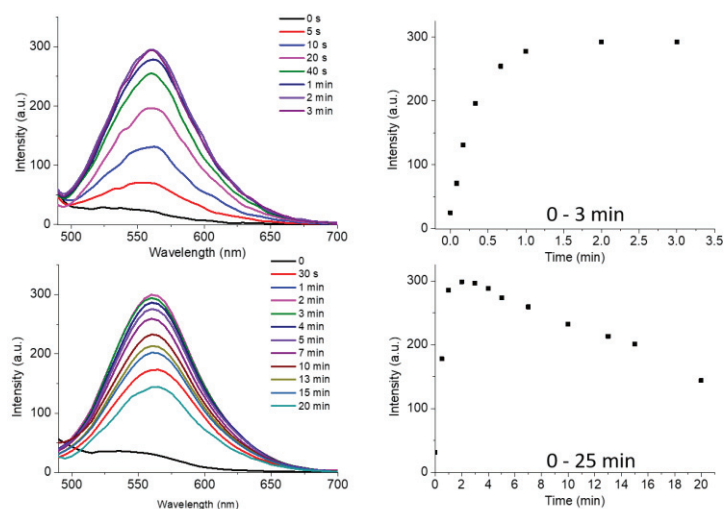


Figure 14: The fluorescence variation of probe responding to thiophenol in aqueous solution with 10% THF.

The fluorescence variation was monitored in the range of 0 - 3 min after adding thiophenol in probe solution. The emission intensity enhanced rapidly under stirring until reaching the maximum after 2 min. The fast emission release illustrated that the probe has high and rapid reactivity with PhSH. From 1 min to 3 min, the fluorescence intensity was stable states. However, the fluorescence intensity began to decrease after 4 min. The probe has low photostability due to the low water-solubility. With increasing stirring time, the poorly water-soluble hydroxy TPE-DCM **IV-5** could be aggregated and precipitated, separated out from the solution, leading to a decrease of the emission signal in solution. The probe could provide a rapid fluorescence enhancement when the excess thiophenol (100 μM) reacted completely with relatively small amount of probe (10 μM). Due to the unstable fluorescence signal, we could not use this probe for subsequent concentration titration because the response time couldn't be ascertained when detecting traces of thiophenol.

IV.4 Self-assembly of TPE-glycocluster and TPE-DCM-based probe for PhSH

detection

According to our previous work (Chapter III), TPE-glycoclusters could capture DCM probes into their hydrophobic core. TPE-DCM probes with similar structure was speculated to self-assemble with TPE-glycoclusters easily, thus could improve the water-solubility, reactivity, and photostability.

IV.4.1 TPE-glycoclusters self-assembly with **IV-7** for thiophenol detection

We have synthesized TPE-based glycoclusters with two or four glycosides. TPE-glycoclusters were only utilized to promote water-solubility of the probe. Because thiophenol was not an endogenous element existing in cells, Hence, we didn't consider the biological influence from different glycosides, and just chose TPE-glycoclusters with galactose for subsequent investigation. Firstly, we mixed TPE2S (**III-3a**, 1000 μM) and **IV-7** concentration during 20 min in PBS buffer with 5% THF (the best condition explored in IV.4.3) and measured fluorescence variation, before adding thiophenol (100 μM) in the mixture (Fig. 15).

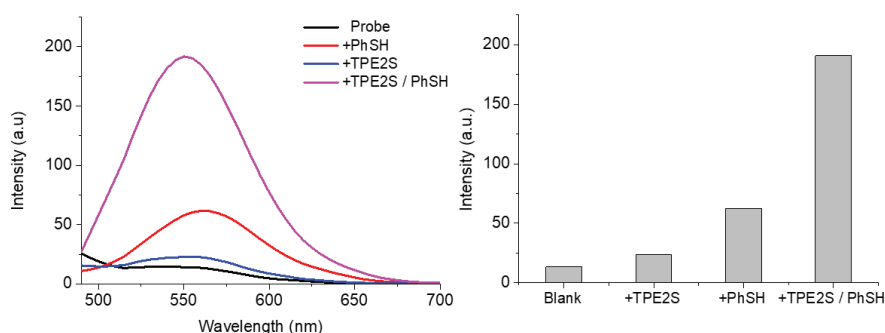


Figure 15: TPE2S improving fluorescence intensity of **IV-7** for the detection of thiophenol.

The basic fluorescence intensity of the glyco-dots (blue line) was higher than only **IV-7** (black line) in solution, which illustrated that TPE2S could interact with probe and influence the emission properties. The low emission intensity was still suitable for thiophenol detection. After adding

thiophenol and stirring during 5 min, the glyco-dots emitted twice higher emission intensity (pink line) than **IV-7** (red line) in aqueous solution. Therefore, we compared the ability of TPE2S and TPE4S self-assembly with **IV-7** to improve the fluorescence intensity. The same concentration (1000 μM) of TPE2S (**III-3a**) and TPE4S (**III-5a**) was incubated with **IV-7** (10 μM) respectively during 30 min, and then addition of thiophenol (100 μM) in PBS solution.

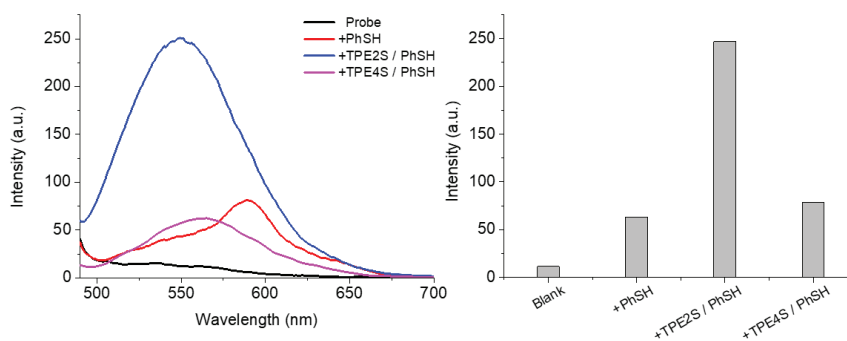


Figure 16: The comparison of TPE2S and TPE4S heightening the emission intensity.

The probe **IV-7** showed a red-shifted but lower fluorescence emission (red line) after incubation with thiophenol when highly aggregated in PBS solution. We didn't add THF in solution because the water-solubility of glyco-dot was enough after self-assembly with TPE4S. Blue-shifted fluorescence emission of glyco-dot was observed after reacting with thiophenol, which was indicated that TPE-glycoclusters partly decreased the aggregation degree of probe in PBS buffer. TPE2S (blue line) exhibited much better ability to increase emission intensity than TPE4S (pink line). For weaker performance of TPE4S, a mechanism was speculated: TPE2S has a higher affinity with **IV-7** due to the small volume and one side on the TPE core without glycosides decoration decreasing the steric hinderance. The glycosides on TPE4S may impede TPE-DCM from entering the hydrophobic core of aggregated TPE4S thus decreasing its fluorescence. TPE2S showing a better performance, it will be conjugated with **IV-7** to construct glyco-dot for thiophenol detection.

To explore appropriate ratio between TPE2S and **IV-7**, the fluorescence variation was measured with different concentrations of TPE2S. The TPE2S was self-assembled with probe (10 μM) during 30 min, and then incubated with excess thiophenol (100 μM) in PBS buffer (Fig. 17).

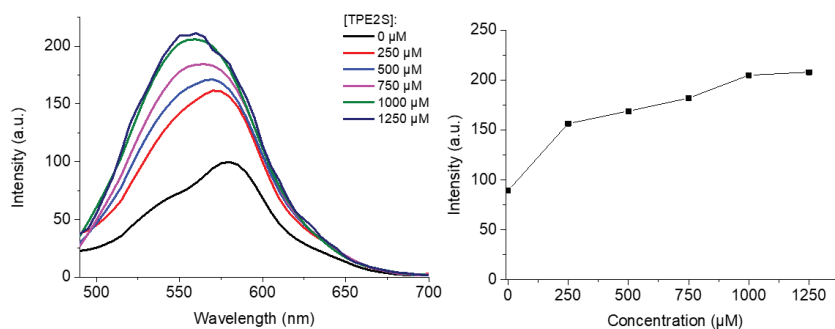


Figure 17: Glyco-dots conjugated by different concentration of TPE2S for thiophenol response.

The TPE2S could promote the emission intensity of **IV-7** in PBS buffer. Following concentration of TPE2S increase, the enhancing tendency was slowing down until reaching maximum at 1000 μM (TPE2S:**IV-7** = 100:1). The emission wavelength slightly blue-shifted from 600 nm to 560 nm, indicating that the TPE2S had captured the probe, disrupted the aggregated state and improved the water-solubility. Hence, we will self-assemble 1000 μM TPE2S with 10 μM probe **IV-7** during 30 min in advanced, and then utilize the resulting glyco-dots for subsequent thiophenol detection.

IV.4.2 AIE affecting fluorescence of glyco-dots for thiophenol response

The hydrophilic TPE2S could self-assemble with hydrophobic probe **IV-7** to generate glyco-dots with good water-solubility. To explore the AIE properties, the glyco-dots were incubated with thiophenol (100 μM) during 5 min in aqueous solution with different ratio of THF.

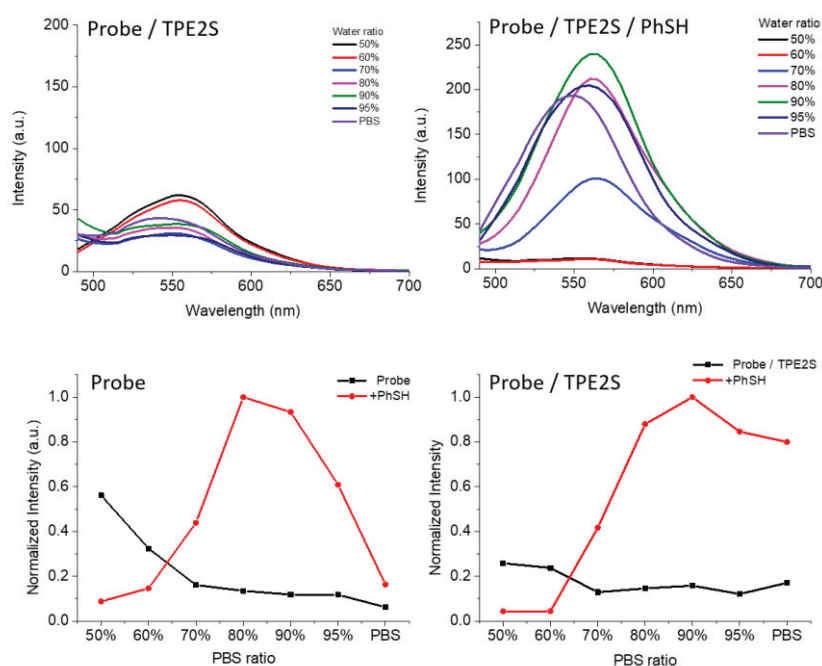


Figure 18: The AIE properties of glyco-dots for thiophenol response in THF/PBS mixtures.

The fluorescence variation was measured before and after incubating with thiophenol in THF/PBS solutions with water ratio increase. The AIE performances of **IV-7** and relative glyco-dots were compared to display the effect of TPE2S (Fig. 18). The fluorescence emission quenching of glyco-dots upon increase of water without thiophenol, illustrated that the glyco-dot still displayed ACQ characteristics when the sulfonate detector was still on the fluorophore. After incubating thiophenol in each sample, the fluorescence intensity increased up to 90% then decreased slightly after 90% PBS ratio. This weak emission intensity in aqueous solution with trace THF was associated with slightly poor water-solubility of glyco-dots to overcome the ACQ effect. while the molecules have conjugated with TPE2S. According to these results, probe conjugated with TPE2S displayed the AIE property and almost completely overcome ACQ effect quenching fluorescence to increase emission intensity.

IV.4.3 Response time of glyco-dots for thiophenol detection

We measured the responding time of glyco-dots after incubating excess thiophenol (1000 μM) in 100% or 95% PBS buffer with THF.

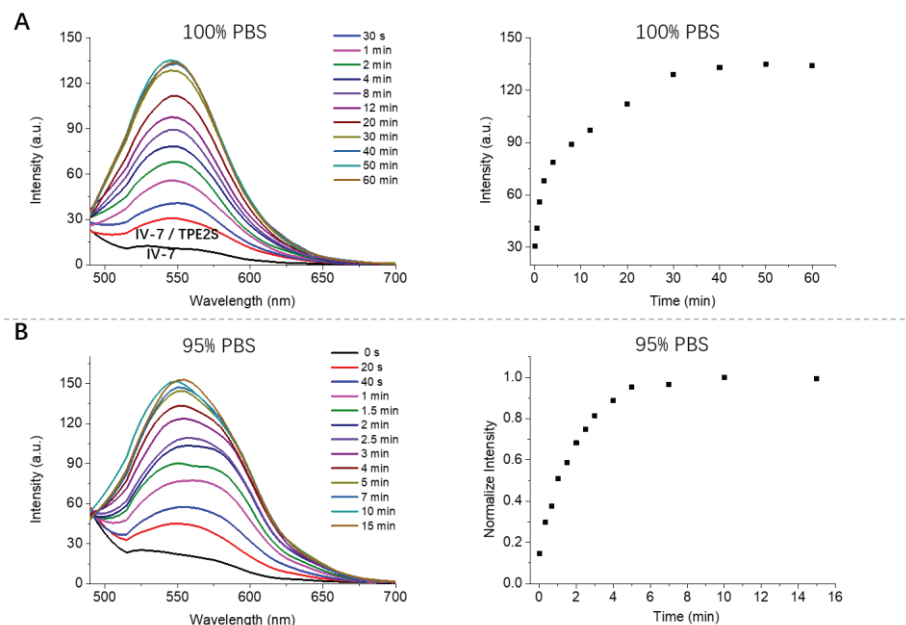


Figure 19: Response time of glyco-dots for thiophenol detection in (A) 100% PBS buffer or (B) 95% PBS buffer with THF.

After incubating excess thiophenol, the fluorescence variation of both samples displayed similar fluorescence increasing tendency over time. When the emission intensity reached its maximum, the fluorescence signal was stable indicating that TPE2S would increase the water-solubility and prevented the precipitation in aqueous solution mixed with less THF. The glyco-dots required longer time (more than 30 min) to reach of probe **IV-7** maximal intensity in 100% PBS buffer than in 95% PBS buffer (about 5-6 min). We believed that the hydrophobic core constructed by TPE2S and probe could have good affinity for the dissociative thiophenol, thus increasing the reaction probability. Small amount of THF would spread thiophenol in solution thus shortening the responding time. The glyco-dots detection of thiophenol with stable emission intensity in 95% PBS solution during 5 min was sufficient for subsequent applications.

IV.4.4 Influence of thiophenol concentration

Concentration titration for analyte is the most essential parameter for evaluation of fluorescent probes, which could not only reflect the sensitivity, but also calculate the limit of detection (LOD) and the standard titration curve. The glyco-dots self-assembled from TPE2S and **IV-7** were appropriate to explore the relationship between fluorescence enhancement and concentration of thiophenol. Hence, the fluorescence variation of prefabricated glyco-dot with **IV-7** (10 μM) and TPE2S (1000 μM) was monitored, followed by adding thiophenol continuously and stirring 5 min in 95% PBS solution with THF. Meanwhile, the concentration titration of **IV-7** without TPE2S was measured as a control.

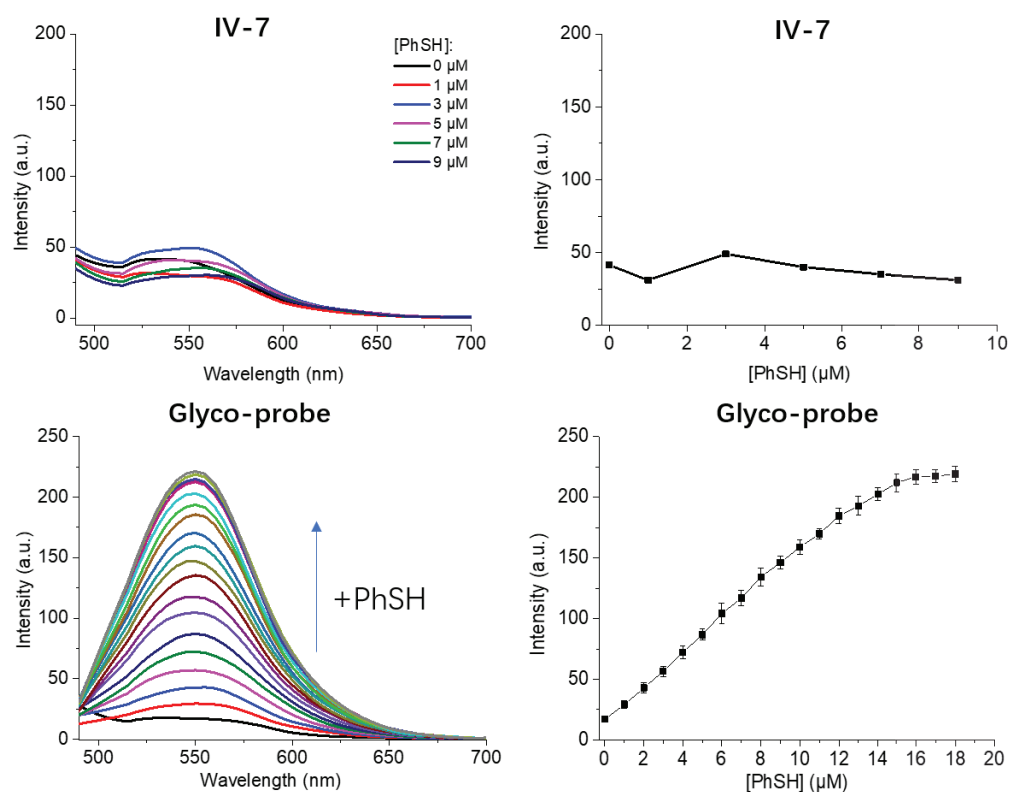


Figure 20: Fluorescence variation of **IV-7** and glyco-dots responding to different concentration of thiophenol.

The probe **IV-7** without TPE2S did not display a fluorescence signal with increasing concentration of thiophenol. This result shows that the probe **IV-5** precipitated leading to fluorescence quenching. However, the glyco-dot after self-assembling with TPE2S, exhibited homogenous fluorescence enhancement upon sequential addition of 1 μM thiophenol and stirring 5 min. The improved water-solubility gave the excellent photostability in 95% buffer avoiding from probe precipitation. The approximate linear fluorescence enhancement from 0 to 14 μM demonstrates that the glyco-dot could monitor the concentration of thiophenol accurately. Above 14 μM , the fluorescence intensity slowly reached a maximum probably due to a complete reaction of **IV-7** (10 μM) with excess PhSH (>14 μM , Fig. 20). Therefore, we calculated and fitted the concentration line to obtain the standard linear relation between thiophenol concentration and fluorescence increase ($I-I_0$, Fig. 21).

We calculated fluorescence increase value but not fluorescence intensity to consider the difference of fluorescence that could arise from glyco-dot concentration. According to computational formula of LOD, the limit of determination was 9.5 nM (according to $3\delta/k$) which is an excellent ability to detect traces of thiophenol in aqueous solution. We believed that outstanding water-solubility could improve the reactivity with thiophenol thus becoming more sensitive than other probes.

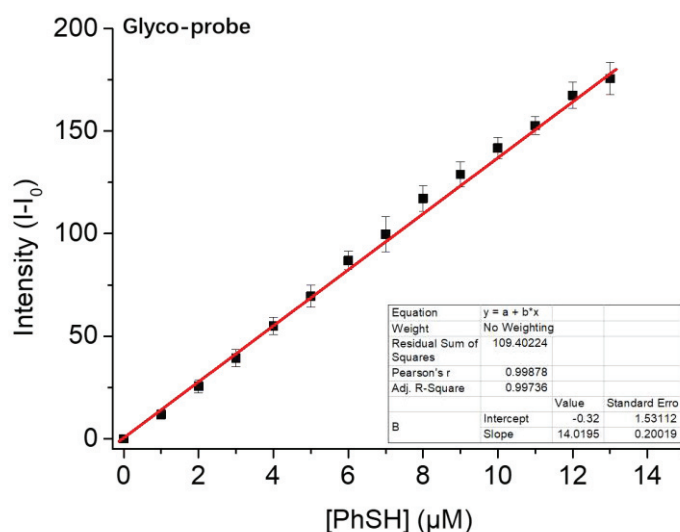


Figure 21: The standard titration of glyco-dot for thiophenol quantification. (I: fluorescence intensity. I₀: initial fluorescence intensity)

IV.4.5 Detection of thiophenol in environmental water samples

Thiophenol as a pollutant, usually exists in industrial wastewater which is harmful for wildlife (fish) and environment. The desirable performance of glyco-dot quantifying thiophenol in environmental water samples is adapted for further application. Hence, the two environmental water samples from Saône River and Rhône River (Lyon, France) will be evaluated for thiophenol quantification (Fig. 22). The glyco-dot was stirred with different concentration of thiophenol and fluorescence variation was monitored every 5 min in river samples with 5% THF. Then, the acquired fluorescence data was related to the relevant PhSH concentration from the standard titration line, and compared with the results in PBS buffers.

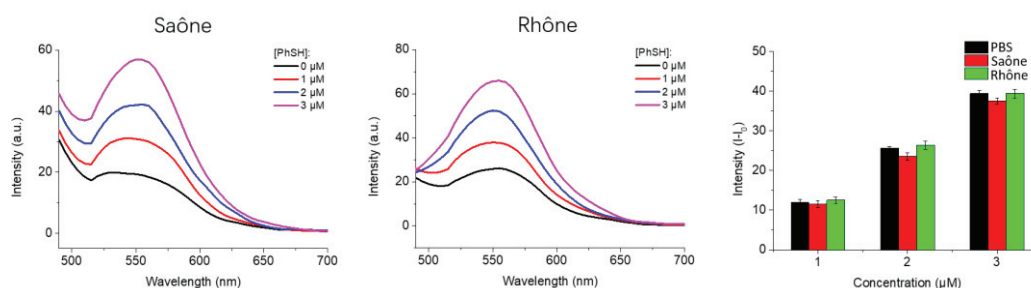


Figure 22: Fluorescence variation of glyco-dot for quantifying different thiophenol in Saône River and Rhône River (Lyon, France).

The glyco-dot provided homogenous fluorescence enhancements upon addition of different concentrations of thiophenol (0-3 µM). Even though the initial fluorescence intensity of two samples is slightly different, the fluorescence increasing value (I-I₀) were similar to the data measured in PBS solution. We have known concentration of PhSH (0-3 µM) in environmental water samples (Table 1). The fluorescence signal recovery was always near 100% from the expected intensities

from the titration curve. Therefore, we can assume that the glyco-dot self-assembled by TPE2S and **IV-7** can detect and quantify the thiophenol in environmental water samples.

Table 1: The glyco-dot self-assembled by TPE2S and **IV-7** quantified thiophenol in environmental samples

| Sample | Thiophenol spiked (μM) | Thiophenol recovered (μM) | Recovery (%) |
|--------------------------|-------------------------------------|--|--------------|
| Saône River water | 0 | Not detect | 0 |
| | 1.00 | 0.97 \pm 0.09 | 97 |
| | 2.00 | 1.84 \pm 0.12 | 92 |
| | 3.00 | 2.86 \pm 0.11 | 95 |
| Rhône River water | 0 | Not detect | 0 |
| | 1.00 | 1.05 \pm 0.06 | 105 |
| | 2.00 | 2.06 \pm 0.08 | 103 |
| | 3.00 | 3.07 \pm 0.14 | 102 |

IV.4.6 Size variation of glyco-dots after intermolecular self-assembly

To verify the process of intermolecular self-assembly between probe **IV-7** and TPE2S, dynamic light scattering (DLS) was employed to measure the size of **IV-17**, TPE2S and supramolecular glyco-dot in aqueous solution mixed with 5% THF (Fig. 23).

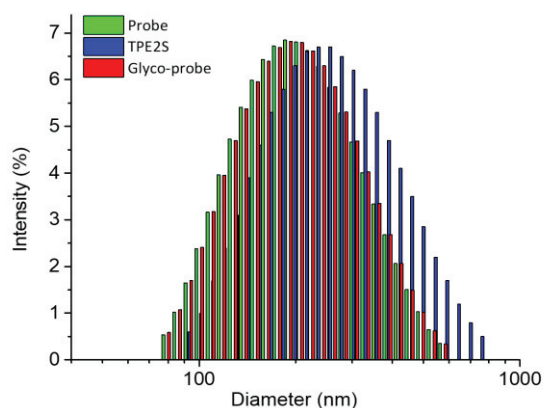


Figure 23: Particle size of **IV-7**, TPE2S and the relevant glyco-dot in aqueous solution.

The probe **IV-7** (green bars) and TPE2S (blue bars) have a large size (100 nm), which indicated that both molecules were highly aggregated in aqueous solution. Based on the two glycosides with TEG linker, the size of TPE2S was larger than **IV-7**, but the water-solubility was insufficient in 95% PBS buffer. When self-assembling the **IV-7** and TPE-glycoclusters together, the size of the resulting glyco-dot was average between the two independent ingredients. This result revealed the TPE2S could dissociate the initial aggregation state of **IV-7** and create a shell around the probe to construct

the amphiphilic glyco-dot with **IV-7** inserted into the hydrophobic cavity of the aggregated TPE2S glycoclusters.

IV.5 Conclusion

Thiophenol is an important organosulfur compound frequently applied in organic synthesis, agrochemical, pharmaceutical and dye industries. Thiophenol and its relevant derivatives are a main kind of polluting compounds with terrible toxicity for wildlife and environment. Fluorescence analysis, as a convenient, cheaper, sensitive, rapid and accurate detecting method, is widely explored. 2,4-dinitrobenzene has high reactivity with thiophenol and its conjugation on fluorophore, quenched the fluorescence through a sulfonate. Many fluorescent probes have been designed and synthesized for thiophenol detection with distinct emission signal variations, excellent sensitivity and selectivity, long-wavelength emission, quantifying thiophenol in environmental samples and other advantages. However, major probes with low water-solubility displayed ACQ effect thus requiring organic solvents including MeCN, EtOH, DMSO and THF.

To overcome these drawbacks, we designed a novel AIE fluorophore with large Stokes shift, good photostability and long-wavelength emission. The TPE moiety with AIE property and a DCM core were conjugated through C=C double bond to build up an electronic “pull-push” system. The probe **IV-7** with sulfonyl ester bond and **IV-7a** with ether bond were obtained and evaluated for thiophenol detection. The fluorescence of **IV-7a** was not quenched enough and had no reactivity for thiophenol after verification by HRMS. Probe **IV-7** displayed obvious fluorescence enhancement for thiophenol detection.

Then, some fundamental parameters of probe **IV-7** were measured about thiophenol detection. The probe could release 25-fold fluorescence enhancement at 565-575 nm with slight red-shifting absorption and emission after reacting thiophenol. The response mechanism was demonstrated through mass spectrometry and HPLC analysis. The probe **IV-7** could detect thiophenol and its derivatives selectively but no fluorescence changes for other thiolated amino acids, ions and aliphatic thiols in neutral or basic pH aqueous solution mixed with 10% THF. Even though the probe displayed obvious AIE performance in solution mixed 60%-80% THF, but the emission intensity was still quenched by ACQ effect due to the limited water-solubility. Unfortunately, the fluorescence emission was not stable after responding to thiophenol, because of precipitation leading to emission intensity decrease in 90% PBS buffer with THF. Therefore, the probe **IV-7** by itself was not an appropriate candidate to detect and quantify thiophenol in aqueous solution.

To improve the water-solubility of **IV-7**, TPE-glycoclusters were self-assembled with **IV-7** to construct a glyco-dot for thiophenol detection. After comparison with TPE4S, TPE2S performed better for fluorescence emission in 95% PBS buffer. After stirring TPE2S and **IV-7** during 30 min, the self-assemble glyco-dot still displayed AIE properties in aqueous solution, and exhibited stable fluorescence intensity over time. The water-soluble glyco-dot showed a linear fluorescence intensity enhancement upon addition of thiophenol, leading to a lower limit of detection of 9.5 nM for PhSH. The standard titration curve was calculated for thiophenol in 95% PBS buffer. This glyco-dot could

detect thiophenol in environment water samples (Saône River and Rhône River, Lyon, France).

In conclusion, we have designed and synthesized AIE fluorescent probes, which could self-assemble with TPE-glycoclusters. The resulting glyco-dot have high water-solubility, excellent sensitivity and selectivity for thiophenol detection, distinct AIE properties in aqueous solution, and could be applied to environmental samples.

Chapter V

Long-wavelength AIE Fluorescent Glycoclusters for Glycosidase Detection

V.1 Introduction

Glycosylation is one of most ubiquitous modifications for more than 50% proteins. The carbohydrates can be associated to protein (glycoprotein, proteoglycans and glycosphingolipids). They play an essential role in many biological processes such as fertilisation, neuronal development, inflammatory responses. Therefore, numerous glycosidases are necessary to hydrolyse stable glycosidic linkages^[233]. Exoglycosidases are hydrolysing the non-reducing terminal monosaccharide units, operating both in the process of transglycosylation and the reverse hydrolysis modes (Fig.1)^[234]. The concentration level of glycosidases is usually the critical marker for several pathological conditions including Gaucher's disease, Parkinson's disease and cancer^[106, 107, 235]. Fluorescent analysis is a popular pathway to trace concentration of cellular enzymes and imaging cells or tissues in the meantime. Here, some typical fluorescent probes for glycosidases detection will be introduced.

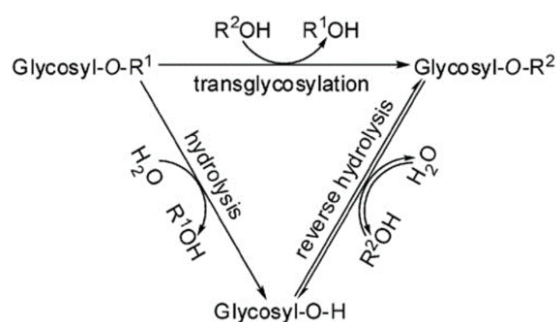


Figure 1: Hydrolysis by glycosidases.

V.1.1 Fluorescent probes for glycosides detection

β -Galactosidase is one of the most important enzymes involved in examine transcription and transfection efficiencies. It has been also demonstrated as a critical biomarker for cell senescence, cell growth, transcriptional regulation, gene expression and primary ovarian cancer diagnosis^[106, 236] *in vivo*. The numerous significances of β -galactosidase have attracted attention from researchers for the design of highly sensitive and selective detection methods. In comparison to detection methods including magnetic resonance imaging (MRI)^[237], single photoemission computed tomography (SPECT)^[238], positron emission tomography (PET)^[239], colorimetric^[240], fluorogenic^[241], chemiluminescence^[242] and bioluminescence^[243], fluorescent probes are widely designed and reported to detect β -galactosidase due to high sensitivity, inexpensive instruments and bioimaging ability. At present, a few fluorescent probes have been reported to monitor β -galactosidase activities in live cells or tissues. Traditionally, conjugating galactose on phenolic hydroxy group through glycosylation was the most prevalent method to control fluorescence intensity. The phenol substitution would quench the fluorescence emission through decreasing intramolecular electron density to block the ICT effect. β -Galactosidase could hydrolyse glycosidic bond (C-O) between galactose and the phenolic fluorophore in suitable reacting conditions and generate fluorescence enhancement. The hydrophilic galactose will improve water-solubility of the whole probe thus increasing biological compatibility for cell imaging.

A rhodamine derivative fluorescent probe was designed and synthesized^[244]. Galactose was

modified on the phenolic hydroxyl of the rhodamine ring to quench fluorescence emission efficiently. After incubation with β -galactosidase, a 76-fold fluorescence emission was obtained in PBS buffer which allowed the detection of intracellular enzyme and imaging cells (Fig. 2A). However, short Stokes shift, green emission wavelength, high sensitivity for pH variation frequently interfered the accuracy of results. Based on 4-hydroxyl-1,8-naphthalimide, a versatile two-photon probe was reported for ratiometric imaging of β -galactosidase *in vivo* (Fig. 2B)^[245]. Galactose decoration on fluorophore didn't quench the fluorescence but blue-shifted the absorption and emission wavelengths. With glycosidic bond cleavage by enzyme, weak yellow fluorescence peak was found at 545 nm accompanied by a decrease at 440 nm. Even though 680-fold enhancement of F_{545} / F_{440} ratio was observed *in vitro*, the weak fluorescence imaging intensity was still not enough to detect endogenous enzyme variations in cells or in tissues.

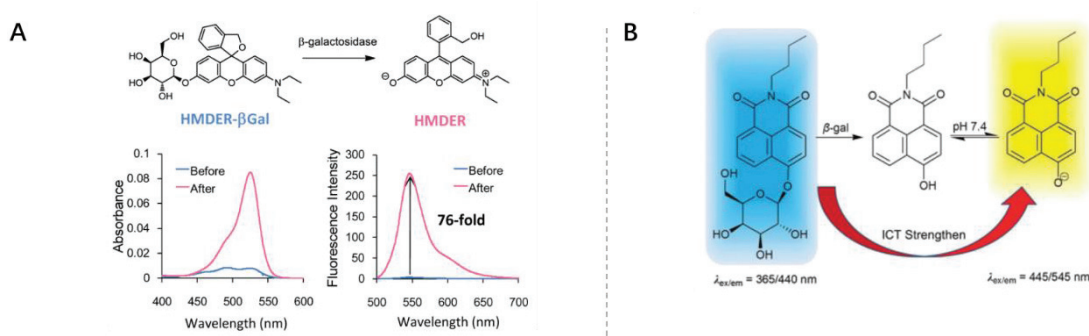


Figure 2: (A) Rhodamine based probes enhanced 76-fold fluorescence intensity after responding to β -galactosidase^[244]. (B) 4-hydroxyl-1,8-naphthalimide based two-photon probe ratiometrically detect β -galactosidase^[245].

A near-infrared probe based on cyanine derivatives was designed to detect enzyme with colour variation of probes in solution (Fig. 3A)^[235]. This probe exhibited high cell compatibility, efficient cell entry, a strong enzyme-associated fluorescence response in visible region and prolonged retention of the intracellular fluorescence signal. 6-Aminostyryl-benzothiazole was conjugated with galactose to construct a glyco-probe for enzyme detection in senescent cells (Fig. 3B)^[246]. After incubation with β -galactosidase rapidly, the fluorescence emission displayed a 200-fold increase due to the recovered ICT effect. The probe could track β -galactosidase selectively in senescent cells and monitor the concentration variation followed by whole process of cell senescence.

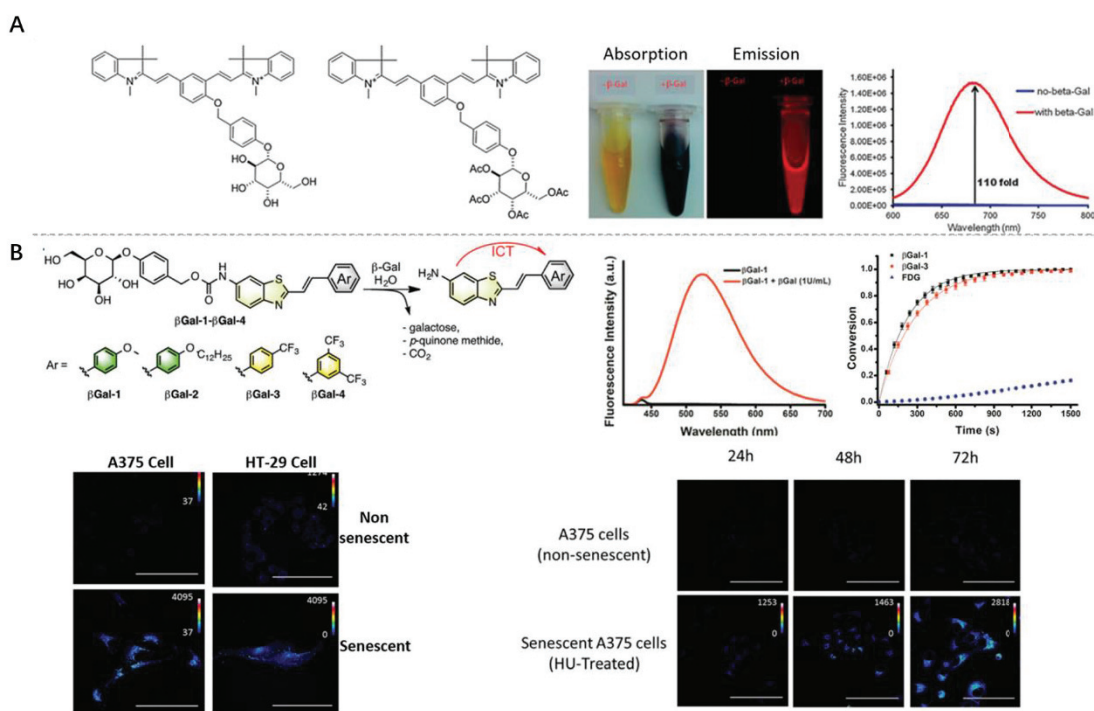


Figure 3: (A) Cyanine based fluorescent probes for β -galactosidase detection^[235]. (B) Highly sensitive probes applied to the real-time monitoring of intracellular β -galactosidase in senescent cells^[246].

Traditional organic fluorescent probes exhibited excellent optical properties for β -galactosidase detection but ACQ effect usually limited the emission intensity in aqueous solution. Intermolecular self-assembly systems were reported to detect enzymes. However, some self-assembly were too unstable or the fluorescence quenching mode for enzyme detection were not suitable to monitor instantaneous variation of β -galactosidase accurately in cell imaging^[247, 248]. Hence, AIE fluorophores were investigated based on their excellent fluorescence properties in aqueous environments. Tetraphenylethylene is a classic AIE dye with high fluorescence emission and outstanding photostability. On account of these advantages, TPE derivatives were conjugated with galactose on pyridine moieties to quench fluorescence through the positively charged pyridinium^[249]. Glycosidic bond cleaved by β -galactosidase resulted in a phenol intermediate, accompanied by 1,6-elimination of *p*-quinone to generate TPE dyes with poor water-solubility. Aggregated TPE dyes in aqueous solution could release strong fluorescence signal based on AIE and overcome biological luminescence interference. The TPE-based probes exhibited good selectivity for β -galactosidase *in vitro* and monitored higher enzyme level of OVCA3 cancer cell than HeLa cells *in vivo* (Fig. 4).

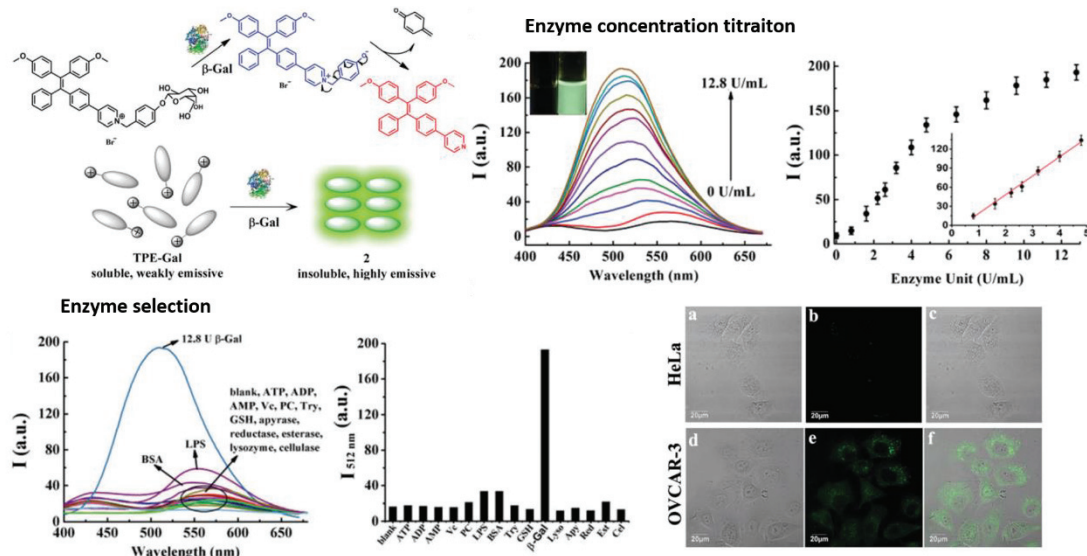


Figure 4: TPE-based glyco-probe for β -galactosidase detection and imaging intracellular enzyme in OVCAR-3 cells^[249].

The short-wavelength emission of TPE was not suitable for further biological applications. DCM derivatives are promising due to their simple synthesis, near-infrared emission and good photostability. Hence, the probe with benzopyran structure was reported for β -galactosidase detection (Fig.5A)^[250]. After enzyme cleavage of the glycosidic bond, the probe could release two types of fluorescence emission when excited at different wavelengths, followed by colour change of probe in solution. The NIR probe exhibited sensitive and selective response for β -galactosidase and excellent photostability *in vitro*. *In vivo*, it could monitor intracellular β -galactosidase with colour variation of emission in HEK-293T or OVCAR-3 cells, and selective detection of the enzyme in mice tumor. Due to the ACQ effect, the solution of poor water-soluble probe had to be mixed with 30% DMSO to maintain the fluorescence maximal intensity which impaired its biological compatibility. Hence, ethylamino substituted nitrogen on the fluorophore was introduced (Fig. 5B) to synthesize a new probe with quinoline structure (QM)^[108]. The new core has particular AIE properties through controlling the rotation of the ethyl groups. The AIE-active QM probe was composed of a hydrophilic galactose moiety that could recognize and react with β -galactosidase leading to fluorescence enhancement. The hydrolysed QM dye (QM-OH) was aggregated due to poor water-solubility which was verified by DLS data and SEM analysis. In HEK-293T cells, the probe could respond to excess enzyme in SKOV-3 ovarian cells with green fluorescence. After cleavage, QM-OH tended to accumulate in mitochondria and endoplasmic reticulum mainly through subcellular colocalization. Compared with the DCM probe with ACQ structure, AIE-active QM probe exhibited long-term tracking of β -galactosidase overexpressed in living cells with high fidelity.

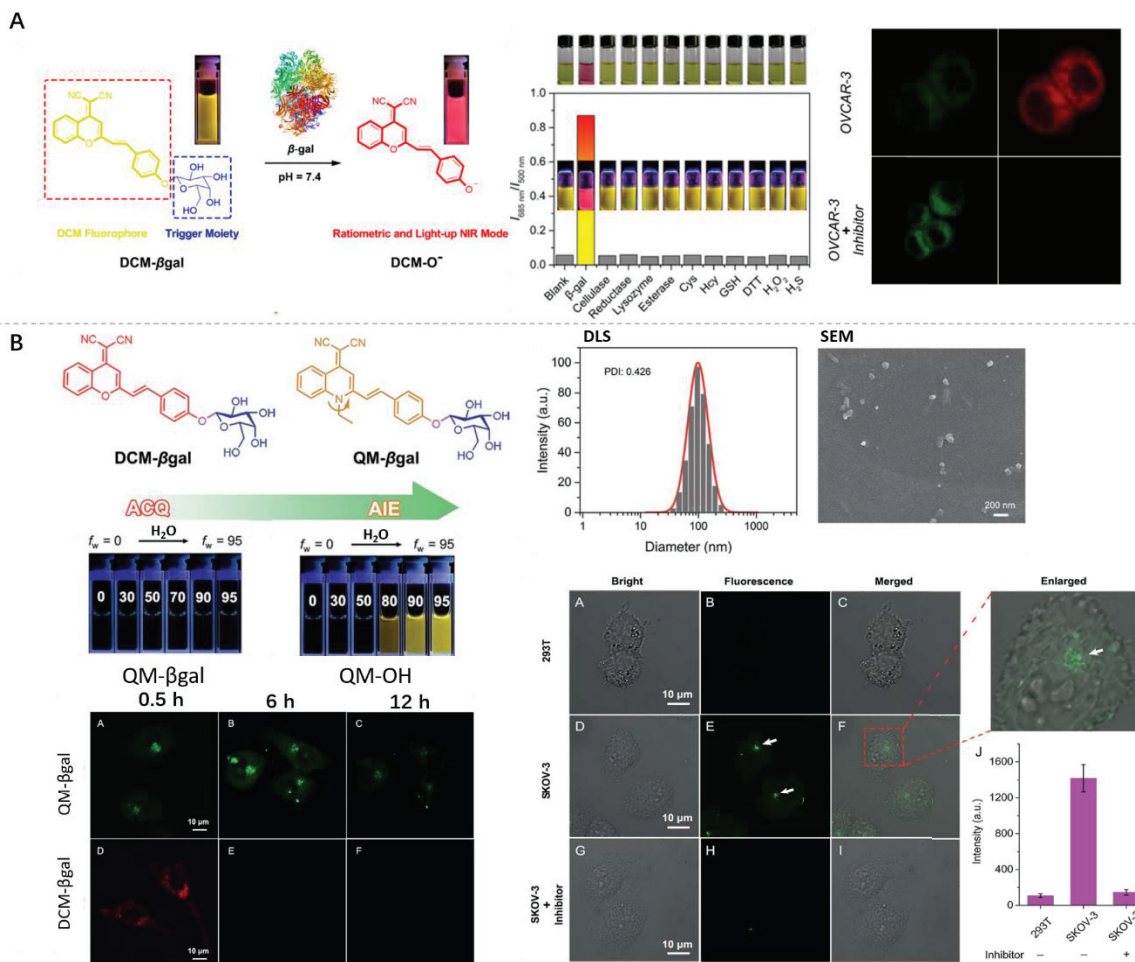


Figure 5: (A) ACQ-active DCM probe^[250] and (B) AIE-active QM probe^[108] for β -galactosidase detection in aqueous solution.

α -L-fucosidase (AFU), as a lysosome enzyme widely existing in all mammalian cells at low concentrations, is another critical glycosidase to catalyse L-fucose residues hydrolysis from glycoconjugates with high activity at pH 4 to 6.5. AFU is an important biomarker closely related to several human diseases such as fucosidosis^[251] and carcinoma^[252, 253]. Some studies demonstrated that AFU was overexpressed in hepatocellular carcinoma (HCC)^[254], hence this enzyme became a specific and sensitive indicator for early HCC diagnosis. Several fluorescent probes or system were reported with some drawbacks including low photostability, weak emission, susceptible interference by biological factors. The difficult glycosylation of fucose to generate glycosylated phenols towards fluorescent AFU probes, prevented the design of fluorophores.

A ratiometric fluorescent probe based on a naphthalimide derivative was designed for AFU detection (Fig. 6)^[255]. A similar conjugation strategy as probes for galactosidase was applied and fucose was modified on the hydroxy group to blue-shift the emission wavelength through ICT influence. After incubation with AFU, the variation of emission wavelength allowed a sensitive detection even in low concentration of enzyme. HPLC and HRMS analyses confirmed verified the response mechanism directly. The probe could trace endogenous enzyme and change fluorescence signal from green to red in HEK293T cells over time. Meanwhile, the probe able to detect the enzyme in zebrafish showing that the probe has enough photostability for detection in living systems.

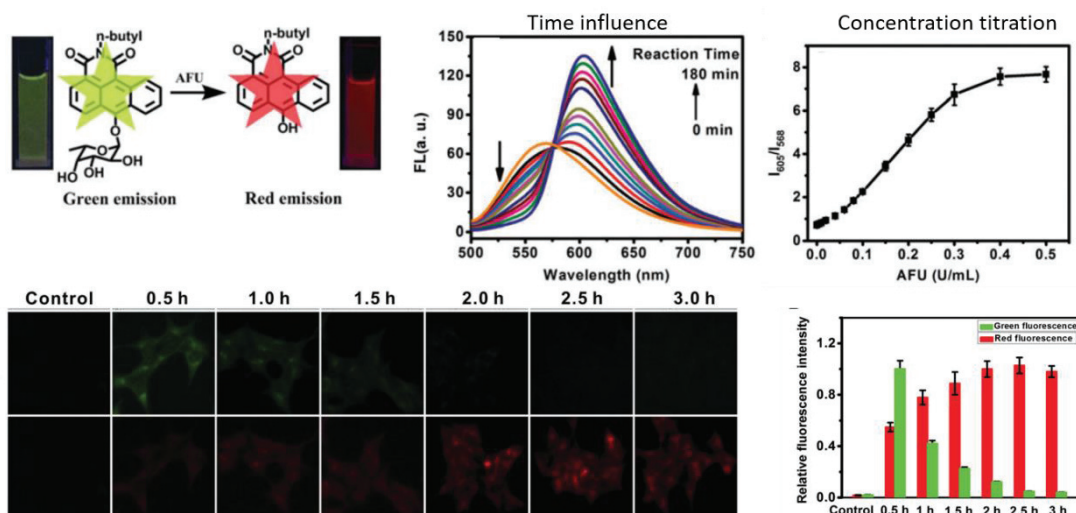


Figure 6: Ratiometric fluorescent probe based on 1,8-naphthalimide derivatives for endogenous AFU detection^[255].

β -Glucosidases are a group of glycosyl hydrolases for cleavage of β -glucosidic disaccharides or others glucose-containing molecules. As an abundant enzyme widely existing in microorganisms, plants, mammals and humans, it is essential in biological processes. Therefore, a FRET fluorescent probe was designed for β -glucosidase (GCD) and phosphodiesterase I (PDE) detection with two fluorescence emission (Fig.7A)^[256]. Based on 7-hydroxycoumarin and meso-tetraphenylporphyrin (TPP), glucose was glycosylated on hydroxyl groups to quench fluorescence and block energy transfer through a phosphoester bond. This probe displayed preferable response for two enzymes and distinct colour variation in Huh7 cell imaging. Besides, a novel coumarin probe, based on excited-state intramolecular proton transfer (ESIPT) phenomenon, for evaluation of β -glucosidase with fluorescence enhancement was designed (Fig.7B)^[257]. The *p*-fluorophenyl group modified on hydroxycoumarin could extend the emission wavelength efficiently. Poor solubility, low photostability and short emission wavelength were still impairing further development of probes for glycosidase detection.

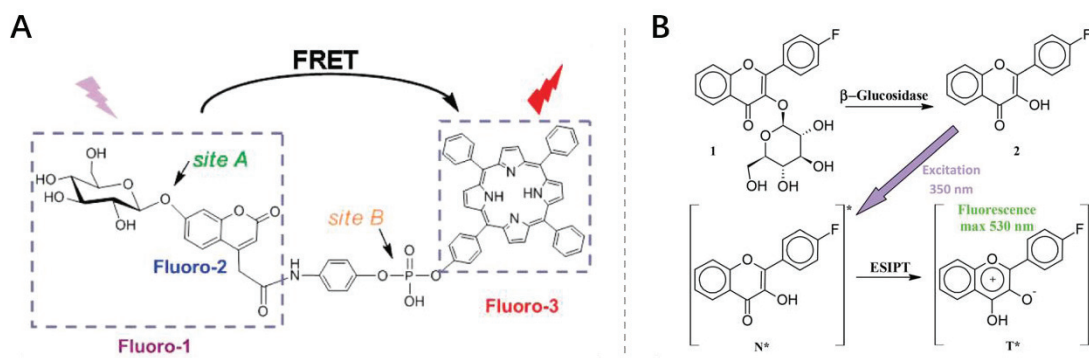


Figure 7: (A) 7-hydroxycoumarin and meso-tetraphenylporphyrin based FRET probe detecting β -glucosidase and phosphodiesterase I^[256]. (B) Flavonol-based fluorescent indicator for determination of β -glucosidase activity^[257].

V.1.2 Project design

A fluorescent probe should be designed with different response mechanisms and several

improvements including near-infrared emission wavelength, distinct emission intensity variation, high water-solubility, preferable photostability, sensitive and selective response for enzyme, universal structural design for different glycosidase and AIE properties. As previously reported^[144], water-solubility can be improved by glycoclusters conjugation to control optical properties of the probe through AIE effect in aqueous solution. Therefore, several monosaccharides conjugated on a NIR fluorophore with AIE properties maybe quench fluorescence in aqueous solution primarily. After glycosidase hydrolysis, water-solubility variation will reduce and the probe will aggregate followed by fluorescence enhancement due to AIE effect (Fig.8).

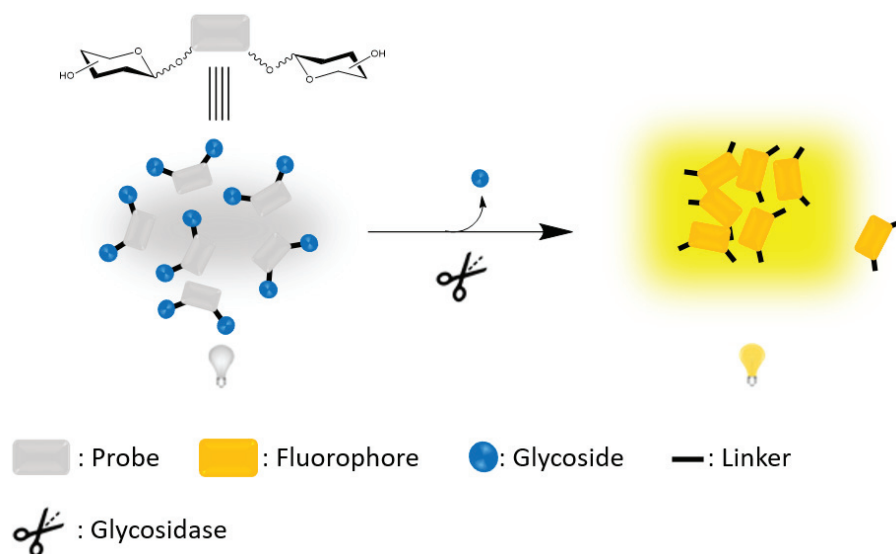


Figure 8: The responding process of AIE probe for glycosidases through water-solubility variation.

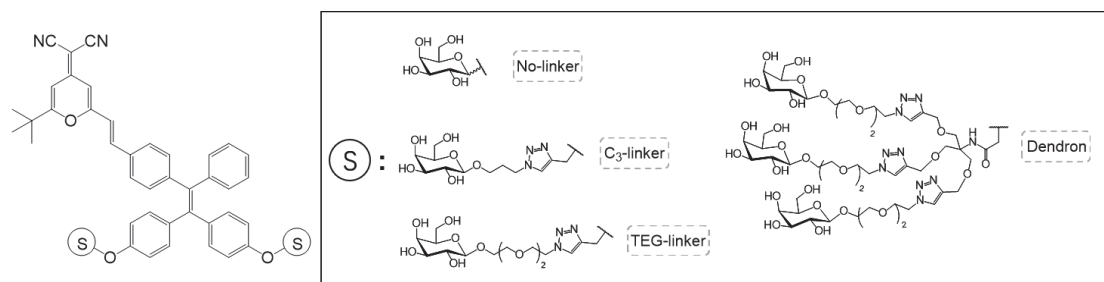
V.1.2.1 AIE fluorophore design

As typical AIE fluorophore, the short emission wavelength of TPE restricted its further biological imaging in cells or tissues, while it performs excellent AIE fluorescence properties. DCM derivatives have red fluorescence emission, good photostability and simple synthesis procedures, but poor water-solubility interferes with fluorescence intensity by ACQ effect in aqueous solution. Hence, combining TPE and DCM may be a reasonable approach to synthesize a novel fluorophore with the advantages of TPE and DCM derivatives. Multiple modifiable positions on the fluorophore to control emission wavelength or intensity, is necessary for fluorophore design.

Due to the detection of glycosidases through fluorescence enhancement, how to quench or decay original emission intensity is a critical aspect to determine relative optical properties for enzyme detection. There are two different ways to quench fluorescence intensity of a dye: (i) monosaccharide is glycosylated with hydroxy on TPE-DCM directly to quench fluorescence by blocking the ICT effect, (ii) after conjugation several monosaccharides with linkers, sufficient water-solubility allows probe to disperse in aqueous solution alone with low initial fluorescence emission. The appropriate number of monosaccharides decorating on fluorophore should be explored, because suitable water-solubility can influence the sensitivity of probes. Here, we will design and synthesize probes with different modifications, and explore their water-solubility for enzyme response *in vitro* (Scheme 1).

We will use either no linker or a C₃-linker or a TEG-linker to study the influence of the ICT

quenching approach. We will also design a dendron with 6 galactosides available for enzyme hydrolysis to investigate the influence of valency.

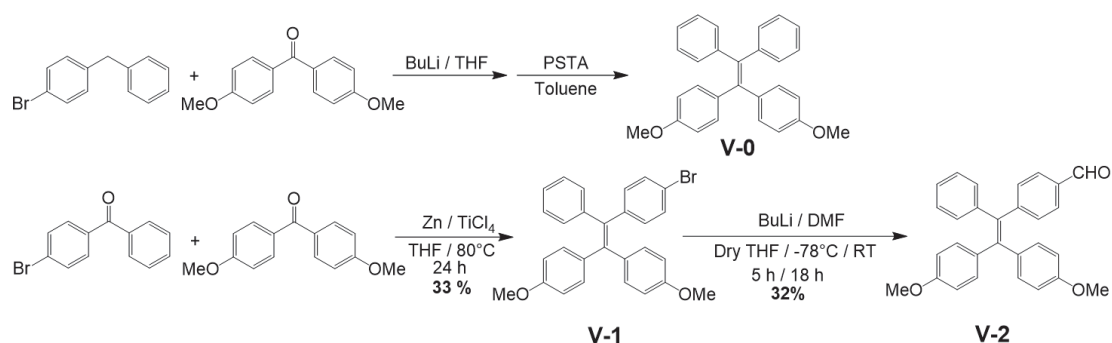


Scheme 1: Chemical structures of TPE-DCM-based glyco-probe for enzyme response.

V.2 Synthesis of the TPE-DCM probes

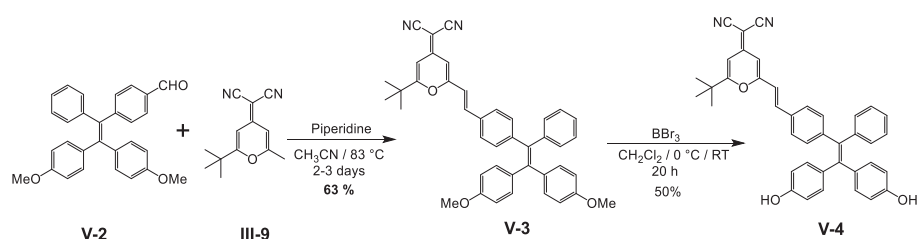
V.2.1 Synthesis of a carbonyl TPE moiety

For the synthesis of compound **V-1**, the Knoevenagel condensation^[102] is an appropriate method to synthesize bisymmetric TPE with multiple functional groups. Therefore, 4-bromodiphenylmethane reacted with *n*-butyllithium then with 4,4'-dimethoxybenzophenone in THF. Acidic dehydration afforded the dimethoxy TPE but not compound **V-1** because the bromine atom has higher reactivity for *n*-butyllithium than hydrogen on methylene leading to compound **V-0**. We then used employ McMurry reaction to synthesize the target compound **V-1** while many by-products would be generated in the meantime (Scheme 2).



Scheme 2: Synthesis scheme of carbonyl TPE **V-2**.

V.2.2 Synthesis of the NIR fluorophore (TPE-DCM)



Scheme 3: Synthesis of dihydroxy TPE-DCM (**V-4**).

Through aldol condensation, the TPE **V-2** and DCM **III-9** were combined with piperidine catalysis at 83°C to obtain the AIE fluorophore **V-3** (Scheme 3). Then, we measured the AIE fluorescence variation of TPE-DCM **V-3** with addition of water in THF (Fig. 9). Compound **V-3** displayed long emission wavelength fluorescence at 610 nm due to establishing intramolecular electron “pull-push” system and extending π - π conjugation system. Compound **V-3** exhibited a fluorescence enhancement in high water ratio in agreement with AIE definition. Hence, compound **V-3** was demethylated with BBr_3 to obtain dihydroxy TPE-DCM **V-4** for further conjugation with glycoside.

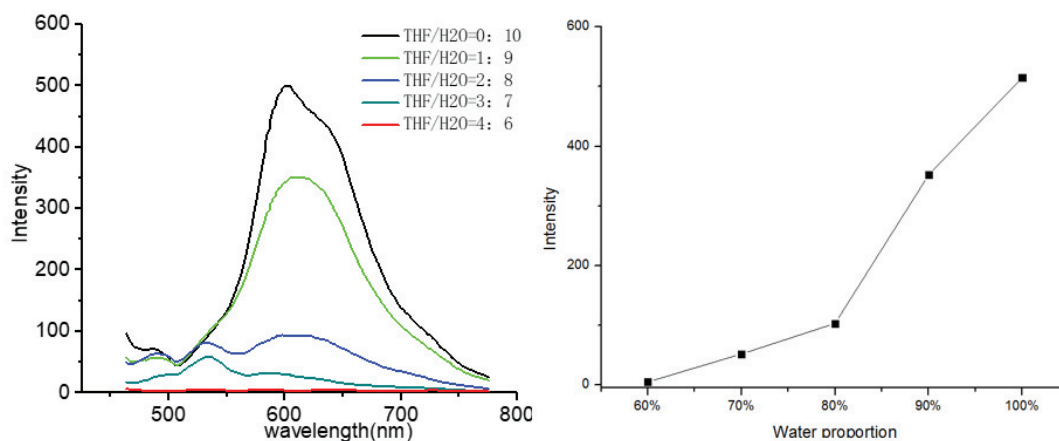
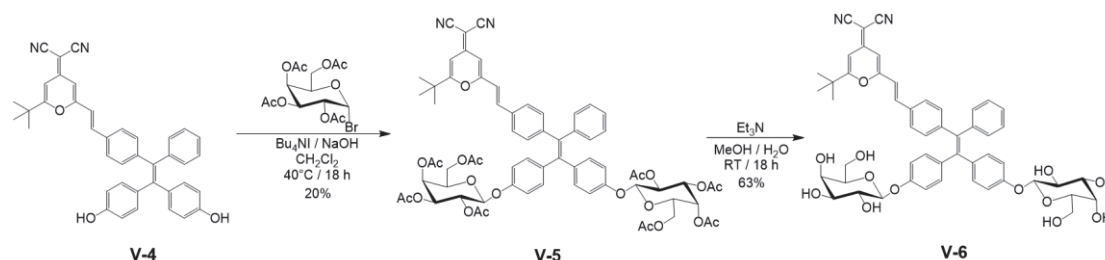


Figure 9: AIE property of fluorophore **V-3** with water ratio increase.

V.2.3 Carbohydrates decorated on fluorophore through glycosylation



Scheme 4: Carbohydrates decoration of TPE-DCM probe through glycosylation without linkers.

1,2,3,4,6-Pentaacetyl- β -D-galactopyranose was reacted with compound **V-4** in basic CH_2Cl_2 solution catalysed by Bu_4NI at 40°C. NaOH as a base, was sufficient to remove proton on hydroxy and promote glycosylation. Compound **V-5** emitted low fluorescence intensity due to galactosides blocking the ICT effect. After deprotection in Et_3N aqueous solution, compound **V-6** with two galactosides exhibited low initial fluorescence intensity and good solubility in aqueous solution.

The fluorescence response of probe **V-6** to β -galactosidase was measured in PBS buffer (pH 6.0 and 7.4). Different concentrations of enzyme (0.01 to 0.06 U/mL) were added in the probe solution (10 μM) and incubated during 10 min before measuring emission intensity. After incubating 0.01 U/mL enzyme, the fluorescence intensity have been increased to maximum at pH 6.0 (Fig. 10A). The emission intensity was not enhanced any more while adding more enzyme in solution. However, the performance of **V-6** at pH 7.4 was different since the fluorescence intensity was decaying with

enzyme concentration increase (Fig. 10B).

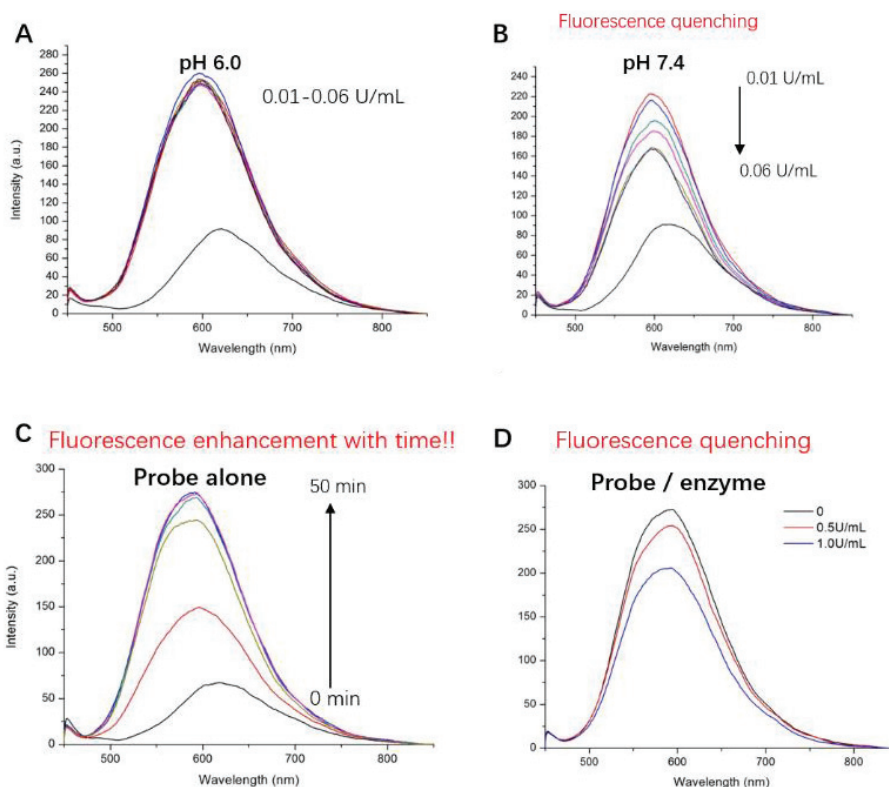
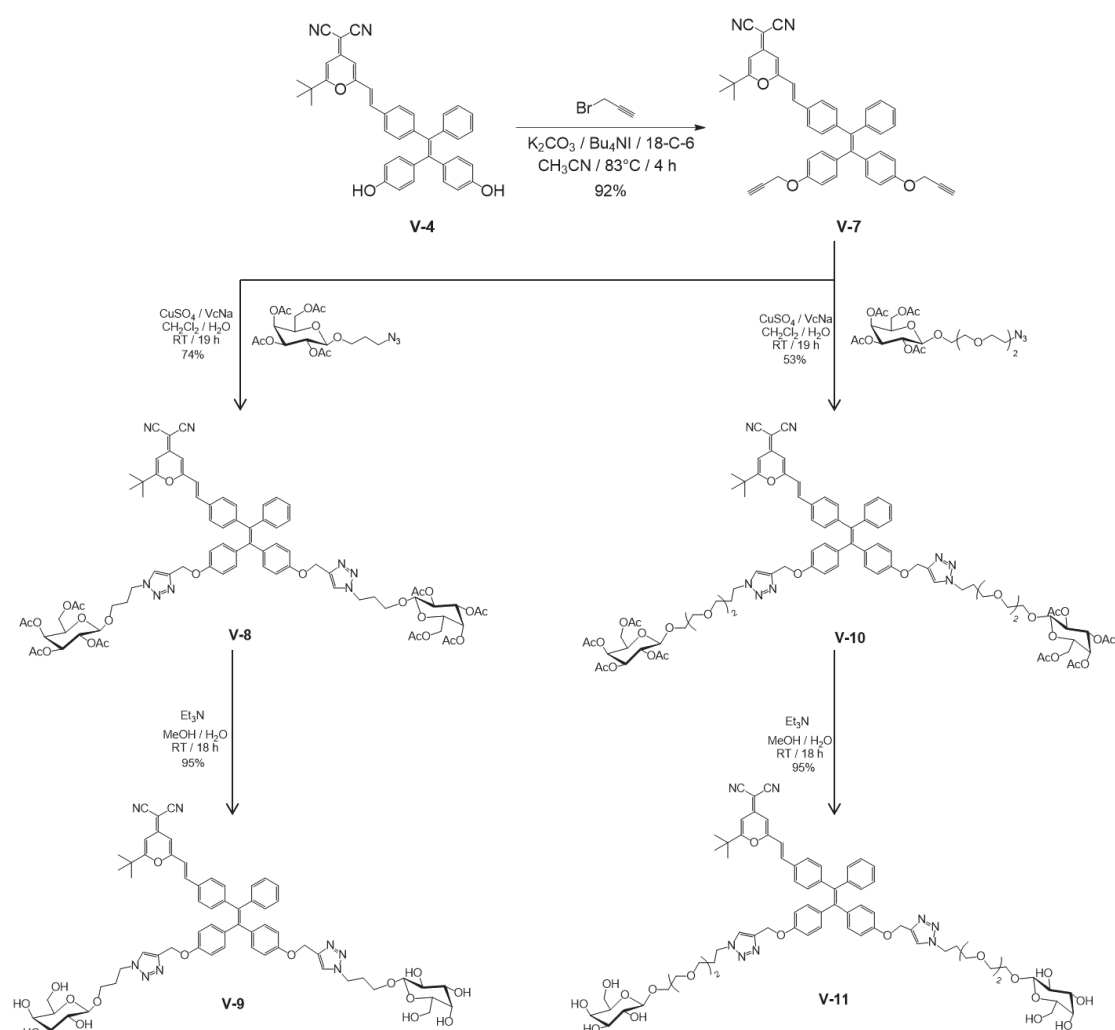


Figure 10: Fluorescence variation of V-6 with enzyme response at (A) pH = 6 and (B) pH=7.4. (C) Fluorescence enhancement due to molecular aggregation. (D) Enzyme reduced to fluorescence decay.

Subsequently, we measured fluorescence variation of the probe V-6 alone with time increase in PBS buffer at pH 7.4 (Fig. 10C). The emission intensity reached a maximum after stirring 20 min, and similar to the sample incubated enzyme at pH 6.0 (Fig. 10A). This phenomenon indicated that the initial emission intensity was not stable due to molecules aggregating slowly in PBS solution. Two galactosides improved water-solubility of V-6 but did not disperse molecules in PBS sufficiently and quench the AIE fluorescence completely. Therefore, the probe still emitted strong fluorescence after molecular aggregation. After incubating with the enzyme, the newly generated fluorophore V-4 released weaker emission than V-6 in aggregated state, which could explain why fluorescence intensity was decreased (Fig. 10D). We speculated that aggregated molecules (V-4 or V-6) displayed emission intensity influenced by their solubility in aqueous buffer which was similar to AIE effect. So, this model was not applicable for galactosidase detection because fluorescence “turn-on” was not reliable after incubation with the enzyme.

V.2.4 Conjugation through C₃ or TEG linkers



Scheme 5: Synthesis of two glycosylated TPE-DCM probes with C₃ (**V-9**) or TEG (**V-11**) linkers.

Propargylation of the dihydroxy TPE-DCM **V-4** was catalysed by Bu_4NI in basic MeCN solution to synthesize dipropargyl TPE-DCM **V-7**. Monosaccharides with different azide linker were combined with fluorophore **V-7** through Cu^{2+} / VcNa catalysis “click” reaction (CuAAC). After deacetylation in Et_3N aqueous solution, the probe **V-11** was supposed to have higher water-solubility and lower initial fluorescence intensity than probe **V-9**, because the hydrophilic TEG linkers could efficiently promote probes to disperse in solution compared with the C₃ linker. Hence, the fluorescence changes of both probes (10 μM) after incubating galactosidase were compared in neutral PBS buffer (Fig. 11).

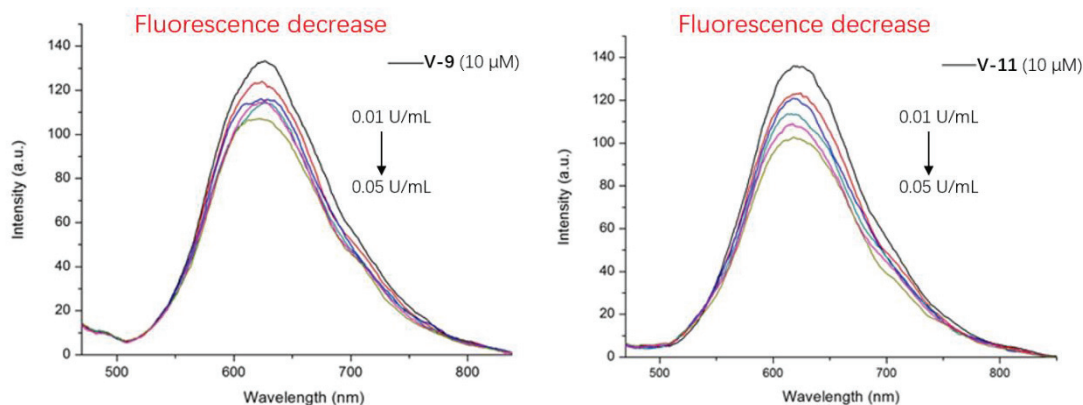


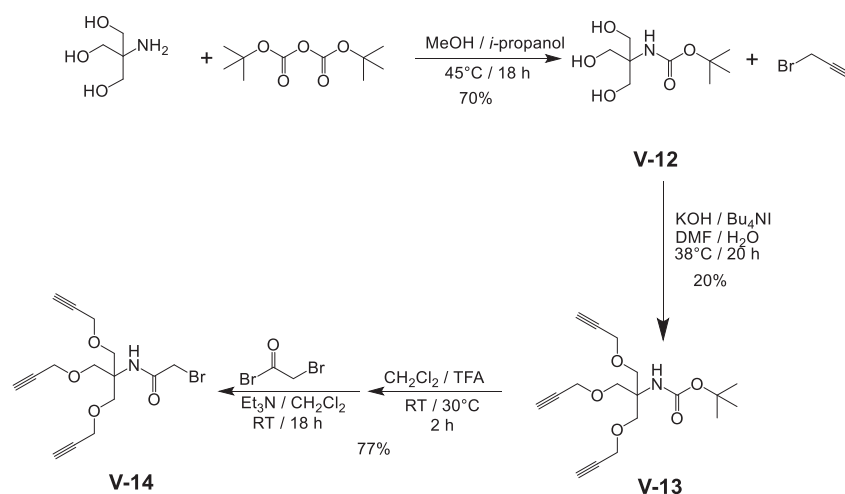
Figure 11: Fluorescence emission of **V-9** and **V-11** upon addition of galactosidases in neutral PBS solution.

The two probes with different linkers, presented similar high fluorescence emission in PBS buffer. These phenomena illustrated that the water-soluble molecules have been at least partially aggregated before adding the enzyme, even though carbohydrates were decorating the fluorophores. With increasing concentration of galactosidase, the monosaccharide hydrophilic moiety was cleaved leading to poorer water-solubility. However, the decreasing trends of emission were similar to the performance of probe **V-6**, which explained that the good solubility obtained from the linker could still influence optical properties while the AIE effect enhanced emission intensity of the probes. Due to the large hydrophobic fluorophore, two monosaccharides were not enough to block AIE fluorescence through high water-solubility of molecules in aqueous environment.

V.2.5 Design and synthesis of TPE-DCM-based glycoclusters

Only two modifiable positions on the TPE-DCM core restricted the conjugation with more carbohydrates directly through “click” reaction, although TEG linkers were expected to provide enough hydrophilic ability to improve the probe dispersion in aqueous solution. We therefore conjugated two trivalent dendrons bearing each three monosaccharides to obtain a higher water solubility.

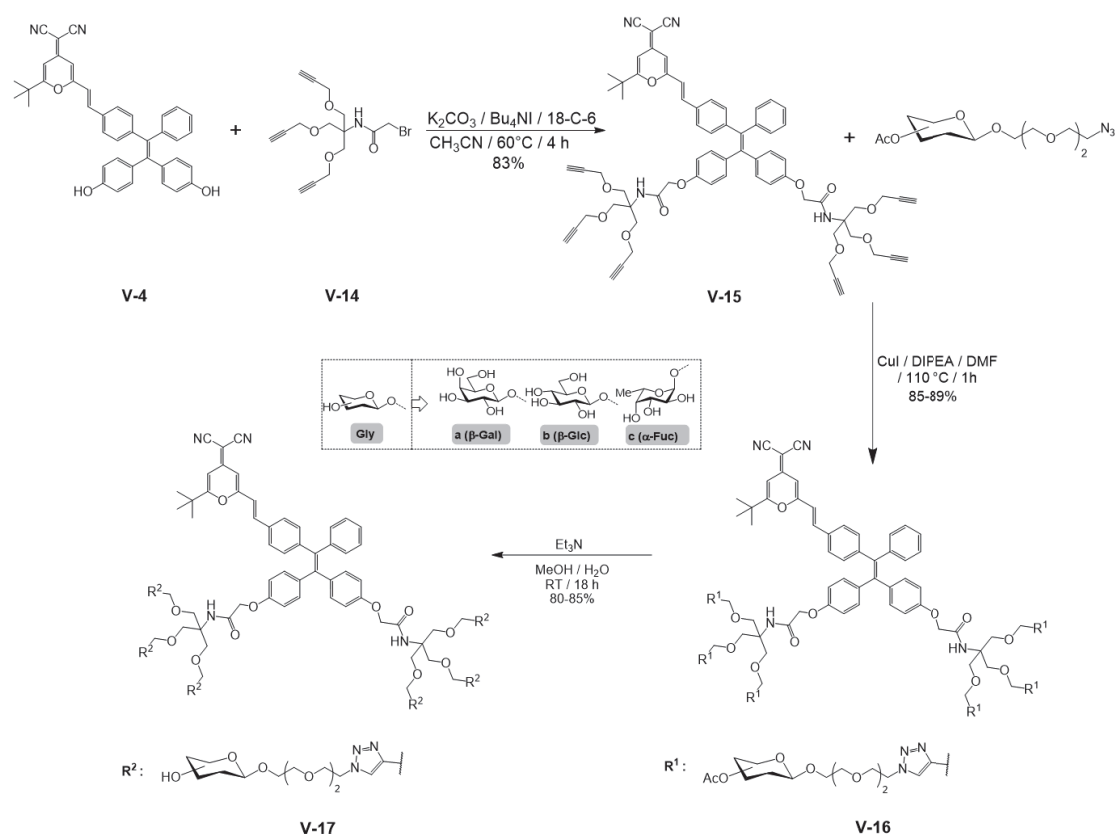
V.2.5.1 Synthesis of the propargylated dendron.



Scheme 6: Synthesis scheme of tripropargyl linker.

Tris(hydroxymethyl)aminomethane (Tris) was protected by di-*t*-butyl dicarbonate (Boc) in MeOH solution with 10% *i*-propanol. Then three equivalents of propargyl bromide were condensed with the compound **V-12** catalysed by KOH and Bu₄NI in DMF and H₂O solution. In this procedure, reacting temperature was the most important parameter for the yield due to low stability of intermediates decomposed by KOH at higher temperatures. The two steps of Boc-deprotection and amidation were combined to synthesize compound **V-14** with three propargyl for “click” reaction and a bromine atom as a precursor for conjugation to the fluorophore (Scheme 6).

V.2.5.2 Synthesis of TPE-DCM-based glycoclusters



Scheme 7: Synthesis of TPE-DCM-based glycoclusters for glycosidase detection.

Two equivalents of compound **V-14** were substituted at the phenol of fluorophore **V-4** to synthesize compound **V-15** with six propargyl moieties for “click” reaction. Compound **V-16a** was obtained from the propargyl fluorophore **V-15** with azido-galactoside catalysed by CuI in basic DMF. Microwaves could accelerate the reaction rate and promote conjugation on the fluorophore overcoming steric hinderance. After deprotection in Et₃N aqueous solution, the terminal probe **V-17a** displayed good water-solubility without any organic solvent assistance. The probe emitting lower fluorescence intensity demonstrated that it was readily soluble and it could detect galactosidase in aqueous solution. Hence, through “click” reaction and deprotection, we synthesized similarly probe **V-17b** for glucosidase and probe **V-17c** for fucosidase detection.

V.3 Water-soluble TPE-DCM-based glycoclusters for galactosidase detection

The novel TPE-DCM-based glycoclusters with six monosaccharides displayed high water-solubility, long emission wavelength and excellent AIE properties, and should have ability to detect glycosidase and respond by fluorescence enhancement. Here, we will display some essential fluorescence data of probe **V-17a** for β -galactosidase (β -Gal) response, and discuss about the relevant working mechanism.

V.3.1 Fluorescence detection of β -galactosidase

For β -galactosidase detection, basic optical data including absorption wavelength, fluorescence wavelength, quantum yield, Stokes-shift and other basic parameters should be measured. Hence, probe **V-17a** (10 μ M) was incubated with β -Gal (10 U/mL) during 50 min at 37°C, and the fluorescence variation was then measured (Fig. 12).

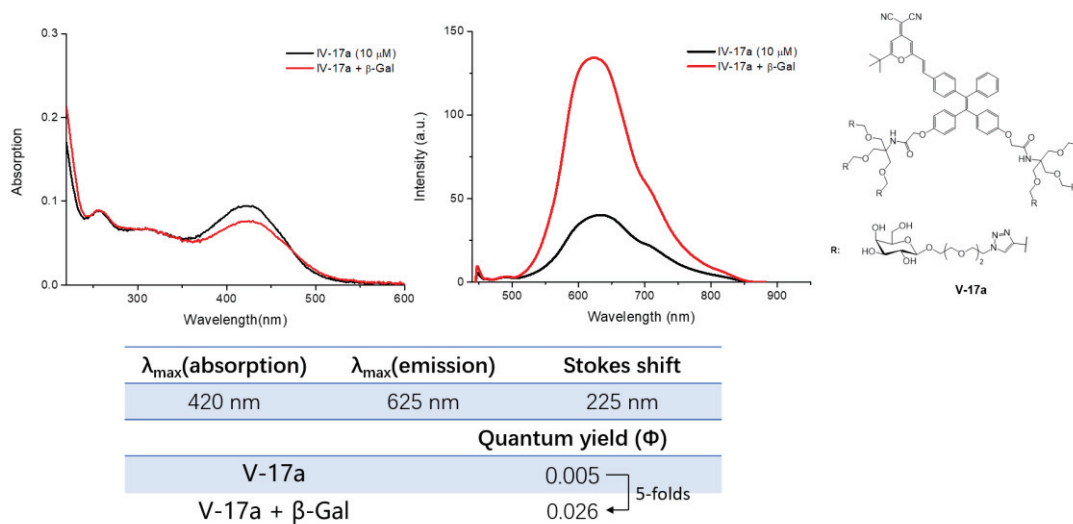


Figure 12: Fluorescence variation of probe **V-17a** after incubation with β -Gal.

The probe dissolved in PBS displayed higher absorption at 420 nm and lower emission at 625 nm, which verified that molecules were in soluble or in a low aggregation state due to high-water solubility. After incubating with β -Gal, the glycosidic bond cleavage led to less hydrophilic probes, thus increasing fluorescence emission through intermolecular aggregation of residues. The unchanged wavelength of absorption and emission after adding β -Gal, illustrated that the fluorophore structure was overall stable apart from the enzyme hydrolysing glycosides. Compared with the fluorophore DCM-OH (**III-10**, $\lambda_{\text{ex}} = 480$ nm, $\lambda_{\text{em}} = 625$ nm), **V-17a** displayed a larger Stokes shift from shorter absorption wavelength and with the same emission wavelength. The response mechanism through AIE effect allowed the probe to perform detection in aqueous solution directly without solubility improvement from other glycoclusters (such as TPE-glycoclusters) or co-solvent. This stable process excluded some interference from interaction between the fluorophore and serum protein (such as BSA and HSA). Hence, **V-17a** exhibited distinct fluorescence enhancement for β -Gal in PBS buffer.

V.3.2 Influence of probe concentration

For detection of the enzyme through AIE effect, the original concentration of the probe was a crucial parameter to influence initial fluorescence intensity. Therefore, we measured the emission intensity with different concentrations of the probe **V-17a** (Fig. 13).

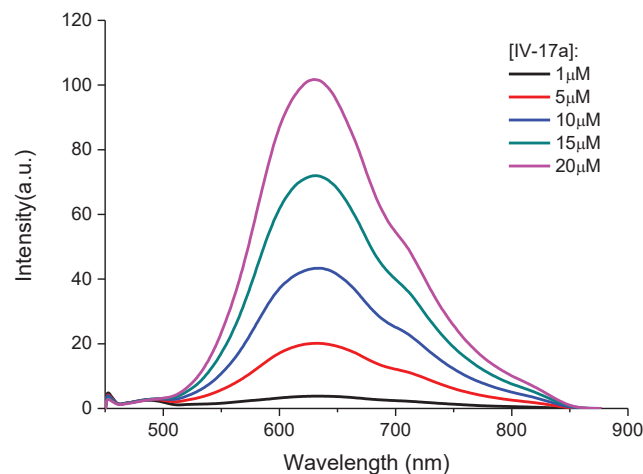


Figure 13: Initial fluorescence intensity with different concentration of **V-17a**.

The fluorescence intensity enhanced with increasing the probe's concentration in aqueous buffer. Although six galactoses were modified on fluorophore, the fluorescence was not totally quenched. We thought that the large hydrophilic moieties may partly impede the rotation of phenyl ring leading to weaker emission. At higher concentration of the probe, a portion of molecules would aggregate together to enhance the emission signal. Hence, for low initial emission and distinct fluorescence response, 10 μM appears as a suitable concentration of **V-17a** for subsequent parameter measurements.

V.3.3 Reverse AIE effect of TPE-DCM-glycoclusters

According to the prospective response mechanism, the sufficient water-solubility of probes was an essential condition for enzyme detection in aqueous solution, so that the molecules would aggregate and release fluorescence by AIE effect after enzyme hydrolysis of the glycosides. To explore the AIE properties, the fluorescence of probes **V-17a** and **V-11** were measured with increasing fraction of water in THF.

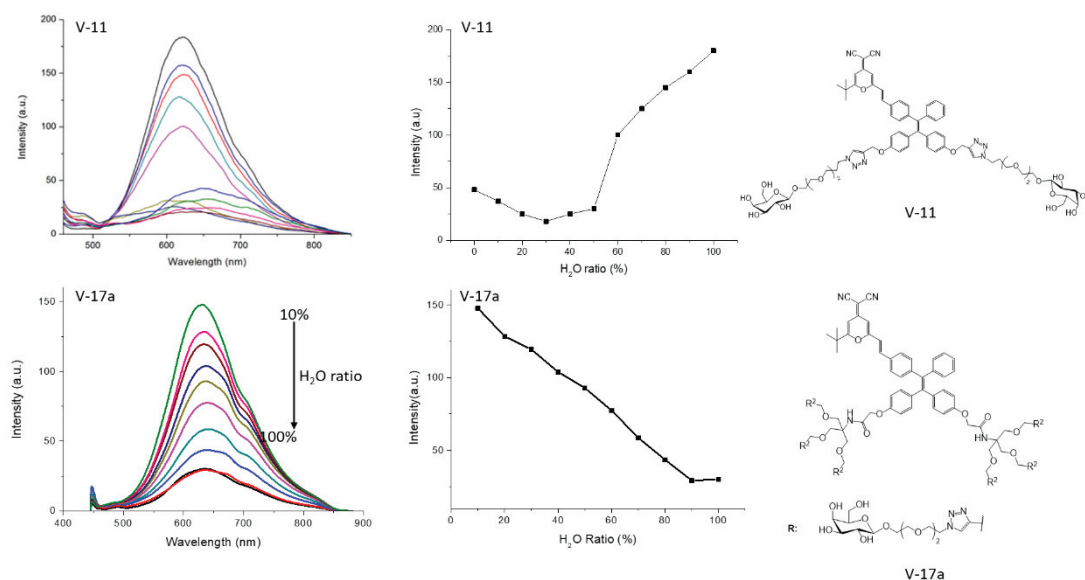


Figure 14: AIE effect influencing the fluorescence intensity of **V-11** and **V-17a** with increasing water ratio in THF.

For probe **V-11**, the water-solubility in THF solutions was too poor to provide a fluorescence signal. Adding water from 0 to 30% into THF promoted the solubility of **V-11** quenching the fluorescence slightly. With continually increase of the water ratio (>50%), the hydrophilic solubility of **V-11** was inadequate leading to fluorescence enhancement rapidly by AIE. Hence, the water-solubility of **V-11** limited its application for galactosidase detection. The probe **V-17a** with six glycosides has optimal water-solubility. Compared with other AIE organic probes, this probe exhibited reverse AIE fluorescence effect when increasing the water ratio from 0 to 100% in THF (Fig. 14). Therefore, probe **V-17a** with weak initial fluorescence intensity in pure water was appropriate to detect galactosidase *in vitro*.

V.3.4 Influence of time for β -Gal detection with probe **V-17a**

While glycoside hydrolysis is not an instantaneous process, the response time needs to be measured for determining enzyme incubation. Hence, we incubated different concentrations of β -Gal with **V-17a**, and measured the fluorescence variation in PBS buffer (Fig. 15).

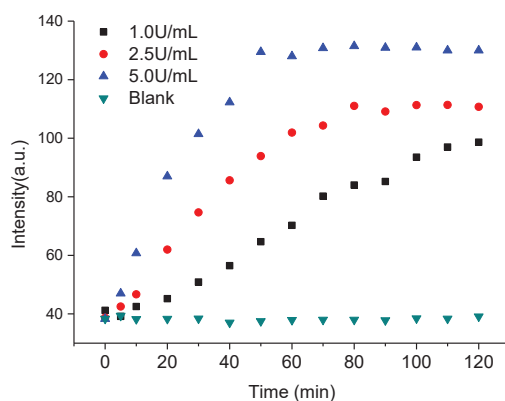


Figure 15: The response time of **V-17a** incubated with increasing concentrations of β -Gal.

The fluorescence intensity kept increasing with time after adding different concentrations of β -Gal, which illustrated that **V-17a** could respond to β -Gal (5.0 U/mL) in aqueous solution. The highest concentration of β -Gal could hydrolyse the glycosides to reach the maximal fluorescence intensity with shorter time (~40 min) and more distinct signal changes (from ~40 to ~130 a.u.). After 50 min incubation with 2.5 or 5.0 U/mL, the fluorescence did not further increase indicating that the enzyme had complete hydrolyse the probe's glycosides. Hence, we will incubate β -Gal with **V-17a** during 50 min in subsequent experiments.

V.3.5 pH influence

We incubated β -Gal (5 U/mL) and **V-17a** together during 50 min and subsequently measured the fluorescence enhancements in different pH PBS solution (Fig. 16). The pH was adjusted by adding Na_2HPO_4 or NaH_2PO_4 aqueous solution.

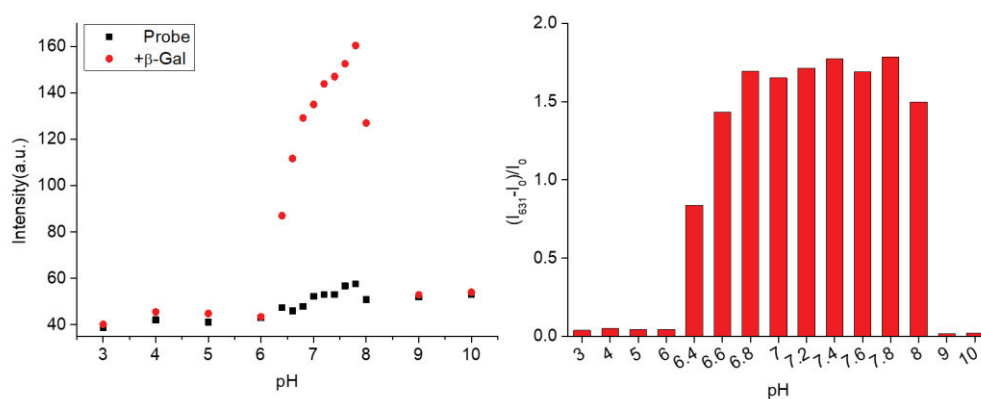


Figure 16: The influence of β -Gal hydrolysis activity in PBS buffer with different pH values.

The basic fluorescence intensity was almost stable at different pH. After incubating β -Gal during 50 min, the samples have no fluorescence emission in acidic (pH 3-6) and basic (pH 9-10) PBS solution. The fluorescence intensity was distinctly changed after incubating enzyme in weak acidic or neutral aqueous solution. The maximal fluorescence enhancement illustrated that the pH range of 6.8-7.8 was the best condition for enzyme hydrolysis. For the responding process, the pH value didn't interfere with the original fluorescence properties of probes, but seriously influenced the enzyme activity for hydrolysing glycosides to change the water-solubility. Hence, the neutral PBS solution (pH 7.4) was applied in subsequent experiments.

V.3.6 TPE-DCM-glycoclusters quantifying β -Gal concentration

The ability of TPE-DCM-glycoclusters for enzyme quantification is the most important requirement for further applications in cell supernatant and biological assay. Therefore, the probe **V-17a** was incubated with different concentrations of β -Gal in neutral PBS buffer during 50 min (Fig. 17)

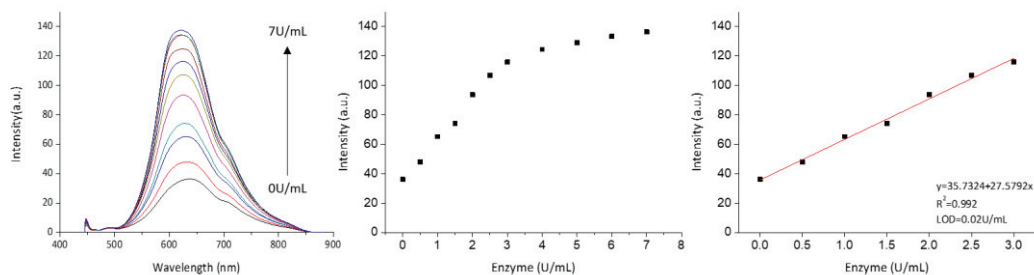


Figure 17: Fluorescence enhancement of **V-17a** upon addition of β -Gal, and relative standard titration line.

The probe **V-17a** emitted low fluorescence emission in PBS buffer before incubating with the enzyme. When incubating different concentrations of β -Gal during the same time (50 min), the fluorescence intensity was increased linearly from 0 to 3 U/mL. The enhancement tendency was weaker when incubating with β -Gal more than 3 U/mL, which illustrated that the hydrolysis of the glycoside from the probe by the enzyme was almost completed. The fluorescence enhancement of **V-17a** showed a linear relationship with enzyme concentration from 0 to 3 U/mL. Therefore, the standard titration line was calculated and fitted to obtain the limit of detection (0.02 U/mL, $LOD = 3\delta/k$) which was compatible with the β -Gal detection *in vivo*.

V.3.7 Selectivity of **V-17a** for β -Gal detection

Although the probe exhibited excellent linear relationship with β -Gal concentration, the specific fluorescence enhancement for only β -Gal response was necessary. The DCM fluorophore and its derivatives normally have high affinity to combine with many proteins such as BSA and HSA, which could amplify the fluorescence signal^[168]. Since the response mechanism to the enzyme is based on AIE effect, the protein selectivity of **V-17a** was required to verify the lack of interference from other enzymes. Hence, we mixed probe **V-17a** with many common amino acids, proteins, lectins and glycosidase during 50 min in neutral PBS solution, and measured the fluorescence variation (Fig. 18).

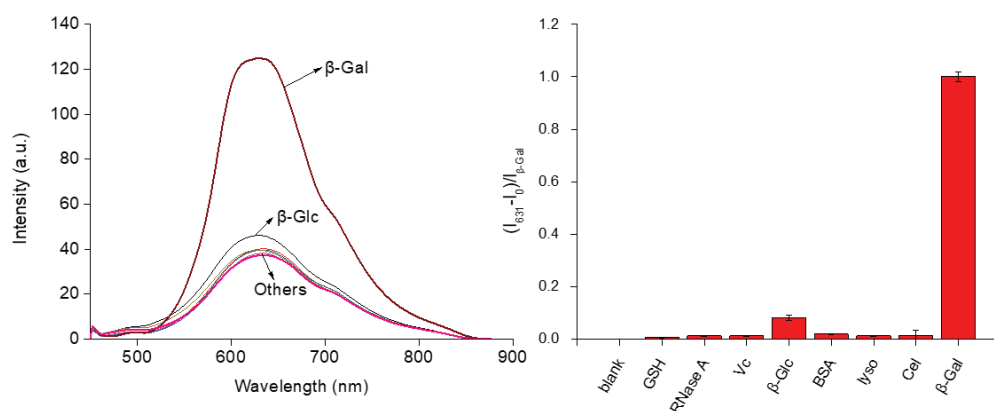


Figure 18: Selectivity of **V-17a** when mixed with common amino acids, proteins, lectins and glycosidases.

Apart from a slight fluorescence enhancement with other proteins, the probe released a large fluorescence signal for β -Gal, which demonstrated **V-17a** has excellent selectivity to recognize and

respond to its particular glycosidase. The weak emission changes after incubating with β -glucosidase (β -Glc) could be due to aggregation into the enzyme through non-selective binding affinity, therefore restricting rotations in the TPE core leading to a weak fluorescence emission based on AIE. It's worth noting that the probe has no fluorescence signal after mixed with BSA, certifying that serum protein (BSA) cannot combine with TPE-DCM probe and interfere with its fluorescence properties. The probe could therefore be employed to detect glycosidase in cells.

V.3.8 Carbohydrate selectivity with V-17a for β -Gal detection

According to the responding mechanism, the β -Gal specifically recognize and hydrolyse the glycosides leading to fluorophore aggregation. The influence of exogenous glycoside in the solution competing with the probe for enzyme hydrolysis can be determined to demonstrate the mechanism. Thus, the different concentrations of galactose or glucose were mixed with V-17a before incubating with β -Gal (5 U/mL) (Fig. 19).

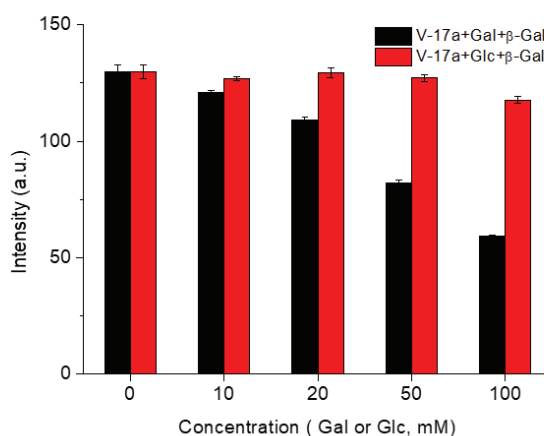


Figure 19: The competition of galactose or glucose with V-17 for β -Gal detection.

With addition of glucose in samples, the fluorescence intensity of each sample was similar after incubating same concentration of β -Gal (red bars). These results illustrated that β -Gal could only recognize the galactose residues on probes and hydrolyse them ignoring the interference from exogenous glucose. But galactoses added in solution could compete with the glycosides and disturb the reaction between enzyme and probe. Thus, the fluorescence enhancement decayed upon addition of galactose. This experiment verified that β -Gal was highly dependent on galactose so that the detecting results would be not accurate enough when abundant galactose would be present in solution.

V.3.9 Dynamic light scattering analysis

According to the mechanism of action of the probe, mass spectrometry or HPLC analysis was quite complicated because multiple residues are hydrolysed leading to multiple portions with lower solubility and aggregated state in PBS buffer. Dynamic light scattering (DLS) was a useful tool to observe the main diameter variation in this process (Fig. 20).

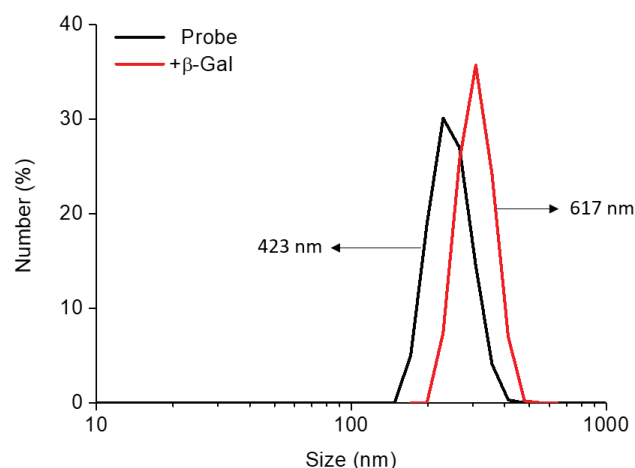


Figure 20: DLS measurement of the size variation of **V-17a** before and after incubation with β -Gal.

Due to the large volume of the probe including fluorophore and multiple glycosides with TEG linker, the size of the particle was 423 nm in PBS buffer (black line). After incubating with β -Gal, the glycosides on the probe were hydrolysed to decrease the water-solubility and promote intermolecular aggregation, leading to aggregated units with increased size to 617 nm (red line). Hence, DLS measurement verified that the enzyme detection through AIE effect was reasonable for subsequently biological assays.

V.3.10 **V-17a** detection of endogenous β -Gal and imaging cells.

β -Galactosidase is a secretory protein excessively existing in senescent cells and ovarian cancer cells. Accurately detecting the enzyme and imaging the cells are fundamental requirements for the probe evaluation. Therefore, the probe **V-17a** was incubated with senescent Wi38 cells, and normal Wi38 cells as control (fibroblasts derived from lung tissue). Meanwhile, the probe **V-17a** was incubated with SKOV3 cells (ovarian cancer cells), and normal HUVEC cells (human umbilical vein endothelial cells) as a control (Fig. 21).

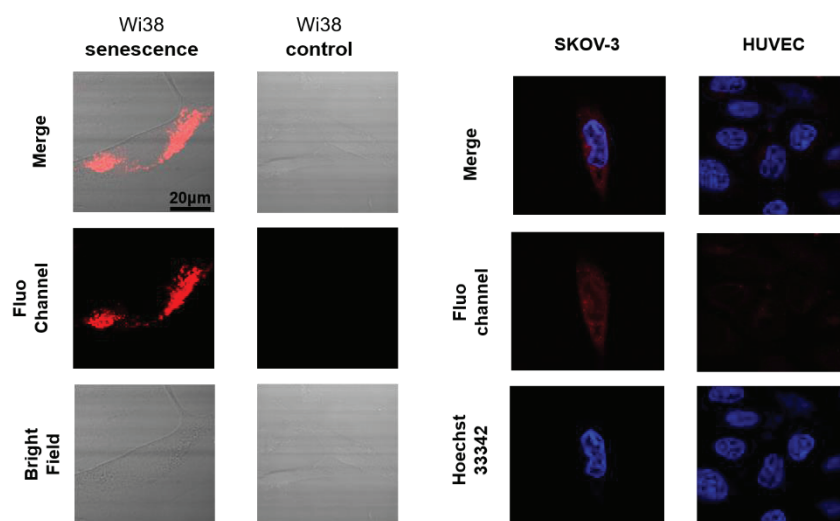


Figure 21: **V-17a** detecting endogenous β -Gal and imaging cells.

The images of normal Wi38 cells without β -Gal in cytoplasm were dark due to probe **V-17a** alone which remain soluble. When incubating with senescent Wi38 cells with excessive endogenous β -Gal in cytoplasm, the glycosides on the probe could be hydrolysed to image the cells after intermolecular aggregation (red fluorescence). Similarly, the probe **V-17a** was allowed to respond to the enzyme and release fluorescence signals in ovarian cancer cells. When comparing the images of the cell nucleus (blue), the β -Gal activity was mainly localizing in the cytoplasm (red). The red fluorescence imaging illustrated that the concentration of β -Gal in SKOV-3 cells was lower than in senescent Wi38 cells. But the fluorescence signal was not found in normal HUVE cells without enzyme. Hence, these results demonstrated that the probe **V-17a** could respond to the endogenous β -Gal and image cells through water-solubility changes and AIE effect.

V.4 Conclusion

Glycosylation is a ubiquitous modification for more than 50% of proteins. Numerous glycosidases participate in the process of polysaccharides hydrolysis. Glycosidases, as important biomarkers, were widely employed to detect diseases such as cancers or cell senescence. Galactosylated fluorescent probes were reported for galactosidase detection *in vitro* and *in vivo*. However, these probes normally have low water-solubility with quenched fluorescence emission by ACQ effect. The short emission wavelength and weak photostability were restricting their further application in biological assays. Besides, direct glycosylation of the phenol on the fluorophore was typically used to control the emission intensity. The glycosylation reactivity was restricting this pathway to detect β -galactosidase (β -Gal).

For overcoming these drawbacks and detecting multiple glycosidases by one probe design model, we combined the TPE and DCM moieties to synthesize a novel AIE fluorophore (TPE-DCM) with long-wavelength emission. The probes emitted fluorescence by AIE effect but not by traditional ICT effect and their water-solubility was changed after enzyme hydrolysis of the glycosides. We designed and synthesized probes containing two glycosides with different linkers (**V-6**, **V-9** and **V-11**), but their limited water-solubility were not suitable for β -Gal detection. For improving their water-solubility, we designed fluorescent glycoclusters with six glycosides (**V-17a**) which were soluble in PBS buffer and displayed low emission intensity.

The best conditions for β -Gal detection with **V-17a** were found when incubating β -Gal with probe (10 μ M) in neutral PBS solution during 50 min. The probe **V-17a** displayed excellent enzyme selectivity for galactosidase, with no influence from serum proteins such as BSA. DLS measurement certified the aggregation process before and after incubating with β -Gal. The probe **V-17a** exhibited linear homogenous fluorescence enhancement with addition of β -Gal. The lower LOD (0.02 U/mL) was sufficient to apply in biological assay. The standard titration of **V-17a** for β -Gal quantification was calculated and fitted. After incubating in senescent cells (Wi38) and ovarian cancer cells (SKOV-3), **V-17a** could respond to the endogenously β -Gal in cytoplasm and imaging the cells with red fluorescence emission.

At present, the measurements of **V-17b** and **V-17c** for each glycosidase detection *in vitro* and *in vivo* are under way in ECUST, China.

In conclusion, the AIE fluorescent probe **V-17a** with long-wavelength emission, excellent water-solubility and novel response mechanism, could sensitively and selectively detect β -Gal *in vitro* and *in vivo*.

Experimental Section

VI.1 General information

VI.1.1 Reagents and solvents

Commercially available reagents were purchased from Sigma-Aldrich, ThermoFisher Scientific, TCI chemicals, Fluorochem or Carbosynth. The solvents were purchased from ThermoFisher Scientific and VWR. Dry solvents (CH₂Cl₂, THF and DMF) were obtained from a PureSolv solvent purification system from Innovative Technology, or purchased from Sigma-Aldrich and ThermoFisher Scientific. Water for HPLC was obtained from an ACCU 20 Ultra Pure Water from Fisher Scientific. Analytical Thin Layer Chromatography (TLC) was carried on Macherey-Nagel silica gel 60 F254 and revealed with a UV lamp at 254 nm. Flash silica gel column chromatography was conducted with a Macherey-Nagel silica 60 M (0.04-0.063 nm).

VI.1.2 Nuclear magnetic Resonance

¹H, ¹³C, DEPT, COSY, DOSY, HSQC, HMBC experiments were performed on Bruker spectrometers: AV 300, AVL 300, AV 400, and AV 500 at 298K in the CCRMN of the University Lyon. The chemical shifts are indicated in ppm (parts per million) in reference to the solvent residual peak. Coupling constants (*J*) are indicated in Hz (Hertz). The abbreviations used for the multiplicity are: s (singlet), b (broad), d (doublet), dd (doublet of doublet), t (triplet), td (triple of doublet), q (quadruplet) and m (multiplet).

VI.1.3 Mass spectrometry

High and low resolution mass spectrometry were performed on an MicroQTOF II (50-20 000 *m/z*) apparatus from Bruker. Electrospray ionization was used in all cases.

VI.1.4 High Performance Liquid Chromatography.

HPLC analysis was performed on UPLC Thermo Scientific Dionex UltiMate 3000 system equipped with a binary pump, an auto-sampler and a variable wavelength UV detector. The column for HPLC analysis was Thermo Scientific Accucore C8 80 Å, 2.1×50 mm, 2.6 μm. The eluent system was H₂O:MeCN = 1:0 to 0:1 during 20 min.

VI.1.5 C18 Chromatography

C18 Chromatography was performed on a CombiFlash Companion system from Serlabo Technologies with a 40 g C18 Reversed-Phase column.

VI.1.6 Absorption and fluorescence and analysis

UV-absorbance spectra were carried out on a Varian Cary 500 spectrophotometer. Fluorescence spectra were recorded on a Varian Cary Eclipse fluorescence spectrophotometer.

VI.1.7 High-resolution transmission electron microscope (TEM)

A droplet of glycocluster (100 μ M) with or without DCM probes (10 μ M) was dropped onto carbon copper grids for HRTEM characterizations. JEOL 2100 equipped with a Gatan Orius charged-coupled device camera and Tridiem energy filter operating at 200 kV was used for TEM images, and the data were processed using Image J software.

VI.1.8 Dynamic light scattering (DLS).

Dynamic light scattering carried out using a Horiba LB-550 Dynamic Light Scattering Nano-Analyzer.

VI.1.9 Cell culture

HepG2, HeLa and 293T cells were cultured in Dulbecco's Modified Eagle's Medium (Invitrogen, Carlsbad, CA, USA) supplemented with 10% fetal bovine serum (Gibco, Gland Island, NY, USA). A549 cells were cultured in F12 supplemented with 10% FBS in a humidified atmosphere of 5% CO₂ and 95% air at 37 °C and split when the cells reached 85% confluency. L02 cells were cultured in Roswell Park Memorial Institute (1640) supplemented with 10% FBS. SKOV-3 cells (human ovarian cancer cell) were cultured at 37 °C under a humidified 5% CO₂ atmosphere in McCoy's 5A (Gibco, Gland Island, NY, USA), which were supplemented with 10% fetal bovine serum (Gibco, Gland Island, NY, USA) and 1% penicillin-streptomycin. WI-38 cells (human embryonic lung diploid fibroblasts cell) were cultured in 5% CO₂ atmosphere under 37°C in Dulbecco's modified Eagle's medium (Sigma, USA) supplemented with 10% fetal bovine serum (Gibco, Gland Island, NY, USA). HeLa cells (human cervical cancer cell) were cultured in 5% CO₂ atmosphere under 37°C in Dulbecco's Modified Eagle's Medium (Invitrogen, Carlsbad, CA, USA) supplemented with 10% fetal bovine serum (Gibco, Gland Island, NY, USA)

VI.1.10 Generation of shASGPR1

HepG2 cells were plated in a 12-well plate 24 h prior to viral infection. The cells at approximately 50% confluency were infected with the lentiviral particles. The plates were incubated overnight and the medium was then changed to fresh complete medium. Two days after infection, the cells were split at 1:5 and incubated for another 24 h in complete medium. Then puromycin (4 μ g/mL) was added to select the stable clones expressing the shRNA. Medium was replaced with fresh puromycin-containing medium every 3-4 days until resistant colonies can be identified. Several colonies were picked, expanded, and then assayed for stable shRNA expression by evaluating level of ASGPR1 mRNA via real-time quantitative polymerase chain reaction (qPCR).

VI.2 Synthesis

VI.2.1 General procedures

General procedure A for formation of TPE core by Knoevenagel condensation

To a solution of diphenylmethane (1.3 eq.) in dry THF (30 mL) was added *n*-butyllithium (1.3 eq., 2.5 M in hexane) dropwise at 0°C and the resulting solution was stirred at 0°C under argon during 45 min. A solution of ketone (1 eq.) in dry THF (20 mL) was then added in the reaction. The solution was stirred at RT under argon during 3.5 h then quenched with saturated aqueous NH₄Cl (40 mL). The solvent was evaporated off and the aqueous layer was extracted with CH₂Cl₂ (4×30 mL). The combined organic layers were washed with brine (3×30 mL), dried (MgSO₄) and concentrated. *p*-Toluenesulfonic acid (0.2 eq.) was added to the solution of crude product in toluene (70 mL). The resulting solution was stirred at 110°C during 18 h. The solvent was evaporated off and the residue dissolved in CH₂Cl₂ (70 mL), washed with saturated aqueous NaHCO₃ (2×50 mL), brine (50 mL), dried (MgSO₄), concentrated and purified by silica gel column chromatography to obtain TPE core.

General procedure B for formation of TPE core by McMurry reaction

To a solution of ketone (A) (1 eq.) and ketone (B) (1.2 eq.) in dry THF (50 mL) was added Zn powder (8 eq.). Pure TiCl₄ (4 eq.) was added to the reaction at 0°C during 30 min, and the mixture was heated to reflux during 20 h. The mixture was then quenched with H₂O (100 mL), evaporated, diluted with EtOAc (150 mL) and filtered over a Celite pad. The organic solution was washed with brine (3×50 mL), dried (Na₂SO₄), concentrated and purified by silica gel column chromatography to obtain the TPE core.

General procedure C for formation of TPE-CHO core

To the solution of TPE-Br (1 eq.) in dry THF (10 mL) was added *n*-butyllithium (2.5 eq., 2.5 M in hexane) at -78°C and continually stirred during 3 h. Then DMF (2-3 mL) was added and stirring was continued at RT during 18 h. The reaction was quenched by saturated aqueous NH₄Cl (15 mL), and diluted with EtOAc (100 mL). The organic layer was washed with brine (2×50 mL), dried (MgSO₄), concentrated and purified by silica gel column chromatography to obtain the TPE-CHO.

General procedure D for aldol condensation

To the solution of carbonyl moiety (R-CHO) (1 eq.) and **III-9** (DCM) in CH₃CN (30 mL) was added piperidine (2.4 eq.) and acetic acid (1.2 eq.). The resulting solution was stirred at 83°C during 18-96 h. The mixture was evaporated and diluted with EtOAc (50 mL), washed with brine (2×50 mL). The organic layer was dried (Na₂SO₄), concentrated and purified by silica gel column chromatography to obtain the relevant fluorophore.

General procedure E for methyl deprotection by BBr₃

To a solution of fluorophore with methoxy group (1 eq.) in dry CH₂Cl₂ (10-15 mL) was added BBr₃ (1.5-2.5 eq., 1 M in CH₂Cl₂) at 0°C. The resulting solution was stirred at 0°C during 10 min, and then at RT during 18 h. The solution was poured into ice-water (50 mL) and the solid compound was dissolved with EtOAc (100-150 mL). The aqueous layer was extracted with EtOAc (2×40 mL). The organic layers were combined, washed with brine (3×50 mL), dried (MgSO₄), concentrated,

and purified by silica gel column chromatography to obtain the hydroxy fluorophore.

General procedure F for substitution of propargyl bromide

To a solution of hydroxy fluorophore (1 eq.), K_2CO_3 (6 eq.) and tetrabutylammonium iodide (4 eq.) in DMF (50 mL) was added propargyl bromide (4 eq., 80 wt% in toluene). The resulting mixture was stirred at 90°C under argon during 18 h. The solvent was evaporated off and the residue diluted with EtOAc (50 mL) and filtered. The filtrate was washed with brine (3×40 mL), dried ($MgSO_4$), concentrated, and purified by silica gel column chromatography to obtain the fluorophore with propargyl groups.

General procedure G for the azide-alkyne “click” conjugation catalysed by $CuSO_4 / VcNa$

To a solution of alkyne moiety (1 eq.), azide moiety (1-2.2 eq.), and copper sulfate (1-2 eq.) in CH_2Cl_2/H_2O (20 mL, 3:1, v/v) was added L-ascorbic acid sodium salt (3-4 eq.). The resulting mixture was stirred vigorously at RT during 20 h. The reaction was diluted with CH_2Cl_2 (40 mL), H_2O (20 mL) and then separated. The aqueous layer was extracted with CH_2Cl_2 (2×30 mL). The combined organic layers were washed with saturated aqueous EDTA (240 mL), dried ($MgSO_4$), concentrated and purified by silica gel column chromatography ($CH_2Cl_2:EtOAc = 2:1$) to afford the desired compound.

General procedure H for the azide-alkyne “click” conjugation catalysed by $CuI / DIPEA$

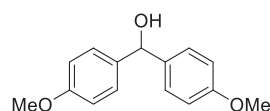
To a solution of alkyne moiety (1 eq.), azide moiety (7 eq.) and copper iodide (0.6 eq.) in dry DMF (4 mL) was added *N,N*-diisopropylethylamine (7 eq.). The resulting mixture was stirred under microwaves activation at 110°C during 60 min. Then the mixture was diluted with EtOAc (50 mL), washed with EDTA aqueous solution (3×50 mL). The combined aqueous layer was extracted with EtOAc (30 mL). The organic layers were combined, dried ($MgSO_4$), concentrated and purified by silica gel column chromatography to obtain the desired compound.

General procedure I for the acetyl deprotection of carbohydrates

To a solution of acetyl protected compound (1 eq.) in mixed solvent with MeOH (8 mL) and H_2O (2 mL) was added Et_3N (2 mL). The resulting mixture was stirred under argon at RT during 20 h. The solution was evaporated and crude product was dissolved with H_2O (2 mL) and purified with C^{18} reverse phase column ($H_2O / MeOH$ system) to afford the terminal product.

VI.2.2 Synthesis

4,4'-Dimethoxybenzhydrol (II-1)

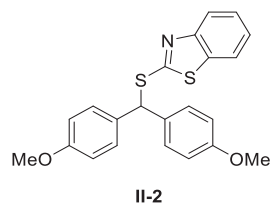


II-1

Prepared according to the literature^[258] from 4,4'-dimethoxybenzophenone (3 g, 12.4 mmol, 1 eq.) and $NaBH_4$ (660 mg, 17.4 mmol, 1.4 eq.) affording compound **II-1** (2.5 g, 83%) as a pure white powder.

$R_f = 0.24$ (CH_2Cl_2)

Di(4-methoxyphenyl)-benzothiazolylthiomethane (II-2)

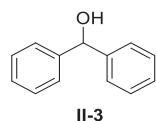


The suspended solution of **II-1** (500 mg, 2.1 mmol, 1 eq.) and 2-mercaptobenzothiazole (685 mg, 4.1 mmol, 2 eq.) in water (25 mL) was stirred intensively at 80°C during 72 h. The mixture was diluted with EtOAc (50 mL) and separated. The aqueous layer was extracted with EtOAc (2×30 mL). The combined organic layer was washed with brine (2×40 mL), dried (MgSO₄), concentrated and purified by silica gel column chromatography (Petroleum ether:CH₂Cl₂ = 1:0 to 1:2) to afford compound **II-2** (394 mg, 48%) as a pale yellow amorphous solid.

R_f = 0.6 (CH₂Cl₂)

¹H NMR (300 MHz, CDCl₃): δ (ppm) 3.79 (s, 6H, 2×OCH₃), 6.87 (d, *J* = 8.7 Hz, 4H, H-Ar), 6.93.-6.96 (m, 1H, H-Btz), 7.03-7.08 (m, 1H, H-Btz), 7.15-7.18 (m, 1H, H-Btz), 7.22 (d, *J* = 8.7 Hz, 4H, H-Ar), 7.43-7.46 (m, 1H, H-Btz).

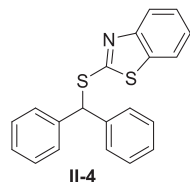
Benzhydrol (II-3)



Prepared according to the literature ^[259] from benzophenone (4.5 g, 24.6 mmol, 1 eq.) and NaBH₄ (3.76 g, 100 mmol, 1.4 eq.) affording compound **II-3** (2.5 g, 83%) as a pure white powder.

R_f = 0.3 (CH₂Cl₂:Petroleum ether = 3:1)

Diphenylbenzothiazolylthiomethane (II-4)

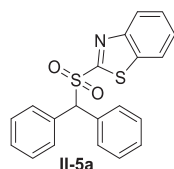


To suspended solution of **II-3** (1.5 g, 8 mmol, 1 eq.) and 2-mercaptobenzothiazole (2.7 g, 16 mmol, 2 eq.) in THF (80 mL) was added conc. H₂SO₄ (0.8 mL) at 0°C. The resulting mixture was stirred at 66°C during 24 h. The solvent was evaporated and the residue was diluted with EtOAc (50 mL) and washed with saturated aqueous NaHCO₃ solution (2×30 mL) and brine (50 mL). The organic layer was dried (MgSO₄), concentrated and purified by silica gel column chromatography (Petroleum ether:CH₂Cl₂ = 1:1) to afford compound **II-4** (2.6 g, 98%) as a pale yellow amorphous solid.

$R_f = 0.35$ (CH_2Cl_2 :Petroleum ether = 1:1)

$^1\text{H NMR}$ (300 MHz, CDCl_3): δ (ppm) 7.23-7.42 (m, 8H, 6×H-Ar, 2×H-Btz), 7.48-7.52 (m, 4H, H-Ar), 7.69 (d, $J = 8.1$ Hz, 1H, H-Btz), 7.86 (d, $J = 7.5$ Hz, 1H, H-Btz).

Diphenyl-benzothiazolysulfonylmethane (**II-5a**)

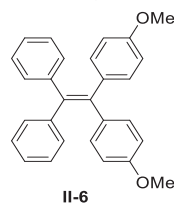


The solution of **II-4** (250 mg, 0.75 mmol, 1 eq.) and *m*-chloroperoxybenzoic acid (650 mg, 3.75 mmol, 5 eq.) in CH_2Cl_2 was stirred at RT during 20 h. The mixture was quenched with 2M $\text{Na}_2\text{S}_2\text{O}_3$ aqueous solution (30 mL), extracted with CH_2Cl_2 (2×30 mL). The combined layers were washed with saturated aqueous NaHCO_3 (2×30 mL), dried (MgSO_4), concentrated and purified by silica gel column chromatography (Cyclohexane: $\text{CH}_2\text{Cl}_2 = 1:3$) to afford compound **II-5a** (195 mg, 72%) as a pale yellow amorphous solid.

$R_f = 0.44$ (Cyclohexane: $\text{CH}_2\text{Cl}_2 = 1:5$)

$^1\text{H NMR}$ (300 MHz, CDCl_3): δ (ppm) 7.30-7.34 (m, 6H, H-Ar), 7.51 (dd, $J = 0.9$ Hz, 6.0 Hz, 1H, H-Btz), 7.56 (dd, $J = 1.2$ Hz, 7.2 Hz, 1H, H-Btz), 7.61-7.65 (m, 4H, H-Ar), 7.86 (d, $J = 7.5$ Hz, 1H, H-Btz), 8.21 (d, $J = 7.5$ Hz, 1H, H-Btz).

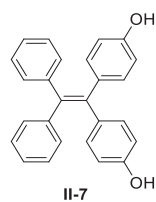
1,1-Di-(4-methoxyphenyl)-2,2-di-phenyl-ethylene (**II-6**)



Prepared according to the general procedure **A** from diphenylmethane (3 g, 17.9 mmol, 1.3 eq.), 4,4'-dimeoxybenzophenone (2.59 g, 13.8 mmol, 1 eq.), *n*-butyllithium (7.2 mL, 17.9 mmol, 1.3 eq., 2.5 M/L in hexane) affording compound **II-6** (4.43 g, 95%) as a white powder^[102].

$R_f = 0.26$ (Cyclohexane:EtOAc = 10:1)

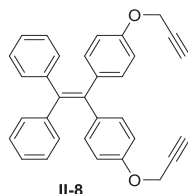
1,1-Di-(4-hydroxyphenyl)-2,2-di-phenyl-ethylene (**II-7**)



Prepared according to the general procedure **E** from compound **II-6** (2 g, 5.1 mmol, 1 eq.) and BBr₃ (7.5 g, 30.6 mmol, 6 eq., 1 M in CH₂Cl₂) affording compound **II-7** (1.75 g, 90%) as a pale yellow powder [182].

R_f = 0.12 (CH₂Cl₂)

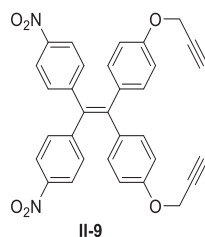
1,1-Di-[4-(2-propyn-1-yloxy)phenyl]-2,2-di-phenyl-ethylene (**II-8**)



Prepared according to the general procedure **F** from compound **II-7** (1.75 g, 4.6 mmol, 1 eq.), K₂CO₃ (3.8 g, 27.6 mmol, 6 eq.), tetrabutylammonium iodide (6.8 g, 18.5 mmol, 4 eq.) and propargyl bromide (2.5 mL, 8.5 mmol, 4 eq., 80 wt% in toluene) affording compound **II-8** (1.43 g, 64%) as a white powder [260].

R_f = 0.67 (CH₂Cl₂)

1,1-Di-[4-(2-propyn-1-yloxy)phenyl]-2,2-di-(4-nitrophenyl)-ethylene (**II-9**)

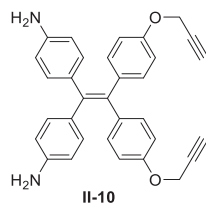


To the solution of **II-8** (356 mg, 0.81 mmol, 1 eq.) in CH₂Cl₂ (10 mL) was added the solution of HNO₃ (2-3 mL) in CH₂Cl₂ (5 mL) at -78°C. The reaction was monitored by TLC until disappearance of starting materials disappearing completely. The resulting mixture was extracted with CH₂Cl₂ (2×30 mL) after quenching with water (30 mL). The combined organic layers were washed with brine (2×30 mL), dried (MgSO₄), concentrated and purified by silica gel column chromatography (Cyclohexane:EtOAc = 5:1) to afford main product of compound **II-9** (320 mg, 75%) as a yellow amorphous solid.

R_f = 0.31 (Cyclohexane:EtOAc = 5:1)

¹H NMR (300 MHz, CDCl₃): δ (ppm) 2.52 (t, 2H, *J* = 2.4 Hz, HC≡C), 4.65 (d, 4H, *J* = 2.4 Hz, CH₂-C≡CH), 6.76 (d, 2H, *J* = 9.0 Hz, H-Ar), 6.94 (d, 2H, *J* = 9.0 Hz, H-Ar), 7.15 (d, 2H, *J* = 9.0 Hz, H-Ar), 8.00 (d, 2H, *J* = 9.0 Hz, H-Ar).

1,1-Di-[4-(2-propyn-1-yloxy)phenyl]-2,2-di-(4-aminophenyl)-ethylene (**II-10**)

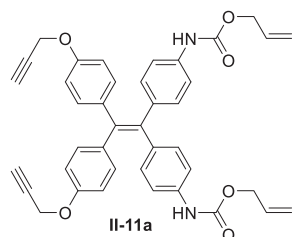


To the solution of compound **II-10** (104 mg, 0.2 mmol, 1 eq.) and $\text{SnCl}_2 \cdot \text{H}_2\text{O}$ (185 mg, 0.8 mmol, 4 eq.) in 1,4-dioxane (15 mL) was added conc. HCl (3 mL). The resulting mixture was stirred at 78°C under argon during 7h. Then, the mixture was quenched by 2M NaOH aqueous solution (40 mL), the residue was filtered. The filtrate was extracted with EtOAc (2×40 mL) and washed with brine (2×30 mL), dried (MgSO_4), concentrated and purified by silica gel column chromatography (CH_2Cl_2 :MeOH = 90:1 to 50:1) to afford compound **II-10** (86 mg, 91%) as a pale yellow amorphous solid.

$R_f = 0.41$ (CH_2Cl_2 :MeOH = 60:1)

$^1\text{H NMR}$ (300 MHz, CD_3OD): δ (ppm) 2.91 (t, 2H, $J = 2.4$ Hz, $\text{HC}\equiv\text{C}$), 4.63 (d, 4H, $J = 2.7$ Hz, $\text{CH}_2\text{-C}\equiv\text{CH}$), 6.47 (d, 4H, $J = 8.7$ Hz, H-Ar), 6.70 (d, 4H, $J = 8.7$ Hz, H-Ar), 6.74 (d, 4H, $J = 8.7$ Hz, H-Ar), 6.90 (d, 4H, $J = 8.7$ Hz, H-Ar).

1,1-Di-[4-(2-propyn-1-yloxy)phenyl]-2,2-di-[4-*N*-(*O*-allylcarbamoyl)phenyl]-ethylene (**II-11a**)

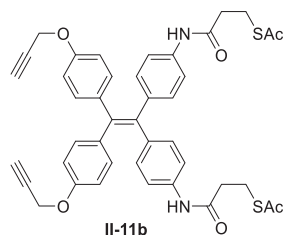


To the solution of compound **II-10** (935 mg, 2 mmol, 1 eq.) and allyl chloroformate (840 mg, 7 mmol, 3.5 eq., 0.75 mL) in dry CH_2Cl_2 (30 mL) was added *N,N*-diisopropylethylamine (DIPEA, 1.4 mL, 8 mmol, 4 eq.). The resulting solution was stirred at RT under argon during 20 h. Then the solvent was evaporated and the residue was purified by silica gel column chromatography (CH_2Cl_2) to afford the compound **II-11a** (802 mg, 63%) as a pale yellow amorphous solid.

$R_f = 0.35$ (CH_2Cl_2)

$^1\text{H NMR}$ (300 MHz, CD_3CN): δ (ppm) 2.78 (t, 2H, $J = 2.4$ Hz, $\text{HC}\equiv\text{C}$), 4.57 (t, 2H, $J = 1.5$ Hz, $\text{CH}_2\text{-CH}=\text{CH}_2$), 4.59 (t, 2H, $J = 1.5$ Hz, $\text{CH}_2\text{-CH}=\text{CH}_2$), 4.57 (d, 4H, $J = 2.4$ Hz, $\text{CH}_2\text{-C}\equiv\text{CH}$), 5.21 (dd, 2H, $J = 1.5$ Hz, 9.0 Hz, $\text{CH}_2\text{-CH}=\text{CH}_2$), 5.34 (dd, 2H, $J = 1.5$ Hz, 9.0 Hz, $\text{CH}_2\text{-CH}=\text{CH}_2$), 5.90-6.03 (m, 2H, $\text{CH}_2\text{-CH}=\text{CH}_2$), 6.74 (d, 4H, $J = 8.7$ Hz, H-Ar), 6.92 (d, 4H, $J = 6.6$ Hz, H-Ar), 6.95 (d, 4H, $J = 6.6$ Hz, H-Ar), 7.20 (d, 4H, $J = 8.7$ Hz, H-Ar), 7.69 (s, 2H, NH)

1,1-Di-[4-(2-propyn-1-yloxy)phenyl]-2,2-di-[4-*N*-(3-acetylthiopropionamide)phenyl]-ethylene (II-11b)

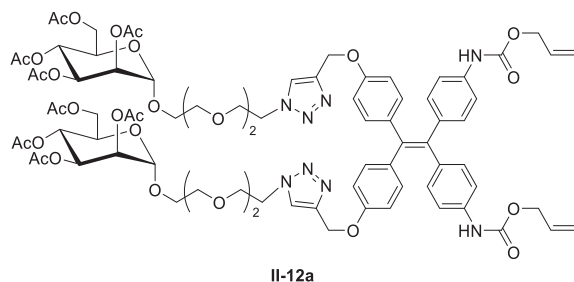


To the solution of compound **II-10** (1.18 g, 2.5 mmol, 1 eq.), 3-acetylthiopropionic acid (1.11 g, 7.5 mmol, 3 eq.) and 2-(6-chloro-1-*H*-benzotriazole-1-yl)-1,1,3,3-tetramethylammonium hexafluorophosphate (3.1 g, 7.5 mmol, 3 eq.) in dry CH₂Cl₂ (30 mL) was added *N,N*-diisopropylethylamine (1.3 mL, 7.5 mmol, 3 eq.). The mixture was stirred at RT under argon during 20 h. Then the reaction was diluted with CH₂Cl₂ (50 mL), washed with saturated NaHCO₃ aqueous solution (40 mL) and brine (2×50 mL). The organic layer was dried (MgSO₄), concentrated and purified with silica gel column chromatography (CH₂Cl₂:MeOH = 100:1 to 60:1) to afford compound **II-11b** (1.16 g, 64%) as a pale yellow amorphous solid.

R_f = 0.29 (CH₂Cl₂:MeOH = 50:1)

¹H NMR (300 MHz, CD₃CN): δ (ppm) 2.23 (s, 6H, CH₃CO), 2.57 (t, 4H, *J* = 6.9 Hz, O-CH₂-CH₂), 2.79 (t, 2H, *J* = 2.4 Hz, HC≡C), 3.10 (t, 4H, *J* = 6.9 Hz, CH₂-CH₂-SAc), 4.67 (d, 4H, *J* = 2.4 Hz, CH₂-C≡CH), 6.74 (d, 4H, *J* = 8.7 Hz, H-Ar), 6.92 (d, 4H, *J* = 6.3 Hz, H-Ar), 6.95 (d, 4H, *J* = 6.6 Hz, H-Ar), 7.31 (d, 4H, *J* = 8.7 Hz, H-Ar), 8.23 (s, 2H, NH).

1,1-Di-(4-{1-[1-(2,3,4,6-tetra-*O*-acetyl- α -D-mannopyranosyloxy)-3,6-dioxaoct-8-yl]-1,2,3-triazol-4-yl-methoxy}phenyl)-2,2-di-[4-*N*-(*O*-allylcarbamoyl)phenyl]-ethylene (II-12a)



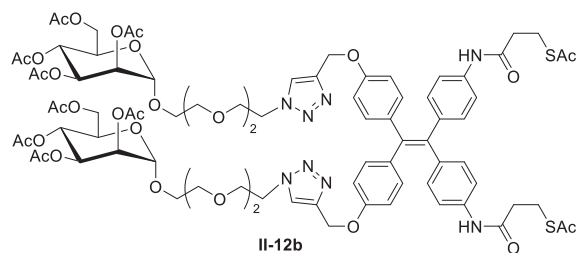
Prepared according to the general procedure **H** from compound **II-11a** (802 mg, 1.26 mmol, 1 eq.), **ManEGN₃**^[261] (1.6 g, 3.15 mmol, 2.5 eq.), copper iodide (CuI, 245 mg, 1.26 mmol, 1 eq.) and DIPEA (0.63 mL, 3.78 mmol, 3 eq.) affording compound **II-12a** (1.41 g, 68%) as a pale yellow amorphous solid.

R_f = 0.23 (CH₂Cl₂:MeOH = 60:1)

¹H NMR (300 MHz, CDCl₃): δ (ppm) 1.98, 2.02, 2.09, 2.14 (4s, 4×6H, CH₃CO), 3.61-3.67 (m, 14H, Man-OCH₂, OCH₂), 3.75-3.82 (m, 2H, Man-OCH₂), 3.90 (t, 4H, *J* = 4.8 Hz, OCH₂CH₂-triaz), 4.02-4.12 (m, 4H, H-5, H-6'), 4.28 (dd, 2H, *J* = 4.8 Hz, 12Hz, H-6), 4.57 (t, 4H, *J* = 5.1 Hz, OCH₂CH₂-

triaz), 4.63 (t, 2H, $J = 1.5$ Hz, $\text{CH}_2\text{-CH=CH}_2$), 4.65 (t, 2H, $J = 1.5$ Hz, $\text{CH}_2\text{-CH=CH}_2$), 4.85 (d, 2H, $J = 1.8$ Hz, H-1), 5.12 (s, 4H, $\text{OCH}_2\text{-triaz}$), 5.22-5.38 (m, 10H, H-2, H-4, H-3, $\text{CH}_2\text{-CH=CH}_2$), 5.88-6.01 (m, 2H, $\text{CH}_2\text{-CH=CH}_2$), 6.72 (d, 4H, $J = 9.0$ Hz, H-Ar), 6.76 (s, 2H, NH), 6.90-6.96 (m, 8H, H-Ar), 7.13 (d, 4H, $J = 8.4$ Hz, H-Ar), 7.79 (s, 2H, H-triaz).

1,1-Di-(4-{1-[1-(2,3,4,6-tetra-*O*-acetyl- α -D-mannopyranosyloxy)-3,6-dioxaoct-8-yl]-1,2,3-triazol-4-yl-methoxy}phenyl)-2,2-di-{4-*N*-[3-(*S*-acetylthiol)propionamide]phenyl}-ethylene (II-12b)

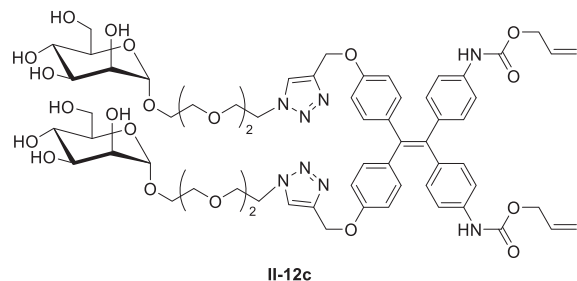


Prepared according to the general procedure **H** from compound **II-11b** (960 mg, 1.32 mmol, 1 eq.), **ManEGN₃** [261] (1.67 g, 3.29 mmol, 2.5 eq.), copper iodide (251 mg, 1.32 mmol, 1 eq.) and DIPEA 0.67 mL, 4 mmol, 3 eq.) affording compound **II-12b** (894 mg, 39%) as a pale yellow amorphous solid.

$R_f = 0.34$ ($\text{CH}_2\text{Cl}_2\text{:MeOH} = 40\text{:}1$)

$^1\text{H NMR}$ (300 MHz, CDCl_3): δ (ppm) 1.96, 2.01, 2.07, 2.13 (4s, 4 \times 6H, $\text{CH}_3\text{CO-Man}$), 2.31 (s, 6H, $\text{CH}_3\text{CO-S}$), 2.63 (t, 4H, $J = 6.6$ Hz, $\text{O-CH}_2\text{-CH}_2$), 3.16 (t, 4H, $J = 6.6$ Hz, $\text{CH}_2\text{-CH}_2\text{-S}$), 3.59-3.65 (m, 14H, Man-OCH_2 , OCH_2), 3.76-3.79 (m, 2H, Man-OCH_2), 3.87 (t, 4H, $J = 5.1$ Hz, $\text{OCH}_2\text{CH}_2\text{-triaz}$), 4.02-4.11 (m, 4H, H-5, H-6'), 4.26 (dd, 2H, $J = 4.8$ Hz, 12Hz, H-6), 4.56 (t, 4H, $J = 5.1$ Hz, $\text{OCH}_2\text{CH}_2\text{-triaz}$), 4.84 (d, 2H, $J = 1.5$ Hz, H-1), 5.10 (s, 4H, $\text{OCH}_2\text{-triaz}$), 5.23-5.32 (m, 6H, H-2, H-4, H-3), 6.70 (d, 4H, $J = 8.7$ Hz, H-Ar), 6.91 (d, 8H, $J = 8.7$ Hz, H-Ar), 7.26 (d, 4H, $J = 8.7$ Hz, H-Ar), 7.78 (s, 2H, NH), 7.79 (s, 2H, H-triaz)

1,1-Di-(4-{1-[1-(α -D-mannopyranosyloxy)-3,6-dioxaoct-8-yl]-1,2,3-triazol-4-yl-methoxy}phenyl)-2,2-di-[4-*N*-(*O*-allylcarbonyl)phenyl]-ethylene (II-12c)

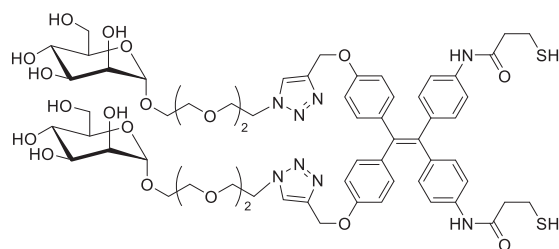


Prepared according to the general procedure **I** from compound **II-12a** (500 mg, 0.3 mmol, 1 eq.), MeOH (10 mL), H_2O (3 mL) and Et_3N (2-3 mL) affording compound **II-12c** (372 mg, 94%) as a pale yellow solid.

$^1\text{H NMR}$ (300 MHz, CD_3OD): δ (ppm) 3.54-3.62 (m, 16H, OCH_2 , Man-OCH_2), 3.65-3.75 (m,

OCH₂CH₂-triaz, H-5, H-6'), 3.80 (d, *J* = 2.7 Hz, 2H, H-6), 3.83-3.87 (m, 4H, CH₂-CH=CH₂), 3.90 (t, 4H, *J* = 4.8 Hz, OCH₂CH₂-triaz), 4.58-4.61 (m, 6H, H-2, H-4, H-3), 4.80 (d, 2H, *J* = 1.8 Hz, H-1), 5.09 (s, 4H, OCH₂-triaz), 5.23 (dd, 2H, *J* = 1.2 Hz, 10.5 Hz, CH₂-CH=CH₂), 5.34 (dd, 2H, *J* = 1.5 Hz, 17.1 Hz, CH₂-CH=CH₂), 5.90-6.03 (m, 2H, CH₂-CH=CH₂), 6.76 (d, 2H, *J* = 8.7 Hz, H-Ar), 6.87-6.92 (m, 8H, H-Ar), 7.16 (d, 4H, *J* = 8.1 Hz, H-Ar), 8.06 (s, 2H, H-triaz).

1,1-Di-(4-{1-[1-(α -D-mannopyranosyloxy)-3,6-dioxaoct-8-yl]-1,2,3-triazol-4-yl-methoxy} phenyl)-2,2-di-[4-*N*-(3-thiolpropionamide)phenyl]-ethylene (II-12b)

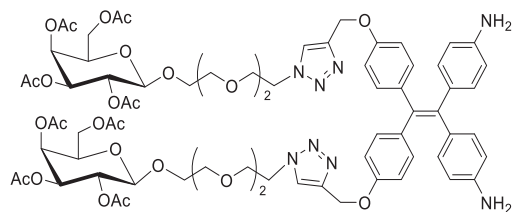


II-12d

Prepared according to the general procedure **I** from compound **II-12b** (500 mg, 0.3 mmol, 1 eq.), MeOH (10 mL), H₂O (3 mL) and Et₃N (2-3 mL) affording compound **II-12c** (372 mg, 94%) as a pale yellow amorphous solid.

¹H NMR (300 MHz, DMSO-*d*₆): δ (ppm) 2.57 (t, *J* = 6.6 Hz, 2H, O-CH₂-CH₂), 2.70 (t, 2H, *J* = 6.6 HZ, CH₂-CH₂-S), 3.59-3.64 (m, 24H, Man-OCH₂, OCH₂, H-5, H-6', H-6, H-2, H-4, H-3), 3.81 (t, 4H, *J* = 5.1 Hz, OCH₂CH₂-triaz), 4.52 (t, 4H, *J* = 5.1 Hz, OCH₂CH₂-triaz), 4.62 (d, 2H, *J* = 1.5 Hz, H-1), 5.03 (s, 4H, OCH₂-triaz), 6.78-6.88 (m, 12H, H-Ar), 7.35 (d, 4H, *J* = 8.4 Hz, H-Ar), 8.15 (s, 2H, H-triaz)

1,1-Di-(4-{1-[1-(α -D-mannopyranosyloxy)-3,6-dioxaoct-8-yl]-1,2,3-triazol-4-yl-methoxy} phenyl)-2,2-di-(4-aminophenyl)-ethylene (II-13)



II-13

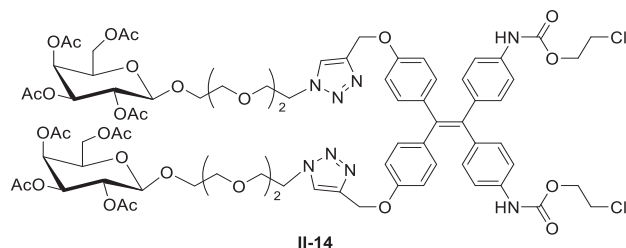
Prepared according to the general procedure **H** from compound **II-10** (510 mg, 1.09 mmol, 1 eq.), compound **GalEGN₃**^[261] (1.12 g, 2.23 mmol, 2.5 eq.), copper iodide (CuI, 103 mg, 0.54 mmol, 1 eq.) and DIPEA (427 mg, 3.3 mmol, 3 eq., 0.54 mL) affording compound **II-13** (1.16 g, 72%) as a pale yellow amorphous solid.

R_f = 0.43 (CH₂Cl₂:MeOH = 30:1)

¹H NMR (300 MHz, Acetone-*d*₆): δ (ppm) 1.90, 1.98, 1.99, 2.11 (4s, 4×6H, CH₃CO), 3.55-3.61 (m, 12H, OCH₂), 3.66-3.72 (m, 4H, Gal-OCH₂), 3.86-3.89 (m, 2H, H-5), 3.92 (t, 4H, *J* = 5.1 Hz, OCH₂CH₂-triaz), 4.11-4.17 (m, 6H, H-1, H-6, H-6'), 4.60 (t, 4H, *J* = 4.8 Hz, OCH₂CH₂-triaz), 4.74-

4.76 (m, 2H, H-3), 5.10 (s, 4H, OCH₂-triaz), 5.11-5.12 (m, 2H, H-2), 5.37 (dd, 2H, *J* = 1.2 Hz, 3.0 Hz, H-4), 6.41 (d, 2H *J* = 8.1 Hz, H-Ar), 6.73 (d, 2H *J* = 8.4 Hz, H-Ar), 6.80 (d, 2H *J* = 8.7 Hz, H-Ar), 6.95 (d, 2H, *J* = 8.4 Hz, H-Ar), 8.07 (s, 2H, H-triaz).

1,1-Di-(4-{1-[1-(α -D-mannopyranosyloxy)-3,6-dioxaoct-8-yl]-1,2,3-triazol-4-yl-methoxy} phenyl)-2,2-di-[4-*N*-[*O*-(2-chloroethyl)carbamoyl]phenyl]-ethylene (II-14)

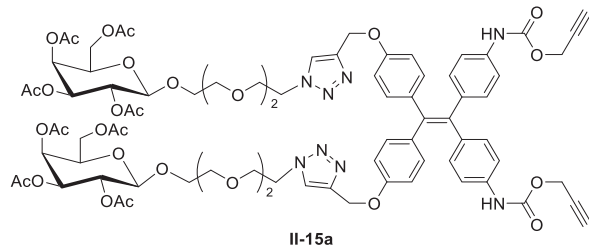


To the solution of the compound **II-13** (100 mg, 0.068 mmol, 1 eq.) and DIPEA (44 mg, 0.34 mmol, 5 eq.) in dry CH₂Cl₂ (3 mL) was added 2-chloroethyl chloroformate at 0°C. The resulting mixture was stirred at RT during 16 h. The mixture was diluted with CH₂Cl₂ (20 mL), washed with saturated NaHCO₃ aqueous solution (20 mL) and brine (20 mL). The organic layer was dried (MgSO₄), concentrated and purified by silica gel column chromatography (CH₂Cl₂:MeOH = 60:1 to 50:1) to afford compound **II-14** (62 mg, 54%) as a pale yellow amorphous solid.

R_f = 0.33 (CH₂Cl₂:MeOH = 40:1)

¹H NMR (300 MHz, CDCl₃): δ (ppm) 2.00, 2.05, 2.06, 2.16 (4s, 4×6H, CH₃CO), 3.61-3.65 (m, 12H, OCH₂), 3.69-3.77 (m, 6H, CH₂CH₂-Cl, Gal-OCH₂), 3.90-3.95 (m, 8H, Gal-OCH₂, H-5, OCH₂CH₂-triaz), 4.16-4.18 (m, 4H, H-6, H-6'), 4.42 (t, 4H, *J* = 5.4 Hz, OCH₂CH₂Cl), 4.54-4.60 (m, 6H, H-1, OCH₂CH₂-triaz), 5.04 (dd, 2H, *J* = 3.6 Hz, 10.5 Hz, H-3), 5.16 (s, 4H, OCH₂-triaz), 5.22 (dd, 2H, *J* = 2.7 Hz, 7.8 Hz, H-2), 5.40 (d, 2H, *J* = 3.6 Hz, H-4), 6.75 (d, 2H, *J* = 8.7 Hz, H-Ar), 6.82 (s, 2H, NH) 6.95 (d, 2H, *J* = 2.7 Hz, H-Ar), 6.98 (d, 2H, *J* = 2.7 Hz, H-Ar), 7.16 (d, 2H, *J* = 8.7 Hz, H-Ar), 7.79 (s, 2H, H-triaz).

1,1-Di-(4-{1-[1-(α -D-mannopyranosyloxy)-3,6-dioxaoct-8-yl]-1,2,3-triazol-4-yl-methoxy} phenyl)-2,2-di-[4-*N*-(*O*-propargylcarbonyl)phenyl]-ethylene (II-15a)



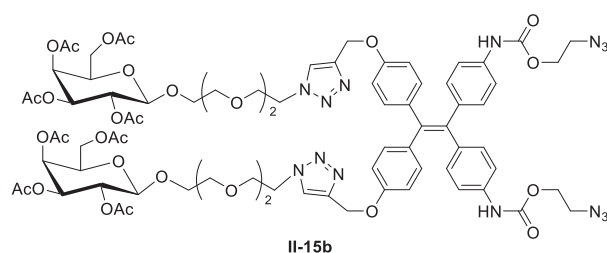
To the solution of compound **II-13** (160 mg, 0.108 mmol, 1 eq.) and propargyl chloroformate (40 mg, 0.33 mmol, 3 eq.) in dry CH₂Cl₂ (4 mL) was added Et₃N (55 mg, 0.54 mmol, 5 eq.) at 0°C. The resulting mixture was stirred at RT during 17 h. The solution was diluted with CH₂Cl₂ (40 mL), washed with saturated NaHCO₃ aqueous solution (30 mL) and brine (30 mL). The organic layer was dried (MgSO₄), concentrated and purified by silica gel column chromatography (CH₂Cl₂:MeOH =

60:1 to 50:1) to afford compound **II-15a** (120 mg, 67%) as a pale yellow amorphous solid.

$R_f = 0.4$ ($\text{CH}_2\text{Cl}_2:\text{MeOH} = 40:1$)

$^1\text{H NMR}$ (300 MHz, CDCl_3): δ (ppm) 1.98, 2.03, 2.04, 2.14 (4s, 4×6H, CH_3CO), 2.52 (t, 2H, $J = 2.4$ Hz, $\text{HC}\equiv\text{C}$), 3.60-3.73 (m, 14H, OCH_2 , Gal- OCH_2), 3.91-3.98 (m, 8H, Gal- OCH_2 , H-5, OCH_2CH_2 -triaz), 4.13-4.18 (m, 4H, H-6, H-6'), 4.54 (d, 2H, $J = 7.8$ Hz, H-1), 4.60 (t, 4H, $J = 5.1$ Hz, OCH_2CH_2 -triaz), 4.78 (d, 4H, $J = 2.4$ Hz, $\text{CH}_2\text{-C}\equiv\text{CH}$), 5.02 (dd, 2H, $J = 3.6$ Hz, 10.5 Hz, H-3), 5.16-5.23 (m, 6H, OCH_2 -triaz, H-2), 5.38 (d, 2H, $J = 3.3$ Hz, H-4), 6.75 (d, 4H, $J = 8.7$ Hz, H-Ar), 6.93 (s, 2H, NH), 7.15-7.25 (m, 12H, H-Ar), 7.89 (s, 2H, H-triaz).

1,1-Di-(4-{1-[1-(α -D-mannopyranosyloxy)-3,6-dioxaoct-8-yl]-1,2,3-triazol-4-yl-methoxy}phenyl)-2,2-di-{4-*N*-[O-(2-azidoethyl)carbamoyl]phenyl}-ethylene (II-15b)

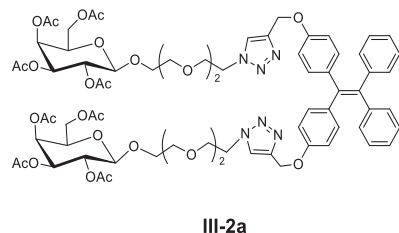


A solution of compound **II-14** (62 mg, 0.037 mmol, 1 eq.), sodium azide (NaN_3 , 7 mg, 0.1 mmol, 2.6 eq.) and Bu_4NI (3 mg, 0.008 mmol, 0.2 eq.) in DMF (2 mL) was stirred at 75°C during 16 h. The mixture was diluted with EtOAc (20 mL), washed with saturated NaHCO_3 aqueous solution (20 mL) and brine (20 mL). The organic layer was dried (MgSO_4), concentrated and purified by silica gel column chromatography ($\text{CH}_2\text{Cl}_2:\text{MeOH} = 60:1$ to 45:1) to afford compound **II-15b** (63 mg, 99%) as a pale yellow amorphous solid.

$R_f = 0.35$ ($\text{CH}_2\text{Cl}_2:\text{MeOH} = 40:1$)

$^1\text{H NMR}$ (300 MHz, CDCl_3): δ (ppm) 1.98, 2.02, 2.03, 2.14 (4s, 4×6H, CH_3CO), 3.54-3.63 (m, 16H, OCH_2 , Gal- OCH_2 , $\text{CH}_2\text{CH}_2\text{N}_3$), 3.89-3.93 (m, 8H, Gal- OCH_2 , H-5, OCH_2CH_2 -triaz), 4.04-4.20 ($\text{OCH}_2\text{CH}_2\text{N}_3$, H-6'), 4.34 (t, 2H, $J = 5.1$ Hz, H-6), 4.52-4.59 (m, 6H, H-1, OCH_2CH_2 -triaz), 5.02 (dd, 2H, $J = 3.6$ Hz, 10.5 Hz, H-3), 5.17-5.23 (m, 6H, H-2, OCH_2 -triaz), 5.38 (d, 2H, $J = 3.3$ Hz, H-4), 6.75 (d, 2H, $J = 8.7$ Hz, H-Ar), 6.93 (s, 2H, NH), 7.18-7.31 (m, H-12, H-Ar), 7.85 (s, 2H, H-triaz).

1,1-Di-(4-{1-[1-(2,3,4,6-tetra-*O*-acetyl- β -D-galactopyranosyloxy)-3,6-dioxaoct-8-yl]-1,2,3-triazol-4-yl-methoxy}phenyl)-2,2-di-phenyl-ethylene (III-2a)



Prepared according to the general procedure **H** from compound **II-8** (360 mg, 0.82 mmol, 1 eq.), **GalEGN₃** [261] (1.26 g, 2.5 mmol, 3 eq.), copper iodide (155 mg, 0.82 mmol, 1 eq.) and DIPEA 0.42 mL, 2.5 mmol, 3 eq.) affording compound **III-2a** (566 mg, 48%) as a pale yellow amorphous solid.

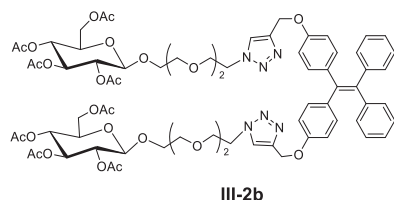
$R_f = 0.31$ (CH₂Cl₂:MeOH = 40:1)

¹H NMR (300 MHz, CDCl₃): δ (ppm) 1.96, 2.01, 2.02, 2.12 (4s, 4×6H, CH₃CO), 3.55-3.61 (m, 12H, OCH₂CH₂O), 3.64-3.73 (m, 2H, Gal-OCH₂), 3.86-3.96 (m, 8H, OCH₂CH₂N, H-5, Gal-OCH₂), 4.09-4.12 (m, 4H, H-6, H-6'), 4.50-4.54 (m, 6H, H-1, OCH₂CH₂N), 4.99 (dd, 2H, $J = 3.6$ Hz, 10.5 Hz, H-3), 5.08 (s, 4H, OCH₂-triaz), 5.15 (dd, 2H, $J = 7.8$ Hz, 10.5 Hz, H-2), 5.35 (dd, 2H, $J = 0.9$ Hz, 3.3 Hz, H-4), 6.69 (d, 4H, $J = 8.7$ Hz, H-Ar), 6.91 (d, 4H, $J = 8.7$ Hz, H-Ar), 6.96-6.99 (m, 4H, Ph), 7.03-7.07 (m, 6H, Ph), 7.77 (s, 2H, H-triaz).

¹³C NMR (75 MHz, CDCl₃): δ (ppm) 20.6, 20.7, 20.7, 20.8 (4×COCH₃), 50.3 (OCH₂CH₂N), 61.3 (C-6), 61.9 (OCH₂-triaz), 67.1 (C-4), 68.8 (C-2), 69.1 (Gal-OCH₂), 69.4 (OCH₂CH₂N), 70.2 (OCH₂), 70.56 (OCH₂), 70.61 (OCH₂), 70.7 (C-5), 70.9 (C-3), 101.3 (C-1), 113.8 (CH-Ar), 124.0 (CH^{triaz}), 126.1 (Ph), 127.7 (Ph), 131.3 (Ph), 132.6 (CH-Ar), 136.8 (C^{Ar}-C=C), 139.6 (C^{Ph}-C=C), 139.8 (C=C), 144.1 (C^{triaz}), 156.9 (C^{Ar}-O), 169.4, 170.1, 170.2, 170.4 (4×COCH₃).

HR-ESI-MS m/z : calcd. for C₇₂H₈₆N₆O₂₆Na₂ [M+2Na]²⁺ 748.2670, found 748.2688.

1,1-Di-(4-{1-[1-(2,3,4,6-tetra-O-acetyl- β -D-glucopyranosyloxy)-3,6-dioxaoct-8-yl]-1,2,3-triazol-4-yl-methoxy}phenyl)-2,2-di-phenyl-ethylene (III-2b)



Prepared according to the general procedure **H** from compound **II-8** (385 mg, 0.88 mmol, 1 eq.), compound **GlcEGN₃** [261] (1.3 g, 2.63 mmol, 3 eq.), copper iodide (165 mg, 0.88 mmol, 1 eq.) and DIPEA (0.45 mL, 2.63 mmol, 3 eq.) affording compound **III-2b** (1.11 g, 87%) as a pale yellow amorphous solid.

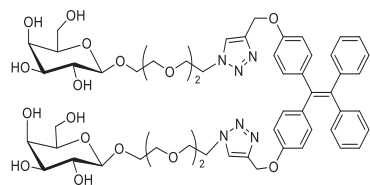
$R_f = 0.30$ (CH₂Cl₂:MeOH, 40:1)

¹H NMR (300 MHz, CDCl₃): δ (ppm) 1.98, 2.00, 2.01, 2.05 (4s, 4×6H, CH₃CO), 3.57-3.60 (m, 12H, OCH₂CH₂O), 3.63-3.71 (m, 4H, H-5, Glc-OCH₂), 3.85-3.93 (m, 6H, OCH₂CH₂N, Glc-OCH₂), 4.11, (dd, $J = 2.4$ Hz, 12.3 Hz, 2H, H-6'), 4.24 (dd, $J = 4.5$ Hz, 12.3 Hz, 2H, H-6), 4.53-4.58 (m, 6H, H-1, OCH₂CH₂N), 4.97 (dd, $J = 7.8$ Hz, 9.6 Hz, H-2), 5.06 (t, $J = 9.6$ Hz, 2H, H-4), 5.11 (s, 4H, OCH₂-triaz), 5.19 (t, $J = 9.6$ Hz, 2H, H-3), 6.71 (d, $J = 8.7$ Hz, 4H, H-Ar), 6.93 (d, $J = 8.7$ Hz, 4H, H-Ar), 6.98-7.01 (m, 4H, Ph), 7.05-7.09 (m, 6H, Ph), 7.78 (s, 2H, H-triaz).

^{13}C NMR (75 MHz, CDCl_3): δ (ppm) 20.68, 20.69, 20.76, 20.83 ($4\times\text{COCH}_3$), 50.5 ($\text{OCH}_2\text{CH}_2\text{N}$), 60.2 (C-6), 60.2 ($\text{OCH}_2\text{-triaz}$), 68.5 (C-4), 69.2 (Glc-OCH_2), 69.5 ($\text{OCH}_2\text{CH}_2\text{N}$), 70.3 (OCH_2), 70.66 (OCH_2), 70.68 (OCH_2), 71.4 (C-2), 71.9 (C-5), 72.9 (C-3), 100.9 (C-1), 113.9 (CH-Ar), 124.0 (CH^{triaz}), 126.2 (Ph), 127.8 (Ph), 131.4 (Ph), 132.7 (CH-Ar), 136.9 ($\text{C}^{\text{Ph-C=C}}$), 139.7 ($\text{C}^{\text{Ar-C=C}}$), 139.9 ($\text{C}=\text{C}$), 144.2 (C^{triaz}), 157.0 ($\text{C}^{\text{Ar-O}}$), 169.4, 169.5, 170.3, 170.7 ($4\times\text{COCH}_3$).

HR-ESI-MS m/z : calcd. for $\text{C}_{72}\text{H}_{88}\text{N}_6\text{O}_{26}$ $[\text{M}+2\text{H}]^{2+}$ 726.2842, found 726.2869.

1,1-Di-(4-{1-[1-(β -D-galactopyranosyloxy)-3,6-dioxaoct-8-yl]-1,2,3-triazol-4-yl-methoxy}phenyl)-2,2-di-phenyl-ethylene (III-3a)



III-3a

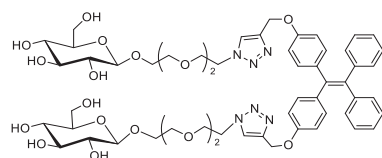
Prepared according to the general procedure I from compound III-2a (510 mg, 0.35 mmol, 1 eq.), MeOH (15 mL), H_2O (5 mL) and Et_3N (4 mL) affording compound III-3a (370 mg, 95%) as a pale yellow amorphous solid.

^1H NMR (300 MHz, CD_3OD): δ (ppm) 3.40-3.47 (m, 4H, H-3, H-5), 3.54-3.66 (m, 14H, H-4, OCH_2), 3.68-3.71 (m, 4H, H-6, H-6'), 3.80 (d, 2H, $J = 2.4$ Hz, H-2), 3.84 (t, 4H, $J = 5.1$ Hz, $\text{OCH}_2\text{CH}_2\text{N}$), 3.89-3.96 (m, 4H, Gal- OCH_2), 4.20 (d, 2H, $J = 7.2$ Hz, H-1), 4.54 (t, 4H, $J = 4.8$ Hz, $\text{OCH}_2\text{CH}_2\text{N}$), 5.03 (s, 4H, $\text{OCH}_2\text{-triaz}$), 6.71 (d, 4H, $J = 8.7$ Hz, H-Ar), 6.88 (d, 4H, $J = 8.7$ Hz, H-Ar), 6.92-6.95 (m, 4H, Ph), 7.01-7.04 (m, 6H, Ph), 8.05 (s, 2H, H-triaz).

^{13}C NMR (75 MHz, CD_3OD): δ (ppm) 51.5 ($\text{OCH}_2\text{CH}_2\text{N}$), 62.2 (C-6), 62.5 ($\text{OCH}_2\text{-triaz}$), 69.6 (Gal- OCH_2), 70.2 ($\text{OCH}_2\text{CH}_2\text{N}$), 70.3 (C-2), 71.29 (OCH_2), 71.38 (OCH_2), 71.4 (OCH_2), 72.5 (C-4), 74.8 (C-5), 76.6 (C-3), 105.0 (C-1), 115.1 (CH-Ar), 126.5 (CH^{triaz}), 127.3 (Ph), 128.8 (Ph), 132.4 (Ph), 133.7 (CH-Ar), 138.1 ($\text{C}^{\text{Ph-C=C}}$), 141.1 ($\text{C}^{\text{Ar-C=C}}$), 141.3 ($\text{C}=\text{C}$), 145.5 (C^{triaz}), 158.3 ($\text{C}^{\text{Ar-O}}$).

HR-ESI-MS m/z : calcd. for $\text{C}_{56}\text{H}_{70}\text{N}_6\text{O}_{18}\text{Na}$ $[\text{M}+\text{Na}]^+$ 1137.4647, found 1137.4644.

1,1-Di-(4-{1-[1-(β -D-glucopyranosyloxy)-3,6-dioxaoct-8-yl]-1,2,3-triazol-4-yl-methoxy}phenyl)-2,2-di-phenyl-ethylene (III-3b)



III-3b

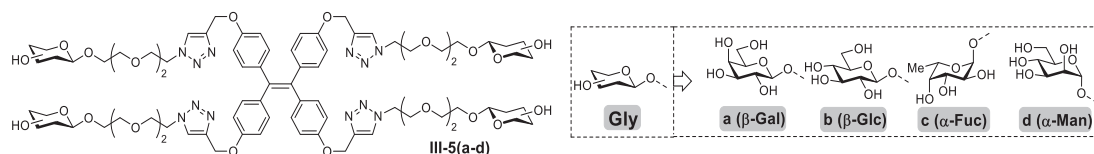
Prepared according to the general procedure I from compound III-2b (1.05 g, 0.72 mmol), MeOH (15 mL), H_2O (5 mL) and Et_3N (4 mL) affording compound III-3b (774 mg, 96%) as a pale yellow amorphous solid.

^1H NMR (300 MHz, CD_3OD): δ (ppm) 3.18-3.29 (m, 8H, H-2, H-3, H-4, H-5), 3.54-3.66 (m, 14H, OCH_2 , H-6'), 3.79-3.91 (m, 10H, Glc-OCH_2 , $\text{OCH}_2\text{CH}_2\text{N}$, H-6), 4.24 (d, 2H, $J = 7.8$ Hz, H-1), 4.56 (t, 4H, $J = 5.1$ Hz, $\text{OCH}_2\text{CH}_2\text{N}$), 5.05 (s, 4H, OCH_2 -triaz), 6.71 (d, 4H, $J = 8.7$ Hz, H-Ar), 6.89 (d, 4H, $J = 8.7$ Hz, H-Ar), 6.93-6.96 (m, 4H, Ph), 7.03-7.06 (m, 6H, Ph), 8.06 (s, 2H, H-triaz).

^{13}C NMR (75 MHz, CD_3OD): δ (ppm) 51.5 ($\text{OCH}_2\text{CH}_2\text{N}$), 62.2 (C-6), 62.8 (OCH_2 -triaz), 69.7 (Gal-OCH_2), 70.3 ($\text{OCH}_2\text{CH}_2\text{N}$), 71.35 (OCH_2), 71.41 (OCH_2), 71.43 (OCH_2), 71.6 (C-2), 75.1 (C-4), 77.9 (C-5), 78.0 (C-3), 104.4 (C-1), 115.1 (CH-Ar), 126.3 (CH^{triaz}), 127.3 (Ph), 128.8 (Ph), 132.4 (Ph), 133.7 (CH-Ar), 138.1 ($\text{C}^{\text{Ph-C=C}}$), 141.4 ($\text{C}^{\text{Ar-C=C}}$), 144.8 ($\text{C}=\text{C}$), 145.5 (C^{triaz}), 158.4 ($\text{C}^{\text{Ar-O}}$).

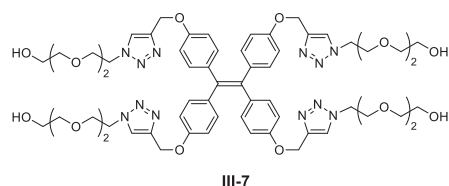
HR-ESI-MS m/z : calcd. for $\text{C}_{56}\text{H}_{70}\text{N}_6\text{O}_{18}\text{Na}$ $[\text{M}+\text{Na}]^+$ 1137.4645, found 1137.4644.

Synthesis of TPE-based glycoclusters with four glycosides (III-5a,b,c,d)



The TPE-based glycoclusters with four glycosides were synthesized in our previous works^[183].

1,1-Di-(4-{1-[1-hydroxyl-3,6-dioxaoct-8-yl]-1,2,3-triazol-4-yl-methoxy}phenyl)-2,2-di-phenylethylene (III-7)



Prepared according to the general procedure **H** from compound **III-4**^[183] (100 mg, 0.18 mmol, 1 eq.), 2-[2-(2-azidoethoxy)ethoxy]ethanol^[183] (**III-6**, 192 mg, 1.09 mmol, 6 eq.), copper iodide (14 mg, 0.073 mmol, 0.4 eq.) and DIPEA (0.2 mL, 1.09 mmol, 6 eq.) affording compound **III-7** (130 mg, 57%) as a pale yellow oil.

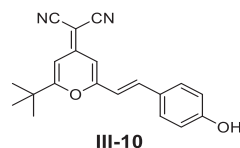
$R_f = 0.27$ ($\text{CH}_2\text{Cl}_2:\text{MeOH} = 10:1$)

^1H NMR (300 MHz, CDCl_3): δ (ppm) 3.48 (t, 8H, $J = 4.8$ Hz, $\text{OCH}_2\text{CH}_2\text{OH}$), 3.53 (s, 16H, $\text{OCH}_2\text{CH}_2\text{O}$), 3.63 (t, 8H, $J = 4.2$ Hz, $\text{OCH}_2\text{CH}_2\text{OH}$), 3.81 (t, 8H, $J = 5.4$ Hz, $\text{OCH}_2\text{CH}_2\text{N}$), 4.48 (t, 8H, $J = 5.1$ Hz, $\text{OCH}_2\text{CH}_2\text{N}$), 5.04 (s, 8H, OCH_2 -triaz), 6.66 (d, 8H, $J = 8.7$ Hz, H-Ar), 6.87 (d, 8H, $J = 8.7$ Hz, H-Ar), 7.79 (s, 4H, H-triaz).

^{13}C NMR (75 MHz, CDCl_3): δ (ppm) 50.6 ($\text{OCH}_2\text{CH}_2\text{N}$), 61.9 (OCH_2 -triaz), 62.2 (CH_2OH), 69.6 (OCH_2), 70.6 (OCH_2), 70.9 (OCH_2), 72.9 (OCH_2), 114.3 (CH-Ar), 124.6 (CH^{triaz}), 132.9 (CH-Ar), 137.5 ($\text{C}^{\text{Ph-C=C}}$), 138.9 ($\text{C}=\text{C}$), 144.2 (C^{triaz}), 157.0 ($\text{C}^{\text{Ar-O}}$).

HR-ESI-MS m/z : calcd. for $\text{C}_{62}\text{H}_{82}\text{N}_{12}\text{O}_{16}$ $[\text{M}+2\text{H}]^{2+}$ 625.2986, found 625.2956.

(E)-2-[2-(4-Hydroxystyryl)-6-(tert-butyl)-4H-pyran-4-ylidene]propanedinitrile (III-10)



Compound **III-9** was synthesized according to the literature^[262]. Prepared according to the general procedure **D** from compound **III-9** (200 mg, 0.93 mmol, 1 eq.), 4-hydroxybenzaldehyd (0.2 mL, 1.86 mmol, 2 eq.) and piperidine (0.2 mL, 1.86 mmol, 2 eq.) in 1-propanol (10 mL) affording compound **III-10** (118 mg, 40%) as a red amorphous solid.

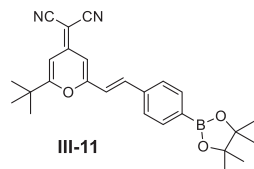
$R_f = 0.4$ (Cyclohexane:EtOAc, 2:1)

$^1\text{H NMR}$ (300 MHz, Acetone- d_6): δ (ppm) 1.34 (s, 9H, CMe_3), 2.72 (s, 1H, OH) 6.45 (d, 1H, $J = 2.1$ Hz, H-3pyran), 6.65 (d, 1H, $J = 2.1$ Hz, H-5pyran), 6.83 (d, 2H, $J = 8.7$ Hz, H-Ar), 7.01 (d, 1H, $J = 15.9$ Hz, $\text{HC}=\text{CH-Ph}$), 7.53 (d, 1H, $J = 16.2$ Hz, $\text{HC}=\text{CH-Ph}$), 7.55 (d, 2H, $J = 8.4$ Hz, H-Ar).

$^{13}\text{C NMR}$ (75 MHz, CDCl_3): δ (ppm) 28.0 (CMe_3), 36.7 (CMe_3), 57.9 ($\text{C}(\text{CN})_2$), 102.5 (C-3pyran), 106.1 (C-5pyran), 115.1 (CN), 115.5 ($\text{HC}=\text{CH-Ph}$), 116.1 (C-Ar), 126.2 ($\text{HC}=\text{CH-C}^{\text{Ar}}$), 129.8 (C-Ar), 138.3 ($\text{HC}=\text{CH-Ph}$), 157.2 ($\text{C}^{\text{Ar-OH}}$), 159.6 (C-2pyran), 160.0 (C-6pyran), 172.4 (C-4pyran).

HR-ESI-MS m/z : calcd. for $\text{C}_{20}\text{H}_{19}\text{N}_2\text{O}_2$ $[\text{M}+\text{H}]^+$ 319.1440, found 319.1441.

(E)-2-{2-[4-(4,4,5,5-Tetramethyl-1,3,2-dioxaborolan-2-yl)styryl]-6-(tert-butyl)-4H-pyran-4-ylidene}propanedinitrile (III-11)



Prepared according to the general procedure **D** from compound **III-9** (200 mg, 0.93 mmol, 1 eq.), 4-formylphenylboronic acid pinacol ester (324 mg, 1.4 mmol, 1.5 eq.) and piperidine (0.2 mL, 1.86 mmol, 2 eq.) affording compound **III-11** (120 mg, 30%) as a red amorphous solid.

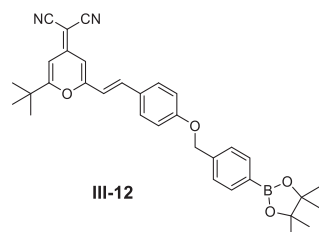
$R_f = 0.25$ (Cyclohexane:EtOAc, 6:1)

$^1\text{H NMR}$ (300 MHz, CDCl_3): δ (ppm) 1.35 (s, 12H, $2 \times \text{CMe}_2$), 1.38 (s, 9H, CMe_3), 6.56 (d, 1H, $J = 2.1$ Hz, H-3pyran), 6.70 (d, 1H, $J = 2.1$ Hz, H-5pyran), 6.80 (d, 1H, $J = 16.2$ Hz, $\text{HC}=\text{CH-Ar}$), 7.41 (d, 1H, $J = 15.9$ Hz, $\text{HC}=\text{CH-Ar}$), 7.54 (d, 2H, $J = 7.8$ Hz, H-Ar), 7.85 (d, 2H, $J = 8.1$ Hz, H-Ar).

$^{13}\text{C NMR}$ (75 MHz, CDCl_3): δ (ppm) 25.0 ($2 \times \text{CMe}_2$), 28.2 (CMe_3), 36.8 (CMe_3), 60.1 ($\text{C}(\text{CN})_2$), 84.2 ($2 \times \text{CMe}_2$), 102.8 (C-3pyran), 107.7 (C-5pyran), 115.1 (CN), 119.4 ($\text{HC}=\text{CH-Ph}$), 127.1 (CH-Ar), 128.8 ($\text{C}^{\text{Ar-B}}$), 135.5 (CH-Ar), 137.0 ($\text{HC}=\text{CH-Ph}$), 137.7 ($\text{HC}=\text{CH-C}^{\text{Ar}}$), 156.7 (C-2pyran), 158.7 (C-6pyran), 172.4 (C-4pyran).

HR-ESI-MS m/z : calcd. for $C_{26}H_{30}BN_2O_3$ $[M+H]^+$ 429.2364, found 429.2344.

(E)-2-(2-{4-[4-(4,4,5,5-Tetramethyl-1,3,2-dioxaborolan-2-yl)-benzyloxy]styryl}-6-(*tert*-butyl)-4*H*-pyran-4-ylidene)-propanedinitrile (III-12)



Compound **III-10** (118 mg, 0.37 mmol, 1 eq.), 4-(bromomethyl)benzeneboronic acid pinacol ester (133 mg, 0.45 mmol, 1.2 eq.) and tetrabutylammonium iodide (Bu_4NI , 137 mg, 0.37 mmol, 1 eq.) were dissolved in acetonitrile (8 mL). Potassium carbonate (103 mg, 138 mmol, 2 eq.) and 18-crown-6 (49 mg, 0.19 mmol, 0.5 eq.) were added to the solution. The resulting mixture was stirred at $80^\circ C$ during 18 h. The mixture was diluted with EtOAc (50 mL), washed with brine (50 mL), 2M HCl (20 mL), and brine (50 mL). The organic layer was dried ($MgSO_4$), concentrated and purified by silica gel column chromatography (cyclohexane: CH_2Cl_2 = 3:1) to afford compound **III-12** (36 mg, 19%) as a yellow amorphous solid.

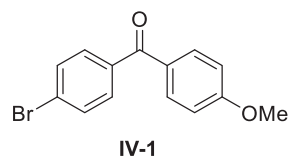
R_f = 0.4 (Cyclohexane:EtOAc, 3:1)

1H NMR (300 MHz, $CDCl_3$): δ (ppm) 1.35 (s, 12H, $2 \times CMe_2$), 1.37 (s, 9H, CMe_3), 5.14 (s, 2H, O- CH_2 -Ph₂), 6.54 (d, 1H, J = 1.8 Hz, H-3pyran), 6.59 (d, 1H, J = 15.9 Hz, $H\bar{C}=\underline{C}H$ -Ph1), 6.64 (d, 1H, J = 2.1 Hz, H-5pyran), 6.98-7.08 (m, 2H, H-Ar₂), 7.36 (d, 1H, J = 15.9 Hz, $H\bar{C}=\underline{C}H$ -Ph1), 7.42 (d, 2H, J = 10.2 Hz, H-Ar₁), 7.48 (d, 2H, J = 8.7 Hz, H-Ar₁), 7.83 (d, 2H, J = 7.8 Hz, H-Ar₂).

^{13}C NMR (75 MHz, $CDCl_3$): δ (ppm) 25.0 ($2 \times CMe_2$), 28.2 (CMe_3), 36.8 (CMe_3), 59.2 ($C(CN)_2$), 70.2 (O- CH_2 -Ph₂), 84.0 ($2 \times CMe_2$), 102.7 (C-3pyran), 106.6 (C-5pyran), 115.5 (CN), 115.7 (C-Ar₂), 116.3 ($H\bar{C}=\underline{C}H$ -Ph1), 126.6 (C-Ar₁), 127.6 (C^{Ar2} -B), 129.6 (C-Ar₁), 135.2 (C-Ar₂), 137.6 ($H\bar{C}=\underline{C}H$ -Ph1), 139.5 (O- CH_2 - C^{Ar2}), 156.8 (C^{Ar1} -OCH₂), 159.4 (C-2pyran), 160.8 (C-6pyran), 172.2 (C-4pyran).

HR-ESI-MS m/z : calcd. for $C_{33}H_{36}BN_2O_4$ $[M+H]^+$ 535.2763, found 535.2768.

4-bromo-4'-methoxybenzophenone (IV-1)

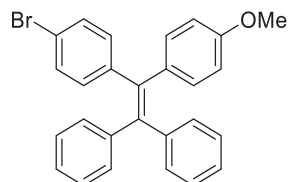


According to the literature^[263], to a solution of 4-bromobenzoylchloride (2 g, 9.2 mmol, 1 eq.) and aluminum chloride (1.82 g, 13.8 mmol, 1.5 eq.) in dry CH_2Cl_2 (14 mL) was added anisole (1.6 g, 13.8 mmol, 1.5 eq., 1.62 mL) at $0^\circ C$. The resulting mixture was stirred at RT during 4 h. The reaction was quenched by 2M HCl (20 mL), diluted with CH_2Cl_2 (30 mL) and separated. The aqueous layer

was extracted with CH₂Cl₂ (2×20 mL). The combined organic layers were washed dried (MgSO₄), concentrated and purified by silica gel column chromatography (Cyclohexane:CH₂Cl₂ = 1:3) to afford compound **IV-1** (2.66 g, 99%) as a white powder.

R_f = 0.15 (Cyclohexane:CH₂Cl₂ = 1:1)

4-bromo-4'-methoxytetraphenylethene (**IV-2**)



IV-2

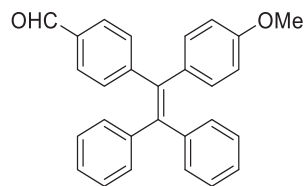
Prepared according to the general procedure **A** from diphenylmethane (1.4 g, 8.3 mmol, 1.2 eq.), *n*-butyllithium (3.4 mL, 8.3 mmol, 1.2 eq., 2.5 M in hexane), compound **IV-1** (2 g, 6.9 mmol, 1 eq.) and *p*-toluenesulfonic acid (240 mg, 1.4 mmol, 0.2 eq.) affording compound **IV-2** (2.21 g, 73%) as pale yellow amorphous solid. The compound has been reported^[264].

R_f = 0.6 (Cyclohexane:CH₂Cl₂ = 3:1)

¹H NMR (300 MHz, CDCl₃): δ (ppm) 3.75 (s, 3H, OCH₃), 6.65, (d, 2H, *J* = 8.7 Hz, H-Ar), 6.92 (dd, 4H, *J* = 3.9 Hz, 8.7Hz, H-Ar), 7.01-7.05 (m, 4H, H-Ar), 7.10-7.13 (m, 6H, H-Ar), 7.23 (d, 2H, *J* = 8.7 Hz, H-Ar).

¹³C NMR (75 MHz, CDCl₃): δ (ppm) 55.3 (OCH₃), 113.3 (CH-Ar), 120.5 (C^{Ar}-Br), 126.6 (CH-Ar), 126.7 (CH-Ar), 127.9 (CH-Ar), 128.0 (CH-Ar), 130.9 (CH-Ar), 131.4 (CH-Ar), 131.41 (CH-Ar), 132.6 (CH-Ar), 133.2 (CH-Ar), 135.5 (C^{Ar}-C=C), 139.4 (C^{Ar}-C=C), 140.8 (C^{Ar}-C=C), 143.1 (C^{Ar}-C=C), 143.7 (C=C), 143.9(C=C), 158.4 (C^{Ar}-OMe).

4-bromo-4'-methoxytetraphenylethene (**IV-3**)



IV-3

Prepared according to the general procedure **C** from compound **IV-2** (700 mg, 1.6 mmol, 1 eq.), *n*-butyllithium (1 mL, 2.4 mmol, 1.5 eq., 2.5 M in hexane), DMF (2-3 mL, excessive) affording compound **IV-3** (410 mg, 66%) as a yellow amorphous solid^[265].

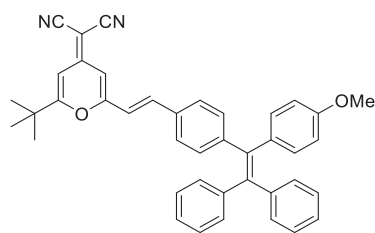
R_f = 0.21 (Cyclohexane:CH₂Cl₂ = 2:1)

¹H NMR (300 MHz, CDCl₃): δ (ppm) 3.03 (s, 3H, OCH₃), 6.67 (d, 2H, *J* = 8.7 Hz, H-Ar), 6.92 (d, 2H, *J* = 9.0 Hz, H-Ar), 6.99-7.06 (m, 4H, H-Ar), 7.0.8-7.26 (m, 6H, H-Ar), 7.62 (d, 2H, *J* = 8.1 Hz,

H-Ar), 9.90 (s, 1H, CHO).

¹³C NMR (75 MHz, CDCl₃): δ (ppm) 55.3 (OCH₃), 113.5 (CH-Ar), 126.9 (CH-Ar), 127.0 (CH-Ar), 127.94 (CH-Ar), 128.01 (CH-Ar), 129.3 (CH-Ar), 131.4 (CH-Ar), 131.5 (CH-Ar), 132.6 (CH-Ar), 133.2 (CH-Ar), 134.4 (C^{Ar}-C=C), 135.8 (C^{Ar}-C=C), 139.5 (C^{Ar}-C=C), 142.3 (C^{Ar}-C=C), 143.38 (C=C), 143.43 (C=C), 151.03 (C^{Ar}-CHO), 158.4 (C^{Ar}-OMe), 192.1 (CHO).

(E)-2-{2-[4-[2,2-diphenyl-1-(4-methoxyphenyl)-1-vinyl]styryl]-6-(tert-butyl)-4H-pyran-4-ylidene}-propanedinitrile (IV-4)



IV-4

Prepared according to the general procedure **D** from compound **IV-3** (400 mg, 1.03 mmol, 1 eq.), compound **III-9** (241 mg, 1.13 mmol, 1.1 eq.) and piperidine (0.21 mL, 2.06 mmol, 2 eq.) affording compound **IV-4** (410 mg, 64%) as a red amorphous solid.

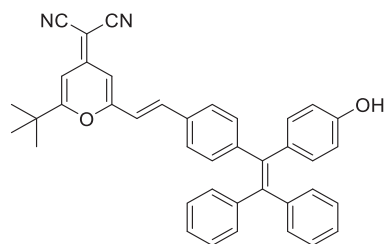
R_f = 0.17 (Cyclohexane:CH₂Cl₂ = 1:4)

¹H NMR (300 MHz, CDCl₃): δ (ppm) 1.37 (s, 9H, C(CH₃)₃), 3.75 (s, 3H, OCH₃), 6.57 (d, 1H, J = 2.1 Hz, H-3pyran), 6.60-6.67 (d, 1H, H-3pyran), 6.61-6.68 (m, 4H, H-5pyran, 2×H-Ar, HC=CH-Ph), 6.94 (d, 2H, J = 8.7 Hz, H-Ar), 7.02-7.08 (m, 5H, H-Ar), 7.09-7.14 (m, 7H, H-Ar), 7.27-7.35 (m, 3H, 2xH-Ar, HC=CH-Ph).

¹³C NMR (75 MHz, CDCl₃): δ (ppm) 28.2 (C(CH₃)₃), 36.8 (C(CH₃)₃), 55.2 (OCH₃), 59.7 (C(CN)₂), 102.7 (C-3pyran), 107.2 (C-5pyran), 113.4 (CH-Ar), 115.3 (2×CN), 118.0 (HC=CH-Ph), 126.7 (CH-Ar), 126.8 (CH-Ar), 127.3 (CH-Ar), 127.9 (CH-Ar), 127.93 (CH-Ar), 131.4 (CH-Ar), 131.5 (CH-Ar), 132.3 (CH-Ar), 132.5 (C^{Ar}-CH=CH-Pyran), 132.7 (CH-Ar), 135.6 (C^{Ar}-C=C), 137.7 (HC=CH-Ph), 137.7 (C^{Ar}-C=C), 141.5 (C^{Ar}-C=C), 143.72 (C=C), 143.75 (C=C), 146.9 (C^{Ar}-C=C), 156.7 (C-6pyran), 158.4 (C^{Ar}-OMe), 159.0 (C-2pyran), 172.3 (C-4pyran).

HR-ESI-MS *m/z*: calcd. for C₄₁H₃₅N₂O₂ [M+H]⁺ 587.2699, found 587.2693.

(E)-2-{2-[4-[2,2-diphenyl-1-(4-hydroxyphenyl)-1-vinyl]styryl]-6-(tert-butyl)-4H-pyran-4-ylidene}-propanedinitrile (IV-5)



IV-5

Prepared according to the general procedure **E** from compound **IV-4** (280 mg, 0.48 mmol, 1 eq.), BBr₃ (0.62 mL, 0.62 mmol, 1.3 eq., 1 M in CH₂Cl₂) affording compound **IV-5** (204 mg, 50%) as a red amorphous solid.

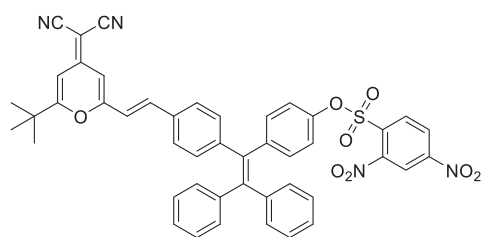
R_f = 0.26 (CH₂Cl₂:MeOH = 70:1)

¹H NMR (300 MHz, CDCl₃): δ (ppm) 1.37 (s, 9H, C(CH₃)₃), 6.57 (d, 1H, *J* = 2.1 Hz, H-3pyran), 6.60-6.67 (m, 4H, H-5pyran, 2×H-Ar, HC=CH-Ph), 6.89 (d, 2H, *J* = 8.4 Hz, H-Ar), 7.02-7.13 (m, 12H, H-Ar), 7.27-7.36 (m, 3H, 2×H-Ar, HC=CH-Ph).

¹³C NMR (75 MHz, CDCl₃): δ (ppm) 28.2 (C(CH₃)₃), 36.8 (C(CH₃)₃), 59.3 (C(CN)₂), 102.8 (C-3pyran), 107.1 (C-5pyran), 114.9 (CH-Ar), 115.3 (2×CN), 118.0 (HC=CH-Ph), 126.66 (CH-Ar), 126.7 (CH-Ar), 127.3 (CH-Ar), 127.85 (CH-Ar), 127.9 (CH-Ar), 131.4 (CH-Ar), 131.5 (CH-Ar), 132.3 (CH-Ar), 132.4 (C^{Ar}-CH=CH-Pyran), 132.8 (CH-Ar), 135.5 (C^{Ar}-C=C), 137.9 (HC=CH-Ph), 139.7 (C^{Ar}-C=C), 141.5 (C^{Ar}-C=C), 143.69 (C=C), 143.71 (C=C), 146.9 (C^{Ar}-C=C), 154.8 (C-6pyran), 156.9 (C^{Ar}-OH), 159.2 (C-2pyran), 172.4 (C-4pyran).

HR-ESI-MS *m/z*: calcd. for C₄₀H₃₃N₂O₂ [M+H]⁺ 573.2542, found 573.2552.

(E)-2-{2-[4-[2,2-diphenyl-1-(4-[2,4-dinitrophenylsulfonate]phenyl)-1-vinyl]styryl]-6-(tert-butyl)-4H-pyran-4-ylidene}-propanedinitrile (IV-7)



IV-7

To a solution of 2,4-dinitrobenzenesulfonyl chloride (**IV-6**, 298 mg, 1.12 mmol, 16 eq.) and Et₃N (0.16 mL, 1.26 mmol, 18 eq.) in CH₂Cl₂ (7 mL) was added the solution of compound **IV-5** (40 mg, 0.07 mmol, 1 eq.) in CH₂Cl₂ (3 mL) at 0°C. The resulting solution was stirred at 0°C under argon during 3 h. The mixture was evaporated when compound **IV-5** disappeared after TLC monitoring, and purified by silica gel column chromatography (Cyclohexane:CH₂Cl₂ = 1:4) to obtain compound **IV-7** (39 mg, 70%) as a red powder.

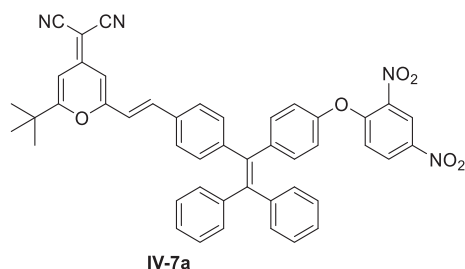
R_f = 0.4 (CH₂Cl₂)

^1H NMR (300 MHz, CDCl_3): δ (ppm) 1.36 (s, 9H, $\text{C}(\underline{\text{CH}}_3)_3$), 6.56 (d, 1H, $J = 2.1$ Hz, H-3pyran), 6.65 (d, 1H, $J = 2.1$ Hz, H-5pyran), 6.66 (d, 1H, $J = 16.2$ Hz, $\underline{\text{H}}\text{C}=\text{CH}-\text{Ph}$), 6.91-7.04 (m, 10H, H-Ar), 7.11-7.16 (m, 6H, H-Ar), 7.28-7.34 (m, 3H, $2\times\text{H}-\text{Ar}$, $\text{HC}=\underline{\text{C}}\text{H}-\text{Ph}$), 8.10 (d, 1H, $J = 8.7$ Hz, H-Ar2), 8.47 (dd, 1H, $J = 2.1$ Hz, 8.7 Hz, H-Ar2), 8.61 (d, 1H, $J = 2.4$ Hz, H-Ar2).

^{13}C NMR (75 MHz, CDCl_3): δ (ppm) 28.2 ($\text{C}(\underline{\text{C}}\text{H}_3)_3$), 36.8 ($\underline{\text{C}}(\text{CH}_3)_3$), 59.9 ($\underline{\text{C}}(\text{CN})_2$), 102.8 (C-3pyran), 107.4 (C-5pyran), 115.3 (CH-Ar), 115.3 ($2\times\text{CN}$), 118.5 ($\underline{\text{H}}\text{C}=\text{CH}-\text{Ph}$), 120.3 (CH-Ar2), 121.7 (CH-Ar), 126.2 (CH-Ar2), 127.1 (CH-Ar), 127.4 (CH-Ar), 127.08 (CH-Ar), 128.02 (CH-Ar), 131.27 (CH-Ar), 131.34 (CH-Ar), 132.1 (CH-Ar), 133.0 ($\underline{\text{C}}^{\text{Ar}}-\text{CH}=\text{CH}-\text{Pyran}$), 133.2 (CH-Ar), 133.6 ($\text{C}^{\text{Ar}2}-\text{C}=\text{C}$), 133.9 (CH-Ar2), 137.3 ($\text{HC}=\underline{\text{C}}\text{H}-\text{Ph}$), 138.3 ($\underline{\text{C}}^{\text{Ar}}-\text{C}=\text{C}$), 142.8 ($\text{C}^{\text{Ar}2}-\text{NO}_2$), 142.9 ($\text{C}^{\text{Ar}2}-\text{NO}_2$), 143.7 (C=C), 143.8 (C=C), 145.4 ($\underline{\text{C}}^{\text{Ar}}-\text{C}=\text{C}$), 147.3 ($\underline{\text{C}}^{\text{Ar}}-\text{C}=\text{C}$), 150.1 (C-6pyran), 155.5 ($\text{C}^{\text{Ar}2}-\text{SO}_2$), 156.9 ($\underline{\text{C}}^{\text{Ar}}-\text{OSO}_2$), 158.9 (C-2pyran), 172.3 (C-4pyran).

HR-ESI-MS m/z : calcd. for $\text{C}_{46}\text{H}_{35}\text{N}_4\text{O}_8\text{S}$ $[\text{M}+\text{H}]^+$ 803.2176, found 803.2170.

(E)-2-{2-[4-[2,2-diphenyl-1-(4-[2,4-dinitrophenoxy]phenyl)-1-vinyl]styryl]-6-(tert-butyl)-4H-pyran-4-ylidene}-propanedinitrile (IV-7a)



To a solution of compound **IV-5** (50 mg, 0.087 mmol, 1 eq.), 2,4-dinitrobenzenesulfonyl chloride (**IV-6**, 298 mg, 1.12 mmol, 16 eq.), 1-ethyl-3-(3-dimethylaminopropyl)carbodiimide hydrochloride (EDCI, 84 mg, 0.44 mmol, 5 eq.), 4-dimethylaminopyridine (DMAP, 11 mg, 0.087 mmol, 1 eq.) in and in CH_2Cl_2 (10 mL) was added Et_3N (0.2 mL, 1.49 mmol, 17 eq.). The resulting solution was stirred at RT under argon during 20 h. The mixture was diluted with CH_2Cl_2 (50 mL), washed with 2M HCl aqueous solution (30 mL) and brine (2×50 mL). The organic layer was dried (MgSO_4), concentrated and purified by silica gel column chromatography (Cyclohexane: $\text{CH}_2\text{Cl}_2 = 1:3$) to obtain compound **IV-7a** (33 mg, 51%) as a red powder.

$R_f = 0.7$ (CH_2Cl_2)

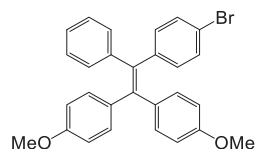
^1H NMR (300 MHz, CDCl_3): δ (ppm) 1.37 (s, 9H, $\text{C}(\underline{\text{CH}}_3)_3$), 6.56 (d, 1H, $J = 2.1$ Hz, H-3pyran), 6.66 (d, 1H, $J = 2.1$ Hz, H-5pyran), 6.67 (d, 1H, $J = 15.9$ Hz, $\underline{\text{H}}\text{C}=\text{CH}-\text{Ph}$), 6.91 (d, 1H, $J = 8.7$ Hz, H-Ar), 6.95 (d, 1H, $J = 9.0$ Hz, H-Ar2) 7.03-7.10 (m, 5H, H-Ar), 7.12-7.19 (m, 9H, H-Ar), 7.30-7.35 (m, 3H, $2\times\text{H}-\text{Ar}$, $\text{HC}=\underline{\text{C}}\text{H}-\text{Ph}$), 8.34 (dd, 1H, $J = 3.0$ Hz, 9.3 Hz, H-Ar2), 8.61 (d, 1H, $J = 2.7$ Hz, H-Ar2).

^{13}C NMR (75 MHz, CDCl_3): δ (ppm) 28.2 ($\text{C}(\underline{\text{C}}\text{H}_3)_3$), 36.8 ($\underline{\text{C}}(\text{CH}_3)_3$), 60.0 ($\underline{\text{C}}(\text{CN})_2$), 102.8 (C-3pyran), 107.4 (C-5pyran), 115.3 ($2\times\text{CN}$), 118.44 (CH-Ar2), 118.46 ($\underline{\text{H}}\text{C}=\text{CH}-\text{Ph}$), 120.1 (CH-Ar), 122.3 (CH-Ar2), 127.28 (CH-Ar), 127.31 (CH-Ar), 127.6 (CH-Ar), 128.04 (CH-Ar), 128.11 (CH-Ar), 128.9 (CH-Ar2), 131.35 (CH-Ar), 131.39 (CH-Ar), 132.2 (CH-Ar), 133.0 ($\underline{\text{C}}^{\text{Ar}}-\text{CH}=\text{CH}-\text{Pyran}$),

133.7 (CH-Ar), 137.4 (HC=CH-Ph), 138.6 (C^{Ar}-C=C), 139.6 (C^{Ar}-C=C), 141.6 (C^{Ar2}-NO₂), 142.0 (C^{Ar2}-NO₂), 142.94 (C=C), 143.12 (C=C), 143.6 (C^{Ar}-C=C), 145.7 (C^{Ar}-C=C), 152.1 (C-6pyran), 155.5 (C^{Ar2}-O), 156.7 (C^{Ar}-O), 158.9 (C-2pyran), 172.3 (C-4pyran).

HR-ESI-MS *m/z*: calcd. for C₄₆H₃₅N₄O₆ [M+2Na]²⁺ 739.2557, found 739.2551.

1-(4-bromophenyl)-2,2-(4-methoxyphenyl)-1-phenyl-ethene (V-1)

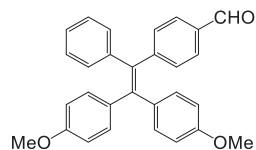


V-1

Prepared according to the general procedure **B** from bromobenzophenone (2 g, 7.7 mmol, 1 eq.), 4,4'-dimethoxybenzophenone (2.23 g, 9.2 mmol, 1.2 eq.), Zn powder (4 g, 61.6 mmol, 8 eq.), pure TiCl₄ (2 mL, 16.8 mmol, 4 eq.) affording compound **V-1** (1.27 g, 33%) as a pale yellow amorphous solid [266].

R_f = 0.27 (Cyclohexane:CH₂Cl₂ = 3:1)

1-(4-formylphenyl)-2,2-(4-methoxyphenyl)-1-phenyl-ethene (V-2):

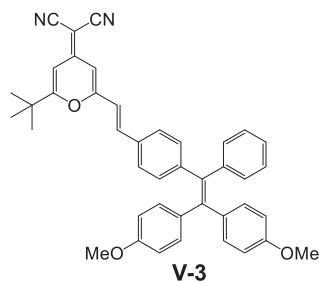


V-2

Prepared according to the general procedure **C** from compound **V-1** (1.265 g, 2.7 mmol, 1 eq.), *n*-butyllithium (2.7 mL, 6.7 mmol, 2.5 eq., 2.5 M in hexane) and DMF (1.2 mL) affording compound **V-2** (873 mg, 77%) as a yellow amorphous solid [266].

R_f = 0.34 (Cyclohexane:CH₂Cl₂ = 1:1)

(*E*)-2-{2-[4-[2,2-di-(4-methoxyphenyl)-1-phenyl-1-vinyl]styryl]-6-(*tert*-butyl)-4*H*-pyran-4-ylidene}-propanedinitrile (V-3)



V-3

Prepared according to the general procedure **D** from compound **V-2** (880 mg, 2.1 mmol, 1 eq.), compound **III-9** (492 mg, 2.3 mmol, 1.1 eq.), piperidine (0.5 mL, 5 mmol, 2.4 eq.) and acetic acid (0.15 mL, 2.5 mmol, 1.2 eq.) affording compound **V-3** (819 mg, 63%) as a red amorphous solid.

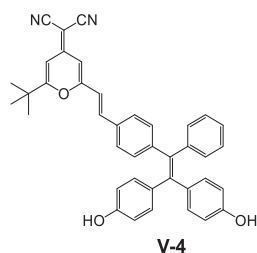
$R_f = 0.29$ (Cyclohexane:CH₂Cl₂ = 5:1)

¹H NMR (300 MHz, CDCl₃): δ (ppm) 1.37 (s, 9H, C(CH₃)₃), 3.75 (d, 6H, $J = 3.3$ Hz, 2×OCH₃), 6.55 (d, 1H, $J = 2.1$ Hz, H-3pyran), 6.62-6.68 (m, 6H, H-5pyran, 4×H-Ar, HC=CH-Ph), 6.95 (dd, 4H, $J = 7.8$ Hz, 9 Hz, H-Ar), 7.00-7.14 (m, 7H, H-Ar), 7.26-7.37 (m, 3H, 2×H-Ar, HC=CH-Ph).

¹³C NMR (75 MHz, CDCl₃): δ (ppm) 28.1 (C(CH₃)₃), 36.7 (C(CH₃)₃), 55.11 (OCH₃), 55.14 (OCH₃), 59.5 (C(CN)₂), 102.6 (C-3pyran), 107.0 (C-5pyran), 113.1 (CH-Ar), 113.2 (CH-Ar), 115.2 (2×CN), 117.7 (HC=CH-Ph), 126.4 (CH-Ar), 127.3 (CH-Ar), 127.9 (CH-Ar), 131.4 (CH-Ar), 132.0 (C^{Ar}-CH=CH-Pyran), 132.2 (CH-Ar), 132.61 (CH-Ar), 132.67 (CH-Ar), 135.9 (C^{Ar}-C=C), 136.0 (C^{Ar}-C=C), 137.7 (HC=CH-Ph), 138.3 (C^{Ar}-C=C), 141.6 (C^{Ar}-C=C), 143.8 (C=C), 147.2 (C=C), 156.6 (C-6pyran), 158.3 (C^{Ar}-OMe), 158.4 (C^{Ar}-OMe), 159.0 (C-2pyran), 172.1 (C-4pyran).

HR-ESI-MS m/z : calcd. for C₄₂H₃₇N₂O₃ [M+H]⁺ 617.2783, found 617.2799.

(E)-2-{2-[4-[2,2-di-(4-hydroxyphenyl)-1-phenyl-1-vinyl]styryl]-6-(tert-butyl)-4H-pyran-4-ylidene}-propanedinitrile (V-4)



Prepared according to the general procedure E from compound V-3 (439 mg, 0.71 mmol, 1 eq.), BBr₃ (1.8 mL, 1.78 mmol, 2.5 eq., 1 M in CH₂Cl₂) affording compound V-4 (204 mg, 50%) as a red amorphous solid.

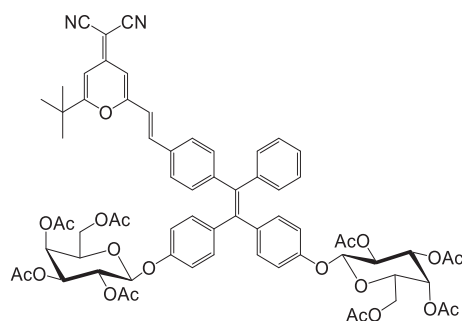
$R_f = 0.26$ (CH₂Cl₂:MeOH = 70:1)

¹H NMR (300 MHz, Acetone-*d*₆): δ (ppm) 1.42 (s, 9H, C(CH₃)₃), 6.56 (d, 1H, $J = 2.1$ Hz, H-3pyran), 6.61 (t, 4H, $J = 9.0$ Hz, H-Ar), 6.80 (d, 1H, $J = 2.1$ Hz, H-5pyran), 6.87 (t, 4H, $J = 9.0$ Hz, H-Ar), 7.03-7.15 (m, 7H, H-Ar), 7.21 (d, 1H, $J = 16.2$ Hz, HC=CH-Ph), 7.50 (d, 2H, $J = 2.1$ Hz, H-Ar), 7.59 (d, 1H, $J = 19.2$ Hz, HC=CH-Ph), 8.30 (d, 2H, $J = 11.4$ Hz, HO-Ph)

¹³C NMR (75 MHz, Acetone-*d*₆): δ (ppm) 28.2 (C(CH₃)₃), 37.5 (C(CH₃)₃), 59.2 (C(CN)₂), 103.1 (C-3pyran), 107.8 (C-5pyran), 115.5 (CH-Ar), 115.7 (CH-Ar), 119.4 (HC=CH-Ph), 127.2 (2×CN), 128.5 (CH-Ar), 128.8 (CH-Ar), 129.6 (C^{Ar}-CH=CH-Pyran), 132.3 (CH-Ar), 132.9 (CH-Ar), 133.5 (CH-Ar), 133.6 (CH-Ar), 133.8 (CH-Ar), 135.9 (C^{Ar}-C=C), 136.0 (C^{Ar}-C=C), 138.5 (HC=CH-Ph), 138.8 (C^{Ar}-C=C), 143.2 (C^{Ar}-C=C), 145.2 (C=C), 148.1 (C=C), 157.3 (C^{Ar}-OH), 157.4 (C^{Ar}-OH), 157.7 (C-6pyran), 160.7 (C-2pyran), 173.7 (C-4pyran).

HR-ESI-MS m/z : calcd. for C₄₀H₃₃N₂O₃ [M+H]⁺ 589.2462, found 589.2486.

(E)-2-{2-[4-[2,2-di-(2,3,4,6-tetra-*O*-acetyl- α -D-galactopyranosyloxyphenyl)-1-phenyl-1-vinyl]styryl]-6-(*tert*-butyl)-4*H*-pyran-4-ylidene}-propanedinitrile (V-5)



V-5

Compound **V-4** (100 mg, 0.24 mmol, 1 eq.), 2,3,4,6-tetra-*O*-acetyl-1-bromo- α -D-galactose (400 mg, 0.97 mmol, 4 eq.), and tetrabutylammonium iodide (358 mg, 0.97 mmol, 4 eq.) were dissolved in CH_2Cl_2 (10 mL). 2M aqueous NaOH (6 mL) was added to the solution and vigorous stirring was continued at 45°C during 20 h. The mixture was diluted with CH_2Cl_2 (50 mL), and washed with 2 M aqueous HCl (2×30 mL) with a colour change from dark to orange. The aqueous layers were combined and extracted with CH_2Cl_2 (2×30 mL). The organic layers were combined, dried (MgSO_4), concentrated and purified by silica gel column chromatography (CH_2Cl_2 :MeOH = 150:1) to obtain compound **V-15** (50 mg, 20%) as red amorphous solid.

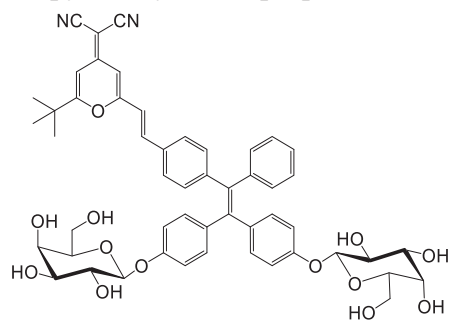
R_f = 0.31 (CH_2Cl_2 :MeOH = 100:1)

^1H NMR (300 MHz, CDCl_3): δ (ppm) 1.36 (s, 9H, $\text{C}(\text{CH}_3)_3$), 2.00, 2.01, 2.05, 2.17 (4s, 4×6H, CH_3CO), 4.01 (t, 2H, J = 6.9 Hz, H-5), 4.07-4.19 (m, 2H, H-6'), 4.18-4.23 (m, 2H, H-6), 4.99 (d, 2H, J = 4.2 Hz, H-1), 5.08 (dd, 2H, J = 3.3 Hz, 10.2 Hz, H-3), 5.42-5.48 (m, 4H, H-2, H-4), 6.55 (d, 1H, J = 2.1 Hz, H-3pyran), 6.66 (d, 1H, J = 2.1 Hz, H-5pyran), 6.64 (d, 1H, J = 15.9 Hz, $\text{HC}=\text{CH}$ -Ph), 6.75 (dd, 4H, J = 5.7 Hz, 8.7 Hz, H-Ar), 6.91-7.14 (m, 12H, H-Ar), 7.28-7.34 (m, 2H, H-Ar, $\text{HC}=\text{CH}$ -Ph).

^{13}C NMR (75 MHz, CDCl_3): δ (ppm) 20.6, 20.7, 20.75, 20.8 (4× COCH_3), 28.2 ($\text{C}(\text{CH}_3)_3$), 36.8 ($\text{C}(\text{CH}_3)_3$), 59.6 ($\text{C}(\text{CN})_2$), 61.4 (C-6), 66.9 (C-4), 68.7 (C-2), 70.9 (C-5), 71.0 (C-3), 99.3 (C-1), 102.7 (C-3pyran), 107.2 (C-5pyran), 115.3 ($\text{HC}=\text{CH}$ -Ph), 116.1 (CH-Ar), 116.3 (CH-Ar), 118.1 (2×CN), 126.8 (CH-Ar), 127.4 (CH-Ar), 128.1 (CH-Ar), 131.3 (CH-Ar), 132.1 (CH-Ar), 132.5 ($\text{C}^{\text{Ar}}\text{-CH}=\text{CH}$ -Pyran), 132.6 (CH-Ar), 132.64 (CH-Ar), 132.67 (CH-Ar), 137.5 ($\text{HC}=\text{CH}$ -Ph), 138.3 ($\text{C}^{\text{Ar}}\text{-C}=\text{C}$), 138.5 ($\text{C}^{\text{Ar}}\text{-C}=\text{C}$), 139.8 ($\text{C}^{\text{Ar}}\text{-C}=\text{C}$), 140.5 ($\text{C}^{\text{Ar}}\text{-C}=\text{C}$), 143.2 (C=C), 146.4 (C=C), 155.4 ($\text{C}^{\text{Ar}}\text{-O}$), 155.6 ($\text{C}^{\text{Ar}}\text{-O}$), 156.7 (C-6pyran), 158.9 (C-2pyran), 170.2, 170.3, 170.4, 170.43 (4× COCH_3), 172.3 (C-4pyran).

HR-ESI-MS m/z : calcd. for $\text{C}_{68}\text{H}_{68}\text{N}_2\text{Na}_2\text{O}_{21}$ $[\text{M}+2\text{Na}]^{2+}$ 647.2022, found 647.2049.

(E)-2-{2-[4-(2,2-di-β-D-galactopyranosyloxyphenyl)-1-phenyl-1-vinyl]styryl]-6-(tert-butyl)-4H-pyran-4-ylidene}-propanedinitrile (V-6)



V-6

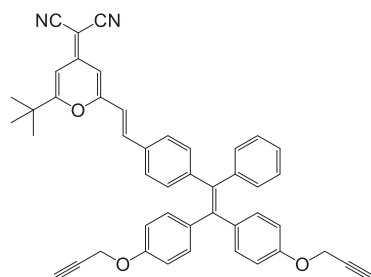
Prepared according to the general procedure **I** from compound **V-5** (50 mg, 0.04 mmol, 1 eq.), MeOH/Et₃N (11 mL, 10:1, v/v) affording compound **V-6** (23 mg, 63%) as a red amorphous solid.

¹H NMR (300 MHz, CD₃OD:DMSO-*d*₆ = 3:1): δ (ppm) 1.42 (s, 9H, C(CH₃)₃), 3.55 (dd, 2H, *J* = 2.4 Hz, 8,7 Hz, H-3), 3.66-3.76 (m, 8H, H-4, H-5, H-6, H-6'), 3.87-3.88 (m, 2H, H-2), 4.83 (dd, 2H, *J* = 2.4 Hz, 7.8 Hz, H-1), 6.58 (d, 1H, *J* = 2.1 Hz, H-3pyran), 6.85-7.19 (m, 17H, H-5pyran, 16×H-Ar), 7.45-7.51 (m, 3H, HC=CH-Ph, 2×H-Ar).

¹³C NMR (75 MHz, CD₃OD:DMSO-*d*₆ = 3:1): δ (ppm) 28.4 (C(CH₃)₃), 37.8 (C(CH₃)₃), 59.0 (C(CN)₂), 62.3 (C-6), 70.1 (C-4), 72.2 (C-2), 74.8 (C-5), 76.9 (C-3), 101.3 (C-1), 102.6 (C-3pyran), 108.1 (C-5pyran), 109.2 (HC=CH-Ph), 116.9 (CH-Ar), 117.0 (CH-Ar), 115.8 (2×CN), 127.75 (CH-Ar), 127.77 (CH-Ar), 128.8 (CH-Ar), 128.9 (CH-Ar), 129.2 (CH-Ar), 132.4 (C^{Ar}-CH=CH-Pyran), 133.1 (CH-Ar), 133.5 (CH-Ar), 133.6 (CH-Ar), 138.7 (HC=CH-Ph), 140.5 (C^{Ar}-C=C), 141.3 (C^{Ar}-C=C), 142.5 (C^{Ar}-C=C), 145.2 (C^{Ar}-C=C), 147.8 (C=C), 148.9 (C=C), 158.1 (C^{Ar}-O), 158.4 (C^{Ar}-O), 160.8 (C-6pyran), 161.2 (C-2pyran), 174.2 (C-4pyran).

HR-ESI-MS *m/z*: calcd. for C₅₂H₅₃N₂O₁₃ [M+H]⁺ 913.3542, found 913.3552.

(E)-2-{2-(4-[2,2-di-O-propargyloxyphenyl]-1-phenyl-1-vinyl)styryl]-6-(tert-butyl)-4H-pyran-4-ylidene}-propanedinitrile (V-7)



V-7

Prepared according to the general procedure **F** from compound **V-4** (1.31 g, 2.2 mmol, 1 eq.), propargyl bromide (0.7 mL, 6.6 mmol, 3 eq.), *n*-tetrabutylammonium iodide (2.4 g, 6.6 mmol, 3 eq.), K₂CO₃ (1.2 g, 8.8 mmol, 4 eq.) and 18-crown-6 (290 mg, 1.1 mmol, 0.5 eq.) affording compound **V-7** (1.35 g, 92%) as a red amorphous solid.

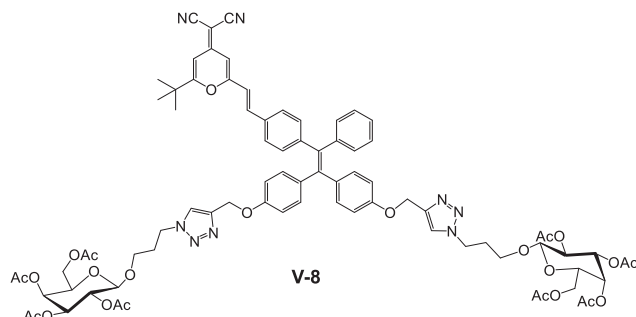
$R_f = 0.31$ (Cyclohexane:CH₂Cl₂ = 1:2)

¹H NMR (300 MHz, CDCl₃): δ (ppm) 1.36 (s, 9H, C(CH₃)₃), 2.51 (dd, 2H, $J = 2.4$ Hz, 3.9 Hz, C≡CH), 4.62 (t, 4H, $J = 2.1$ Hz, CH₂-C≡CH), 6.55 (d, 1H, $J = 2.1$ Hz, H-3pyran), 6.64 (d, 1H, $J = 15.9$ Hz, HC=CH-Ph), 6.65 (d, 1H, $J = 2.1$ Hz, H-5pyran), 6.72 (dd, 4H, $J = 5.7$ Hz, 9 Hz, H-Ar), 6.93-7.14 (m, 12H, H-Ar), 7.29-7.33 (m, 2H, H-Ar, HC=CH-Ph).

¹³C NMR (75 MHz, CDCl₃): δ (ppm) 28.2 (C(CH₃)₃), 36.8 (C(CH₃)₃), 55.86 (CH₂-C≡CH), 55.90 (CH₂-C≡CH), 59.7 (C(CN)₂), 75.6 (CH≡C), 75.7 (CH≡C), 78.56 (CH=C), 78.59 (CH=C), 102.7 (C-3pyran), 107.1 (C-5pyran), 114.1 (CH-Ar), 114.2 (CH-Ar), 115.3 (2xCN), 117.9 (HC=CH-Ph), 126.7 (CH-Ar), 127.4 (CH-Ar), 128.0 (CH-Ar), 131.5 (CH-Ar), 132.2 (CH-Ar), 132.3 (C^{Ar}-CH=CH-Pyran), 132.69 (CH-Ar), 132.76 (CH-Ar), 136.8 (C^{Ar}-C=C), 136.9 (C^{Ar}-C=C), 137.7 (HC=CH-Ph), 138.9 (C^{Ar}-C=C), 141.3 (C^{Ar}-C=C), 143.6 (C=C), 147.0 (C=C), 156.5 (C-6pyran), 156.6 (C^{Ar}-O-propargyl), 156.7 (C^{Ar}-O-propargyl), 159.0 (C-2pyran), 172.3 (C-4pyran).

HR-ESI-MS m/z : calcd. for C₄₆H₃₇N₂O₃ [M+H]⁺ 665.2799, found 665.2722.

(E)-2-{2-[4-(2,2-di-(4-{1-[1-(2,3,4,6-tetra-*O*-acetyl- β -D-galactopyranosyloxy)-3-propyl]-1,2,3-triazol-4-yl-methoxy}phenyl)-1-phenyl-1-vinyl)styryl]-6-(*tert*-butyl)-4H-pyran-4-ylidene}-propanedinitrile (V-8)



Prepared according to the general procedure **G** from compound **V-7** (150 mg, 0.22 mmol, 1 eq.), **GalC₃N₃** (214 mg, 0.49 mmol, 2.2 eq.)^[267], copper sulfate (80 mg, 0.44 mmol, 2 eq.) and L-ascorbic acid sodium salt (178 mg, 0.9 mmol, 4 eq.) affording compound **V-8** (247 mg, 74%) as a red amorphous solid.

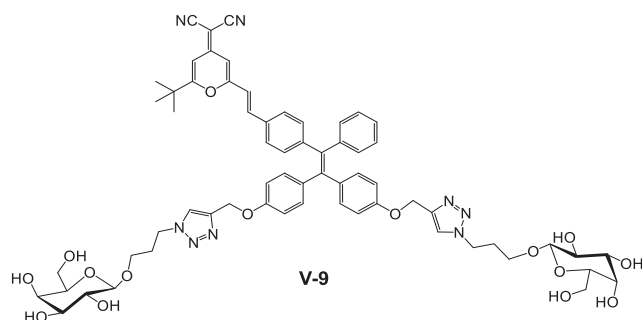
$R_f = 0.2$ (CH₂Cl₂:EtOAc = 2:1)

¹H NMR (300 MHz, CDCl₃): δ (ppm) 1.36 (s, 9H, C(CH₃)₃), 1.99, 2.02, 2.09, 2.16 (4s, 4×6H, CH₃CO), 2.13-2.24 (m, 4H, OCH₂CH₂CH₂-triaz), 3.46-3.56 (m, 2H, H-6'), 3.88-3.93 (m, 4H, H-5, H-6), 4.13-4.17 (m, 4H, OCH₂CH₂CH₂-triaz), 4.47 (d, 2H, $J = 7.8$ Hz, H-1), 4.41-4.51 (m, 4H, OCH₂CH₂CH₂-triaz), 5.02 (dd, 2H, $J = 3.3$ Hz, $J = 10.5$ Hz, H-3), 5.12 (d, 4H, $J = 2.1$ Hz, OCH₂-triaz), 5.18-5.29 (m, 2H, H-2), 5.40 (d, 2H, $J = 3.3$ Hz), 6.55 (d, 1H, $J = 1.8$ Hz, H-3pyran), 6.659 (d, 1H, $J = 2.1$ Hz, H-5pyran), 6.66 (d, 1H, $J = 8.4$ Hz, HC=CH-Ph), 6.74 (dd, 4H, $J = 6.6$ Hz, 8.7 Hz, H-Ar), 6.91-7.14 (m, 12H, H-Ar), 7.30-7.35 (m, 2H, H-Ar, HC=CH-Ph), 7.62 (d, 2H, $J = 7.8$ Hz, H-triaz).

^{13}C NMR (75 MHz, CDCl_3): δ (ppm) 20.7, 20.78, 20.79, 21.0 ($4\times\text{COCH}_3$), 28.2 ($\text{C}(\text{CH}_3)_3$), 30.3 ($\text{OCH}_2\text{CH}_2\text{CH}_2\text{-triaz}$), 36.8 ($\text{C}(\text{CH}_3)_3$), 46.9 ($\text{OCH}_2\text{CH}_2\text{CH}_2\text{-triaz}$), 59.6 ($\text{C}(\text{CN})_2$), 60.5 ($\text{OCH}_2\text{CH}_2\text{CH}_2\text{-triaz}$), 61.4 ($\text{CH}_2\text{-triaz}$), 65.9 (C-6), 67.1 (C-4), 68.9 (C-2), 78.88 (C-5), 78.89 (C-3), 101.3 (C-1), 102.7 (C-3pyran), 107.1 (C-5pyran), 113.96 (CH-Ar), 114.09 (CH-Ar), 115.3 ($2\times\text{CN}$), 117.9 ($\text{HC}=\text{CH-Ph}$), 123.3 (CH^{triaz}), 127.4 (CH-Ar), 128.0 (CH-Ar), 131.5 (CH-Ar), 132.2 (CH-Ar), 132.3 ($\text{C}^{\text{Ar}}\text{-CH}=\text{CH-Pyran}$), 132.75 (CH-Ar), 132.77 (CH-Ar), 132.8 (CH-Ar), 136.50 ($\text{C}^{\text{Ar}}\text{-C}=\text{C}$), 136.57 ($\text{C}^{\text{Ar}}\text{-C}=\text{C}$), 137.7 ($\text{HC}=\text{CH-Ph}$), 138.9 ($\text{C}^{\text{Ar}}\text{-C}=\text{C}$), 141.4 ($\text{C}^{\text{Ar}}\text{-C}=\text{C}$), 143.6 (C=C), 144.4 (C^{triaz}), 147.0 (C=C), 156.7 (C-6pyran), 157.2 ($\text{C}^{\text{Ar}}\text{-O}$), 157.4 ($\text{C}^{\text{Ar}}\text{-O}$), 159.1 (C-2pyran), 169.7, 170.2, 170.3, 170.5 ($4\times\text{COCH}_3$) 172.3 (C-4pyran).

HR-ESI-MS m/z : calcd. for $\text{C}_{88}\text{H}_{88}\text{N}_8\text{O}_{23}$ [$\text{M}+2\text{H}$] $^+$ 764.2976, found 764.2947.

(E)-2-{2-(4-[2,2-di-(4-[1-(1- β -D-galactopyranosyloxy-3-propyl)-1,2,3-triazol-4-yl-methoxy]phenyl)-1-phenyl-1-vinyl]styryl)-6-(*tert*-butyl)-4H-pyran-4-ylidene}-propanedinitrile (V-9)



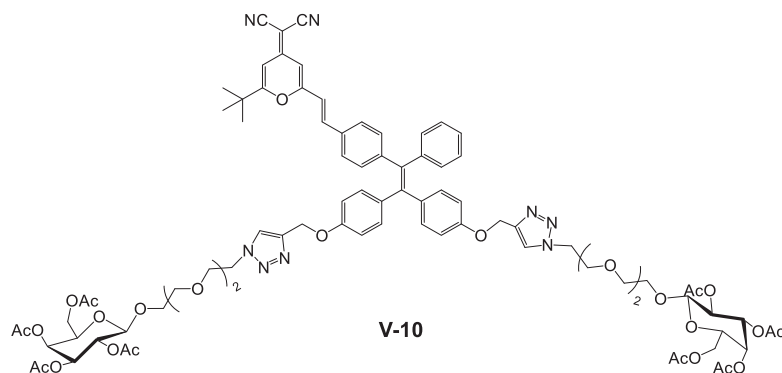
Prepared according to the general procedure I from compound V-8 (115 mg, 0.075 mmol, 1eq.), and in $\text{MeOH}/\text{H}_2\text{O}/\text{Et}_3\text{N}$ (17 mL, 12:3:2, v/v/v) affording compound V-9 (92 mg, 95%) as a red amorphous solid.

^1H NMR (300 MHz, CD_3OD): δ (ppm) 1.40 (s, 9H, $\text{C}(\text{CH}_3)_3$), 2.17-2.21 (m, 4H, $\text{OCH}_2\text{CH}_2\text{CH}_2\text{-triaz}$), 3.34-3.58 (m, 8H, H-2, H-3, H-5, H-6'), 3.72-3.76 (m, 4H, $\text{OCH}_2\text{CH}_2\text{CH}_2\text{-triaz}$), 3.82-3.91 (m, 4H, H-4, H-6), 4.20 (dd, 2H, $J = 2.1$ Hz, 7.2 Hz, H-1), 4.56-4.61 (m, 4H, $\text{OCH}_2\text{CH}_2\text{CH}_2\text{-triaz}$), 5.09 (s, 4H, $\text{OCH}_2\text{-triaz}$), 6.58 (d, 1H, $J = 2.1$ Hz, H-3pyran), 6.74-6.80 (m, 5H, H-5pyran, $4\times\text{H-Ar}$), 6.91-7.12 (m, 12H, $\text{HC}=\text{CH-Ph}$, $11\times\text{H-Ar}$), 7.40-7.47 (m, $\text{HC}=\text{CH-Ph}$, $2\times\text{H-Ar}$), 8.12 (d, 2H, $J = 2.1$ Hz, H-triaz).

^{13}C NMR (75 MHz, CD_3OD): δ (ppm) 28.3 ($\text{C}(\text{CH}_3)_3$), 31.5 ($\text{OCH}_2\text{CH}_2\text{CH}_2\text{-triaz}$), 37.7 ($\text{C}(\text{CH}_3)_3$), 48.3 ($\text{OCH}_2\text{CH}_2\text{CH}_2\text{-triaz}$), 59.1 ($\text{C}(\text{CN})_2$), 60.8 ($\text{OCH}_2\text{CH}_2\text{CH}_2\text{-triaz}$), 62.5 ($\text{CH}_2\text{-triaz}$), 66.7 (C-6), 70.3 (C-4), 72.5 (C-2), 74.9 (C-5), 76.7 (C-3), 102.9 (C-3pyran), 105.0 (C-1), 108.1 (C-5pyran), 115.1 (CH-Ar), 115.3 (CH-Ar), 118.7 ($\text{HC}=\text{CH-Ph}$), 120.2 ($2\times\text{CN}$), 126.1 (CH^{triaz}), 128.67 (CH-Ar), 127.70 (CH-Ar), 129.0 (CH-Ar), 132.5 ($\text{C}^{\text{Ar}}\text{-CH}=\text{CH-Pyran}$), 133.1 (CH-Ar), 132.7 (CH-Ar), 132.8 (CH-Ar), 134.1 (CH-Ar), 137.76 ($\text{C}^{\text{Ar}}\text{-C}=\text{C}$), 137.8 ($\text{C}^{\text{Ar}}\text{-C}=\text{C}$), 138.8 ($\text{HC}=\text{CH-Ph}$), 140.3 ($\text{C}^{\text{Ar}}\text{-C}=\text{C}$), 141.4 (C^{triaz}), 144.5 ($\text{C}^{\text{Ar}}\text{-C}=\text{C}$), 143.6 (C=C), 145.2 (C^{triaz}), 152.0 (C=C), 155.0 (C-6pyran), 158.6 ($\text{C}^{\text{Ar}}\text{-O}$), 158.7 ($\text{C}^{\text{Ar}}\text{-O}$), 159.3 (C-2pyran), 172.2 (C-4pyran).

HR-ESI-MS m/z : calcd. for $C_{64}H_{72}N_8O_{15}$ $[M+2H]^{2+}$ 596.2553, found 596.2537.

(E)-2-{2-[4-(2,2-di-(4-{1-[1-(2,3,4,6-tetra-*O*-acetyl- β -D-galacopyranosyloxy)-3,6-dioxaoct-8-yl]-1,2,3-triazol-4-yl-methoxy}phenyl)-1-phenyl-1-vinyl)styryl]-6-(*tert*-butyl)-4*H*-pyran-4-ylidene}-propanedinitrile (V-10)



Prepared according to the general procedure **H** from compound **V-7** (140 mg, 0.21 mmol, 1 eq.), compound **GalEGN₃** (242 mg, 0.48 mmol, 2.3 eq.), copper iodide (10 mg, 0.05 mmol, 0.2 eq.) and *N,N*-diisopropylethylamine (0.2 mL, 1.05 mmol, 5 eq.) affording compound **V-10** (185 mg, 53%) as red amorphous solid.

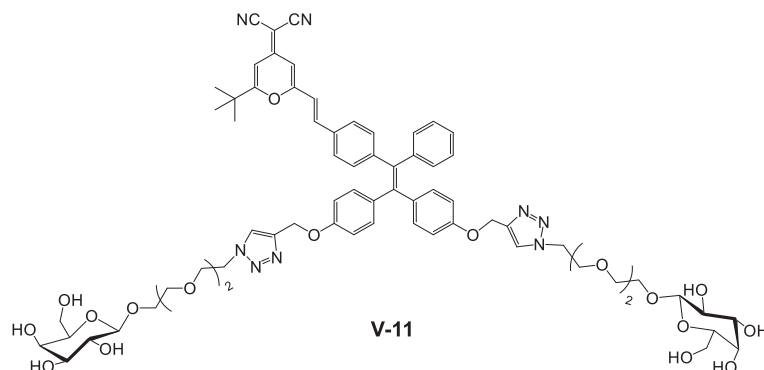
$R_f = 0.20$ (CH_2Cl_2 :MeOH = 40:1)

1H NMR (300 MHz, $CDCl_3$): δ (ppm) 1.35 (s, 9H, $C(CH_3)_3$), 1.96, 2.01, 2.02, 2.12 (4s, 4 \times 6H, CH_3CO), 3.56-3.63 (m, 12H, OCH_2CH_2O), 3.66-3.72 (m, 2H, Gal- OCH_2), 3.86-3.96 (m, 8H, OCH_2CH_2N , H-5, Gal- OCH_2), 4.09-4.15 (m, 4H, H-6, H-6'), 4.51-4.58 (m, 6H, H-1, OCH_2CH_2N), 5.00 (dd, 2H, $J = 3.0$ Hz, 9.0 Hz, H-3), 5.11 (s, 4H, OCH_2 -triaz), 5.15-5.22 (m, 2H, H-2), 5.37 (d, 2H, $J = 3.3$ Hz, H-4), 6.53 (d, 1H, $J = 1.8$ Hz, H-3pyran), 6.65 (d, 1H, $J = 1.8$ Hz, H-5pyran), 6.66 (d, 1H, $J = 15.9$ Hz, $HC=CH$ -Ph), 6.73 (dd, 4H, $J = 6.9$ Hz, 9 Hz, H-Ar), 6.91-7.13 (m, 12H, H-Ar), 7.26-7.34 (m, 2H, H-Ar, $HC=CH$ -Ph), 7.78 (d, 2H, $J = 5.4$ Hz, H-triaz).

^{13}C NMR (75 MHz, $CDCl_3$): δ (ppm) 20.7, 20.76, 20.79, 20.8 (4 \times $COCH_3$), 28.2 ($C(CH_3)_3$), 36.8 ($C(CH_3)_3$), 50.4 (OCH_2CH_2N), 59.5 ($C(CN)_2$), 61.3 (OCH_2 -triaz), 61.9 (C-6), 67.1 (C-4), 68.9 (C-2), 69.3 (Gal- OCH_2), 69.5 (OCH_2CH_2N), 70.3 (C-5), 70.65 (OCH_2), 70.70 (OCH_2), 70.8 (OCH_2), 70.9 (C-3), 101.4 (C-1), 102.7 (C-3pyran), 107.1 (C-5pyran), 113.96 (CH-Ar), 114.09 (CH-Ar), 115.3 (2 \times CN), 117.9 ($HC=CH$ -Ph), 124.1 (CH^{triaz}), 127.4 (CH-Ar), 128.0 (CH-Ar), 131.5 (CH-Ar), 132.2 (CH-Ar), 132.24 (C^{Ar} -CH=CH-Pyran), 132.71 (CH-Ar), 132.74 (CH-Ar), 132.8 (CH-Ar), 136.4 (C^{Ar} -C=C), 136.5 (C^{Ar} -C=C), 137.7 ($HC=CH$ -Ph), 138.8 (C^{Ar} -C=C), 141.3 (C^{Ar} -C=C), 143.7 (C=C), 144.0 (C^{triaz}), 147.0 (C=C), 156.7 (C-6pyran), 157.2 (C^{Ar} -O), 157.4 (C^{Ar} -O), 159.1 (C-2pyran), 169.5, 170.2, 170.3, 170.5 (4 \times $COCH_3$) 172.3 (C-4pyran).

HR-ESI-MS m/z : calcd. for $C_{86}H_{100}N_8O_{27}$ $[M+2H]^{2+}$ 838.3343, found 838.3352.

(*E*)-2-{2-[4-(2,2-di-(4-{1-[1-(β-D-galacopyranosyloxy)-3,6-dioxaoct-8-yl]-1,2,3-triazol-4-yl-methoxy}phenyl)-1-phenyl-1-vinyl)styryl]-6-(*tert*-butyl)-4*H*-pyran-4-ylidene}-propanedinitrile (V-11)



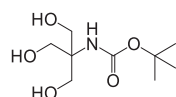
Prepared according to the general procedure **I** from compound **V-10** (120 mg, 0.072 mmol, 1 eq.), and in MeOH/H₂O/Et₃N (8 mL / 2 mL / 2 mL) affording compound **V-11** (92 mg, 95%) as a red amorphous solid.

¹H NMR (300 MHz, CD₃OD): δ (ppm) 1.37 (s, 9H, C(CH₃)₃), 3.64-3.73 (m, 22H, OCH₂, H-2, H-3, H-4, H-5, H-6'), 3.82-3.99 (m, 10H, OCH₂CH₂N, Gal-OCH₂, H-6), 4.23 (dd, 2H, *J* = 2.4 Hz, 7.2 Hz, H-1), 4.58 (m, 2H, OCH₂CH₂N), 5.07 (s, 4H, OCH₂-triaz), 6.55 (d, 1H, *J* = 2.1 Hz, H-3pyran), 6.74-6.78 (m, 4H, H-5pyran, HC=CH-Ph, 2×H-Ar), 6.90-7.10 (m, 13H, H-Ar), 7.35-7.38 (m, 3H, 2×H-Ar, HC=CH-Ph), 8.09 (s, 2H, H-triaz).

¹³C NMR (75 MHz, CD₃OD): 26.9 (C(CH₃)₃), 36.3 (C(CH₃)₃), 50.1 (OCH₂CH₂N), 57.7 (C(CN)₂), 60.6 (OCH₂-triaz), 68.2 (C-6), 68.87 (Gal-OCH₂), 68.93 (OCH₂CH₂N), 69.7 (OCH₂), 69.85 (OCH₂), 69.89 (OCH₂), 70.0 (C-4), 71.1 (C-2), 72.1 (C-5), 73.5 (C-3), 102.0 (C-3pyran), 103.6 (C-1), 106.6 (C-5pyran), 113.75 (CH-Ar), 113.94 (CH-Ar), 115.0 (2×CN), 118.0 (HC=CH-Ph), 125.0 (CH^{triaz}), 127.3 (CH-Ar), 127.6 (CH-Ar), 131.1 (CH-Ar), 131.7 (CH-Ar), 131.8 (C^{Ar}-CH=CH-Pyran), 132.37 (CH-Ar), 132.41 (CH-Ar), 132.7 (CH-Ar), 136.38 (C^{Ar}-C=C), 136.4 (C^{Ar}-C=C), 137.5 (HC=CH-Ph), 138.9 (C^{Ar}-C=C), 141.3 (C^{Ar}-C=C), 143.7 (C=C), 144.1 (C^{triaz}), 146.6 (C=C), 156.0 (C-6pyran), 157.2 (C^{Ar}-O), 157.3 (C^{Ar}-O), 159.7 (C-2pyran), 172.8 (C-4pyran).

HR-ESI-MS *m/z*: calcd. for C₇₀H₈₄N₈O₁₉ [M+H]⁺ 670.2921, found 670.2914.

***N*-(*t*-butyloxycarbonyl)tris(hydroxymethyl)aminomethane (V-12)**

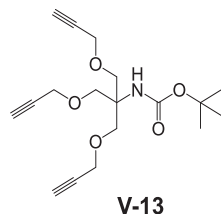


V-12

A suspension of tris(hydroxymethyl)aminomethane (4 g, 33 mmol, 1 eq.) and di-*t*-butyl dicarbonate (9.4 g, 43 mmol, 1.3 eq.) in MeOH/*i*-PrOH (30 mL, 2:1, v/v) was stirred at 82°C during 18 h. The

reaction was then evaporated when all starting material had been dissolved. The solid residue was diluted with EtOAc (50 mL) then filtered and washed with EtOAc (3×40 mL) and dried under vacuum to obtain compound **V-12** (5.05 g, 70%) as a white powder^[268].

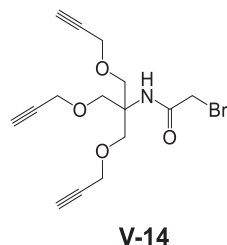
***N*-(*t*-butyloxycarbonyl)tris(propargyloxymethyl)aminomethane (V-13)**



To a solution of compound **V-12** (1 g, 4.5 mmol, 1 eq.), potassium hydroxide (KOH, 1.5 g, 27.3 mmol, 6 eq.) and tetrabutylammonium iodide (360 mg, 0.45 mmol, 0.1 eq.) in DMF/H₂O (18 mL, 5:1, v/v) was added propargyl bromide (2.15 g, 18.1 mmol, 4 eq.). The resulting solution was stirred at 38°C during 20 h. The solution was diluted with EtOAc (50 mL) and washed with brine (2×40 mL), 2M aqueous HCl (20 mL). The organic layer was dried (Na₂SO₄), concentrated and purified by silica gel column chromatography (Cyclohexane:EtOAc = 4:1) to obtain compound **V-13** (285 mg, 20%) as a pale yellow oil^[268].

R_f = 0.57 (Cyclohexane:EtOAc = 4:1)

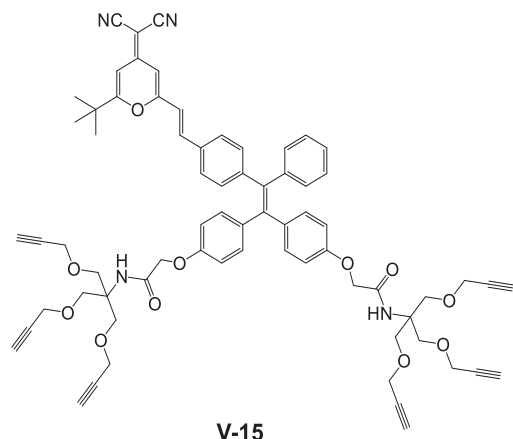
***N*-(2-bromoacetyl)tris(propargyloxymethyl)aminomethane (V-14)**



To a solution of compound **V-13** (250 mg, 0.75 mmol, 1 eq.) in CH₂Cl₂ (4 mL) was added trifluoroacetic acid (1 mL). The reaction was stirred at 30°C during 2 h. The mixture was then evaporated and toluene (2×10 mL) was used to co-evaporate TFA. The resulting crude product was dissolved with CH₂Cl₂ (10 mL) before adding triethylamine (0.22 mL, 1.5 mmol, 2 eq.) and 2-bromoacetyl bromide (0.08 mL, 0.97 mmol, 1.3 eq.). The solution was stirred at room temperature during 18 h. The solution was then diluted with CH₂Cl₂ (50 mL), washed by brine (50 mL), 2M aqueous HCl (30 mL), and brine (50 mL). The organic layer was dried (MgSO₄), concentrated, and purified with silica gel column chromatograph (Cyclohexane:EtOAc = 3:1) to obtain compound **V-14** (204 mg, 77%) as a pale yellow oil^[269].

R_f = 0.2 (Cyclohexane:EtOAc = 3:1)

(E)-2-{2-[4-(2,2-di-{N-[tris(propargyloxymethyl)methyl]-2-oxy-acetamido}phenyl-1-phenyl-1-vinyl)styryl]-6-(tert-butyl)-4H-pyran-4-ylidene}-propanedinitrile (V-15)



V-15

To a solution of compound **V-14** (152 mg, 0.26 mmol, 1 eq.) and compound **V-4** (200 mg, 0.56 mmol, 2.2 eq.), potassium carbonate (141 mg, 1.02 mmol, 4 eq.) and tetrabutylammonium iodide (189 mg, 0.52 mmol, 2 eq.) in acetonitrile (15 mL) was added 18-crown-6 (35 mg, 0.13 mmol, 0.5 eq.). The resulting solution was stirred at 60°C during 18 h. The mixture was concentrated, diluted with EtOAc (50 mL), washed with brine (50 mL), 2M aqueous HCl (30 mL) and brine (30 mL). The aqueous fractions were combined and extracted with EtOAc (40 mL). The organic layers were combined, dried (MgSO₄), concentrated, and purified by silica gel column chromatography (Cyclohexane:EtOAc = 2.5:1) to obtain compound **V-15** (241 mg, 83%) as a red amorphous solid.

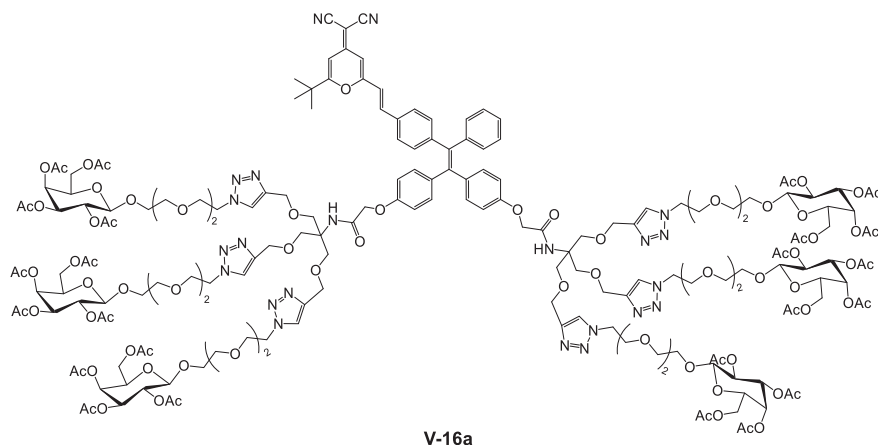
$R_f = 0.17$ (Cyclohexane:EtOAc = 2.5:1)

¹H NMR (300 MHz, CDCl₃): 1.37 (s, 9H, C(CH₃)₃), 2.42-2.44 (m, 6H, HC≡C), 3.87 (s, 12H, (O-CH₂)₃-C), 4.15 (d, 12H, $J = 2.7$ Hz, CH₂-C≡CH), 4.34 (s, 4H, OCH₂CO), 6.56 (d, 1H, $J = 2.1$ Hz, H-3pyran), 6.49-6.71 (m, 6H, H-5pyran, HC=CH-Ph, 2×H-Ar), 6.88 (d, 2H, $J = 3$ Hz, NH), 6.39-6.70 (m, 8H, H-Ar), 7.14-7.16 (m, 3H, H-Ar), 7.29-7.32 (m, 3H, 2×H-Ar, HC=CH-Ph).

¹³C NMR (75 MHz, CDCl₃): 28.2 (C(CH₃)₃), 36.8 (C(CH₃)₃), 58.7 (CH₂-C≡CH), 59.3 ((O-CH₂)₃-C), 59.7 (C(CN)₂), 67.4 (OCH₂CO), 68.4 ((O-CH₂)₃-C), 74.85 and 74.9 (HC≡C), 79.51 and 79.54 (HC≡C), 102.7 (C-3pyran), 107.2 (C-5pyran), 114.2 (CH-Ar), 114.3 (CH-Ar), 115.2 and 115.23 (2×CN), 118.1 (HC=CH-Ph), 126.8 (CH-Ar), 127.4 (CH-Ar), 128.1 (CH-Ar), 131.4 (CH-Ar), 132.1 (CH-Ar), 132.4 (C^{Ar}-CH=CH-Pyran), 132.7 (CH-Ar), 132.8 (CH-Ar), 137.1 (C^{Ar}-C=C), 137.2 (C^{Ar}-C=C), 137.5 (HC=CH-Ph), 139.3 (C^{Ar}-C=C), 140.8 (C^{Ar}-C=C), 143.4 (C=C), 146.7 (C=C), 156.0 (C-6pyran), 156.1 (C^{Ar}-O-propargyl), 156.6 (C^{Ar}-O-propargyl), 158.9 (C-2pyran), 167.8 and 167.87 (CH₂CONH) 172.2 (C-4pyran).

HR-ESI-MS m/z : calcd. for C₇₀H₆₇N₄O₁₁ [M+H]⁺ 1139.4801, found 1139.4807.

(E)-2-{2-[4-(2,2-di-{N-[tris{1-[1-(2,3,4,6-tetra-*O*-acetyl- β -D-galacopyranosyloxy)-3,6-dioxaoct-8-yl]-1,2,3-triazol-4-yl-methoxy}methyl]-2-oxy-acetamido}phenyl-1-phenyl-1-vinyl)styryl]-6-(*tert*-butyl)-4*H*-pyran-4-ylidene}-propanedinitrile (V-16a)



Prepared according to the general procedure **H** from compound **V-15** (100 mg, 0.088 mmol, 1 eq.), **GalEGN₃** (354 mg, 0.7 mmol, 8 eq.) [183], copper iodide (10 mg, 0.052 mmol, 0.6 eq.) and *N,N*-diisopropylethylamine (0.13 mL, 0.7 mmol, 8 eq.) affording compound **V-16a** (185 mg, 53%) as red amorphous solid.

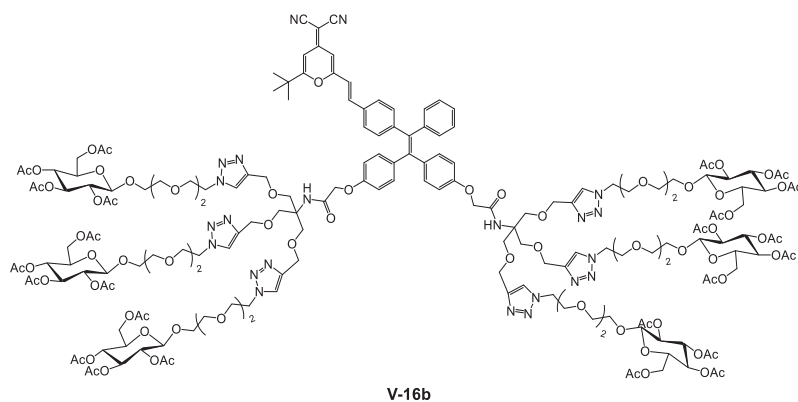
$R_f = 0.26$ ($\text{CH}_2\text{Cl}_2:\text{MeOH} = 20:1$)

¹H NMR (300 MHz, CDCl_3): 1.35 (s, 9H, $\text{C}(\text{CH}_3)_3$), 1.96, 2.02, 2.021, 2.12 (4s, $4 \times 18\text{H}$, CH_3CO), 3.57-3.61 (m, 36H, $\text{OCH}_2\text{CH}_2\text{O}$), 3.67-3.74 (m, 8H, Gal- OCH_2), 3.80 (s, 12H, $(\text{O}-\text{CH}_2)_3\text{-C}$), 3.85-3.97 (m, 24H, $\text{OCH}_2\text{CH}_2\text{N}$, H-5, Gal- OCH_2), 4.08-4.19 (m, 12H, H-6, H-6'), 4.28 (s, 4H, OCH_2CO), 4.50-4.61 (m, 30H, H-1, $\text{OCH}_2\text{CH}_2\text{N}$, $\text{OCH}_2\text{-triaz}$), 5.02 (dd, 6H, $J = 3.3$ Hz, 10.5 Hz, H-3), 5.14-5.21 (m, 6H, H-2), 5.37 (dd, 6H, $J = 3.3$ Hz, 10.5 Hz, H-4), 6.53 (d, 2H, $J = 2.1$ Hz, H-3pyran), 6.60-6.75 (m, 6H, H-5pyran, $\text{HC}=\text{CH-Ph}$, $2 \times \text{H-Ar}$), 6.90-7.04 (m, 10H, $2 \times \text{NH}$, $8 \times \text{H-Ar}$), 7.14-7.16 (m, 3H, H-Ar), 7.29-7.32 (m, 3H, $2 \times \text{H-Ar}$, $\text{HC}=\text{CH-Ph}$), 7.70 (s, 6H, H-triaz).

¹³C NMR (75 MHz, CDCl_3): 20.5, 20.56, 20.58, 20.7 ($4 \times \text{COCH}_3$), 28.0 ($\text{C}(\text{CH}_3)_3$), 36.6 ($\text{C}(\text{CH}_3)_3$), 50.0 ($\text{OCH}_2\text{CH}_2\text{N}$), 53.5 ($(\text{O}-\text{CH}_2)_3\text{-C}$), 59.6 ($\text{C}(\text{CN})_2$), 61.1 (C-6), 64.6 ($\text{OCH}_2\text{-triaz}$), 67.0 (C-4), 67.1 (OCH_2CO), 68.6 (C-2), 68.7 ($(\text{O}-\text{CH}_2)_3\text{-C}$), 69.0 (Gal- OCH_2), 69.3 ($\text{OCH}_2\text{CH}_2\text{N}$), 70.1 (C-5), 70.37 (OCH_2), 70.47 (OCH_2), 70.5 (OCH_2), 70.7 (C-3), 101.2 (C-1), 102.5 (C-3pyran), 107.0 (C-5pyran), 113.9 (CH-Ar), 114.1 (CH-Ar), 115.1 ($2 \times \text{CN}$), 118.0 ($\text{HC}=\text{CH-Ph}$), 123.7 (CH^{triaz}), 126.6 (CH-Ar), 127.3 (CH-Ar), 127.9 (CH-Ar), 131.2 (CH-Ar), 131.94 (CH-Ar), 131.98 (CH-Ar), 132.3 ($\text{C}^{\text{Ar}}\text{-CH}=\text{CH-Pyran}$), 132.6 (CH-Ar), 136.90 ($\text{C}^{\text{Ar}}\text{-C}=\text{C}$), 136.92 ($\text{C}^{\text{Ar}}\text{-C}=\text{C}$), 137.4 ($\text{HC}=\text{CH-Ph}$), 139.1 ($\text{C}^{\text{Ar}}\text{-C}=\text{C}$), 140.7 ($\text{C}^{\text{Ar}}\text{-C}=\text{C}$), 143.3 (C=C), 144.3 and 144.4 (C^{triaz}), 146.4 (C=C), 155.7 ($\text{C}^{\text{Ar}}\text{-O}$), 155.9 ($\text{C}^{\text{Ar}}\text{-O}$), 156.6 (C-6pyran), 158.9 (C-2pyran), 167.4 (NHCOCH_2) 169.3, 170.0, 170.1, 170.2 ($4 \times \text{COCH}_3$), 172.1 (C-4pyran).

HR-ESI-MS m/z : calcd. for $\text{C}_{190}\text{H}_{252}\text{N}_{22}\text{Na}_4\text{O}_{83}$ $[\text{M}+4\text{Na}]^{4+}$ 1065.3936, found 1065.3937.

(E)-2-{2-[4-(2,2-di-{N-[tris{1-[1-(2,3,4,6-tetra-*O*-acetyl- β -D-glucopyranosyloxy)-3,6-dioxaoct-8-yl]-1,2,3-triazol-4-yl-methoxy}methyl]-2-oxy-acetamido}phenyl-1-phenyl-1-vinyl)styryl]-6-(*tert*-butyl)-4*H*-pyran-4-ylidene}-propanedinitrile (V-16b)



Prepared according to the general procedure **H** from compound **V-15** (90 mg, 0.079 mmol, 1 eq.), **GlcEGN₃** (320 mg, 0.63 mmol, 8 eq.) [183], copper iodide (9 mg, 0.047 mmol, 0.6 eq.) and *N,N*-diisopropylethylamine (0.1 mL, 0.63 mmol, 8 eq.) affording compound **V-16b** (185 mg, 53%) as red amorphous solid.

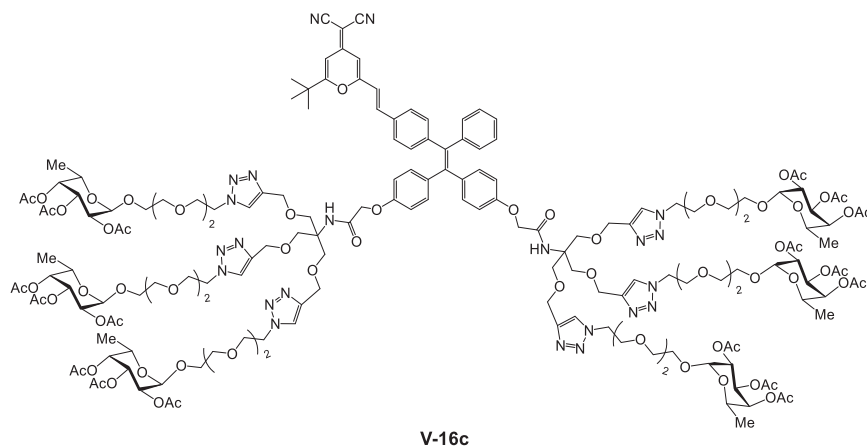
$R_f = 0.20$ ($\text{CH}_2\text{Cl}_2:\text{MeOH} = 25:1$)

¹H NMR (300 MHz, CDCl_3): 1.30 (s, 9H, $\text{C}(\text{CH}_3)_3$), 1.92, 1.94, 1.941, 2.00 (4s, $4 \times 18\text{H}$, CH_3CO), 3.51-3.57 (m, 36H, $\text{OCH}_2\text{CH}_2\text{O}$), 3.63-3.71 (m, 12H, H-5, Glc-OCH_2), 3.74 (s, 12H, $(\text{O-CH}_2)_3\text{-C}$), 3.79-3.90 (m, 18H, $\text{OCH}_2\text{CH}_2\text{N}$, Glc-OCH_2), 4.06 (dd, 6H, $J = 2.4$ Hz, 12.3 Hz, H-6'), 4.16-4.22 (m, 10H, H-6, OCH_2CO), 4.54 (t, 12H, $J = 5.4$ Hz, $\text{OCH}_2\text{CH}_2\text{N}$), 4.50-4.54 (m, 18H, H-1, $\text{OCH}_2\text{-triaz}$), 4.88-4.94 (m, 6H, H-2), 4.97-5.04 (m, 6H, H-4), 5.14 (t, 6H, $J = 9.3$ Hz, H-3), 6.47 (d, 2H, $J = 1.8$ Hz, H-3pyran), 6.54-6.69 (m, 6H, H-5pyran, $\text{HC}=\text{CH-Ph}$, $2 \times \text{H-Ar}$), 6.84-6.98 (m, 10H, $2 \times \text{NH}$, $8 \times \text{H-Ar}$), 7.04-7.06 (m, 3H, H-Ar), 7.23-7.28 (m, 3H, $2 \times \text{H-Ar}$, $\text{HC}=\text{CH-Ph}$), 7.63 (s, 6H, H-triaz).

¹³C NMR (75 MHz, CDCl_3): 20.55, 20.56, 20.6, 20.7 ($4 \times \text{COCH}_3$), 28.0 ($\text{C}(\text{CH}_3)_3$), 36.6 ($\text{C}(\text{CH}_3)_3$), 50.1 ($\text{OCH}_2\text{CH}_2\text{N}$), 53.5 ($(\text{O-CH}_2)_3\text{-C}$), 59.6 ($\text{C}(\text{CN})_2$), 61.9 (C-6), 64.7 ($\text{OCH}_2\text{-triaz}$), 67.1 (OCH_2CO), 68.3 (C-4), 68.6 ($(\text{O-CH}_2)_3\text{-C}$), 69.1 (Glc-OCH_2), 69.4 ($\text{OCH}_2\text{CH}_2\text{N}$), 70.1 (OCH_2), 70.4 (OCH_2), 70.5 (OCH_2), 71.2 (C-2), 71.7 (C-5), 72.7 (C-3), 100.7 (C-1), 102.5 (C-3pyran), 107.1 (C-5pyran), 114.0 (CH-Ar), 114.2 (CH-Ar), 115.1 ($2 \times \text{CN}$), 118.0 ($\text{HC}=\text{CH-Ph}$), 123.68 and 123.73 (CH^{triaz}), 126.6 (CH-Ar), 127.4 (CH-Ar), 127.9 (CH-Ar), 131.25 (CH-Ar), 131.29 (CH-Ar), 132.0 (CH-Ar), 132.3 ($\text{C}^{\text{Ar}}\text{-CH}=\text{CH-Pyran}$), 132.6 (CH-Ar), 136.94 ($\text{C}^{\text{Ar}}\text{-C}=\text{C}$), 136.96 ($\text{C}^{\text{Ar}}\text{-C}=\text{C}$), 137.4 ($\text{HC}=\text{CH-Ph}$), 139.1 ($\text{C}^{\text{Ar}}\text{-C}=\text{C}$), 140.7 ($\text{C}^{\text{Ar}}\text{-C}=\text{C}$), 143.4 (C=C), 144.3 and 144.4 (C^{triaz}), 146.5 (C=C), 155.8 ($\text{C}^{\text{Ar}}\text{-O}$), 155.9 ($\text{C}^{\text{Ar}}\text{-O}$), 156.6 (C-6pyran), 158.9 (C-2pyran), 167.4 (NHCOCH_2), 169.2, 169.3, 170.1, 170.5 ($4 \times \text{COCH}_3$), 172.2 (C-4pyran).

HR-ESI-MS m/z : calcd. for $\text{C}_{190}\text{H}_{256}\text{N}_{22}\text{O}_{83}$ [$\text{M}+4\text{H}$]⁴⁺ 1043.4116, found 1043.4168.

(E)-2-[2-[4-(2,2-di-{N-[tris{1-[1-(2,3,4-tri-*O*-acetyl- α -L-fucopyranosyloxy)-3,6-dioxaoct-8-yl]-1,2,3-triazol-4-yl-methoxy}methyl]-2-oxy-acetamido}phenyl-1-phenyl-1-vinyl)styryl]-6-(*tert*-butyl)-4*H*-pyran-4-ylidene}-propanedinitrile (V-16c)



Prepared according to the general procedure **H** from compound **V-15** (35 mg, 0.031 mmol, 1 eq.), **FucEGN₃** (97 mg, 0.215 mmol, 7 eq.) [183], copper iodide (4 mg, 0.019 mmol, 0.6 eq.) and *N,N*-diisopropylethylamine (0.036 mL, 0.215 mmol, 7 eq.) affording compound **V-16c** (185 mg, 53%) as red amorphous solid.

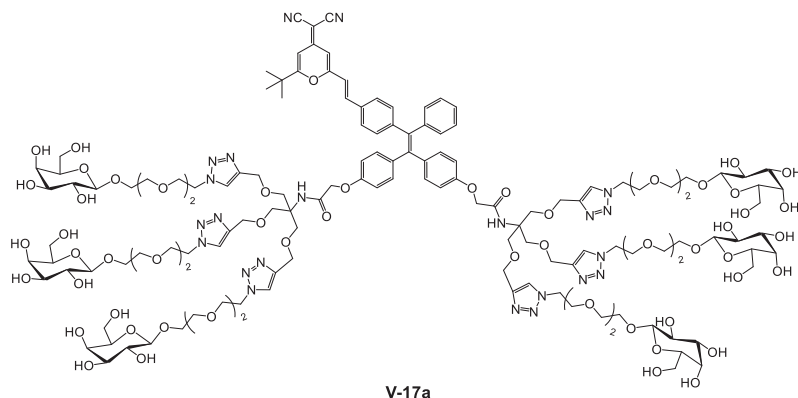
$R_f = 0.20$ ($\text{CH}_2\text{Cl}_2:\text{MeOH} = 30:1$)

$^1\text{H NMR}$ (300 MHz, CDCl_3): 1.04 (d, 18H, $J = 6.6$ Hz, H-6), 1.29 (s, 9H, $\text{C}(\text{CH}_3)_3$), 1.90, 1.97, 2.08 (3s, $3 \times 18\text{H}$, CH_3CO), 3.50-3.59 (m, 36H, $\text{OCH}_2\text{CH}_2\text{O}$, Fuc- OCH_2), 3.66-3.73 (m, 6H, Fuc- OCH_2), 3.74 (s, 12H, $(\text{O}-\text{CH}_2)_3\text{-C}$), 3.81 (d, 12H, $J = 5.1$ Hz, $\text{OCH}_2\text{CH}_2\text{N}$), 4.14 (q, 6H, $J = 6.6$ Hz, H-5), 4.21 (s, 4H, OCH_2CO), 4.45 (t, 12H, $J = 5.4$ Hz, $\text{OCH}_2\text{CH}_2\text{N}$), 4.51 (bs, 12H, $\text{OCH}_2\text{-triaz}$), 4.99-5.05 (m, 12H, H-1, H-2), 5.19-5.21 (m, 6H, H-4), 5.24-5.30 (m, 6H, H-3), 6.47 (d, 2H, $J = 2.1$ Hz, H-3pyran), 6.54-6.69 (m, 6H, H-5pyran, $\text{HC}=\text{CH}-\text{Ph}$, $2 \times \text{H-Ar}$), 6.84-6.98 (m, 10H, $2 \times \text{NH}$, $8 \times \text{H-Ar}$), 7.04-7.06 (m, 3H, H-Ar), 7.23-7.28 (m, 3H, $2 \times \text{H-Ar}$, $\text{HC}=\text{CH}-\text{Ph}$), 7.63 (s, 6H, H-triaz).

$^{13}\text{C NMR}$ (75 MHz, CDCl_3): 15.8 (C-6), 20.6, 20.63, 20.7 ($3 \times \text{COCH}_3$), 28.0 ($\text{C}(\text{CH}_3)_3$), 36.9 ($\text{C}(\text{CH}_3)_3$), 50.0 ($\text{OCH}_2\text{CH}_2\text{N}$), 53.5 ($(\text{O}-\text{CH}_2)_3\text{-C}$), 59.6 ($\text{C}(\text{CN})_2$), 64.2 (C-5), 64.61 and 64.67 ($\text{OCH}_2\text{-triaz}$), 67.1 (OCH_2CO), 67.3 (Fuc- OCH_2), 67.9 (C-3), 68.1 (C-2), 68.6 ($(\text{O}-\text{CH}_2)_3\text{-C}$), 69.4 ($\text{OCH}_2\text{CH}_2\text{N}$), 70.1 (OCH_2), 70.44 (OCH_2), 70.48 (OCH_2), 71.1 (C-4), 96.1 (C-1), 102.5 (C-3pyran), 107.0 (C-5pyran), 113.9 (CH-Ar), 114.1 (CH-Ar), 115.1 ($2 \times \text{CN}$), 118.0 ($\text{HC}=\text{CH}-\text{Ph}$), 123.62 and 123.66 (CH^{triaz}), 126.5 (CH-Ar), 127.3 (CH-Ar), 127.9 (CH-Ar), 131.3 (CH-Ar), 132.0 (CH-Ar), 132.3 ($\text{C}^{\text{Ar}}\text{-CH}=\text{CH}-\text{Pyran}$), 132.6 (CH-Ar), 132.61 (CH-Ar), 136.91 ($\text{C}^{\text{Ar}}\text{-C}=\text{C}$), 136.93 ($\text{C}^{\text{Ar}}\text{-C}=\text{C}$), 137.4 ($\text{HC}=\text{CH}-\text{Ph}$), 139.1 ($\text{C}^{\text{Ar}}\text{-C}=\text{C}$), 140.7 ($\text{C}^{\text{Ar}}\text{-C}=\text{C}$), 143.3 (C=C), 144.3 and 144.4 (C^{triaz}), 146.5 (C=C), 155.8 ($\text{C}^{\text{Ar}}\text{-O}$), 155.9 ($\text{C}^{\text{Ar}}\text{-O}$), 156.6 (C-6pyran), 158.9 (C-2pyran), 167.4 ($\text{NHC}=\text{OCH}_2$), 169.9, 170.3, 170.5 ($3 \times \text{COCH}_3$), 172.1 (C-4pyran).

HR-ESI-MS m/z : calcd. for $\text{C}_{178}\text{H}_{244}\text{N}_{22}\text{O}_{71}$ $[\text{M}+4\text{H}]^{4+}$ 956.4034, found 956.4035.

(E)-2-{2-[4-(2,2-di-{N-[tris{1-[1-(β-D-galacopyranosyloxy)-3,6-dioxaoct-8-yl]-1,2,3-triazol-4-yl-methoxy}methyl]-2-oxy-acetamido}phenyl-1-phenyl-1-vinyl)styryl]-6-(tert-butyl)-4H-pyran-4-ylidene}-propanedinitrile (V-17a)



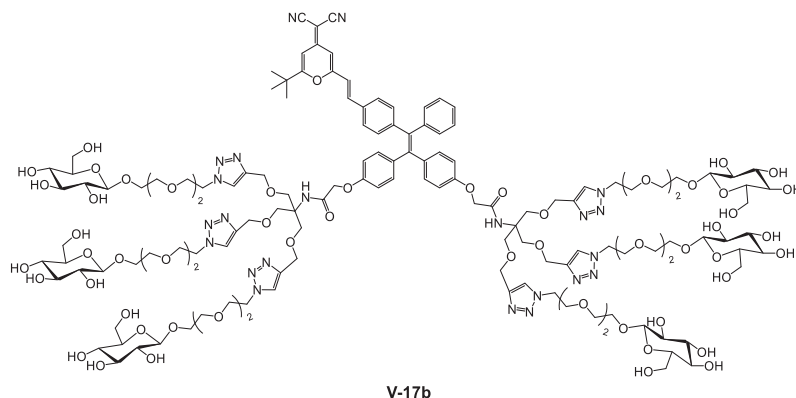
To a solution of compound **V-16a** (238 mg, 0.057 mmol, 1 eq.) in MeOH/H₂O (12 mL, 5:1, v/v) was added KOH powder (84 mg, 1.48 mmol, 26 eq.). The resulting mixture was stirred under argon at RT during 90 min. The solution was neutralized (pH = 7) with 0.6 M HCl aqueous solution and concentrated. The crude product was dissolved with H₂O (4 mL) and purified with C¹⁸ reverse phase column (H₂O/MeOH = 1:0 to 0:1) to afford compound **V-17a** (153 mg, 85%) as a red amorphous solid.

¹H NMR (300 MHz, D₂O/εCD₃OD): 1.48 (s, 9H, C(CH₃)₃), 3.66-3.77 (m, 54H, OCH₂, H-2, H-3, H-5), 3.82-3.92 (m, 30H, Gal-OCH₂, (O-CH₂)₃-C, H-6'), 4.00-4.14 (OCH₂CH₂N, H-4, H-6), 4.43 (dd, 6H, *J* = 2.7 Hz, 5.4 Hz, H-1), 4.51 (s, 4H, OCH₂CO), 4.67-4.72 (m, 24H, OCH₂CH₂N, OCH₂-triaz), 6.67 (d, 1H, *J* = 1.5 Hz, H-3pyran), 6.78-6.86 (m, 6H, H-5pyran, HC=CH-Ph, 2×H-Ar), 7.00-7.13 (m, 10H, 2×NH, 8×H-Ar), 7.23-7.24 (m, 3H, H-Ar), 7.47-7.53 (m, 3H, 2×H-Ar, HC=CH-Ph), 8.13, 8.16 (bs, 6H, H-triaz).

¹³C NMR (75 MHz, D₂O/εCD₃OD): 28.3 (C(CH₃)₃), 37.6 (C(CH₃)₃), 51.3 (OCH₂CH₂N), 58.0 (C(CN)₂), 60.9 ((O-CH₂)₃-C), 62.2 (Gal-OCH₂), 65.1 (OCH₂-triaz), 68.2 (OCH₂CO), 69.55 (OCH₂CH₂N), 69.56 (C-6), 70.0 ((O-CH₂)₃-C), 70.07 (C-4), 71.0 (OCH₂), 71.1 (OCH₂), 71.2 (OCH₂), 72.3 (C-2), 74.5 (C-5), 76.4 (C-3), 103.4 (C-3pyran), 104.6 (C-1), 108.0 (C-5pyran), 115.2 (CH-Ar), 115.4 (CH-Ar), 116.5 (2×CN), 119.4 (HC=CH-Ph), 126.2 (CH^{triaz}), 127.8 (CH-Ar), 128.6 (CH-Ar), 129.0 (CH-Ar), 131.2 (CH-Ar), 132.9 (CH-Ar), 133.52 (CH-Ar), 133.57 (CH-Ar), 133.9 (C^{Ar}-CH=CH-Pyran), 138.28 (C^{Ar}-C=C), 138.3 (C^{Ar}-C=C), 138.3 (HC=CH-Ph), 140.7 (C^{Ar}-C=C), 142.0 (C^{Ar}-C=C), 144.5 (C^{triaz}), 147.6 (C=C), 157.4 (C^{Ar}-O), 157.5 (C^{Ar}-O), 158.8 (C-6pyran), 161.4 (C-2pyran), 170.5 (NHCOCH₂), 174.7 (C-4pyran).

HR-ESI-MS *m/z*: calcd. for C₁₄₂H₂₀₇N₂₂O₅₉ [M+3H]³⁺ 1054.7952, found 1054.7901.

(E)-2-{2-[4-(2,2-di-{N-[tris{1-[1-(β-D-glucopyranosyloxy)-3,6-dioxaoct-8-yl]-1,2,3-triazol-4-yl-methoxy}methyl]-2-oxy-acetamido}phenyl-1-phenyl-1-vinyl)styryl]-6-(tert-butyl)-4H-pyran-4-ylidene}-propanedinitrile (V-17b)



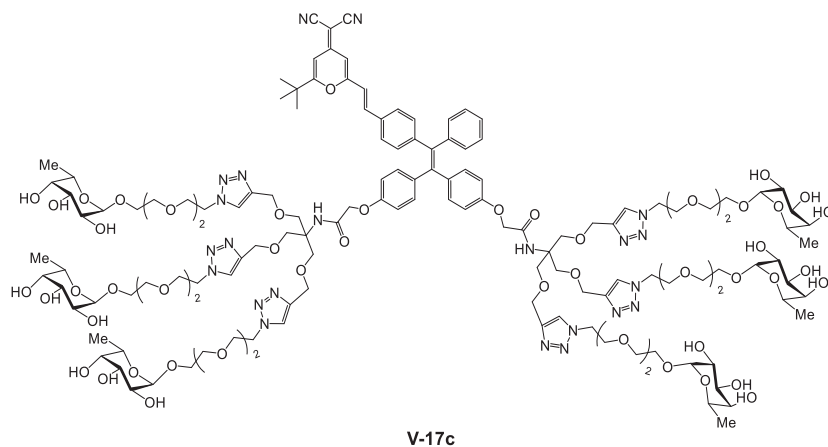
Prepared according to the general procedure **I** from compound **V-16b** (260 mg, 0.062 mmol, 1 eq.) MeOH (14 mL), H₂O (3 mL) and Et₃N (3 mL) affording the compound **V-17b** (170 mg, 87%) as a red amorphous solid.

¹H NMR (300 MHz, D₂O/εCD₃OD): 1.60 (s, 9H, C(CH₃)₃), 3.43-3.49 (m, 24H, H-2, H-3, H-4, H-5), 3.78-3.87 (m, 36H, OCH₂), 3.89-3.98 (m, 12H, Glc-OCH₂, H-6'), 4.00-4.06 (m, 12H, (O-CH₂)₃-C), 4.08-4.15 (m, 18H, H-6, OCH₂CH₂N), 4.17-4.23 (m, 6H, Glc-OCH₂), 4.57 (dd, 6H, *J* = 2.1 Hz, 6.0 Hz, H-1), 4.61 (s, 4H, OCH₂CO), 4.78-4.79 (m, 24H, OCH₂CH₂N, OCH₂-triaz), 6.79 (d, 1H, *J* = 1.5 Hz, H-3pyran), 6.90-6.99 (m, 6H, H-5pyran, HC=CH-Ph, 2×H-Ar), 7.12-7.26 (m, 10H, 2×NH, 8×H-Ar), 7.33-7.37 (m, 3H, H-Ar), 7.60-7.66 (m, 3H, 2×H-Ar, HC=CH-Ph), 8.21, 8.23 (bs, 6H, H-triaz).

¹³C NMR (75 MHz, D₂O/εCD₃OD): 28.5 (C(CH₃)₃), 37.9 (C(CH₃)₃), 51.6 (OCH₂CH₂N), 58.4 (C(CN)₂), 61.3 ((O-CH₂)₃-C), 62.8 (Gal-OCH₂), 65.4 (OCH₂-triaz), 68.2 (OCH₂CO), 69.8 (C-6), 69.9 ((O-CH₂)₃-C), 70.3 (OCH₂CH₂N), 71.3 (OCH₂), 71.36 (OCH₂), 71.4 (OCH₂), 71.6 (C-2), 75.0 (C-5), 77.85 (C-3), 77.89 (C-4), 103.6 (C-3pyran), 104.3 (C-1), 108.1 (C-5pyran), 115.5 (CH-Ar), 115.7 (CH-Ar), 116.7 (2×CN), 119.7 (HC=CH-Ph), 126.2 (CH^{triaz}), 127.9 (CH-Ar), 128.8 (CH-Ar), 129.2 (CH-Ar), 132.4 (CH-Ar), 133.1 (CH-Ar), 133.74 (CH-Ar), 133.79 (CH-Ar), 134.2 (C^{Ar}-CH=CH-Pyran), 138.56 (C^{Ar}-C=C), 138.62 (C^{Ar}-C=C), 139.1 (HC=CH-Ph), 141.0 (C^{Ar}-C=C), 142.2 (C^{Ar}-C=C), 144.8 (C^{triaz}), 147.8 (C=C), 157.7 (C^{Ar}-O), 157.8 (C^{Ar}-O), 158.9 (C-6pyran), 161.4 (C-2pyran), 170.6 (NHCOCH₂), 174.9 (C-4pyran).

HR-ESI-MS *m/z*: calcd. for C₁₄₂H₂₀₇N₂₂O₅₉ [M+3H]³⁺ 1054.7952, found 1054.7942.

(E)-2-{2-[4-(2,2-di-{N-[tris{1-[1-(α -L-fucopyranosyloxy)-3,6-dioxaoct-8-yl]-1,2,3-triazol-4-yl-methoxy}methyl]-2-oxy-acetamido}phenyl-1-phenyl-1-vinylstyryl]-6-(*tert*-butyl)-4H-pyran-4-ylidene]-propanedinitrile (V-17c)



Prepared according to the general procedure **I** from compound **V-16c** (101 mg, 0.026 mmol, 1 eq.) MeOH (8 mL), H₂O (2 mL) and Et₃N (2 mL) affording the compound **V-17c** (52 mg, 66%) as a red amorphous solid.

¹H NMR (300 MHz, D₂O/ ϵ CD₃OD): 1.40 (d, 9H, J = 1.8 Hz, C-6), 1.42 (d, 9H, J = 1.8 Hz, C-6), 1.61 (s, 9H, C(CH₃)₃), 3.79-3.87 (m, 44H, Fuc-OCH₂, OCH₂), 3.92-3.93 (m, 6H, C-4), 3.95-4.03 (m, 30H, C-2, C-3, Fuc-OCH₂, (O-CH₂)₃-C), 4.13 (m, 12H, OCH₂CH₂N), 4.18-4.24 (m, 6H, H-5), , 4.61 (s, 4H, OCH₂CO), 4.78-4.79 (m, 24H, OCH₂CH₂N, OCH₂-triaz), 5.04 (t, 6H, J = 2.4 Hz, H-1), 6.78 (d, 1H, J = 1.5 Hz, H-3pyran), 6.90-7.00 (m, 6H, H-5pyran, HC=CH-Ph, 2×H-Ar), 7.13-7.26 (m, 10H, 2×NH, 8×H-Ar), 7.32-7.35 (m, 3H, H-Ar), 7.60-7.66 (m, 3H, 2×H-Ar, HC=CH-Ph), 8.20, 8.22 (bs, 6H, H-triaz).

¹³C NMR (75 MHz, D₂O/ ϵ CD₃OD): 16.7 (C-6), 28.3 (C(CH₃)₃), 37.7 (C(CH₃)₃), 51.4 (OCH₂CH₂N), 58.4 (C(CN)₂), 61.1 ((O-CH₂)₃-C), 65.2 (OCH₂-triaz), 67.6 (C-5), 68.2 (Fuc-OCH₂), 68.4 (OCH₂CO), 68.4 ((O-CH₂)₃-C), 69.9 (C-2), 70.2 (OCH₂CH₂N), 71.17 (OCH₂), 71.19 (OCH₂), 71.2 (OCH₂), 71.5 (C-3), 73.4 (C-4), 100.4 (C-1), 103.4 (C-3pyran), 108.0 (C-5pyran), 115.32 (CH-Ar), 115.5 (CH-Ar), 116.4 (2×CN), 119.4 (HC=CH-Ph), 125.9 (CH^{triaz}), 127.7 (CH-Ar), 128.7 (CH-Ar), 129.0 (CH-Ar), 132.2 (CH-Ar), 133.0 (CH-Ar), 133.56 (CH-Ar), 133.62 (CH-Ar), 134.1 (C^{Ar}-CH=CH-Pyran), 138.36 (C^{Ar}-C=C), 138.42 (C^{Ar}-C=C), 138.9 (HC=CH-Ph), 141.8 (C^{Ar}-C=C), 142.1 (C^{Ar}-C=C), 144.6 (C=C), 145.5 (C^{triaz}), 147.6 (C=C), 157.5 (C^{Ar}-O), 157.7 (C^{Ar}-O), 158.7 (C-6pyran), 161.2 (C-2pyran), 170.4 (NHCOCH₂), 174.7 (C-4pyran).

HR-ESI-MS m/z : calcd. for C₁₄₂H₂₀₇N₂₂O₅₃ [M+3H]³⁺ 1022.8054, found 1022.8077.

VI.3 Fluorescence measurements

VI.3.1 Supramolecular glyco-dots with DCM probe and TPE-glycocluster for ONOO⁻ detection

Supramolecular self-assembly of glyco-dots. DCM probe (1 mM, DMSO) was added to a solution

of TPE-based glycoclusters (15 mM, PBS buffer). The resulting mixture was stirred during 30 min to produce the supramolecular glyco-probes for subsequent experiments.

General. DCM probe (1 mM, DMSO, 10 μ L) or glyco-dots (10 μ L) was added in 1 mL PBS buffer or mixed with MeCN to prepare the probe solution and measured the fluorescence. Then the prefabricated ONOO⁻ solution was adding in the solution and stirred 30s before measuring the fluorescence intensity.

Preparation of ROS/RNS

H₂O₂ : The purchased hydrogen peroxide was diluted in deionizer water to afford the solution. The concentration of H₂O₂ was determined from the absorption at 240 nm ($\epsilon = 43.6 \text{ M}^{-1}\text{cm}^{-1}$).

ClO⁻ : The purchased sodium hypochlorite was dissolved in NaOH solution(0.1 mol L⁻¹). The concentration of ClO⁻ was determined from the absorption at 292 nm ($\epsilon = 350 \text{ M}^{-1}\text{cm}^{-1}$).

ROO[•] : ROO[•] was generated from 2,2'-azobis-(2-amidinopropane) dihydrochloride. AAPH (2,2'-azobis-(2-amidinopropane) dihydrochloride, 1 M) was added into deionized water, and then stirred at 37 °C for 30 min.

•OH : Hydroxyl radical was generated by the Fenton reaction. To prepare •OH solution, hydrogen peroxide (H₂O₂, 10 eq.) was added to Fe(ClO₄)₂ in deionized water.

O₂⁻ : Superoxide was generated from KO₂. KO₂ and 18-crown-6 ether (2.5 eq.) was dissolved in DMSO to afford a 0.25 M solution.

NO : Nitric oxide (NO) was prepared by treating sulfuric acid (3.6 M) solution with sodium nitrite solution (7.3 M) and its stock solution (2 mM) was prepared by bubbling NO into deoxygenated deionized water for 30 min.

NO₂⁻ : The purchased sodium nitrite was dissolved in deionizer water to afford the solution.

HNO: The purchased Angeli's salt was dissolved in PBS buffer (0.05 M, PBS, pH 7.4) to afford the solution. Angeli's salt can readily decompose at physiological pH to yield nitroxyl anion (HNO) and nitric oxide (NO).

ONOO⁻ : Simultaneously, 0.6 M KNO₂, 0.6 M in HCl, 0.7 M in H₂O₂ was added to a 3 M NaOH solution at 0 °C. The concentration of peroxyxynitrite was estimated by using extinction coefficient of 1670 cm⁻¹M⁻¹ at 302 nm in 0.1 M sodium hydroxide aqueous solution.

Fluorescence imaging of cells. Cells were seeded on a black 96-well microplate with optically clear bottom (Greiner bio-one, Germany) overnight. Then, the cells were incubated with **glyco-dots** in the absence and presence of SIN-1 for 30 min. Then, the cells were gently washed with PBS (phosphate buffered saline) three times, and stained with Hoechst 33342 (5 μ g/mL) at 37 °C in a humidified atmosphere of 5% CO₂ in air for 5 min. Then, cells were washed with PBS three times. The fluorescence images were recorded using an Operetta high content imaging system and quantified by the Columbus image data analysis system (Perkinelmer, US).

VI.3.2 Supramolecular glyco-dot with TPE-DCM probe and TPE2S for thiophenol detection

Supramolecular self-assembly of glyco-dots. TPE-DCM probe (1 mM, DMSO) was added to a solution of TPE-based glycoclusters (**TPE2S**, 10 mM, PBS buffer). The resulting mixture was stirred during 30 min to produce the supramolecular glyco-dots for subsequent experiments.

General. TPE-DCM probe (1 mM, DMSO, 10 μ L) or glyco-dots (10 μ L) was added in 1 mL PBS buffer with different ratio of THF, to prepare the probe solution and measured the fluorescence. Then the prepared thiophenol (in EtOH) was adding in the solution and stirred 5 min before measuring the fluorescence intensity.

VI.3.3 TPE-DCM-based glycocluster for glycosidase detection

General. TPE-DCM glycoclusters (1 mM, PBS buffer, 10 μ L) was added in 1 mL PBS buffer to prepare the probe solution and measured the fluorescence. Then the glycosidase solution was added in the solution and incubated during 50 min before measuring the fluorescence intensity.

Fluorescence imaging of cells. Cells were seeded on a black 96-well microplate with optically clear bottom (Greiner bio-one, Germany) overnight. Then, the cells were incubated with **TPE-DCM glycoclusters** for 30 min. Then, the cells were gently washed with PBS (phosphate buffered saline) three times, and stained with Hoechst 33342 (5 μ g/mL) at 37 °C in a humidified atmosphere of 5% CO₂ in air for 5 min. Then, cells were washed with PBS three times. The fluorescence images were recorded using the Laser Scanning Confocal Microscopy.

Reference

VII. Reference

- [1] F. Ibrahim, A.K. El-Deen, S.A. El Abass, and K. Shimizu. An ecofriendly green liquid chromatographic method for simultaneous determination of nicotinamide and clindamycin phosphate in pharmaceutical gel for acne treatment. *J Food Drug Anal*, **2017**, *25*: 741-747.
- [2] A.J. Signes-Pastor, *et al.* Urinary Arsenic Speciation in Children and Pregnant Women from Spain. *Expo Health*, **2017**, *9*: 105-111.
- [3] M. Iammarino, A. Di Taranto, and A.R. Ientile. Monitoring of sulphites levels in shrimps samples collected in Puglia (Italy) by ion-exchange chromatography with conductivity detection. *Food Addit Contam Part B Surveill*, **2014**, *7*: 84-89.
- [4] R. Sowmya, *et al.* Detection of calcium based neutralizers in milk and milk products by AAS. *J Food Sci Technol*, **2015**, *52*: 1188-1193.
- [5] M.Z. Mo, *et al.* Laser wakefield generated X-ray probe for femtosecond time-resolved measurements of ionization states of warm dense aluminum. *Rev Sci Instrum*, **2013**, *84*: 123106.
- [6] Y. Long, W. Zhang, F. Wang, and Z. Chen. Simultaneous determination of three curcuminoids in *Curcuma longa* L. by high performance liquid chromatography coupled with electrochemical detection. *J Pharm Anal*, **2014**, *4*: 325-330.
- [7] R. Karami-Osboo, *et al.* A validated dispersive liquid-liquid microextraction method for extraction of ochratoxin A from raisin samples. *J Food Sci Technol*, **2015**, *52*: 2440-2445.
- [8] B.A. Kairdolf, X. Qian, and S. Nie. Bioconjugated Nanoparticles for Biosensing, in Vivo Imaging, and Medical Diagnostics. *Anal Chem*, **2017**, *89*: 1015-1031.
- [9] X. Yang, *et al.* Novel and remarkable enhanced-fluorescence system based on gold nanoclusters for detection of tetracycline. *Talanta*, **2014**, *122*: 36-42.
- [10] C.A. Smurthwaite, *et al.* Fluorescent genetic barcoding in mammalian cells for enhanced multiplexing capabilities in flow cytometry. *Cytometry A*, **2014**, *85*: 105-113.
- [11] H.D. MacGillavry and T.A. Blanpied. Single-Molecule Tracking Photoactivated Localization Microscopy to Map Nano-Scale Structure and Dynamics in Living Spines. *Curr Protoc Neurosci*, **2013**, *65*: 2 20 21-19.
- [12] M. Esaki, *et al.* Safety and efficacy of a turkey herpesvirus vector laryngotracheitis vaccine for chickens. *Avian Dis*, **2013**, *57*: 192-198.
- [13] G. Grynkiewicz, M. Poenie, and R.Y. Tsien. A New Generation of Ca-2+ Indicators with Greatly Improved Fluorescence Properties. *J Biol Chem*, **1985**, *260*: 3440-3450.
- [14] J. Zhang, *et al.* Fluorogenic probes for disease-relevant enzymes. *Chem Soc Rev*, **2019**, *48*: 683-722.
- [15] Z. Gu, *et al.* Detection of Mercury Ion by Infrared Fluorescent Protein and Its Hydrogel-Based Paper Assay. *Analytical Chemistry*, **2011**, *83*: 2324-2329.
- [16] L. Xue, *et al.* Rational Design of a Ratiometric and Targetable Fluorescent Probe for Imaging Lysosomal Zinc Ions. *Inorg Chem*, **2012**, *51*: 10842-10849.
- [17] M. Sun, *et al.* Palladacycle Based Fluorescence Turn-On Probe for Sensitive Detection of Carbon Monoxide. *ACS Sens*, **2018**, *3*: 285-289.
- [18] X. Gu, C. Liu, Y.C. Zhu, and Y.Z. Zhu. A boron-dipyrromethene-based fluorescent probe for colorimetric and ratiometric detection of sulfite. *J Agric Food Chem*, **2011**, *59*: 11935-11939.
- [19] T. Hirata, *et al.* Protein-Coupled Fluorescent Probe To Visualize Potassium Ion Transition on Cellular Membranes. *Anal Chem*, **2016**, *88*: 2693-2700.
- [20] X. Sun, *et al.* A water-soluble boronate-based fluorescent probe for the selective detection of peroxynitrite and imaging in living cells. *Chemical Science*, **2014**, *5*: 3368.
- [21] J. Kim, *et al.* A boronate-based fluorescent probe for the selective detection of cellular peroxynitrite. *Chem Commun*

- (*Camb*), **2014**, *50*: 9353-9356.
- [22] G. Castro-Falcon, D. Hahn, D. Reimer, and C.C. Hughes. Thiol Probes To Detect Electrophilic Natural Products Based on Their Mechanism of Action. *ACS Chem Biol*, **2016**, *11*: 2328-2336.
- [23] L.D. Lavis and R.T. Raines. Bright building blocks for chemical biology. *ACS Chem Biol*, **2014**, *9*: 855-866.
- [24] B. Valeur and I. Leray. Design principles of fluorescent molecular sensors for cation recognition. *Coordin Chem Rev*, **2000**, *205*: 3-40.
- [25] L. Xue, *et al.* Rational design of a ratiometric and targetable fluorescent probe for imaging lysosomal zinc ions. *Inorg Chem*, **2012**, *51*: 10842-10849.
- [26] Z.C. Xu, *et al.* Zn²⁺-Triggered Amide Tautomerization Produces a Highly Zn²⁺-Selective, Cell-Permeable, and Ratiometric Fluorescent Sensor. *Journal of the American Chemical Society*, **2010**, *132*: 601-610.
- [27] S. Sun, *et al.* Naphthylamine-rhodamine-based ratiometric fluorescent probe for the determination of Pd²⁺ ions. *Org Lett*, **2014**, *16*: 1132-1135.
- [28] D. Wang, *et al.* Computational design of two-photon fluorescent probes for intracellular free zinc ions. *J Phys Chem B*, **2014**, *118*: 10101-10110.
- [29] A.J. Huxley, M. Schroeder, H.Q. Gunaratne, and A.P. de Silva. Modification of fluorescent photoinduced electron transfer (PET) sensors/switches to produce molecular photo-ionic triode action. *Angew Chem Int Ed Engl*, **2014**, *53*: 3622-3625.
- [30] Z.R. Grabowski, K. Rotkiewicz, and W. Rettig. Structural changes accompanying intramolecular electron transfer: Focus on twisted intramolecular charge-transfer states and structures. *Chemical Reviews*, **2003**, *103*: 3899-4031.
- [31] Q. Ma, *et al.* A novel acidic pH fluorescent probe based on a benzothiazole derivative. *Spectrochim Acta A Mol Biomol Spectrosc*, **2017**, *177*: 6-13.
- [32] F. Li, *et al.* A fluorescent "on-off-on" probe for sensitive detection of ATP based on ATP displacing DNA from nanoceria. *Talanta*, **2018**, *179*: 285-291.
- [33] H. Kaur, *et al.* Highly selective and sensitive fluorescence sensing of nanomolar Zn(2+) ions in aqueous medium using Calix[4]arene passivated Carbon Quantum Dots based on fluorescence enhancement: Real-time monitoring and intracellular investigation. *Anal Chim Acta*, **2018**, *1009*: 1-11.
- [34] K. Vongnam, *et al.* A highly selective turn-on fluorescent sensor for glucosamine from amidoquinoline-naphthalimide dyads. *Biosens Bioelectron*, **2016**, *86*: 472-476.
- [35] Y. Mei, *et al.* Fluorescence quenching based alkaline phosphatase activity detection. *Talanta*, **2018**, *176*: 52-58.
- [36] H. Zhu, *et al.* An "enhanced PET"-based fluorescent probe with ultrasensitivity for imaging basal and elesclomol-induced HClO in cancer cells. *J Am Chem Soc*, **2014**, *136*: 12820-12823.
- [37] S. Guo, *et al.* Highly Selective Red-Emitting Fluorescent Probe for Imaging Cancer Cells in Situ by Targeting Pim-1 Kinase. *ACS Appl Mater Interfaces*, **2018**, *10*: 1499-1507.
- [38] T.W. Shiue, *et al.* Nitric oxide turn-on fluorescent probe based on deamination of aromatic primary monoamines. *Inorg Chem*, **2012**, *51*: 5400-5408.
- [39] L. Yuan, W. Lin, K. Zheng, and S. Zhu. FRET-based small-molecule fluorescent probes: rational design and bioimaging applications. *Acc Chem Res*, **2013**, *46*: 1462-1473.
- [40] K.E. Sapsford, L. Berti, and I.L. Medintz. Materials for fluorescence resonance energy transfer analysis: beyond traditional donor-acceptor combinations. *Angew Chem Int Ed Engl*, **2006**, *45*: 4562-4589.
- [41] I.L. Medintz and H. Mattoussi. Quantum dot-based resonance energy transfer and its growing application in biology. *Phys Chem Chem Phys*, **2009**, *11*: 17-45.
- [42] H. Zhang, *et al.* A FRET-based ratiometric fluorescent probe for nitroxyl detection in living cells. *ACS Appl Mater Interfaces*, **2015**, *7*: 5438-5443.
- [43] A.M. Dennis, *et al.* Quantum Dot-Fluorescent Protein FRET Probes for Sensing Intracellular pH. *Acs Nano*, **2012**, *6*:

- 2917-2924.
- [44] B. Gao, *et al.* A selective “turn-on” fluorescent sensor for Hg²⁺ based on “reactive” 7-hydroxycoumarin compound. *Sensors and Actuators B: Chemical*, **2012**, *162*: 391-395.
- [45] B.D. Wagner. The Use of Coumarins as Environmentally-Sensitive Fluorescent Probes of Heterogeneous Inclusion Systems. *Molecules*, **2009**, *14*: 210-237.
- [46] S. Bouasla, *et al.* Coumarin Derivatives Solvent-Free Synthesis under Microwave Irradiation over Heterogeneous Solid Catalysts. *Molecules*, **2017**, *22*.
- [47] A. Loudet, *et al.* B,O-Chelated Azadipyromethenes as Near-IR Probes. *Organic Letters*, **2008**, *10*: 4771-4774.
- [48] W. Zhao and E.M. Carreira. Conformationally restricted aza-bodipy: a highly fluorescent, stable, near-infrared-absorbing dye. *Angewandte Chemie*, **2005**, *117*: 1705-1707.
- [49] J.O. Flores-Rizo, *et al.* 8-Alkoxy-and 8-aryloxy-BODIPYs: straightforward fluorescent tagging of alcohols and phenols. *The Journal of organic chemistry*, **2013**, *78*: 5867-5877.
- [50] J.C. Carlson, L.G. Meimetis, S.A. Hilderbrand, and R. Weissleder. BODIPY–tetrazine derivatives as superbright bioorthogonal turn-on probes. *Angewandte Chemie International Edition*, **2013**, *52*: 6917-6920.
- [51] A. Baeyer. Ueber eine neue Klasse von Farbstoffen. *Berichte der deutschen chemischen Gesellschaft*, **1871**, *4*: 555-558.
- [52] M. Ceresole. Verfahren zur Darstellung von Farbstoffen aus der Gruppe des Meta-amidophenolphthaleins. *DR patent*, **1887**.
- [53] Y. Urano, *et al.* Evolution of fluorescein as a platform for finely tunable fluorescence probes. *Journal of the American Chemical Society*, **2005**, *127*: 4888-4894.
- [54] H. Wang, G. Zhou, H. Gai, and X. Chen. A fluorescein-based probe with high selectivity to cysteine over homocysteine and glutathione. *Chemical Communications*, **2012**, *48*: 8341-8343.
- [55] R. Wang, C. Yu, F. Yu, and L. Chen. Molecular fluorescent probes for monitoring pH changes in living cells. *TrAC Trends in Analytical Chemistry*, **2010**, *29*: 1004-1013.
- [56] L.D. Lavis, T.-Y. Chao, and R.T. Raines. Fluorogenic label for biomolecular imaging. *ACS chemical biology*, **2006**, *1*: 252-260.
- [57] K.B. Li, *et al.* Hepatoma-selective imaging of heavy metal ions using a 'clicked' galactosylrhodamine probe. *Chem Commun (Camb)*, **2014**, *50*: 11735-11737.
- [58] K.B. Li, *et al.* Revisit of a dipropargyl rhodamine probe reveals its alternative ion sensitivity in both a solution and live cells. *Analyst*, **2013**, *138*: 7087-7089.
- [59] K.B. Li, *et al.* One-step click engineering considerably ameliorates the practicality of an unqualified rhodamine probe. *ACS Appl Mater Interfaces*, **2014**, *6*: 19600-19605.
- [60] P. Jin, *et al.* A NIR luminescent copolymer based on platinum porphyrin as high permeable dissolved oxygen sensor for microbioreactors. *AIChE Journal*, **2013**, *59*: 2743-2752.
- [61] Y. Yang, Q. Zhao, W. Feng, and F. Li. Luminescent chemodosimeters for bioimaging. *Chemical reviews*, **2012**, *113*: 192-270.
- [62] X. Wu, *et al.* Constructing NIR silica–cyanine hybrid nanocomposite for bioimaging in vivo: a breakthrough in photostability and bright fluorescence with large Stokes shift. *Chemical Science*, **2013**, *4*: 1221-1228.
- [63] C. Tang, S. VanSlyke, and C. Chen. Electroluminescence of doped organic thin films. *Journal of Applied Physics*, **1989**, *65*: 3610-3616.
- [64] Z. Guo, W. Zhu, and H. Tian. Dicyanomethylene-4H-pyran chromophores for OLED emitters, logic gates and optical chemosensors. *Chemical Communications*, **2012**, *48*: 6073-6084.
- [65] X. Huang, *et al.* A colorimetric and fluorescent turn-on sensor for pyrophosphate anion based on a dicyanomethylene-4 H-chromene framework. *Chemical Communications*, **2008**: 5143-5145.

- [66] Z. Guo, W. Zhu, and H. Tian. Hydrophilic copolymer bearing dicyanomethylene-4 H-pyran moiety as fluorescent film sensor for Cu²⁺ and pyrophosphate anion. *Macromolecules*, **2009**, *43*: 739-744.
- [67] W. Chen, *et al.* Recent advances in electrochemical sensing for hydrogen peroxide: a review. *Analyst*, **2012**, *137*: 49-58.
- [68] C. Behl, J. Davis, R. Lesley, and D. Schubert. Hydrogen peroxide mediates amyloid β protein toxicity. *Cell*, **1994**, *77*: 817-827.
- [69] K.J. Barnham, C.L. Masters, and A.I. Bush. Neurodegenerative diseases and oxidative stress. *Nature reviews Drug discovery*, **2004**, *3*: 205.
- [70] H. Li, *et al.* A two-photon NIR-to-NIR fluorescent probe for imaging hydrogen peroxide in living cells. *Biosens Bioelectron*, **2017**, *94*: 536-543.
- [71] M. Li, *et al.* A near-infrared colorimetric fluorescent chemodosimeter for the detection of glutathione in living cells. *Chemical Communications*, **2014**, *50*: 1751-1753.
- [72] X. Wu, *et al.* In vivo and in situ tracking cancer chemotherapy by highly photostable NIR fluorescent theranostic prodrug. *J Am Chem Soc*, **2014**, *136*: 3579-3588.
- [73] S. Banerjee, S. Kar, J.M. Perez, and S. Santra. Quantum dot-based OFF/ON probe for detection of glutathione. *The Journal of Physical Chemistry C*, **2009**, *113*: 9659-9663.
- [74] D. Xie, *et al.* Targeted fluorescence imaging enhanced by 2D materials: a comparison between 2D MoS₂ and graphene oxide. *Chemical Communications*, **2016**, *52*: 9418-9421.
- [75] D.-K. Ji, *et al.* Receptor-targeting fluorescence imaging and theranostics using a graphene oxide based supramolecular glycoconjugate. *Journal of Materials Chemistry B*, **2015**, *3*: 9182-9185.
- [76] D.K. Ji, *et al.* Targeted Intracellular Production of Reactive Oxygen Species by a 2D Molybdenum Disulfide Glycosheet. *Adv Mater*, **2016**, *28*: 9356-9363.
- [77] Z. Guo, A. Shao, and W.-H. Zhu. Long wavelength AIEgen of quinoline-malononitrile. *Journal of Materials Chemistry C*, **2016**, *4*: 2640-2646.
- [78] A. Shao, *et al.* Insight into aggregation-induced emission characteristics of red-emissive quinoline-malononitrile by cell tracking and real-time trypsin detection. *Chemical Science*, **2014**, *5*: 1383.
- [79] G. Qian, *et al.* Simple and Efficient Near-Infrared Organic Chromophores for Light-Emitting Diodes with Single Electroluminescent Emission above 1000 nm. *Advanced Materials*, **2009**, *21*: 111-116.
- [80] S.W. Thomas, G.D. Joly, and T.M. Swager. Chemical sensors based on amplifying fluorescent conjugated polymers. *Chemical reviews*, **2007**, *107*: 1339-1386.
- [81] R. Hu, N.L. Leung, and B.Z. Tang. AIE macromolecules: syntheses, structures and functionalities. *Chem Soc Rev*, **2014**, *43*: 4494-4562.
- [82] J. Luo, *et al.* Aggregation-induced emission of 1-methyl-1, 2, 3, 4, 5-pentaphenylsilole. *Chemical communications*, **2001**: 1740-1741.
- [83] J. Mei, *et al.* Aggregation-induced emission: the whole is more brilliant than the parts. *Advanced materials*, **2014**, *26*: 5429-5479.
- [84] J. Mei, *et al.* Aggregation-Induced Emission: Together We Shine, United We Soar! *Chem Rev*, **2015**, *115*: 11718-11940.
- [85] J. Chen, *et al.* Synthesis, light emission, nanoaggregation, and restricted intramolecular rotation of 1, 1-substituted 2, 3, 4, 5-tetraphenylsiloles. *Chemistry of materials*, **2003**, *15*: 1535-1546.
- [86] B. ZhongáTang. Photoluminescence and electroluminescence of hexaphenylsilole are enhanced by pressurization in the solid state. *Chemical Communications*, **2008**: 2989-2991.
- [87] Y. Ren, *et al.* Enhanced emission efficiency and excited state lifetime due to restricted intramolecular motion in silole aggregates. *The Journal of Physical Chemistry B*, **2005**, *109*: 1135-1140.

- [88] B. Chen, *et al.* Conjugation versus rotation: good conjugation weakens the aggregation-induced emission effect of siloles. *Chemical Communications*, **2014**, 50: 4500-4503.
- [89] E. Zhao, *et al.* How do substituents affect silole emission? *Journal of materials chemistry C*, **2013**, 1: 5661-5668.
- [90] H. Lee, *et al.* Dual Role of a Fluorescent Peptidyl Probe Based on Self-Assembly for the Detection of Heparin and for the Inhibition of the Heparin-Digestive Enzyme Reaction. *ACS Appl Mater Interfaces*, **2018**, 10: 2282-2290.
- [91] J. Li, *et al.* Aggregation-Induced Fluorescence Probe for Monitoring Membrane Potential Changes in Mitochondria. *ACS Appl Mater Interfaces*, **2018**, 10: 12150-12154.
- [92] J. Luo, K. Song, F. long Gu, and Q. Miao. Switching of non-helical overcrowded tetrabenzoheptafulvalene derivatives. *Chemical Science*, **2011**, 2: 2029-2034.
- [93] N.L. Leung, *et al.* Restriction of Intramolecular Motions: The General Mechanism behind Aggregation-Induced Emission. *Chemistry—A European Journal*, **2014**, 20: 15349-15353.
- [94] L. Yao, *et al.* Highly Efficient Near-Infrared Organic Light-Emitting Diode Based on a Butterfly-Shaped Donor–Acceptor Chromophore with Strong Solid-State Fluorescence and a Large Proportion of Radiative Excitons. *Angewandte Chemie International Edition*, **2014**, 53: 2119-2123.
- [95] Y. Dong, *et al.* Aggregation-induced emissions of tetraphenylethene derivatives and their utilities as chemical vapor sensors and in organic light-emitting diodes. *Applied physics letters*, **2007**, 91: 011111.
- [96] Z. Zhao, J. WY Lam, and B. Zhong Tang. Aggregation-induced emission of tetraarylethene luminogens. *Current Organic Chemistry*, **2010**, 14: 2109-2132.
- [97] Y. Hong, J.W. Lam, and B.Z. Tang. Aggregation-induced emission. *Chemical Society Reviews*, **2011**, 40: 5361-5388.
- [98] R.T. Kwok, C.W. Leung, J.W. Lam, and B.Z. Tang. Biosensing by luminogens with aggregation-induced emission characteristics. *Chemical Society Reviews*, **2015**, 44: 4228-4238.
- [99] D. Ding, K. Li, B. Liu, and B.Z. Tang. Bioprobes based on AIE fluorogens. *Accounts of chemical research*, **2013**, 46: 2441-2453.
- [100] N. Stühr-Hansen. Utilization of microwave heating in the McMurry reaction for facile coupling of aldehydes and ketones to give alkenes. *Tetrahedron letters*, **2005**, 46: 5491-5494.
- [101] J.E. McMurry, M.P. Fleming, K.L. Kees, and L.R. Krepski. Titanium-induced reductive coupling of carbonyls to olefins. *The Journal of Organic Chemistry*, **1978**, 43: 3255-3266.
- [102] H.-T. Feng, *et al.* Multicolor Emissions by the Synergism of Intra/Intermolecular Slipped π - π Stacks of Tetraphenylethylene-DiBODIPY Conjugate. *Chemistry of Materials*, **2015**, 27: 7812-7819.
- [103] S. Song, *et al.* Monomer emission and aggregate emission of TPE derivatives in the presence of gamma-cyclodextrin. *Org Lett*, **2014**, 16: 2170-2173.
- [104] M. Fang, *et al.* A cyanine-based fluorescent cassette with aggregation-induced emission for sensitive detection of pH changes in live cells. *Chemical Communications*, **2018**, 54: 1133-1136.
- [105] W. Qin, *et al.* Biocompatible Nanoparticles with Aggregation-Induced Emission Characteristics as Far-Red/Near-Infrared Fluorescent Bioprobes for In Vitro and In Vivo Imaging Applications. *Advanced Functional Materials*, **2012**, 22: 771-779.
- [106] G.P. Dimri, *et al.* A biomarker that identifies senescent human cells in culture and in aging skin in vivo. *Proceedings of the National Academy of Sciences*, **1995**, 92: 9363-9367.
- [107] S.K. Chatterjee, M. Bhattacharya, and J.J. Barlow. Glycosyltransferase and glycosidase activities in ovarian cancer patients. *Cancer research*, **1979**, 39: 1943-1951.
- [108] K. Gu, *et al.* An enzyme-activatable probe liberating AIEgens: on-site sensing and long-term tracking of beta-galactosidase in ovarian cancer cells. *Chem Sci*, **2019**, 10: 398-405.
- [109] C.R. Bertozzi and L.L. Kiessling. Chemical glycobiology. *Science*, **2001**, 291: 2357-2364.
- [110] A. Bernardi, *et al.* Multivalent glycoconjugates as anti-pathogenic agents. *Chemical Society reviews*, **2013**, 42: 4709-

4727.

- [111] R.A. Dwek. Glycobiology: toward understanding the function of sugars. *Chemical reviews*, **1996**, *96*: 683-720.
- [112] J. Axford. Glycobiology and medicine: an introduction. *Journal of the Royal Society of Medicine*, **1997**, *90*: 260-264.
- [113] P.K. Grewal, *The Ashwell–Morell receptor*, in *Methods in enzymology*. 2010, Elsevier. p. 223-241.
- [114] K. Bridges, J. Harford, G. Ashwell, and R.D. Klausner. Fate of receptor and ligand during endocytosis of asialoglycoproteins by isolated hepatocytes. *Proceedings of the National Academy of Sciences*, **1982**, *79*: 350-354.
- [115] M. Meier, *et al.* Crystal structure of the carbohydrate recognition domain of the H1 subunit of the asialoglycoprotein receptor. *Journal of molecular biology*, **2000**, *300*: 857-865.
- [116] Y.-H. Tang, *et al.* Discovery of a sensitive Cu (II)-cyanide “off-on” sensor based on new C-glycosyl triazolyl bis-amino acid scaffold. *Organic & biomolecular chemistry*, **2012**, *10*: 555-560.
- [117] M.H. Lee, *et al.* Hepatocyte-Targeting Single Galactose-Appended Naphthalimide: A Tool for Intracellular Thiol Imaging in Vivo. *Journal of the American Chemical Society*, **2012**, *134*: 1316-1322.
- [118] L. Dong, *et al.* Glycosylation enhances the aqueous sensitivity and lowers the cytotoxicity of a naphthalimide zinc ion fluorescence probe. *Chem Commun (Camb)*, **2015**, *51*: 11852-11855.
- [119] K.-B. Li, D. Zhou, X.-P. He, and G.-R. Chen. Ratiometric glyco-probe for transient determination of thiophenol in full aqueous solution and river water. *Dyes and Pigments*, **2015**, *116*: 52-57.
- [120] K.-B. Li, *et al.* Hepatoma-selective imaging of heavy metal ions using a ‘clicked’ galactosylrhodamine probe. *Chemical Communications*, **2014**, *50*: 11735-11737.
- [121] X.P. He, *et al.* Rapid Identification of the Receptor-Binding Specificity of Influenza A Viruses by Fluorogenic Glycofoldamers. *Angewandte Chemie International Edition*, **2016**, *55*: 13995-13999.
- [122] M.H. Lee, *et al.* Disulfide-cleavage-triggered chemosensors and their biological applications. *Chem Rev*, **2013**, *113*: 5071-5109.
- [123] X. Sun, Y. Wang, and Y. Lei. Fluorescence based explosive detection: from mechanisms to sensory materials. *Chem Soc Rev*, **2015**, *44*: 8019-8061.
- [124] H.N. Kim, W.X. Ren, J.S. Kim, and J. Yoon. Fluorescent and colorimetric sensors for detection of lead, cadmium, and mercury ions. *Chem Soc Rev*, **2012**, *41*: 3210-3244.
- [125] N. Jayaraman, K. Maiti, and K. Naresh. Multivalent glycoliposomes and micelles to study carbohydrate-protein and carbohydrate-carbohydrate interactions. *Chem Soc Rev*, **2013**, *42*: 4640-4656.
- [126] A. Martinez, C.O. Mellet, and J.M.G. Fernández. Cyclodextrin-based multivalent glycoconjugates: covalent and supramolecular conjugates to assess carbohydrate–protein interactions. *Chemical Society Reviews*, **2013**, *42*: 4746-4773.
- [127] W. Weis, *et al.* Structure of the influenza virus haemagglutinin complexed with its receptor, sialic acid. *Nature*, **1988**, *333*: 426.
- [128] Y.M. Chabre and R. Roy. Multivalent glycoconjugate syntheses and applications using aromatic scaffolds. *Chemical Society Reviews*, **2013**, *42*: 4657-4708.
- [129] S. Cecioni, A. Imberty, and S. Vidal. Glycomimetics versus multivalent glycoconjugates for the design of high affinity lectin ligands. *Chemical reviews*, **2014**, *115*: 525-561.
- [130] S. Howorka, J. Nam, H. Bayley, and D. Kahne. Stochastic detection of monovalent and bivalent protein–ligand interactions. *Angewandte Chemie*, **2004**, *116*: 860-864.
- [131] M. Mammen, G. Dahmann, and G.M. Whitesides. Effective inhibitors of hemagglutination by influenza virus synthesized from polymers having active ester groups. Insight into mechanism of inhibition. *Journal of medicinal chemistry*, **1995**, *38*: 4179-4190.
- [132] P.I. Kitov, *et al.* Shiga-like toxins are neutralized by tailored multivalent carbohydrate ligands. *Nature*, **2000**, *403*: 669.

- [133] R. Roy. Syntheses and some applications of chemically defined multivalent glycoconjugates. *Current opinion in structural biology*, **1996**, *6*: 692-702.
- [134] J.J. Lundquist and E.J. Toone. The cluster glycoside effect. *Chemical reviews*, **2002**, *102*: 555-578.
- [135] K.C.Y. Baptiste Thomas, Marion Donnier-Maréchal, Guo Rong Chen, Xiao Peng He, Sébastien Vidal. Fluorescent glycoconjugates and their application. *Submitted*.
- [136] J. Yariv, M. Rapport, and L. Graf. The interaction of glycosides and saccharides with antibody to the corresponding phenylazo glycosides. *Biochemical Journal*, **1962**, *85*: 383.
- [137] T.K. Dam and C.F. Brewer, *Carbohydrate-lectin cross-linking interactions: structural, thermodynamic, and biological studies*, in *Methods in enzymology*. 2003, Elsevier. p. 455-486.
- [138] L.R. Olsen, *et al.* X-ray crystallographic studies of unique cross-linked lattices between four isomeric biantennary oligosaccharides and soybean agglutinin. *Biochemistry*, **1997**, *36*: 15073-15080.
- [139] M. Delbianco, P. Bharate, S. Varela-Aramburu, and P.H. Seeberger. Carbohydrates in Supramolecular Chemistry. *Chem Rev*, **2016**, *116*: 1693-1752.
- [140] Y.M. Chabre and R. Roy. Multivalent glycoconjugate syntheses and applications using aromatic scaffolds. *Chem Soc Rev*, **2013**, *42*: 4657-4708.
- [141] Q. Chen, *et al.* Glucosamine hydrochloride functionalized tetraphenylethylene: a novel fluorescent probe for alkaline phosphatase based on the aggregation-induced emission. *Chem Commun (Camb)*, **2010**, *46*: 4067-4069.
- [142] T. Kato and K. Hatanaka. Flow cytometric analysis of lectin-oligosaccharide interactions by using fluorescent oligosaccharide probes. *Journal of bioscience and bioengineering*, **2011**, *112*: 202-204.
- [143] X.M. Hu, *et al.* Tetraphenylethylene-based Glycoconjugate as a Fluorescence “Turn-On” Sensor for Cholera Toxin. *Chemistry—An Asian Journal*, **2011**, *6*: 2376-2381.
- [144] J.X. Wang, *et al.* Sugar-bearing tetraphenylethylene: novel fluorescent probe for studies of carbohydrate-protein interaction based on aggregation-induced emission. *Org Biomol Chem*, **2011**, *9*: 2219-2226.
- [145] K. Shiraiishi, T. Sanji, and M. Tanaka. A displacement assay for the sensing of protein interactions using sugar-tetraphenylethylene conjugates. *Tetrahedron Letters*, **2010**, *51*: 6331-6333.
- [146] K.R. Wang, D. Han, G.J. Cao, and X.L. Li. Synthesis and predetermined supramolecular chirality of carbohydrate-functionalized perylene bisimide derivatives. *Chem Asian J*, **2015**, *10*: 1204-1214.
- [147] K.-R. Wang, *et al.* Fluorescence turn-on sensing of protein based on mannose functionalized perylene bisimides and its fluorescence imaging. *Biosensors and Bioelectronics*, **2014**, *58*: 27-32.
- [148] M. Marradi, F. Chiodo, I. Garcia, and S. Penades. Glyconanoparticles as multifunctional and multimodal carbohydrate systems. *Chem Soc Rev*, **2013**, *42*: 4728-4745.
- [149] J. Yao, M. Yang, and Y. Duan. Chemistry, biology, and medicine of fluorescent nanomaterials and related systems: new insights into biosensing, bioimaging, genomics, diagnostics, and therapy. *Chem Rev*, **2014**, *114*: 6130-6178.
- [150] Z. Skeete, *et al.* Design of functional nanoparticles and assemblies for theranostic applications. *ACS Appl Mater Interfaces*, **2014**, *6*: 21752-21768.
- [151] M. Grzelczak, J. Perez-Juste, P. Mulvaney, and L.M. Liz-Marzán. Shape control in gold nanoparticle synthesis. *Chemical Society Reviews*, **2008**, *37*: 1783-1791.
- [152] N.L. Rosi and C.A. Mirkin. Nanostructures in biodiagnostics. *Chemical reviews*, **2005**, *105*: 1547-1562.
- [153] T.A. Taton, G. Lu, and C.A. Mirkin. Two-color labeling of oligonucleotide arrays via size-selective scattering of nanoparticle probes. *Journal of the American Chemical Society*, **2001**, *123*: 5164-5165.
- [154] J.F. Parker, C.A. Fields-Zinna, and R.W. Murray. The story of a monodisperse gold nanoparticle: Au25L18. *Accounts of chemical research*, **2010**, *43*: 1289-1296.
- [155] J. Turkevich, P.C. Stevenson, and J. Hillier. A study of the nucleation and growth processes in the synthesis of colloidal gold. *Discussions of the Faraday Society*, **1951**, *11*: 55-75.

- [156] O. Martínez-Ávila, *et al.* Gold manno-glyconanoparticles: Multivalent systems to block HIV-1 gp120 binding to the lectin DC-SIGN. *Chemistry—A European Journal*, **2009**, *15*: 9874-9888.
- [157] A.J. Reynolds, A.H. Haines, and D.A. Russell. Gold glyconanoparticles for mimics and measurement of metal ion-mediated carbohydrate–carbohydrate interactions. *Langmuir*, **2006**, *22*: 1156-1163.
- [158] C.L. Schofield, *et al.* Colorimetric detection of *Ricinus communis* Agglutinin 120 using optimally presented carbohydrate-stabilised gold nanoparticles. *Analyst*, **2008**, *133*: 626-634.
- [159] A. Aykaç, *et al.* β -Cyclodextrin-bearing gold glyconanoparticles for the development of site specific drug delivery systems. *Langmuir*, **2013**, *30*: 234-242.
- [160] C.H. Lu, *et al.* A graphene platform for sensing biomolecules. *Angewandte Chemie*, **2009**, *121*: 4879-4881.
- [161] D.-K. Ji, Y. Zhang, X.-P. He, and G.-R. Chen. An insight into graphene oxide associated fluorogenic sensing of glycode–lectin interactions. *Journal of Materials Chemistry B*, **2015**, *3*: 6656-6661.
- [162] D.K. Ji, G.R. Chen, X.P. He, and H. Tian. Simultaneous Detection of Diverse Glycoligand-Receptor Recognitions Using a Single-Excitation, Dual-Emission Graphene Composite. *Advanced Functional Materials*, **2015**, *25*: 3483-3487.
- [163] X.P. He, *et al.* Dynamic tracking of pathogenic receptor expression of live cells using pyrenyl glycoanthraquinone-decorated graphene electrodes. *Chem Sci*, **2015**, *6*: 1996-2001.
- [164] A.M. Jastrzębska, P. Kurtycz, and A.R. Olszyna. Recent advances in graphene family materials toxicity investigations. *Journal of Nanoparticle Research*, **2012**, *14*: 1320.
- [165] A. Magrez, *et al.* Cellular toxicity of carbon-based nanomaterials. *Nano letters*, **2006**, *6*: 1121-1125.
- [166] J. Voskuhl, M.C. Stuart, and B.J. Ravoo. Sugar-decorated sugar vesicles: Lectin–carbohydrate recognition at the surface of cyclodextrin vesicles. *Chemistry—A European Journal*, **2010**, *16*: 2790-2796.
- [167] X.-P. He, *et al.* Fluorogenic supramolecular complexes formed between pyrenyl- β -cyclodextrin and glyco-rhodamine for the selective detection of lectins. *Chemical Communications*, **2014**, *50*: 14141-14144.
- [168] Y. Liu, *et al.* Supramolecular assembly of fluorogenic glyco-dots from perylenediimide-based glycoclusters for targeted imaging of cancer cells. *Chem Commun (Camb)*, **2017**, *53*: 11937-11940.
- [169] K.B. Li, *et al.* Foldable glycoprobes capable of fluorogenic crosslinking of biomacromolecules. *Chem Sci*, **2016**, *7*: 6325-6329.
- [170] V.K. Tiwari, *et al.* Cu-Catalyzed Click Reaction in Carbohydrate Chemistry. *Chem Rev*, **2016**, *116*: 3086-3240.
- [171] B. Worrell, J. Malik, and V.V. Fokin. Direct evidence of a dinuclear copper intermediate in Cu (I)-catalyzed azide-alkyne cycloadditions. *Science*, **2013**, *340*: 457-460.
- [172] J.E. Hein and V.V. Fokin. Copper-catalyzed azide–alkyne cycloaddition (CuAAC) and beyond: new reactivity of copper (I) acetylides. *Chemical Society Reviews*, **2010**, *39*: 1302-1315.
- [173] P. Wu, *et al.* Efficiency and fidelity in a click-chemistry route to triazole dendrimers by the copper (I)-catalyzed ligation of azides and alkynes. *Angewandte Chemie International Edition*, **2004**, *43*: 3928-3932.
- [174] W. Tang and M.L. Becker. "Click" reactions: a versatile toolbox for the synthesis of peptide-conjugates. *Chem Soc Rev*, **2014**, *43*: 7013-7039.
- [175] A.B. Lowe. Thiol–ene “click” reactions and recent applications in polymer and materials synthesis: a first update. *Polym. Chem.*, **2014**, *5*: 4820-4870.
- [176] A.B. Lowe. Thiol-ene “click” reactions and recent applications in polymer and materials synthesis. *Polym. Chem.*, **2010**, *1*: 17-36.
- [177] A. Dondoni and A. Marra. Recent applications of thiol–ene coupling as a click process for glycoconjugation. *Chemical Society Reviews*, **2012**, *41*: 573-586.
- [178] T. Mukaiyama, T. Sato, and J. Hanna. Reductive coupling of carbonyl compounds to pinacols and olefins by using TiCl_4 and Zn. *Chemistry Letters*, **1973**, *2*: 1041-1044.

- [179] M. Ephritikhine. A new look at the McMurry reaction. *Chemical Communications*, **1998**: 2549-2554.
- [180] S. Surprenant, W.Y. Chan, and C. Berthelette. Efficient synthesis of substituted vinyl ethers using the Julia olefination. *Organic letters*, **2003**, *5*: 4851-4854.
- [181] N. Dussart, H.V. Trinh, and D. Gueyrard. Modified Julia Olefination on Anhydrides: Extension and Limitations. Application to the Synthesis of Maculalactone B. *Org Lett*, **2016**, *18*: 4790-4793.
- [182] M.V. Ramakrishnam Raju and H.-C. Lin. Self-Assembly of Tetraphenylethene-Based [2] Catenane Driven by Acid-Base-Controllable Molecular Switching and Its Enabled Aggregation-Induced Emission. *Organic letters*, **2014**, *16*: 5564-5567.
- [183] M. Donnier-Marechal, *et al.* Tetraphenylethylene-based glycoclusters with aggregation-induced emission (AIE) properties as high-affinity ligands of bacterial lectins. *Org Biomol Chem*, **2018**, *16*: 8804-8809.
- [184] P.R. Blakemore. The modified Julia olefination: alkene synthesis via the condensation of metallated heteroarylalkylsulfones with carbonyl compounds. *Journal of the Chemical Society, Perkin Transactions 1*, **2002**: 2563-2585.
- [185] J.V. Allen, *et al.* On the use of the modified Julia olefination for bryostatin synthesis. *Tetrahedron Letters*, **2008**, *49*: 6352-6355.
- [186] B. Bourdon, *et al.* Synthesis of enol ethers from lactones using modified Julia olefination reagents: application to the preparation of tri- and tetrasubstituted exoglycals. *Tetrahedron letters*, **2008**, *49*: 747-749.
- [187] Y. Lin, *et al.* An elastic hydrogen-bonded cross-linked organic framework for effective iodine capture in water. *Journal of the American Chemical Society*, **2017**, *139*: 7172-7175.
- [188] R. Evans, *et al.* Quantitative Interpretation of Diffusion-Ordered NMR Spectra: Can We Rationalize Small Molecule Diffusion Coefficients? *Angewandte Chemie International Edition*, **2013**, *52*: 3199-3202.
- [189] K.-T. Lin, *et al.* Peroxynitrite induces apoptosis of HL-60 cells by activation of a caspase-3 family protease. *American Journal of Physiology-Cell Physiology*, **1998**, *274*: C855-C860.
- [190] K.B. Li, *et al.* Fluorogenic boronate-based probe-lactulose complex for full-aqueous analysis of peroxynitrite. *Talanta*, **2017**, *165*: 593-597.
- [191] P. Pacher, J.S. Beckman, and L. Liaudet. Nitric oxide and peroxynitrite in health and disease. *Physiological reviews*, **2007**, *87*: 315-424.
- [192] R. Radi. Peroxynitrite, a stealthy biological oxidant. *J Biol Chem*, **2013**, *288*: 26464-26472.
- [193] F. Yu, P. Li, B. Wang, and K. Han. Reversible near-infrared fluorescent probe introducing tellurium to mimetic glutathione peroxidase for monitoring the redox cycles between peroxynitrite and glutathione in vivo. *J Am Chem Soc*, **2013**, *135*: 7674-7680.
- [194] F. Yu, *et al.* A near-IR reversible fluorescent probe modulated by selenium for monitoring peroxynitrite and imaging in living cells. *J Am Chem Soc*, **2011**, *133*: 11030-11033.
- [195] J. Park, C.H. Heo, H.M. Kim, and J.-I. Hong. Two-photon fluorescent probe for peroxynitrite. *Tetrahedron Letters*, **2016**, *57*: 715-718.
- [196] X. Li, *et al.* A 1,8-naphthalimide-based fluorescent probe for selective and sensitive detection of peroxynitrite and its applications in living cell imaging. *RSC Advances*, **2017**, *7*: 34287-34292.
- [197] T. Peng, *et al.* A rationally designed rhodamine-based fluorescent probe for molecular imaging of peroxynitrite in live cells and tissues. *Chem Sci*, **2016**, *7*: 5407-5413.
- [198] D. Yang, *et al.* A highly selective fluorescent probe for the detection and imaging of peroxynitrite in living cells. *Journal of the American Chemical Society*, **2006**, *128*: 6004-6005.
- [199] Z.-N. Sun, *et al.* BODIPY-based fluorescent probe for peroxynitrite detection and imaging in living cells. *Organic letters*, **2009**, *11*: 1887-1890.
- [200] J. Zhang, X. Zhen, J. Zeng, and K. Pu. A Dual-Modal Molecular Probe for Near-Infrared Fluorescence and

- Photoacoustic Imaging of Peroxynitrite. *Anal Chem*, **2018**, *90*: 9301-9307.
- [201] X. Jia, *et al.* FRET-Based Mito-Specific Fluorescent Probe for Ratiometric Detection and Imaging of Endogenous Peroxynitrite: Dyad of Cy3 and Cy5. *J Am Chem Soc*, **2016**, *138*: 10778-10781.
- [202] D. Cheng, *et al.* Selective Visualization of the Endogenous Peroxynitrite in an Inflamed Mouse Model by a Mitochondria-Targetable Two-Photon Ratiometric Fluorescent Probe. *J Am Chem Soc*, **2017**, *139*: 285-292.
- [203] A. Sikora, *et al.* Direct oxidation of boronates by peroxynitrite: mechanism and implications in fluorescence imaging of peroxynitrite. *Free Radic Biol Med*, **2009**, *47*: 1401-1407.
- [204] F. Yu, *et al.* A fluorescent probe directly detect peroxynitrite based on boronate oxidation and its applications for fluorescence imaging in living cells. *Analyst*, **2012**, *137*: 3740-3749.
- [205] M. Weber, A.B. Mackenzie, S.D. Bull, and T.D. James. Fluorescence-Based Tool To Detect Endogenous Peroxynitrite in M1-Polarized Murine J774.2 Macrophages. *Anal Chem*, **2018**, *90*: 10621-10627.
- [206] A.C. Sedgwick, *et al.* Long-wavelength fluorescent boronate probes for the detection and intracellular imaging of peroxynitrite. *Chem Commun (Camb)*, **2017**, *53*: 12822-12825.
- [207] X. Sun, *et al.* Reaction-based Indicator displacement Assay (RIA) for the selective colorimetric and fluorometric detection of peroxynitrite. *Chem Sci*, **2015**, *6*: 2963-2967.
- [208] G. Eda and M. Chhowalla. Chemically derived graphene oxide: towards large-area thin-film electronics and optoelectronics. *Advanced materials*, **2010**, *22*: 2392-2415.
- [209] K.P. Loh, Q. Bao, G. Eda, and M. Chhowalla. Graphene oxide as a chemically tunable platform for optical applications. *Nature chemistry*, **2010**, *2*: 1015.
- [210] P. Zheng and N. Wu. Fluorescence and sensing applications of graphene oxide and graphene quantum dots: a review. *Chemistry—An Asian Journal*, **2017**, *12*: 2343-2353.
- [211] A. Eychmüller and A.L. Rogach. Chemistry and photophysics of thiol-stabilized II-VI semiconductor nanocrystals. *Pure and Applied Chemistry*, **2000**, *72*: 179-188.
- [212] J.C. Love, *et al.* Self-assembled monolayers of thiolates on metals as a form of nanotechnology. *Chemical reviews*, **2005**, *105*: 1103-1170.
- [213] I. Rahman and W. MacNee. Lung glutathione and oxidative stress: implications in cigarette smoke-induced airway disease. *American Journal of Physiology-Lung Cellular and Molecular Physiology*, **1999**, *277*: L1067-L1088.
- [214] L. Yang, *et al.* A Triple-Emission Fluorescent Probe for Discriminatory Detection of Cysteine/Homocysteine, Glutathione/Hydrogen Sulfide, and Thiophenol in Living Cells. *ACS Sens*, **2018**, *3*: 1863-1869.
- [215] R. Munday. Toxicity of thiols and disulphides: involvement of free-radical species. *Free Radical Biology and Medicine*, **1989**, *7*: 659-673.
- [216] T.P. Hell and R.C. Lindsay. Toxicological properties of thio- and alkylphenols causing flavor tainting in fish from the upper Wisconsin River. *Journal of Environmental Science & Health Part B*, **1989**, *24*: 349-360.
- [217] P. Amroliya, S.G. Sullivan, A. Stern, and R. Munday. Toxicity of aromatic thiols in the human red blood cell. *Journal of Applied toxicology*, **1989**, *9*: 113-118.
- [218] J.-X. He, T. Akao, and T. Tani. Development of a simple HPLC method for determination of paeoniflorin-metabolizing activity of intestinal bacteria in rat feces. *Chemical and pharmaceutical bulletin*, **2002**, *50*: 1233-1237.
- [219] T. Wang, *et al.* Identification of hydrolytic metabolites of dyfonate in alkaline aqueous solutions by using high performance liquid chromatography–UV detection and gas chromatography–mass spectrometry. *International Journal of Environmental and Analytical Chemistry*, **2010**, *90*: 948-961.
- [220] X. Hu, *et al.* An excited-state intramolecular proton transfer-based probe for the discrimination of thiophenols over aliphatic thiols. *Analytical Methods*, **2016**, *8*: 1425-1430.
- [221] S. Pagidi, N.K. Kalluvettukuzhy, and P. Thilagar. Triarylboron Anchored Luminescent Probes: Selective Detection and Imaging of Thiophenols in the Intracellular Environment. *Langmuir*, **2018**, *34*: 8170-8177.

- [222] X. Liu, *et al.* A red emitting fluorescent probe for instantaneous sensing of thiophenol in both aqueous medium and living cells with a large Stokes shift. *Journal of Materials Chemistry C*, **2016**, *4*: 4320-4326.
- [223] D. Kand, P.S. Mandal, T. Saha, and P. Talukdar. Structural imposition on the off-on response of naphthalimide based probes for selective thiophenol sensing. *RSC Adv.*, **2014**, *4*: 59579-59586.
- [224] H.W. Liu, *et al.* Efficient two-photon fluorescent probe with red emission for imaging of thiophenols in living cells and tissues. *Anal Chem*, **2015**, *87*: 8896-8903.
- [225] L. Xiong, *et al.* Highly Sensitive Squaraine-Based Water-Soluble Far-Red/Near-Infrared Chromofluorogenic Thiophenol Probe. *ACS Sens*, **2017**, *2*: 599-605.
- [226] D. Yu, F. Huang, S. Ding, and G. Feng. Near-infrared fluorescent probe for detection of thiophenols in water samples and living cells. *Anal Chem*, **2014**, *86*: 8835-8841.
- [227] M. Zhang, T. Leng, Y. Shen, and C. Wang. Reaction-based fluorescent probe for the selective and sensitive detection of thiophenols with a large Stokes shift and its application in water samples. *Analyst*, **2018**, *143*: 756-760.
- [228] D.G. Khandare, *et al.* Green synthesis of a benzothiazole based 'turn-on' type fluorimetric probe and its use for the selective detection of thiophenols in environmental samples and living cells. *RSC Advances*, **2016**, *6*: 52790-52797.
- [229] D. Yu, Q. Zhai, S. Yang, and G. Feng. A colorimetric and near-infrared fluorescent turn-on probe for in vitro and in vivo detection of thiophenols. *Analytical Methods*, **2015**, *7*: 7534-7539.
- [230] W. Lv, *et al.* Design and synthesis of norendoxifen analogues with dual aromatase inhibitory and estrogen receptor modulatory activities. *Journal of medicinal chemistry*, **2015**, *58*: 2623-2648.
- [231] D. Zhang, *et al.* Probing Thiophenol Pollutant in Solutions and Cells with BODIPY-Based Fluorescent Probe. *Industrial & Engineering Chemistry Research*, **2017**, *56*: 9303-9309.
- [232] K.R. Kim, H.J. Kim, and J.I. Hong. Electrogenerated Chemiluminescent Chemodosimeter Based on a Cyclometalated Iridium(III) Complex for Rapid and Sensitive Detection of Thiophenol. *Anal Chem*, **2018**.
- [233] H.M. Burke, T. Gunnlaugsson, and E.M. Scanlan. Recent advances in the development of synthetic chemical probes for glycosidase enzymes. *Chem Commun (Camb)*, **2015**, *51*: 10576-10588.
- [234] L. Weignerová, P. Bojarová, and V. Křen, *Glycosidases in synthesis*, in *Carbohydrate Chemistry*. 2009. p. 311-333.
- [235] J. Han, M.S. Han, and C.H. Tung. A fluorogenic probe for beta-galactosidase activity imaging in living cells. *Mol Biosyst*, **2013**, *9*: 3001-3008.
- [236] D.J. Spergel, *et al.* Using reporter genes to label selected neuronal populations in transgenic mice for gene promoter, anatomical, and physiological studies. *Progress in neurobiology*, **2001**, *63*: 673-686.
- [237] A.Y. Louie, *et al.* In vivo visualization of gene expression using magnetic resonance imaging. *Nature biotechnology*, **2000**, *18*: 321.
- [238] M.E. Van Dort, *et al.* Radiosynthesis and Evaluation of 5-[¹²⁵I] Iodoindol-3-yl-β-d-Galactopyranoside as a β-Galactosidase Imaging Radioligand. *Molecular imaging*, **2008**, *7*: 7290.2008. 00020.
- [239] S. Celen, *et al.* Synthesis and evaluation of ¹⁸F-and ¹¹C-labeled phenyl-galactopyranosides as potential probes for in vivo visualization of LacZ gene expression using positron emission tomography. *Bioconjugate chemistry*, **2008**, *19*: 441-449.
- [240] A. Alvarez, M. Ibanez, and R. Rotger. Beta-galactosidase activity in bacteria measured by flow cytometry. *Biotechniques*, **1993**, *15*: 974.
- [241] Y. Zhang, *et al.* Detecting lacZ gene expression in living cells with new lipophilic, fluorogenic beta-galactosidase substrates. *The FASEB Journal*, **1991**, *5*: 3108-3113.
- [242] T.S. Wehrman, *et al.* Luminescent imaging of β-galactosidase activity in living subjects using sequential reporter-enzyme luminescence. *Nature methods*, **2006**, *3*: 295.
- [243] R. Fulton and B.N. Van. Luminescent reporter gene assays for luciferase and beta-galactosidase using a liquid scintillation counter. *Biotechniques*, **1993**, *14*: 762-763.

- [244] M. Kamiya, *et al.* beta-Galactosidase fluorescence probe with improved cellular accumulation based on a spirocyclized rhodol scaffold. *J Am Chem Soc*, **2011**, *133*: 12960-12963.
- [245] X.X. Zhang, *et al.* A versatile two-photon fluorescent probe for ratiometric imaging E. colibeta-galactosidase in live cells and in vivo. *Chem Commun (Camb)*, **2016**, *52*: 8283-8286.
- [246] M. Safir Filho, *et al.* Development of highly sensitive fluorescent probes for the detection of beta-galactosidase activity - application to the real-time monitoring of senescence in live cells. *Analyst*, **2018**, *143*: 2680-2688.
- [247] M. Zhao, *et al.* Fabrication of Stable and Luminescent Copper Nanocluster-Based AIE Particles and Their Application in beta-Galactosidase Activity Assay. *ACS Appl Mater Interfaces*, **2017**, *9*: 32887-32895.
- [248] C. Tang, *et al.* A universal fluorometric assay strategy for glycosidases based on functional carbon quantum dots: β -galactosidase activity detection in vitro and in living cells. *Journal of Materials Chemistry B*, **2017**, *5*: 1971-1979.
- [249] G. Jiang, *et al.* A selective and light-up fluorescent probe for beta-galactosidase activity detection and imaging in living cells based on an AIE tetraphenylethylene derivative. *Chem Commun (Camb)*, **2017**, *53*: 4505-4508.
- [250] K. Gu, *et al.* Real-Time Tracking and In Vivo Visualization of beta-Galactosidase Activity in Colorectal Tumor with a Ratiometric Near-Infrared Fluorescent Probe. *J Am Chem Soc*, **2016**, *138*: 5334-5340.
- [251] B.G. Winchester, *Lysosomal metabolism of glycoconjugates*, in *Biology of the Lysosome*. 1996, Springer. p. 191-238.
- [252] D.J. Becker and J.B. Lowe. Fucose: biosynthesis and biological function in mammals. *Glycobiology*, **2003**, *13*: 41R-53R.
- [253] H. Abdel-Aleem, *et al.* Serum alpha L-fucosidase enzyme activity in ovarian and other female genital tract tumors. *International Journal of Gynecology & Obstetrics*, **1996**, *55*: 273-279.
- [254] E. Waidely, *et al.* Serum protein biomarkers relevant to hepatocellular carcinoma and their detection. *Analyst*, **2016**, *141*: 36-44.
- [255] X. Hou, *et al.* An anthracenecarboximide fluorescent probe for in vitro and in vivo ratiometric imaging of endogenous alpha-L-fucosidase for hepatocellular carcinoma diagnosis. *Materials Chemistry Frontiers*, **2017**, *1*: 660-667.
- [256] Y. Li, *et al.* Simultaneous intracellular beta-D-glucosidase and phosphodiesterase I activities measurements based on a triple-signaling fluorescent probe. *Anal Chem*, **2011**, *83*: 1268-1274.
- [257] I.E. Serdiuk, *et al.* Flavonol-based fluorescent indicator for determination of β -glucosidase activity. *RSC Advances*, **2016**, *6*: 42532-42536.
- [258] A.J. Plajer, *et al.* Different Selectivities in the Insertions into C (sp²)-H Bonds: Benzofulvenes by Dual Gold Catalysis Competition Experiments. *Chemistry-A European Journal*, **2018**, *24*: 10766-10772.
- [259] L. Anthore-Dalion, *et al.* The Halogen-Samarium Exchange Reaction: Synthetic Applications and Kinetics. *Angewandte Chemie International Edition*, **2019**, *58*: 4046-4050.
- [260] A.-X. Ding, *et al.* [12] aneN³ modified tetraphenylethylene molecules as high-performance sensing, condensing, and delivering agents toward DNAs. *ACS applied materials & interfaces*, **2016**, *8*: 14367-14378.
- [261] M. Donnier-Marechal, *et al.* Perylene^{di}imide-based glycoclusters as high affinity ligands of bacterial lectins: synthesis, binding studies and anti-adhesive properties. *Org Biomol Chem*, **2017**, *15*: 10037-10043.
- [262] G. Zhao, *et al.* Facile preparation and investigation of the properties of single molecular POSS-based white-light-emitting hybrid materials using click chemistry. *New Journal of Chemistry*, **2018**, *42*: 555-563.
- [263] L. Han, *et al.* Assessing the Sequence Specificity in Thermal and Polarized Optical Order of Multiple Sequence-Determined Liquid Crystal Polymers. *Macromolecules*, **2018**, *51*: 6209-6217.
- [264] B. Liu and J. Liu, *Methods and compositions for near infrared fluorescent nanodots with aggregation-induced emission characteristics*. 2018, National University of Singapore, Singapore . p. 54pp.
- [265] D. Jana, S. Boxi, P.P. Parui, and B.K. Ghorai. Planar-rotor architecture based pyrene-vinyl-tetraphenylethylene conjugated systems: photophysical properties and aggregation behavior. *Organic & biomolecular chemistry*, **2015**, *13*:

10663-10674.

- [266] X. Cai, *et al.* Organic Nanoparticles with Aggregation-Induced Emission for Bone Marrow Stromal Cell Tracking in a Rat PTI Model. *Small*, **2016**, *12*: 6576-6585.
- [267] A. Kovalová, R. Pohl, and M. Vrabel. Stepwise triple-click functionalization of synthetic peptides. *Organic & biomolecular chemistry*, **2018**, *16*: 5960-5964.
- [268] M. Rao, *et al.* Photocatalytic Supramolecular Enantiodifferentiating Dimerization of 2-Anthracenecarboxylic Acid through Triplet–Triplet Annihilation. *Organic letters*, **2018**, *20*: 1680-1683.
- [269] Z. Chen, *et al.* Synthesis and evaluation of a water-solubility glycosyl-rhodamine fluorescent probe detecting Hg²⁺. *Carbohydrate research*, **2016**, *429*: 81-86.

TITRE:

Conception et synthèse de glyco-sondes fluorescents pour des applications en détection

RESUME

Les sondes fluorescentes sont largement appliquées par exemple à la détection de contaminants ou à l'imagerie cellulaire. Mais l'effet d'agrégation (ACQ) atténue généralement l'intensité de la fluorescence. Par conséquent, le concept d'« aggregated induced emission » (AIE) représente une solution à ces problèmes d'agrégation et plusieurs glycoclusters, glyco-sondes et glyco-assemblages fluorescents ont été conçus et reportés. Nous avons conçu et synthétisé des glyco-polymères fluorescents pour le ciblage cellulaire et l'adressage de médicaments, avec la fluorescence permettant la détection des cellules ciblées. Pour surmonter l'effet ACQ, nous avons conjugué le dicyanométhylène-4H-pyrane (DCM) et le tétraphényléthène (TPE) afin d'obtenir des sondes fluorescentes (AIE) émettant dans le proche infrarouge. Nous avons conçu et synthétisé des sondes fluorescentes AIE pouvant s'auto-assembler avec des glycoclusters à base de TPE. Nous avons conçu et synthétisé des sondes fluorescentes AIE pouvant s'auto-assembler avec des glycoclusters à base de TPE. Nous avons finalement combiné les deux fragments TPE et DCM pour synthétiser un nouveau fluorophore AIE (TPE-DCM). Ensuite, la conjugaison avec des glycosides a conduit à une excellente solubilité dans l'eau. Une application à la détection de glycosidases *in vitro* et dans des dosages cellulaires ou sur des modèles animaux a été possible avec ces sondes.

MOTS-CLES: aggregation induced emission (AIE), glycosylation, tétraphényléthène, Click Chemistry, imagerie des cellules

TITLE:

Design and synthesis of fluorescent glyco-dots for detection and cell imaging

ABSTRACT

Fluorescent probes are widely developed and applied to the detection of contaminants or in cell imaging. But the ACQ effect usually quenched the fluorescence intensity. Aggregated-induced emission (AIE) appears to solve these problems and several fluorescent glycoclusters, glyco-probes and glyco-complexes were designed and reported for biological analysis. We designed and synthesized fluorescent glyco-polymers with multiple glycosides for cell targeting and drug delivery. To overcome the ACQ effect and interference, we conjugated dicyanomethylene-4H-pyran (DCM) and tetraphenylethene (TPE) to obtain near-infrared AIE fluorescent probes for detection and imaging cancer cells. We designed and synthesized AIE fluorescent probes which could self-assemble with TPE-based glycoclusters for thiophenol detection *in vitro* and in environmental water samples. We finally combined both TPE and DCM moieties to synthesize a novel AIE fluorophore (TPE-DCM), and n conjugated with glycosides to obtained AIE fluorescent probes with long-wavelength emission, excellent water-solubility. Application to the detection of glycosidases *in vitro* and in cell assays or animal models was possible with these probes.

KEY WORD: aggregation induced emission (AIE), glycosylation, tetraphenylethene, Click Chemistry, cell imaging

DISCIPLINE: Chimie Organique

UMR-CNRS 5246, ICBMS, Laboratoire de Chimie Organique 2, Batiment Lederer, 43 boulevard du 11 Novembre 1918, F-69622 Villeurbanne CEDEX.